UNIVERSIDADE FEDERAL DE MINAS GERAIS
ESCOLA DE ENGENHARIA
PROGRAMA DE PÓS-GRADUAÇÃO EM ENGENHARIA QUÍMICA

Leonardo Fortuna Carneiro

Analysis of the computational and mathematical impacts of simplifying assumptions in proton-exchange membrane fuel cell models

BELO HORIZONTE – MG
2025

Leonardo Fortuna Carneiro

Analysis of the computational and mathematical impacts of simplifying assumptions in proton-exchange membrane fuel cell models

Dissertação apresentada ao Programa de Pós-Graduação em Engenharia Química da Universidade Federal de Minas Gerais, como requisito parcial à obtenção do título de Mestre em Engenharia Química.

Linha de pesquisa: Engenharia de sistemas em processos

Orientador: Prof. Esly Ferreira da Costa Junior

Coorientadores: Tulio Matencio; Samuel Tadeu de Paula Andrade

Belo Horizonte
2025

Carneiro, Leonardo Fortuna.
C289a Analysis of the computational and mathematical impacts of simplifying assumptions in proton-exchange membrane fuel cell models [recurso eletrônico] / Leonardo Fortuna Carneiro. – 2025.
1 recurso online (186 f. : il., color.) : pdf.

Orientador: Esly Ferreira da Costa Júnior.
Coorientadores: Tulio Matencio, Samuel Tadeu de Paula Andrade.

Dissertação (mestrado) – Universidade Federal de Minas Gerais, Escola de Engenharia.

Apêndices: f. 154-186.

Bibliografia: f. 145-153.

1. Engenharia química – Teses. 2. Eletroquímica – Teses. 3. Modelagem matemática – Teses. 4. Modelagem computacional – Teses. 5. Células a combustível – Teses. 6. Membranas (Tecnologia) – Teses. I. Costa Júnior, Esly Ferreira da. II. Matencio, Tulio. III. Andrade, Samuel Tadeu de Paula. IV. Universidade Federal de Minas Gerais. Escola de Engenharia. V. Título.

CDU: 66.0(043)

Ficha catalográfica elaborada pelo bibliotecário Marcio A. A. Gomes CRB/6 2812
Biblioteca Prof. Mário Werneck, Escola de Engenharia da UFMG

UNIVERSIDADE FEDERAL DE MINAS GERAIS

FOLHA DE APROVAÇÃO

"ANALYSIS OF THE COMPUTATIONAL AND MATHEMATICAL IMPACTS OF SIMPLIFYING ASSUMPTIONS IN PROTON EXCHANGE MEMBRANE FUEL CELL MODELS"

Leonardo Fortuna Carneiro

Dissertação submetida à Banca Examinadora designada pelo Colegiado do Programa de Pós-Graduação em Engenharia Química da Escola de Engenharia da Universidade Federal de Minas Gerais, como parte dos requisitos à obtenção do título de **MESTRE EM ENGENHARIA QUÍMICA**.

321ª DISSERTAÇÃO APROVADA EM 6 DE FEVEREIRO DE 2025 POR:

Documento assinado eletronicamente por **Tulio Matencio**, **Membro de comissão**, em 06/02/2025, às 11:28, conforme horário oficial de Brasília, com fundamento no art. 5º do Decreto nº 10.543, de 13 de novembro de 2020.

Documento assinado eletronicamente por **Esly Ferreira da Costa Junior**, **Professor do Magistério Superior**, em 06/02/2025, às 11:29, conforme horário oficial de Brasília, com fundamento no art. 5º do Decreto nº 10.543, de 13 de novembro de 2020.

Documento assinado eletronicamente por **Rudolf Huebner**, **Professor do Magistério Superior**, em 06/02/2025, às 11:29, conforme horário oficial de Brasília, com fundamento no art. 5º do Decreto nº 10.543, de 13 de novembro de 2020.

Documento assinado eletronicamente por **Gerhard Ett**, **Usuário Externo**, em 06/02/2025, às 11:30, conforme horário oficial de Brasília, com fundamento no art. 5º do Decreto nº 10.543, de 13 de novembro de 2020.

Documento assinado eletronicamente por **Samuel Tadeu de Paula Andrade**, **Usuário Externo**, em 06/02/2025, às 11:33, conforme horário oficial de Brasília, com fundamento no art. 5º do Decreto nº 10.543, de 13 de novembro de 2020.

A autenticidade deste documento pode ser conferida no site https://sei.ufmg.br/sei/controlador_externo.php?acao=documento_conferir&id_orgao_acesso_externo=0, informando o código verificador **3894293** e o código CRC **F706584A**.

Referência: Processo nº 23072.203725/2025-76 SEI nº 3894293

ACKNOWLEDGEMENTS

I knew from a young age that I wanted to be a scientist. No other career would be capable of fulfilling my desire to learn and contribute to a subject that fascinates me. Whether this is a curse or a blessing, I let the future decide: I can only play the hand that I have been dealt. So, I am deeply grateful to everyone who helped me during the first steps of my academic career.

Firstly, I thank my close family for trusting – much more than me – that my dedication would be fruitful. Among them, I particularly thank my sister, whose interest in my work acted as a major motivation.

Furthermore, I am grateful for all the contributions and lessons my professors gave me at UFMG. Without the aid of Esly F. da Costa Junior, Tulio Matencio, and Samuel T. de P. Andrade, this dissertation would certainly be of much lower quality. Also, I thank CNPq (Process 350339/2023-6 and 405937/2022-4), CAPES, and FAPEMIG for the financial support during this time.

Lastly, I thank my friends for their companionship and patience during these last years. I know that I am absent – and sometimes even negligent – due to my dedication to my research, but every moment I was with them was essential to me. I especially thank Lucas Paladini for helping me during the hardest parts of these years and for believing in me even when I was not able to.

To Toby, my dog.

ABSTRACT

Modeling is an area of great importance for the development and optimization of fuel cells and, therefore, is the subject of significant research. However, most of the models in the literature do not discuss the impact of the simplifying assumptions made during modeling, focusing the analysis only on the global description. Furthermore, few works discuss the computational cost of their model, even though this is important for many applications.

With these challenges in mind, this work seeks to analyze the impact of simplifying assumptions on the modeling of PEM-type fuel cells to quantify both the computational cost and the effect on the predicted results. In this case, the simplifications evaluated are the use of the reaction entropy of the system as a constant value with temperature, the use of the Tafel equation instead of Butler-Volmer to describe the reaction kinetics, the impact of using different sorption isotherms, and the assumption that an average value can approximate water's diffusivity in the electrolyte. To this purpose, a one-dimensional, isothermal, and single-phase model was implemented, as well as variations that allow the evaluation of each of the analyzed assumptions. All tests were performed using typical operational conditions for fuel cells, with high and low values for critical parameters – namely temperature, relative humidity, transfer coefficients, membrane thickness, and three electro-osmotic drag coefficients.

The results for the assumption of a constant reaction entropy showed only small deviations when compared to the robust description, but no statistically significant computational improvement was obtained using it. As for the use of the Tafel equation, the cathodic activation overvoltage had insignificant differences from the one obtained from Butler-Volmer, while the anodic one was not well represented but had a negligible value. Furthermore, a small computational improvement was observed when this assumption was used, which was more significant when the interval between current densities was smaller in the model. The usage of a mean diffusivity – which permitted the development of analytical solutions for the water transport inside the membrane – caused considerable deviations when the membrane was not well humidified. This behavior was attributed to underestimating the back-diffusion, which significantly affects the water profile and, consequently, the ohmic overvoltage. Regarding the computational improvement, a considerable reduction in time was observed for all tests when the assumption was used along with the larger interval between current densities. However, for the smaller one, the models with the polynomial and piecewise linear descriptions of the electro-osmotic drag coefficient presented, in some cases, worse performances when compared to their non-simplified versions. Thus, this assumption can provide significant improvements, but is only useful under well-humidified conditions and with considerable steps in current density. Finally, the use of different sorption isotherms caused a substantial change in the water profile in the membrane, also impacting the ohmic overvoltage. This indicates that the common practice of using parametrizations obtained for different membranes can significantly harm the model's accuracy.

Keywords: Proton-exchange membrane fuel cell, Mathematical modeling, Fuel cell, Electrochemistry, Numerical simulation.

RESUMO

A modelagem é uma área de grande importância para o desenvolvimento e otimização de células a combustível e, portanto, é objeto de um número significativo de pesquisas. Todavia, a maioria dos modelos da literatura não discute o impacto das hipóteses utilizadas para a simplificação da modelagem, concentrando a análise apenas na descrição global. Além disso, poucos trabalhos discutem o custo computacional de seus modelos, embora isso seja importante para diversas aplicações.

Com esses desafios em mente, este trabalho busca analisar o impacto de hipóteses simplificadoras na modelagem de células a combustível do tipo PEM, para quantificar o custo computacional e o efeito nos resultados previstos. Nesse caso, as simplificações avaliadas são o uso da entropia de reação do sistema como um valor constante com a temperatura, o uso da equação de Tafel em vez da de Butler-Volmer para descrever a cinética da reação, o impacto do uso de diferentes isotermas de sorção e a suposição de que a difusividade da água no eletrólito pode ser aproximada por um valor médio. Para esse fim, foi implementado um modelo unidimensional, isotérmico e monofásico, bem como variações que permitem a avaliação de cada uma das suposições analisadas. Todos os testes foram realizados em condições de operação típicas para células a combustível, com valores altos e baixos para parâmetros críticos – os quais são a temperatura, umidade relativa, coeficientes de transferência, espessura da membrana e três coeficientes de arraste eletro-osmótico.

Os resultados para a hipótese de uma entropia de reação constante mostraram apenas pequenos desvios quando comparados com a descrição robusta, mas nenhum aprimoramento computacional estatisticamente significativo foi obtido com seu uso. Quanto ao uso da equação de Tafel, o sobrepotencial de ativação catódico teve diferenças insignificantes em relação à obtida com Butler-Volmer, enquanto o anódico não foi bem representado, mas teve um valor desprezível. Além disso, uma pequena melhoria computacional foi observada quando essa hipótese foi usada, o que foi mais significativo quando o intervalo entre densidades de corrente foi menor no modelo. O uso de uma difusividade média – que permitiu o desenvolvimento de soluções analíticas para o transporte de água dentro da membrana – causou desvios consideráveis quando a membrana não estava bem umidificada. Esse comportamento foi atribuído à subestimação da retrodifusão, que afeta significativamente o perfil da água e, consequentemente, o sobrepotencial ôhmico. Com relação à melhoria computacional, foi observada uma redução considerável no tempo para todos os testes quando a suposição foi usada junto com o tamanho maior do intervalo entre densidades de corrente. No entanto, para o menor, os modelos com as descrições polinomiais e lineares por partes do coeficiente de arraste eletro-osmótico apresentaram piores desempenhos em alguns casos quando comparados às suas versões não simplificadas. Portanto, essa suposição pode proporcionar melhorias significativas, mas só é útil em condições bem umidificadas e com passos consideráveis na densidade de corrente. Por fim, o uso de diferentes isotermas de sorção causou uma mudança substancial no perfil da água na membrana, afetando também o sobrepotencial ôhmico. Isso indica que a prática comum de usar parametrizações obtidas para diferentes membranas pode prejudicar significativamente a exatidão do modelo.

Palavras-chave: Célula a combustível de membrana polimérica trocadora de prótons, Modelagem matemática, Célula a combustível, Eletroquímica, Simulação numérica.

LIST OF FIGURES

LIST OF TABLES

LIST OF ABBREVIATIONS AND ACRONYMS

FC	Fuel cell
PEMFC	Polymer Electrolyte Membrane Fuel Cell
HOR	Hydrogen Oxidation Reaction
ORR	Oxygen Reduction Reaction
SEM	Scanning electron microscopy
LE	Liquid-equilibrated
VE	Vapor-equilibrated
CL	Catalyst layer
GDL	Gas diffusion layer
PEM	Proton-exchange membrane
IAPWS	International Association for the Properties of Water and Steam
ODE	Ordinary Differential Equation

LIST OF SYMBOLS

P	Pressure	[Pa]
p	Partial pressure	[Pa]
T	Temperature	[K]
c	Concentration	[mol·m^{-3}]
A	Area	[m^2]
J	Molar flux	[mol·m^{-2}·s^{-1}]
i	Electric current	[A]
j	Current density	[A·m^{-2}]
n	Number of moles of electrons transferred	[mol]
G	Gibbs Energy	[J]
F	Faraday constant	[A·s·mol^{-1}]
E	Reversible voltage	[V]
V	Voltage or Volume	[V or m^3]
W	Work	[J]
Q	Heat	[J]
R	Electrical resistance	[Ω]
x	Mole fraction	[mol·mol^{-1}]
M	Correction factor	[ ]
s	Liquid water saturation	[ ]
H	Enthalpy	[J]
L	Distance	[m]
S_e	Standard error of the estimate	[ ]

Greek Symbols

α	Transfer coefficient or empirical constant	[ ]
α^*	Ratio between net water molar flux in the membrane and net hydrogen flux in the anode	[ ]
β	Symmetry coefficient	[ ]
Δ	Variation (final value - initial value)	[ ]
ρ	Density	[kg·m^3]

ν	Stoichiometric coefficient or number of rate-determining steps	[ ]
η	Overvoltage	[V]
λ	Water content in the electrolyte	[ ]
σ	Electrical conductivity	[S·m^{-1}]
φ	Volume fraction of water in the membrane.	[ ]
ϕ	Phase potential	[V]
ξ	Electro-osmotic drag coefficient	[ ]
ε	Efficiency or Porosity	[ ]
τ	Tortuosity	[ ]
H	Regularization function	[ ]
ζ	Correction factor	[ ]

Superscripts

A	Anode	[ ]
C	Cathode	[ ]
M	Membrane	[ ]
$\bar{X}$	Molar quantity of property X	[ ]
$\hat{X}$	Mass quantity of property X	[ ]
0	Standard-state	[ ]

Subscripts

H_2	Hydrogen	[ ]
O_2	Oxygen	[ ]
H_2O	Water	[ ]
H^+	Proton	[ ]
e^-	Electron	[ ]
in	Inlet	[ ]
out	Outlet	[ ]
rxn	Reaction	[ ]
$Thermo$	Thermodynamic (reversible) value.	[ ]
$prod.$	Products	[ ]

$react.$	Reactants	[ ]
i	Species i	[ ]
HHV	Higher Heating Value	[ ]
ele	Electrical	[ ]
act	Activation	[ ]
oxi	Oxidation	[ ]
red	Reduction	[ ]
ch	Chemical	[ ]
fwd	Forward direction of an equilibrium	[ ]
bwd	Backward direction of an equilibrium	[ ]
amb	Ambient	[ ]
$Cool$	Cooling	[ ]
tn	Thermoneutral	[ ]
cl	Clamping (relative to the clamping pressure)	[ ]

TABLE OF CONTENTS

1 INTRODUCTION

The development of sustainable and reliable sources of energy is one of the most important goals for the prosperity of future generations (CHU; MAJUMDAR, 2012). Among the existing alternatives, the change for a hydrogen economy – that is, the system where the main energy carriers are hydrogen and electricity (PENNER, 2006) – has been discussed since the 19th century as a promising possibility (BOCKRIS, 2013). This molecule has a high energy content and has the potential, on adequate conditions, to have a clean cycle (INCER-VALVERDE et al., 2023), as even its combustion yields only water as a product.

Therefore, as hydrogen becomes more relevant as an energy source, methods for producing and using it sustainably also increase in relevancy. To meet this demand, the usage of fuel cells and electrolyzers is taken in high regard due to their reliable, quiet, and efficient operation (SMITH, 2000). A cycle, as exemplified in Figure 1, where electrolyzers powered by sustainable energy produce the hydrogen that is fed to fuel cells when needed, could ensure almost completely clean energy.

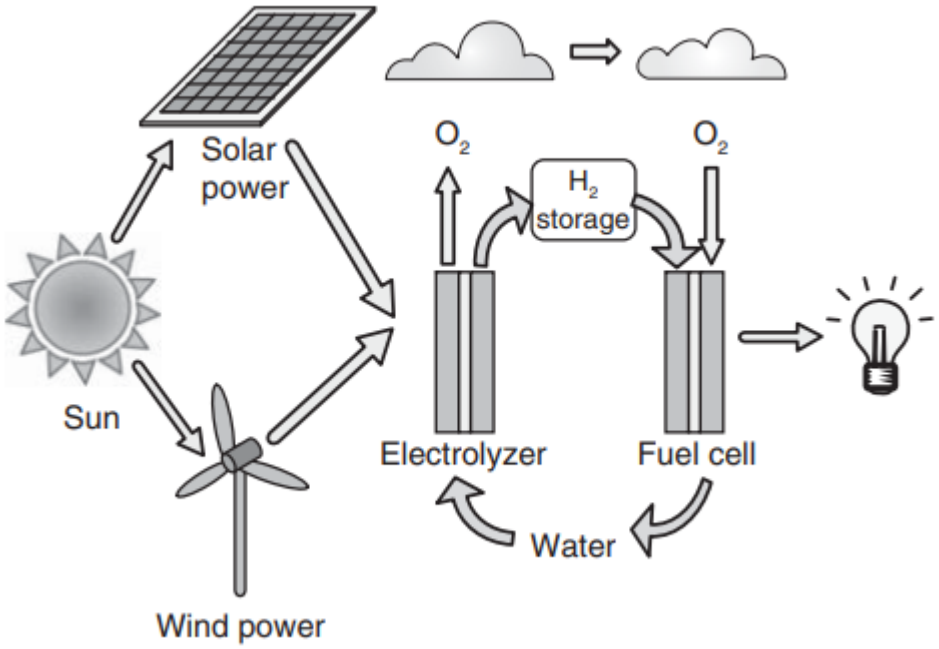

Figure 1 - Possible cycle for clean hydrogen production and usage.
Source: O'HAYRE et al., 2016, p. 22.

Fuel cells are devices capable of converting electrochemical energy directly into electric energy. As they do not demand transformations to either mechanical energy or heat, fuel cells can have high efficiencies, which, when related to their low

environmental impact (EG&G TECHNICAL SERVICES INC., 2004), makes them strong candidates for replacing traditional combustion engines in a significant number of applications. In contrast to batteries, these devices are open systems, which enables independent scaling between their capacity and power because they can produce energy as long as the reactant is available (O'HAYRE et al., 2016, p. 9). This independence also permits the separation between the energy storage – in this case, made in the form of hydrogen – and power production, which can yield advantages in enabling the optimization of each function without harming the performance of the other part (SMITH, 2000). Moreover, as some types of fuel cells can be operated in a different cycle, being also able to produce hydrogen with electrical energy and water as inputs – that is, working as an electrolyzer – their upsides in a hydrogen-based economy become even more evident.

Even though all fuel cells operate under the same basic principles, different types exist, each requiring specific operating conditions, fuel types, and offering particular advantages and disadvantages. They are categorized according to their electrolytes, as this choice determines the electrochemical reactions that happen in the system and, consequently, the necessary conditions for operation (O'HAYRE et al., 2016, p. 12-13). Table 1 presents the main types of fuel cells along with some of their characteristics.

Table 1 - Major fuel cell types.

	PEMFC	**PAFC**	**AFC**	**MCFC**	**SOFC**
Electrolyte	Polymer membrane	Liquid H_3PO_4 (immobilized)	Liquid KOH (immobilized)	Molten Carbonate	Ceramic
Charge carrier	H^+	H^+	OH^-	CO_3^{2-}	O^{2-}
Operating Temperature	80°C	200°C	60-220°C	650°C	600-1000°C
Catalyst	Platinum	Platinum	Platinum	Nickel	Perovskites
Cell components	Carbon based	Carbon based	Carbon based	Stainless based	Ceramic based
Fuel compatibility	H_2, methanol	H_2	H_2	H_2, CH_4	H_2, CH_4, CO

Source: O'HAYRE et al., 2016.

Among the presented types, polymer electrolyte membrane fuel cells (PEMFC) – the focus of this work – are considered of special interest to important applications, such as transportation and portable power generation, because they operate in low

temperatures and have high power density (BARBIR, 2013, p. 8). For example, most motor companies work exclusively with PEMFCs for their fuel cell vehicles (WANG et al., 2011). These devices also present other considerable advantages, such as very fast start-up and response times (although much slower than those of batteries), compactness, which may be essential for several applications, and the possibility of reverse operation as an electrolyzer. Therefore, understanding and optimizing the operation of these devices is an important topic of scientific research (ABDEREZZAK, 2018).

Even though fuel cells and electrolyzers are taken in high regard as a technology, significant scientific advances are still necessary to make their widespread usage commercially viable. One major barrier to this technology is the price, as the membrane – usually coated with an expensive catalyst – is significantly costly. Therefore, improvements are needed to ensure better commercial viability (ALASWAD et al., 2020) (PAREKH, 2022).

Given the increasing importance of fuel cells, computational methods for simulating them become a necessity, because they provide indispensable information for the design and optimization of such complex systems. However, detailed models can be too computationally demanding for applications where the model must be applied repeatedly (NÓBREGA, 2023). Thus, understanding the impact of each modeling approach for fuel cells on both precision and computational demand is necessary, as it enables researchers to balance their needs when elaborating new models for specific applications.

2 OBJECTIVES

2.1 GENERAL OBJECTIVE

The objective of this study is to evaluate different approaches found in the scientific literature for modeling some of the main phenomena occurring in polymer electrolyte membrane fuel cells, aiming to understand the impact of simplifying assumptions on model accuracy and computational demand.

2.2 SPECIFIC OBJECTIVES

- Elaboration of a one-dimensional, steady-state PEMFC model capable of using different methods available in the literature for describing each discussed phenomenon.
- Usage of this model to evaluate the computational demand and effect in the predicted result related to different modeling approaches for the following variations:
    - Constant entropy of reaction or describing its dependence with temperature when evaluating the thermodynamic potential.
    - Description of the reaction's kinetics using the Butler-Volmer Equation or the simpler Tafel Equation.
    - Different sorption isotherms used to describe the water content on the boundaries of the membrane.
    - Description of water's diffusivity inside the membrane as a function of the water content or using a mean value.
- Refinement of modeling strategies for PEMFC that exist in the literature, proposing analytical methods when possible.

3 LITERATURE REVIEW

3.1 Basic PEMFC operation

Fuel cells (FC) are capable of transforming the chemical energy contained in a fuel into electrical energy (direct current) in a single reaction step, without demanding any other energy conversion and with no moving parts (BARBIR, 2013, p. 1). However, differently from batteries – which also do this – fuel cells are open systems, that is, their capacity and power are not convoluted. As long as fuel is provided, they will be able to generate power and will maintain constant voltage. These characteristics grant them significant advantages, such as good scaling between power demands and quick recharge, simply made by refueling the system (O'HAYRE et al., 2016, p. 8-11).

To generate power, a fuel cell reacts a fuel (most commonly hydrogen) with oxygen (usually from air). This is also how a combustion engine works – and FCs share many characteristics with them – but the energy conversion process is intrinsically different. While a combustion engine directly reacts both reactants and obtains work by converting the energy released by the reaction with the movement of mechanical parts, fuel cells spatially separate each reaction, making it so that two electrochemical half-reactions occur instead (O'HAYRE et al., 2016, p. 6). This is done by using different layers in the cell, which can be grouped into two electrodes (anode and cathode) and one electrolyte.

The electrodes are the places where the electrochemical reaction takes place. They are highly porous structures that contain, along with other components, the catalyst for the half-reactions. The anode – the electrode where the fuel is fed – is characterized by the occurrence of the oxidation reaction, where electrons are liberated, while the cathode contains the reduction reaction, consuming electrons (O'HAYRE et al., 2016, p. 15-16). As for the electrolytes, they are materials that permit ion passage but prevent both the reactant and electron flows (O'HAYRE et al., 2016 p. 6). Thus, using an external circuit, it is possible to produce an electrical current when the electrons are demanded or liberated from the half-reactions, which can perform work on a load (EG&G TECHNICAL SERVICES INC., 2004, p. 2).

The exact reaction that will take place in the electrodes depends both on the used fuel and on the electrolyte (EG&G TECHNICAL SERVICES INC., 2004, p. 2). In a PEMFC using hydrogen, the focus of this work, the anodic reaction is the hydrogen

oxidation reaction (HOR), presented in Equation 1, and the cathodic one is the oxygen reduction reaction (ORR), Equation 2 (SPIEGEL, 2008). Note that the H^+ ion is present in both reactions, as it is conducted by the polymeric electrolytes used in PEMFCs. If other electrolytes are used so that other ions are conducted, the reactions would be different.

$$H_2 \rightarrow 2H^+ + 2e^- \quad (1)$$

$$\frac{1}{2}O_2 + 2H^+ + 2e^- \rightarrow H_2O \quad (2)$$

Although those reactions are essentially the only energy conversion step, the operation of a fuel cell cannot be reduced just to them. Their energy production process, according to O'Hayre *et al.* (2016, p. 16), can be divided into four major steps: reactant transport, electrochemical reaction, ionic and electronic conductions, and product removal from the fuel cell.

First, as open systems, fuel cells demand a constant supply of fuel and oxidant. If either is not present in a sufficient quantity for the reaction, it will not happen, which can be especially limiting in high current operations (O'HAYRE et al., 2016, p. 17). Thus, ensuring an efficient delivery of reactants is a major step in fuel cell operation.

Once the reactants reach the catalyst, they may undergo electrochemical reactions. As these reactions are the source of the electrons that provide the needed current for the system, their kinetics are determinant in the amount of work one can obtain from a fuel cell (O'HAYRE et al., 2016, p. 17).

Then, as the reaction produces and demands electrons and ions, transporting them is necessary. For the electrons, the transport is made by conduction in the external circuit, while the ions are transported by specific mechanisms involving the electrode. These are usually much less efficient than electron transport, which may hinder cell operation. Thus, it is desirable to work with thin electrolytes to minimize the resistance to this process (O'HAYRE et al., 2016, p. 17).

Finally, to avoid the system's dilution, which would hinder the transport mechanisms, the obtained products should be removed. Usually, the same mechanisms associated with feeding the reactants to the fuel cell cause the product to exit, however, under certain conditions this might not suffice, resulting in considerable efficiency losses (O'HAYRE et al., 2016, p. 18).

3.1.1 Fuel cell components

To enable each of the previously discussed steps to take place efficiently, an adequate structure is needed. It is essential, for example, that the structure permits easy access to the catalyst for the reactants, prevents reactant crossover, and ensures that electrons and ions can be moved between the electrodes. Also, as the voltage produced by one fuel cell is limited by thermodynamics, a stack arranged in series is demanded to reach higher voltages (O'HAYRE et al., 2016, p. 46). So, materials should be carefully selected to minimize contact resistances, which hinder the fuel cell's performance.

Figure 2 presents the basic parts of a PEMFC, where the location of each layer and its plate-like geometry are evident. The function of those and the materials used in their construction are presented in the following topics.

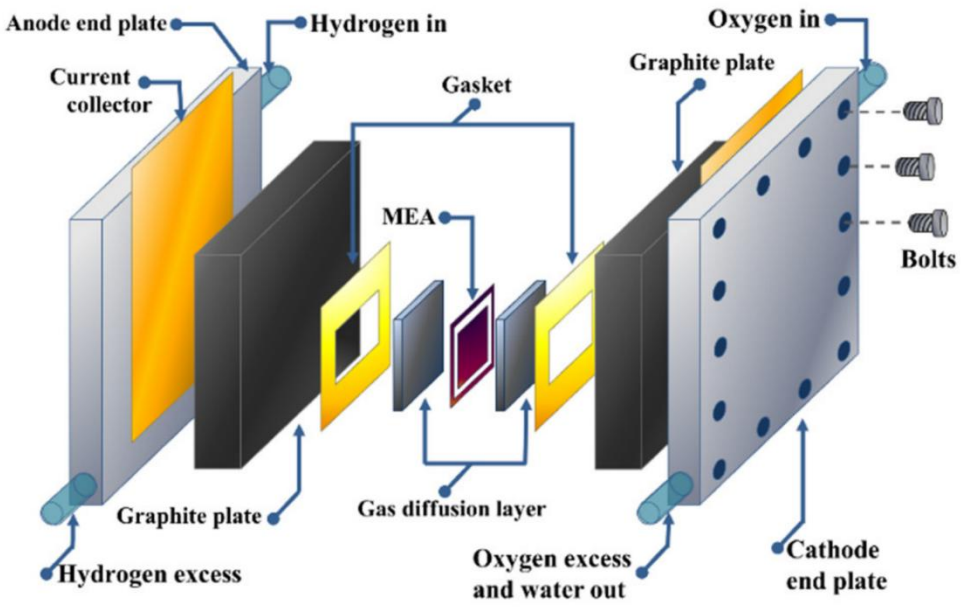

Figure 2 - Components of a PEMFC.
Source: TELLEZ-CRUZ et al., 2021

3.1.1.1 Flow channel

Flow channels are regions of advective transport of reactants (and products) that aim to ensure efficient reactant distribution (or product removal) in a fuel cell so that mass transfer losses are minimized (O'HAYRE et al., 2016, p. 183). They are also involved in harvesting the generated current (O'HAYRE et al., 2016, p. 196). In

addition, they provide mechanical support for a PEMFC stack, permit heat removal, and facilitate water management in the system (BAROUTAJI et al., 2016). There are many requirements for material selection for this application, such as chemical compatibility, corrosion resistance, electrical conductivity, and high mechanical strength (O'HAYRE et al., 2016, p. 196).

The materials used for the construction of flow channels are mainly graphite and metal alloys. Graphite has the benefits of high corrosion resistance, good conductivity, and relatively low contact resistance (BAROUTAJI et al., 2016), however, its brittleness and costly machining requirements are significant problems for their cost-effectiveness (O'HAYRE et al., 2016, p. 196). Metal alloys, on the other hand, besides the higher mechanical strength, are easier to fabricate and can be made thinner. Their main hindrance is the vulnerability to corrosion, as the oxide layer significantly decreases the fuel cell efficiency due to the rise in electrical resistance (BAROUTAJI et al., 2016). This problem is circumvented by the usage of corrosion-resistant alloys and surface coatings, but increasing the stability of such coatings is still necessary (O'HAYRE et al., 2016, p. 197).

An intensive area of research is the configuration of flow channels, aiming to minimize the mass transport losses in them. Many researchers have used Computational Fluid Dynamics modeling to understand and optimize these structures (BAROUTAJI et al., 2016). Common types of patterns used are exemplified in Figure 3, however, as this work is focused on low-dimensional modeling, their characteristics will not be discussed here. For further details, the review of Manso *et al.* (2012) is recommended.

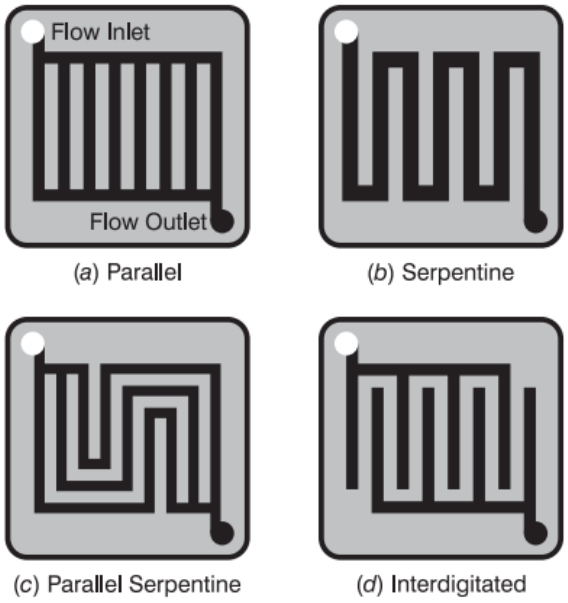

Figure 3 - Usual flow field patterns.
Source: O'HAYRE et al., 2016, p. 198.

3.1.1.2 Gas diffusion layer (GDL)

The gas diffusion layer is located between the flow channel and the catalyst. It has the functions of permitting diffusive transport to the inner layers, mechanically supporting the catalyst and membrane, conducting electrons involved in the reaction, aiding in water and heat removal, and protecting the thin catalyst layer from corrosion and erosion that would happen if the advective flow was directly made in its surface (BAROUTAJI et al., 2016) (EG&G TECHNICAL SERVICES INC., 2004, p. 3-4). Note that each electrode has one gas diffusion layer, thus, two are present in a fuel cell.

The most common materials for GDL are porous carbon paper or carbon cloth, with thicknesses between 100 and 300 μm (MAIYALAGAN; PASUPATHI, 2010). This choice is justified by the high porosity (usually more than 70%) and conductivity of these materials (O'HAYRE et al., 2016, p. 311). Figure 4 presents SEM (scanning electron microscopy) micrographs of them, in which their porosity is especially apparent.

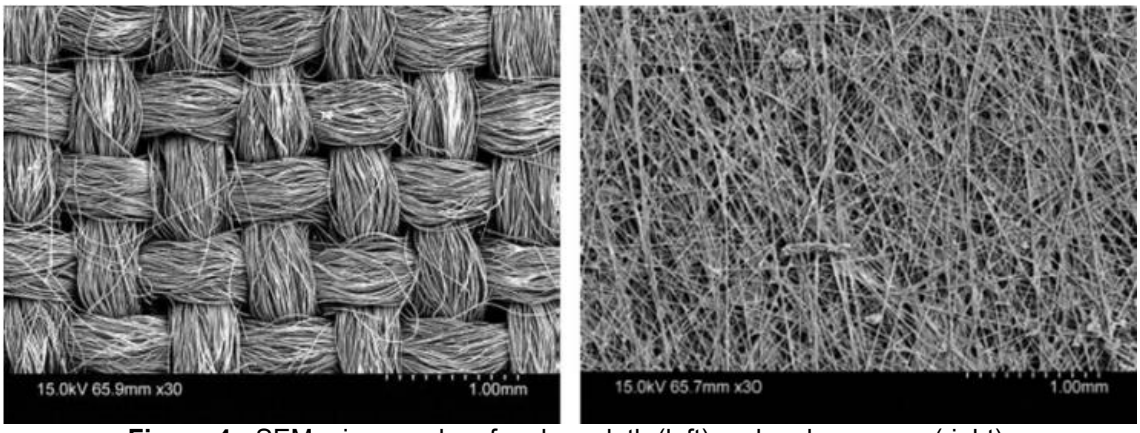

Figure 4 - SEM micrographs of carbon cloth (left) and carbon paper (right).
Source: BARBIR, 2013, p. 98.

As PEMFC normally operates in temperatures where it is likely that liquid water will be present, GDL is commonly coated with a hydrophobic material to prevent water from blocking its pores (BAROUTAJI et al., 2016). This coating is usually made of polytetrafluoroethylene (PTFE). Using an optimal amount of this material is important, as the coating will reduce the pore size, but its absence will result in flooding (MAIYALAGAN; PASUPATHI, 2010).

3.1.1.3 Catalyst layer (CL)

The catalyst layer is a thin region where the catalyst for each half-reaction is present (BARBIR, 2013, p. 92). Due to their high price, it is desirable to use the least amount of catalyst possible while ensuring a highly effective surface area for the reaction. This is usually achieved by using nanoscale particles of the material along with high-surface-area carbon support (O'HAYRE et al., 2016, p. 310). Ensuring this high availability of catalyst is crucial for fuel cell performance, as the reaction can only occur where electrolyte, gas, and electrically connected catalyst regions are in contact (O'HAYRE; BARNETT; PRINZ, 2005). Maximizing the quantity of these regions – named triple phase boundary (TPB) – depends on ensuring high contact between the needed components. With this objective and to diminish mass transport losses, fuel cells are organized into thin plates and their reaction rate is intrinsically linked to their area (O'HAYRE et al., 2016, p. 15). Figure 5 schematically presents the concept of the TPB.

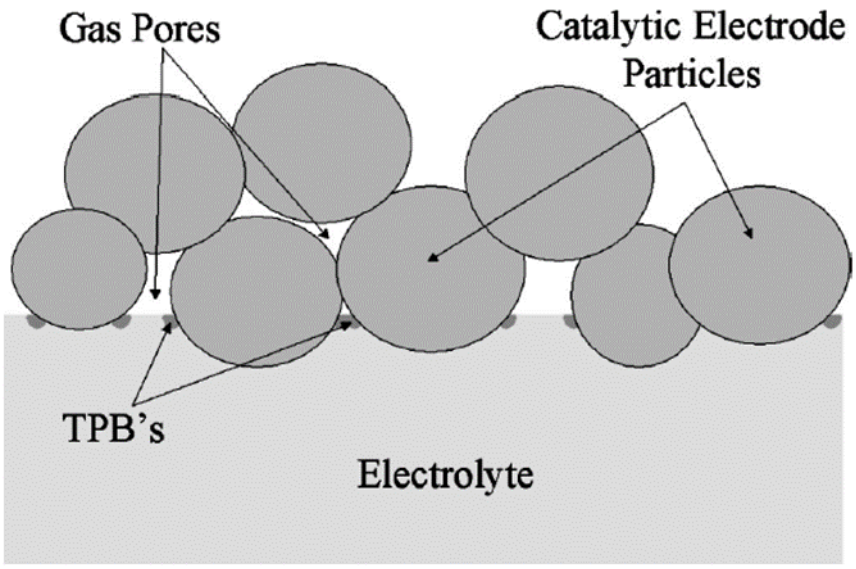

Figure 5 - Simplified illustration of the TPB.
Source: O'HAYRE; BARNETT; PRINZ, 2005.

The material whose performance as a catalyst is considered the best for both HOR and ORR reactions is platinum, an expensive and rare metal (MAIYALAGAN; PASUPATHI, 2010). However, advances in nanotechnology have considerably lowered the platinum load needed, as the area is the most important factor, not the catalyst's mass (BARBIR, 2013, p. 93-94). Even if the usage of this expensive material may not be an economic hindrance in the future, it still presents a significant limitation related to its durability. In the presence of CO, which is also a product in many hydrogen production processes, the platinum is poisoned, degrading the fuel cell performance (BAROUTAJI et al., 2016). This is undesirable not only due to the catalyst loss but also because it restricts the PEMFC into using only pure – thus, more expensive – hydrogen. To reduce this poisoning effect, multiple alloys of platinum have been studied (MAIYALAGAN; PASUPATHI, 2010), among which Pt-Ru has demonstrated the most significant potential (BAROUTAJI et al., 2016).

Although platinum is used in both electrodes, it is significantly less active for the ORR – which also is a more sluggish reaction – than for the HOR (O'HAYRE et al., 2016, p. 314-315). Therefore, the load in the cathode is normally higher than the one in the anode, and the interest in developing more effective catalysts is even greater for this reaction. Further discussion about alternative catalysts and alternatives for such optimization are beyond the scope of this work, nevertheless, it is one of the most important developments for the commercial viability of PEMFCs.

3.1.1.4 Electrolyte

Electrolytes are responsible for providing a conductive path for the ions involved in the half-reactions while also being impermeable to the gases and electrons (EG&G TECHNICAL SERVICES INC., 2004). In the case of PEMFC, the electrolytes are thin polymeric membranes capable of conducting protons (H^+). A considerable amount of them use water-related mechanisms in this transport and, thus, are dependent on their hydration level to work properly (O'HAYRE et al., 2016, p. 304).

The most used materials for applications below 100°C are sulfonated polymers made by the combination of perfluorinated back-bones with sulfonated chains (BAROUTAJI et al., 2016). The commercial name of this polymer is Nafion®, whose structure is presented in Figure 6, originally patented by DuPont. It should be noted that there are multiple types of Nafion, with their properties (mainly resistance and conductivity) changing according to the equivalent weight (EW) – mass of polymers per mol of active sites (BARBIR, 2013) (ABDEREZZAK, 2018).

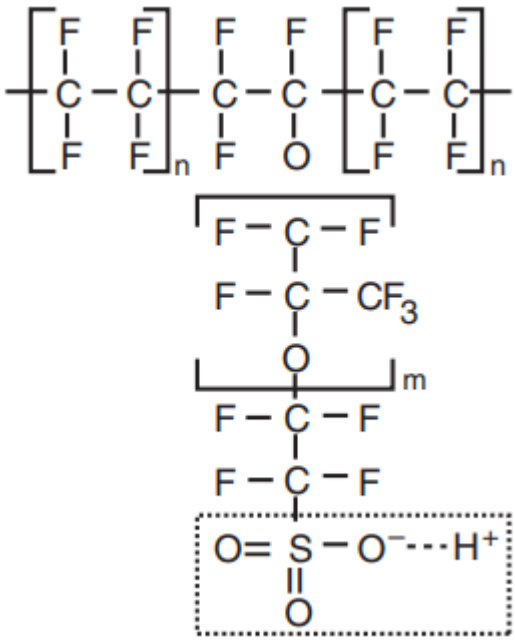

Figure 6 - Structure of Nafion.
Source: O'HAYRE et al., 2016, p. 137.

This polymer – more specifically, ionomer – presents a high proton conductivity and chemical resistance, where the first property is related to the chains and the second to the backbone (MAIYALAGAN; PASUPATHI, 2010). Nevertheless, it also has significant disadvantages, such as an environmentally unfriendly production

process, very high material cost, limitations for high-temperature operation, and the necessity of strict humidity control to ensure good conductivity (BAROUTAJI et al., 2016).

To measure this humidity in the membrane, it is common to define the water content in Nafion, λ, as the number of water molecules per sulfonic acid group present in the polymer (BARBIR, 2013, p. 76-77). The value of λ depends on the humidity of the system, reaching values up to 22 when the membrane is equilibrated with liquid water. However, when water vapor is used, it normally only reaches values of approximately 14 (BARBIR, 2013, p. 77). This phenomenon of the same water activity ($a_{H_2O} = 1$) yielding different values of λ (14 or 22) for different phases is called Schroeder's paradox. Another interesting phenomenon related to water uptake can be seen when studying an isotherm relating water activity to λ, as the one presented in Figure 7.

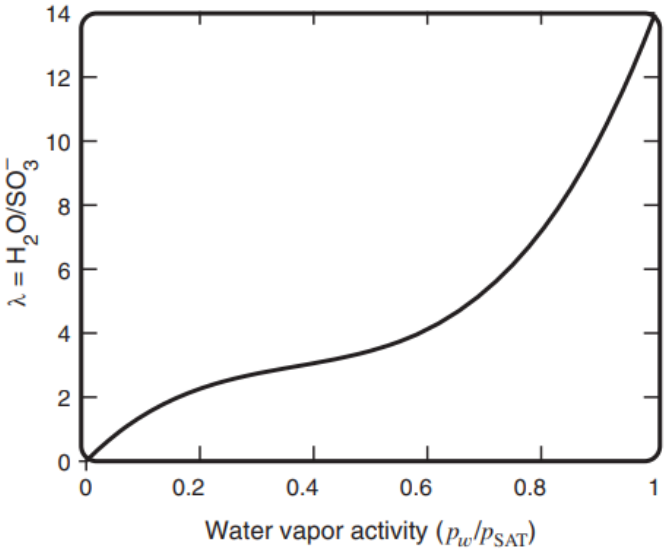

Figure 7 - Isotherm relating water uptake and λ for Nafion 117 at 303K.
Source: O'HAYRE et al., 2016, p. 138.

In low water activities (up to 0.75), λ increases slowly to about 5 due to solvation. Then, λ increases rapidly to 14.4, as the polymer swells with the water filling its pores (BARBIR, 2013, p. 77-78). Understanding these relations is crucial, as they enable the description of the conductivity as a function of usual variables (a_{H_2O}, in this case).

There are also other promising materials for electrolytes in fuel cells. For example, sulfonated hydrocarbon polymers, which are less expensive and more easily

recycled but have lower ionic conductivity and chemical stability (O'HAYRE et al., 2016, p. 305). Also, Phosphoric Acid Doped Polybenzimidazole (PBI) is interesting due to its high thermal resistance, which enables operation above 100ºC, which significantly eases water management. In this work, however, the modeling is restricted to Nafion membranes, as they are more commonly discussed in scientific literature.

3.1.1.5 Other components

Although the fuel cell's most critical parts are the two electrodes and the electrolyte, there are a considerable number of secondary parts that are important to ensure an efficient and stable operation of fuel cells. Some of them will be mentioned in this topic, but as they normally are not directly described in fuel cell modeling, the discussion will be brief.

Considering that fuel cells normally are operated as a stack to obtain the desired voltage, it is necessary to have a means to connect the cells. This is done by the usage of a bipolar plate, which connects the anode of one cell to the cathode of the adjacent one (BARBIR, 2013, p. 104). To be able to do this, they should be impermeable to gases, be electrically conductive, have adequate strength, and be corrosion resistant. Due to their good compromise between these properties, these plates are usually made of metal alloys or graphite-composite materials (BARBIR, 2013, p. 106).

Furthermore, to ensure that gas will not leak out of the edges of the stack, gaskets are used. They are normally made of polymeric material and are located around the edges of each cell (O'HAYRE et al., 2016, p. 349).

Finally, the end plates are present in a stack to unitize the components. Their main goal is to provide a uniform pressure distribution between the components of the PEMFC, which is important to reduce the contact resistance between them (ASGHARI; SHAHSAMANDI; ASHRAF KHORASANI, 2010).

3.2 PEMFC Thermodynamics

3.2.1 Thermodynamic voltage

Fuel cells operate by transforming energy, therefore, as with all other known energy conversion processes, they must obey the laws of thermodynamics (BARBIR, 2013). By analyzing the thermodynamic properties of the system, it is possible to calculate the maximum performance that can be achieved by them, which works as the limit for a real operation (O'HAYRE et al., 2016, p. 25).

Specifically, in a fuel cell, the main interest regarding thermodynamics is the evaluation of the maximum electrical work that can be obtained. As demonstrated in Appendix A, this value is equal to the variation of Gibbs energy caused by the electrochemical reaction. Using this deduction, the maximum voltage – the potential of a system to do electrical work – that can be obtained from a fuel cell can be calculated by Equation 3, where $\Delta\overline{G_{rxn}}$ is the molar Gibbs energy of the reaction, n is the number of electrons involved and F is the Faraday constant.

$$E_{Thermo} = -\frac{\Delta\overline{G_{rxn}}}{nF} \tag{3}$$

The only restriction for this equation is that the reaction must take place in constant pressure and temperature, which is almost always the case for fuel cells. Theoretically, using adequate values for the Gibbs energy of reactants and products, the thermodynamic voltage could be calculated for a system in any pressure or temperature, however, this is not common practice in the literature. Usually, the standard-state[1] voltage at certain pressure and temperature conditions is used, and correction terms for the activity of reactant and products, pressure, and temperature are added to obtain the value in the desired conditions.

For obtaining the temperature correction, consider Equation 4, which defines the differential of Gibbs energy (G) as a function of its canonical variables: temperature (T), and pressure (P) (SMITH et al., 2017, p. 212).

$$dG = -SdT + VdP \tag{4}$$

Considering molar properties and constant pressure, Equation 5 is reached.

[1] All substances in their pure, most stable forms with unit activity (O'HAYRE et al., 2016, p. 33).

$$\left(\frac{d\overline{G}}{dT}\right)_P = -\overline{S} \tag{5}$$

Then, writing this equation for the reaction and using the relation between Gibbs energy and voltage presented in Equation 3, Equation 6 is obtained. In it, $\Delta\overline{S_{rxn}}$ is the molar entropy of the reaction.

$$\left(\frac{dE}{dT}\right)_P = \frac{\Delta\overline{S_{rxn}}}{nF} \tag{6}$$

In this equation, the majority of the literature considers that the entropy is approximately constant with temperature so that the expression can be easily integrated to obtain Equation 7, which describes how voltage varies with temperature for constant pressure (O'HAYRE et al., 2016, p. 47-48) (KULIKOVSKY, 2019, p. 5). In this equation, E^0 and T_0 are, respectively, the voltage and temperature at the standard-state.

$$E_T(T) = E^0 + \frac{\Delta\overline{S_{rxn}}}{nF}(T - T_0) \tag{7}$$

However, as entropy is a function of temperature, a more accurate result is obtained by integrating an expression that describes the variation of the reaction's entropy with temperature, as proposed by Equation 8 (O'HAYRE et al., 2016, p. 48).

$$E_T(T) = E^0 + \frac{1}{nF}\int_{T_0}^{T} \Delta\overline{S_{rxn}} dT \tag{8}$$

Moreover, a correction is needed for both the pressure and concentration of reactants in the system. This can be done, as proposed throughout the literature, with the Nernst equation, presented in Equation 9, where a_i is the activity of species i, and ν_i is its stoichiometric coefficient.

$$E = E^0 - \frac{RT}{nF}\ln\left(\frac{\prod a_{prod.}^{\nu_i}}{\prod a_{react.}^{\nu_i}}\right) \tag{9}$$

For an ideal gas, which is commonly assumed for all gases when modeling fuel cells, the activity may be written as a function of the partial pressure of the substance, as seen in Equation 10, where p_i is the partial pressure of i and P^0 is the standard-state pressure (1 atm) (O'HAYRE et al., 2016, p. 50). For liquid species, for example water, the activity is equal to 1.

$$a_i = \frac{p_i}{P^0} \tag{10}$$

Thereby, using Equations 9 and 10, the Nernst equation for a PEMFC with the reaction written so that 1 mol of hydrogen is consumed is presented in Equation 11.

$$E = E^0 - \frac{RT}{2F}\ln\left(\frac{\left(\frac{p_{H_2O(g)}}{P^0}\right)}{\left(\frac{p_{H_2}}{P^0}\right)\left(\frac{p_{O_2}}{P^0}\right)^{0.5}}\right) \quad (11)$$

Finally, as the Nernst equation does not consider the temperature correction term, the description of the thermodynamic voltage of a PEMFC fuel cell may be done by combining Equations 8 (or 7 if the simplified relation is assumed) with 11, yielding Equation 12.

$$E_{Thermo} = E^0 + \frac{1}{2F}\int_{T_0}^{T}\Delta\overline{S_{rxn}}dT - \frac{RT}{2F}\ln\left(\frac{\left(\frac{p_{H_2O(g)}}{P^0}\right)}{\left(\frac{p_{H_2}}{P^0}\right)\left(\frac{p_{O_2}}{P^0}\right)^{0.5}}\right) \quad (12)$$

3.2.2 Fuel cell efficiency

Efficiency can be defined as the ratio between useful energy output and total energy input in the system (BARBIR, 2013, p. 24). For a fuel cell, the useful energy is the electrical work, and the energy input is the energy provided to the system by the reaction, given by the enthalpy of the reaction between hydrogen and oxygen. More precisely, the value that should be used is the higher heating value (HHV) for hydrogen combustion, as more energy is released by the reaction if liquid water is produced (O'HAYRE et al., 2016, p. 61).

It should be noted that, as in combustion, it is not possible to use all energy released by the reaction, as there are thermodynamic barriers to the energy conversion process. The maximum efficiency (ε_{Thermo}) is obtained by considering the theoretical electrical work that would be obtained with a reversible process ($W_{ele,Thermo}$), as presented in Equation 13. The negative sign in the work is due to the convention used, where negative work is done by the system.

$$\varepsilon_{Thermo} = \frac{-W_{ele,Thermo}}{\Delta H_{rxn,HHV}} \quad (13)$$

The maximum electrical work obtainable is given by the Gibbs energy, as shown in Appendix A. Thus, the maximum efficiency for a fuel cell is given by Equation 14.

$$\varepsilon_{Thermo} = -\frac{\Delta\overline{G_{rxn}}}{\Delta H_{rxn,HHV}} \quad (14)$$

For a combustion engine, this efficiency is limited by the Carnot cycle, whose efficiency is given by Equation 15 (SMITH et al., 2017, p. 177). T_C is the temperature

of the lower-temperature reservoir, while T_H is the one for the higher-temperature reservoir.

$$\varepsilon_{Carnot} = 1 - \frac{T_C}{T_H} \tag{15}$$

Considering a Carnot cycle that has a temperature of heat rejection of 273.15 K, the maximum efficiency of a PEMFC and a heat engine may be compared, as shown in Figure 8. It can be seen that, as the temperature rises, the heat engine's maximum efficiency rises and the fuel cell's decreases. Another remark about this figure is the slope change at 373.15 K, explained by the presence of only vapor water after this temperature, which was a different molar entropy when compared to liquid water (O'HAYRE et al., 2016, p. 62).

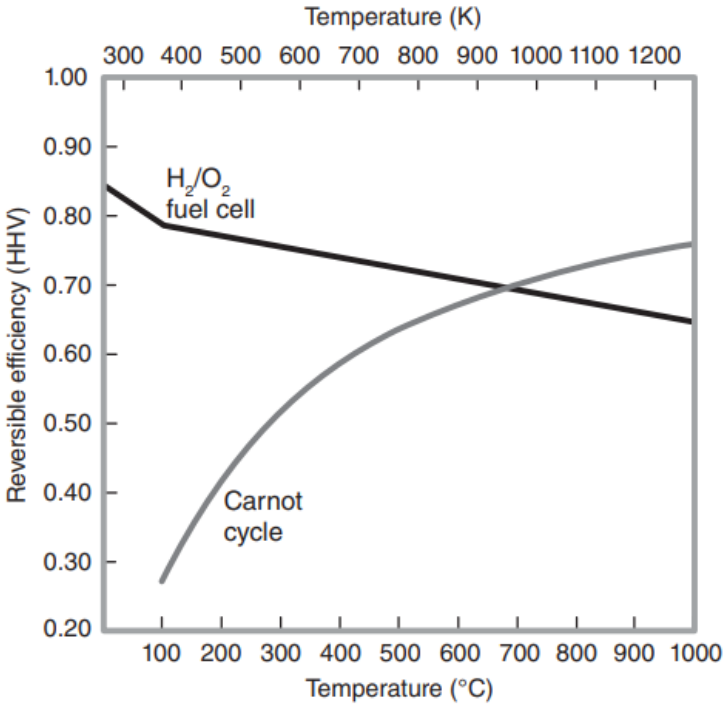

Figure 8 - Comparison between the maximum efficiency of a PEMFC and a Carnot engine.
Source: O'HAYRE et al., 2016, p. 62.

However, neither of these devices can operate at their maximum efficiency, so these results must be considered with caution. For example, one may conclude that higher efficiencies would be obtained if fuel cells are operated in lower temperatures, but efficiency losses – such as the kinetic losses – will decrease with temperature, thus, the real efficiency does not have a simple relation with the reversible one (O'HAYRE et al., 2016, p. 48).

3.3 PEMFC Kinetics

In a PEMFC, two electrochemical half-reactions take place: the hydrogen oxidation reaction (Equation 1) and the oxygen reduction reaction (Equation 2). Both of them, when written as in those equations, represent a global process of the mechanism happening in the electrode. The actual reaction involves a series of steps; for example, Kuhn *et al.* (2007) proposed a pathway for the ORR at low current densities, which is presented in Equations 16 (a) to (d). Note that the mechanism involves chemisorption of the molecules, which reinforces the discussion made in topic 3.1.1.3 about the triple phase boundary and heterogeneous nature of involved electrochemical reactions.

$$O_2 \rightleftharpoons 2O_{ad} \quad (16a)$$

$$2O_{ad} + e^- \rightleftharpoons O_{ad}^- \quad (16b)$$

$$O_{ad}^- + H^+ \rightharpoonup HO_{ad} \quad (16c)$$

$$HO_{ad} + H^+ + e^- \rightleftharpoons H_2O \quad (16d)$$

All steps happening in the reaction mechanism of HOR and ORR have finite rates, but they vary significantly. Thus, it is usual to ignore the fast steps, considering them instantaneous, and approach each reaction as an equivalent single-step single-electron transfer process when considering the reaction speed (KULIKOVSKY, 2019, p. 9).

Another important consideration about the reaction kinetics, which arises from the fact that the reaction is composed of a sequence of steps, is the existence of an activated state. Even though the reaction is spontaneous ($\Delta G_{rxn} < 0$), there is a necessity to pass through a state where the system has higher energy. This creates an energy barrier that must be overcome for the completion of the reaction – the activation energy (O'HAYRE et al., 2016, p. 82-84). To complete a reaction, due to the existence of this barrier, some energy will have to be spent. This will also impact the voltage of the fuel cell, resulting in a loss in relation to the thermodynamic voltage that is called activation overvoltage (η_{act}) (ABDEREZZAK, 2018, p. 68).

To calculate the activation overvoltage, which represents the kinetic losses in a fuel cell, some fundamental concepts of electrochemical reactions must be presented. The first one is the intrinsic relation between the produced current and reaction rate: each mole of fuel that undergoes an electrochemical reaction releases a specific number of electrons. Therefore, as current is the flow of charges, the rate at which the

reaction occurs can be directly related to the measured current (O'HAYRE et al., 2016, p. 78-79) (ABDEREZZAK, 2018, p. 87). Using the concept of current density (j) – that can be thought of as a normalized reaction rate – to normalize the area of a fuel cell, the flux of fuel into the reaction (J_i) is given by Faraday's law (Equation 17), where n is the number of electrons involved in the reaction and F is the Faraday constant.

$$J_i = \frac{j}{nF} \tag{17}$$

Furthermore, another key concept is that electrochemical reactions can occur in both directions, oxidation and reduction, according to the electrode potential (O'HAYRE et al., 2016, p. 80). In a specific voltage, both reactions will have the same rate, that is, the system will be in a dynamic equilibrium. If the electrode potential is made more negative than the equilibrium one, the reduction reaction will be favored, while in the opposite case – a more positive potential – will result in oxidation being the preferred reaction (O'HAYRE et al., 2016, p. 81).

Although there is no net current when the reaction is in equilibrium, both the oxidation and the reduction are happening in the electrode because this equilibrium is dynamic. Thus, considering that reaction rate is related to current density, there is a current related to both directions of the equilibrium, which have the same intensity and opposite directions so that the net current is zero. This current density that represents the charge transfer rate at equilibrium is the exchange current density, j_0 (ABDEREZZAK, 2018, p. 69). This value depends on the concentration of reactants and temperatures, as presented in Equation 18 (ABDEREZZAK, 2018, p. 70) (BARBIR, 2013, p. 38).

$$j_0 = j_0^{ref} a_c L_c \left(\frac{p_i}{p_i^{re}}\right)^{\gamma} e^{\left[-\frac{E_{act}}{RT}\left(1-\frac{T}{T_{ref}}\right)\right]} \tag{18}$$

In this equation, j_0^{ref} is the exchange current density per unit area of catalyst (A·cm^{-2} of catalyst) at a reference temperature and pressure; T is the temperature, p_i is the reactant partial pressure; E_{act} is the activation energy for the reaction; R is the ideal gas constant; γ is a pressure coefficient with values between 0.5 and 1; a_c is the specific surface area of the catalyst (cm^2·mg^{-1} of catalyst) and L_c is the catalyst loading (mg of catalyst·cm^{-2}). The product between a_c and L_c is called electrode roughness, given in unit of area of catalyst per unit of area of the electrode (BARBIR, 2013, p. 38).

Finally, as an electrochemical reaction is being evaluated, it should be considered that Gibbs energy consists of both electrical and chemical terms (BARBIR,

2013, p. 35). This makes it so that, for oxidation and reduction, Equations 19 and 20 can be respectively written.

$$\Delta G = \Delta G_{ch} - \alpha_{Oxi} FE \tag{19}$$

$$\Delta G = \Delta G_{ch} + \alpha_{Red} FE \tag{20}$$

Here, α is known as the transfer coefficient of the reaction, which is commonly confused in the literature with β, the symmetry factor (BARBIR, 2013, p. 35). While the meaning of β varies according to the model used to interpret the system (GUIDELLI et al., 2014, p. 255), its usage must be restricted to a one-electron transfer step or a single one-electron transfer step in an electrode reaction with multiple steps (GUIDELLI et al., 2014, p. 257). The transfer coefficient, on the other hand, involves kinetic, stoichiometric, and rate-defining step considerations (BOCKRIS; NAGY, 1973). Due to the complexity of the multiple electron transfer steps, its value cannot be assumed. They should be obtained experimentally by means of measuring the Tafel slope and calculated with Equations 21 and 22 (GUIDELLI et al., 2014, p. 257).

$$\alpha_{ano} = \left(\frac{RT}{F}\right)\frac{d \ln j_a}{dE} \tag{21}$$

$$\alpha_{cat} = -\left(\frac{RT}{F}\right)\frac{d \ln j_c}{dE} \tag{22}$$

An important difference between α and β is that, while the sum of the symmetry coefficient of the oxidation and reduction reaction (β_{oxi} and β_{red}, respectively) is equal to 1, that does not have to be the case for the transfer coefficient (BARBIR, 2013, p. 36). The more accurate description would be that, if oxidation and reduction directions in an electrode have the same rate-determining steps, Equation 23 applies, where ν is the number of rate-determining steps and n is the number of electrons involved (GUIDELLI et al., 2014, p. 257).

$$\alpha_{oxi} + \alpha_{red} = \frac{n}{\nu} \tag{23}$$

3.3.1 Butler-Volmer Equation

Using all concepts presented before, it is possible to obtain a relation between net current density and activation overvoltage – the Butler-Volmer equation, presented in Equations 24 for the anode and 25 for the cathode (BARBIR, 2013, p. 37) (SPIEGEL, 2008, p. 61-62). A deduction of this equation was made by Dickinson *et* Hinds (2019),

in which special attention was given to each of the used assumptions; thus, it is recommended for a more profound understanding.

$$j_{ano} = j_{0,ano}\left[e^{\left(\frac{\alpha_{oxi,ano}F\eta_{act,ano}}{RT}\right)} - e^{\left(\frac{-\alpha_{red,ano}F\eta_{act,ano}}{RT}\right)}\right] \quad (24)$$

$$j_{cat} = j_{0,cat}\left[e^{\left(\frac{\alpha_{red,cat}F\eta_{act,cat}}{RT}\right)} - e^{\left(\frac{-\alpha_{oxi,cat}F\eta_{act,cat}}{RT}\right)}\right] \quad (25)$$

Note that the activation overpotential (η_{act}) was defined in these equations in a manner that it always has a positive value. Also, due to its complexity, obtaining the value of η_{act} involves solving a nonlinear equation.

While the usage of this equation is common for obtaining the value of η_{act} (NÓBREGA, 2023), the values of the transfer coefficient vary considerably. For example, values used in some models that use the Butler-Volmer equation and values calculated experimentally are presented in Table 2. Note that some values in this table are written with an explicit multiplicative factor. This is due to the fact that many authors define the Butler-Volmer equation with $\alpha \cdot n$ – where n is the number of electrons involved in the half-reaction – instead of just α.

Table 2 - Values of the transfer coefficient in literature.

Authors	Type	$\alpha_{oxi,ano}$	$\alpha_{red,ano}$	$\alpha_{red,cat}$	$\alpha_{oxi,cat}$
Tang *et al.,* (2017)	Model	2 · 0.50	2 · 0.50	2 · 0.40	2 · 0.60
Jiao *et* Li (2009)	Model	2 · 0.50	2 · 0.50	4 · 0.50	4 · 0.50
Futter *et al.* (2018)	Model	2 · 0.50	2 · 0.50	2 · 0.25 and 2 · 0.50	2 · 0.25 and 2 · 0.50
Chaudhary *et al.*, (2014)	Model	0.50	0.50	1	1
Vetter *et* Schumacher (2019)	Model	2 · 0.50	2 · 0.50	2 · 0.50	2 · 0.50
Iranzo *et al.*, (2010)	Experiment	-	-	0.95 and 1.05	-
Zhang *et al.* (2008)	Experiment	-	-	Function of RH and T	-
Shabani (2010)	Experiment	2 · 0.69	2·(1 - 0.69)	4 · 0.33	4·(1 - 0.33)

Source: the author.

Another common difference from Equations 24 and 25 is that some authors consider that the sum of the transfer coefficient in the forward and reverse directions

must equal one. Equation 26 shows this other common formulation of the Butler-Volmer expression, where x can be the cathode or anode (O'HAYRE et al., 2016, p. 90).

$$j_x = j_{0,x}\left[e^{\left(\frac{\alpha_x n_x F \eta_{act,x}}{RT}\right)} - e^{\left(\frac{-(1-\alpha_x) n_x F \eta_{act,x}}{RT}\right)}\right] \quad (26)$$

For this to be valid, according to Equation 23 (GUIDELLI et al., 2014, p. 257), the number of rate-determining steps must be equal to the number of electrons involved in the reaction. However, a more plausible explanation for its usage in literature, as n is written explicitly in this formulation, is the assumption that the transfer coefficient written is actually the symmetry coefficient, β, and that the multiple electron exchange process coefficient α is equal to the product between the number of electrons involved in the process (n_{ano} = 2 and n_{cat} = 4) and β.

Although it may not be initially evident, the Butler-Volmer equation depends on the concentration of the involved species. This dependency is present in the exchange current density's description, as presented before. Further detailing about this will be provided in topic 3.5, as changes in the concentration are intrinsically related to mass transport in a fuel cell.

A final consideration regarding the applicability of the Butler-Volmer equation must be made. Fundamentally, this equation is only exact for a single reversible elementary step, which is neither the case for HOR nor for ORR (RAZDAN; LIN; BHAN, 2023). However, with the usage of adequate transfer coefficients, it is still considered an excellent estimation for multi-step reactions whose rate-determining step is much slower than the others (O'HAYRE et al., 2016, p. 92). Dickinson and Hinds (2019) presented a profound discussion about misconceptions around this equation, in which they argue that, due to the nature of the transfer coefficient, the Butler-Volmer equation is inherently an empirical treatment for the equations involved in a fuel cell, therefore, simpler models – such as the Tafel equation, discussed in the next section – should be prioritized, as they yield approximately the same results, but with fewer parameters to evaluate.

3.3.2 Tafel equation and linear form of the Butler-Volmer equation

The Tafel equation is an empirical relation noted by Tafel that relates overvoltage and current density. It is presented in Equation 27 (PETRII et al., 2007).

$$\eta = a + b \log j \tag{27}$$

This relation predates the Butler-Volmer Equation, however, both can be considered related, as the Tafel equation can be obtained from that equation if one considers that the forward reaction dominates (O'HAYRE et al., 2016, p. 98). To demonstrate this, consider that the current density in the system is significantly larger than the exchange current density, that is, the reaction deviates from the equilibrium, and, thus, η_{act} is also significant. This makes it so that the terms related to the backward reaction – that is, oxidation of oxygen and reduction of hydrogen – are negligible when compared to the other, resulting in Equation 28.

$$j_x = j_{0,x}\left[e^{\left(\frac{\alpha_{fwd,x}F\eta_{act,x}}{RT}\right)}\right] \tag{28}$$

Differently from the Butler-Volmer equation, here one may write an explicit relation for the activation overvoltage in the electrode – Equation 29 – in which the Tafel experimental constants may be related to physical variables. Nevertheless, this relation should be considered carefully, as the transfer coefficient is intrinsically an experimental value that is obtained from the Tafel equation (GUIDELLI et al., 2014b, p. 260).

$$\eta_{act,} = \frac{-RT}{\alpha_x F}\ln j_0 + \frac{RT}{\alpha_x F}\ln j \tag{29}$$

The Tafel equation has fewer parameters to be calculated than the Butler-Volmer equation but is reported to provide precise results if its assumption is respected. Due to this precision and ease of use, it is widely used for calculating η_{act} (NÓBREGA, 2023) and is the recommendation of Dickinson and Hinds (2019) in their review of the Butler-Volmer equation for PEMFC modeling. Figure 9 shows a comparison between the Butler-Volmer and Tafel equations, where it is noticeable that a deviation exists in low overvoltages, but a good fit is reached after these initial values.

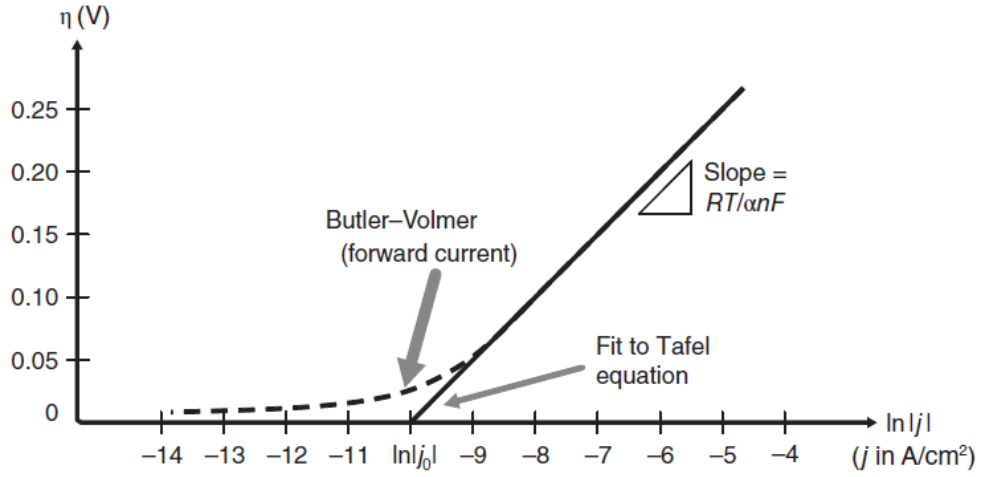

Figure 9 - Comparison Between Tafel and Butler-Volmer equations.
Source: O'HAYRE et al., 2016, p. 98.

As for the case where the j is considerably smaller than j_0, the exponential terms are small. Expanding each exponential in a Taylor series and neglecting the powers higher than one (that is, $e^x \approx 1 + x$ for small x), Equation 30 is obtained.

$$j_x = j_{0,x}\left[\left(1 + \frac{\alpha_{fwd,x} F \eta_{act,x}}{RT}\right) - \left(1 + \frac{-\alpha_{bwd,x} F \eta_{act,x}}{RT}\right)\right] \quad (30)$$

Grouping the terms, Equation 31 is reached, which is the "linear form" of the Butler-Volmer equation presented by Wang (2004) and used by about 41 other works from 1989 to 2018 (DICKINSON; HINDS, 2019).

$$j_x = j_{0,x}\left[(\alpha_{fwd,x} + \alpha_{bwd,x})\left(\frac{F\eta_{act,x}}{RT}\right)\right] \quad (31)$$

As in the Tafel equation, η_{act} can be explicitly written for the system, yielding Equation 32.

$$\eta_{act,x} = \frac{j_x}{j_{0,}} \frac{RT}{(\alpha_{fwd,x} + \alpha_{bwd,x})F} \quad (32)$$

The linear description is commonly used to describe the anode kinetics, as the HOR reaction is much faster than ORR (WANG, 2004), so the activation overvoltage in the anode is expected to be small when compared to the cathode. Therefore, one may use this approximation to avoid the necessity of solving the non-linear Butler-Volmer equation, which could demand a considerable amount of computational time if the model is to be resolved multiple times.

3.3.3 Minimizing activation losses

The previously presented equations for fuel cell kinetics highlight an important characteristic: if more current is demanded from a fuel cell (in other words, more reaction is being done), the activation overvoltage will increase because more energy is required to overcome the activation barrier. As obtaining the maximum amount of power ($V \cdot i$) is desirable, reducing the intensity of this process is essential to attain a high efficiency.

Considering the Butler-Volmer equation (Equations 24 and 25) or its simplification (Equations 29 and 32), an inverse relation can be seen between exchange current density and activation overvoltage. Therefore, considering that this is one of the few parameters that one may vary according to controllable variables, increasing the efficiency of fuel cells involves maximizing j_0. This may be done, as seen in Equation 18, in four main ways: increase the electrode roughness, increase temperature, decrease the activation energy of the reaction, and increase reactant concentration. Each of these alternatives will be discussed in the following paragraphs.

Probably the most intuitive way of accelerating a catalytic reaction is increasing either the catalyst load or the surface area of this catalyst – in other words, raising the electrode roughness (area of catalyst per area of electrode). However, as the catalyst materials are considerably expensive, increasing their usage is not an attractive option, as it is desired to make fuel cells as cheap as possible to permit commercial viability. So, to conciliate both objectives, the catalyst load should be reduced, but with an accompanying development in nanotechnology to enable the available catalytic area to be at least maintained. State-of-art catalysts have a specific area of about 600 – 1000 $cm^2\ mg^{-1}$, while the theoretical limit for platinum is 2400 $cm^2\ mg^{-1}$, that is, a significant margin for improvement still exists (BARBIR, 2013, p. 38).

Another intuitive option is increasing the fuel cell temperature, as it will increase the thermal energy available to the system, making it more likely that reactants will have the energy to reach the activated state (O'HAYRE et al., 2016, p. 96). However, this effect has limited applicability, as the activation energy also increases with temperature, thus, after a certain limit (overvoltage values greater than $\Delta E_{act}/(\alpha F)$), increases in temperature will begin to increase η_{act} (O'HAYRE et al., 2016, p. 99-100). However, as there are other types of overvoltage in a fuel cell, this effect is difficult to

detect, which explains why authors like Song *et al.* (2007) and Santarelli *et* Torchio (2007) report increases in fuel cell performance when increasing the temperature.

Besides the temperature, the activation energy also depends on the catalyst used, thus, choosing a better catalyst can significantly increase the ease with which the reaction occurs. The best catalyst activity is obtained by the usage of elements from the platinum family, as they have a good compromise between bonding and reactivity (O'HAYRE et al., 2016, p. 96). Discussing the candidate materials and the implication of the choice in the system is beyond the scope of this work but is of the utmost importance for the commercial viability of PEMFCs.

Finally, the availability of reactants, that is, their concentration on the reactive surface, has an impact on the exchange current density. Maintaining a high concentration involves ensuring good mass transport in the fuel cell and providing a sufficient amount of fuel to diminish the depletion effects of reactants. This effect is one of the reasons why works such as those presented by Santarelli and Torchio (2007) report an increase in performance with higher operating pressures and why operating a cell with pure oxygen instead of air yields better results (ŠTEKL; KADLEC, 2015). More details about this effect will be discussed in section 3.5 about mass transport, but it should be noted that there is a blurry line between attributing this effect to activation overvoltage or concentration overvoltage (voltage loss due to mass transport effects).

3.4 PEMFC Charge Transport

Fuel cells, due to their electrochemical nature, have to move charges to operate. As every material has an intrinsic resistance to charge transport, this process will result in an efficiency loss, which manifests itself as a voltage loss – the ohmic overvoltage, η_{ohmic} (O'HAYRE et al., 2016, p. 121). Specifically, for a PEMFC, there are two types of charges that need to be transported for the operation: electrons, produced in the anode catalyst layer and transported to the cathode catalyst layer by passing each layer of the electrodes, current collectors, and interconnects; and protons, which have to cross the electrolyte (EG&G TECHNICAL SERVICES INC., 2004, p. 10). Also, there is contact resistance associated with the contact regions between the layers of the fuel cell, which are crossed by the charges during transport (O'HAYRE et al., 2016, p. 127).

The voltage loss caused by these resistances obeys Ohm's law (O'HAYRE et al., 2016, p. 122), thus, a description of the ohmic overpotential can be made by using it. This relation is expressed in Equation 33, where R_{ohmic} is the total electrical resistance of the fuel cell, while R_{e^-} and R_{H^+} are respectively the total resistance to electron and proton transport (NÓBREGA, 2023). Those total resistances are the sum of each contribution, as the resistances in a fuel cell can be considered in series (O'HAYRE et al., 2016, p. 127).

$$\eta_{ohmic} = iR_{ohmic} = i(R_{e^-} + R_{H^+}) \tag{33}$$

A more useful form of writing this equation can be obtained if the concept of current density (j) and area-specific resistance (ASR) are used. This last one is defined as the product of the resistance and area, as presented in Equation 34, which normalizes the value to enable comparisons between fuel cells of different sizes (O'HAYRE et al., 2016, p. 124-125). Using these concepts in Equation 33, Equation 35 is obtained.

$$ASR_{ohmic} = A_{cell}R_{ohm} \tag{34}$$

$$\eta_{ohmic} = jASR_{ohmic} \tag{35}$$

Usually, it is considered that the resistance for proton transport in the electrolyte dominates in the system due to its complexity, so it is reasonable to only consider this resistance for calculating the ohmic overpotential (O'HAYRE et al., 2016, p. 128). However, with the usage of thinner membranes, others such as electronic resistance and protonic resistance in the catalyst layer may become relevant (NÓBREGA, 2023). Therefore, both resistances will be discussed in the following topics, with special attention to the protonic resistance in the electrolyte.

3.4.1 Protonic resistance

Protons are produced in the anode catalyst layer and are transported via the electrolyte to the cathode catalyst layer. Thus, protonic resistance exists both in the catalyst layers and in the electrolytes (NÓBREGA, 2023).

The resistance in the membrane is dependent on the characteristics of the polymer used, more specifically, the concentration of fixed charge sites with opposite charges of the carried ion and the free volume available inside the structure (O'HAYRE et al., 2016, p. 135). In this work, the considered material is Nafion because, as

previously discussed, it is the most common material for electrolytes. This polymer has a conductivity – σ, the inverse of resistance – that is dependent on both water content and temperature (O'HAYRE et al., 2016, p. 139). Most models in the literature use an empirical relation obtained by Springer *et al*. (1991) to describe this dependence (NÓBREGA, 2023). This expression was obtained for Nafion 117 by measuring the conductivities at 30°C for a range of values of λ and using measurements for a specific λ at 30°C and 80°C to obtain the activation energy related to the temperature dependence. Equation 36 presents the relation with conductivity in S·m^{-1}.

$$\sigma(T,\lambda) = (0.5139\lambda - 0.326)e^{\left[1268\left(\frac{1}{303}-\frac{1}{T}\right)\right]} \tag{36}$$

An important remark is that the electrolyte used for gathering data for this model (Nafion 117) is significantly thicker than the current state-of-art, nevertheless, the relations deducted for it are still used. This is not a particularity of this expression: most other equations used in the literature are based on outdated membranes (DICKINSON; SMITH, 2020). Therefore, the lack of available data for state-of-the-art electrolytes can potentially hinder the accuracy of the models for newer fuel cells.

Based on Springer's proposition, Mann *et al*. (2000) used results from other works with Nafion membranes to propose another empirical relation for conductivity (S·m^{-1}), presented in Equation 37. In this case, an explicit relation with the current density is considered.

$$\sigma(T,\lambda,j) = \frac{[\lambda - 0.634 - 3j]e^{\left[4.18\left(\frac{T-303}{T}\right)\right]}}{1.816\left[1 + 0.03j + 0.062\left(\frac{T}{303}\right)^2 j^{2.5}\right]} \tag{37}$$

Another proposition for modeling the protonic conductivity was made by Weber and Newman (2004) based on the percolation theory. In this work, they propose one functional form that is assumed to be valid either in liquid or vapor-equilibrated membranes, as the mechanism of conduction is similar in both cases. The conductivity difference caused by the different phases will arise due to the different values of λ that they provide, therefore, their proposition is also capable of modeling Schroeder's paradox. This relation describes conductivity as a function of the water volume fraction (φ) and temperature, whereas the value rises with volume fraction up to about 45% when it becomes a constant because the channels of the membrane are filled with liquid water. Equation 38 presents the proposed function for protonic conductivity (S/m) in Nafion, and Equation 39 equates the volume fraction of water in the membrane, φ. A demonstration of why φ is described by this equation is presented in Appendix B.

Also, Figure 10 presents a plot of the predicted conductivity at 80°C for Springer's and Weber *et* Newman's models as a function of λ. It is noticeable that Springer's correlation gives higher conductivities for λ up to about 6, then Weber et Newman's model predicts higher values.

$$\sigma(T,\lambda) = \begin{cases} 50(\varphi - 0.06)^{1.5} e^{\left[\frac{15000 J/mol}{R}\left(\frac{1}{303.15} - \frac{1}{T}\right)\right]}, & \varphi \leq 0.45 \\ 50(0.39)^{1.5} e^{\left[\frac{15000 J/mol}{R}\left(\frac{1}{303.15} - \frac{1}{T}\right)\right]}, & \varphi > 0.45 \end{cases} \quad (38)$$

$$\varphi = \frac{\lambda \overline{V}_{H2O}}{\overline{V}_m + \lambda \overline{V}_{H2O}} \quad (39)$$

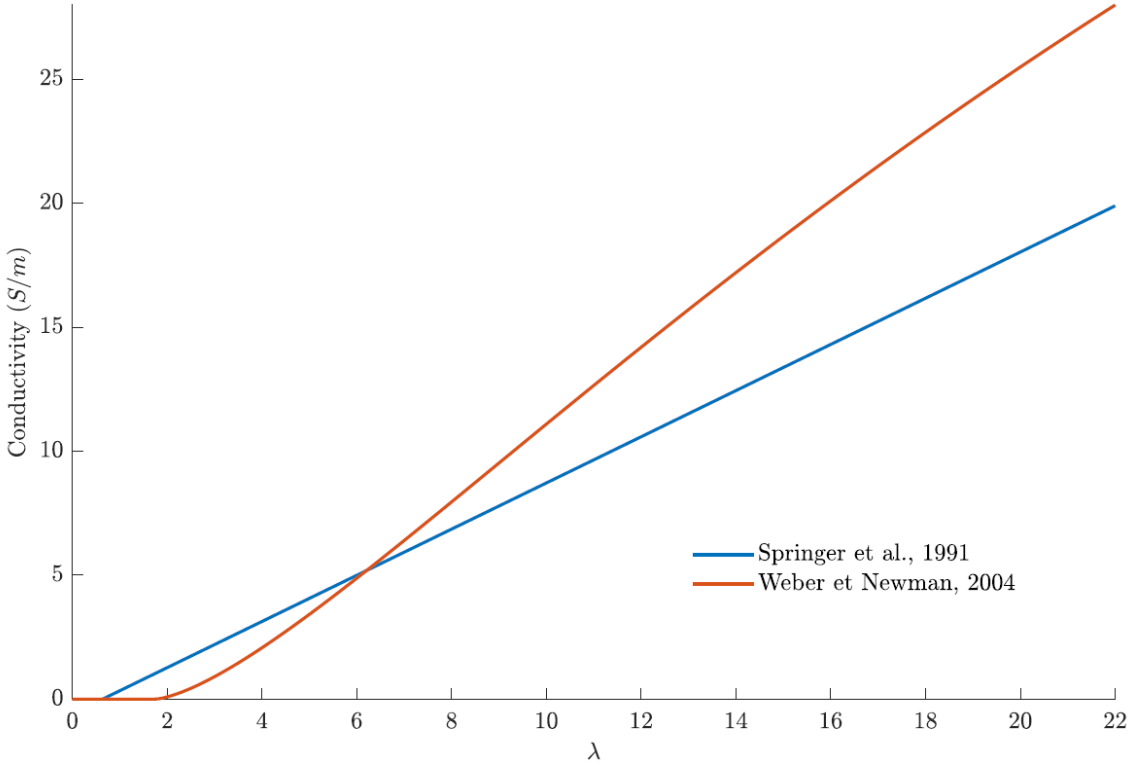

Figure 10 - Comparison between Springer's and Weber et Newman's models for conductivity. Source: The author.

Vetter and Schumacher (2019) used this description in their implementation of a two-phase 1D fuel cell model, with small – but interesting – adjustments. First, instead of (φ - 0.06), they use the maximum value between 0 and (φ - 0.06) to avoid the inconsistency of negative conductivity. Also, the authors add a term – the Bruggeman correction – to account for the different ionomer content in the membrane and catalyst layer, enabling its usage in both layers. Considering these adaptations, Equation 40 is obtained. It should be noted that this equation is not exactly equal to the one presented by Vetter and Schumacher (2019), because they use the reference

temperature at 80ºC instead of 30°C and do not consider that the value is a constant after $\varphi = 0.45$.

$$\sigma(T,\lambda) = \begin{cases} \epsilon_i^{1.5} 50 \max\{(\varphi - 0.06), 0\}^{1.5} e^{\left[\frac{15000 J/mol}{R}\left(\frac{1}{303.15} - \frac{1}{T}\right)\right]}, & \varphi \leq 0.45 \\ \epsilon_i^{1.5} 50 (0.39)^{1.5} e^{\left[\frac{15000 J/mol}{R}\left(\frac{1}{303.15} - \frac{1}{T}\right)\right]}, & \varphi > 0.45 \end{cases} \quad (40)$$

Other authors have also used similar approaches to model the protonic conductivity of the catalyst layers. Both Schröder *et al*. (2021) and Gerteisen *et al.* (2009) used Springer's (1991) conductivity description with the same ionomer fraction on the catalyst layer elevated by 1.5 as the equation to calculate catalyst layer conductivity. Xu *et al*. (2021) proposed that, based on measurements obtained by Makharia *et al.* (2005), in addition to using $\epsilon_i^{1.5}$ in Springer's model, only one-third of the CCL protonic resistance should be considered to calculate the total, as presented in Equation 41. The resistance of the ACL is neglected because the anode reaction is significantly facile (MAKHARIA; MATHIAS; BAKER, 2005).

$$R_{H^+} = R_m + \frac{1}{3} R_{CCL} \quad (41)$$

However, even if the calculation of protonic resistance in the CL only demands a correction factor according to these authors, most models neglect this resistance, only considering the protonic resistance in the membrane (NÓBREGA, 2023).

Therefore, with those descriptions of conductivity, it is possible to calculate ASR by integrating the resistivity along the proton-conducting region. As an example, Equation 42 presents the integral used to calculate protonic ASR in the membrane.

$$ASR_{m,H^+} = \int_0^{t^M} \frac{1}{\sigma(T,\lambda)} dz \quad (42)$$

Note that this integral demands a description of how temperature and λ vary along the analyzed dimension. If the system is isothermal, this integral can be solved by using what is discussed in section 3.5.3 to propose descriptions of a $\lambda(z)$ function, however, if temperatures also vary along the membrane, this phenomenon is coupled with heat transfer, thus, solving an ODE system is needed. There are also other factors that can make the obtention of an analytical $\lambda(z)$ function difficult, which will also be described in section 3.5.3.

3.4.2 Electronic resistance

The total electronic resistance of a fuel cell is calculated by the sum of the resistance of the bipolar plate (R_{BP}) and porous layers (R_{GDL} and R_{CL}), as they are considered in a series association (NÓBREGA, 2023). In other words, this total resistance can be represented by Equation 43.

$$R_{e^-} = R_{CL} + R_{GDL} + R_{BP} \tag{43}$$

The values of those resistances are related to the used material in each layer. Some examples of conductivity for those layers are presented in Table 3 to illustrate the magnitude of those values and the total resistance of an electrode according to those values. The higher value obtained by Bernardi *et* Verbrugge (1992) probably can be explained by the possible inclusion of some contact resistance in the measurement, as highlighted in their article.

Table 3 - Electric conductivities used in the literature.

Reference	$\sigma_{CL}(S/m)$	$\sigma_{GDL}(S/m)$	$\sigma_{BP}(S/m)$	$R_{sum}(\Omega \cdot m)$
Bernardi *et* Verbrugge, 1992	-	-	-	$5.3 \cdot 10^{-2}$
Zhou *et al*., 2014	300	300	20000	$6.72 \cdot 10^{-3}$
Vetter *et* Schumacher, 2019	1250	350	-	$3.66 \cdot 10^{-3}$

Source: the author.

Weber *et al.* (2014), in their review of transport phenomena modeling in PEMFC, affirms that the electrical resistance of the bulk of the thin electrodes is negligible, and the electronic one is mainly influenced by the contact resistances. This resistance is commonly lumped in a fitted parameter (NÓBREGA, 2023), and is represented as a function of the clamping pressure of the fuel cell in some works. Zhou *et al*. (2006) obtained good adjustment of experimental data from other works by using Equation 44, where A, B, and C are empirical parameters, and P is the contact pressure.

$$ASR_{cont.} = A\left(\frac{B}{P}\right)^{C} \tag{44}$$

Analyzing the previous equation, it can be concluded that high pressures decrease the contact resistance, however, it also decrease the porosity of the GDL, which can be a significant hindrance to fuel cell efficiency (ZHOU; WU; MA, 2006). This balance results in the existence of an optimal contact pressure, which will depend

on the bolt torque and gas diffusion layer type (LEE et al., 1999). Understanding this relation can be important because Nitta *et al.* (2008) have reported contact resistances between GDL and CL comparable to the membrane resistances under their experimental conditions.

Moreover, it should be highlighted that the clamping pressure affects many characteristics of the fuel cell. For example, the transport – dependent on the porosity – is affected, so the activation and concentration overvoltages also rely on this value. However, the majority of the reviewed models do not consider the impact of this variable in the model, which hinders their capacity, for example, to describe the impact of the bolt torque in the model.

Finally, relations between contact pressure and electronic conductivity have also been reported in the literature. Hamour *et al*. (2015) fitted Equation 45 to describe the conductivity of GDL made with Quintech carbon cloth, and Equation 46 for a bipolar plate in stainless steel foam. In both equations, P is the applied load ($0 < P < 8$ MPa), and the conductivity is presented in $S \cdot m^{-1}$.

$$\sigma_{GDL} = 10^3 \log(1850P + 49600) \tag{45}$$

$$\sigma_{BP} = 25 \cdot 10^4 \log(51000P + 117000) \tag{46}$$

3.5 PEMFC Mass Transport

A fuel cell demands a constant supply of reactants to be able to produce electricity (BARBIR, 2013, p. 85). Thus, ensuring good mass transport inside it is necessary for their efficiency. As PEMFC performance depends on the concentrations in the catalyst layer, reactant depletion or product accumulation may hinder the operation of the system (O'HAYRE et al., 2016, p. 167).

There are two types of transport, each of which dominates in a region of the fuel cell. In the gas channels, advective transport dictates the system, and in the electrode (GDL and CL), diffusive transport is dominant (O'HAYRE et al., 2016, p. 168). Even though the description of the flow channels is important in fuel cell design, it will not be discussed in this work. Therefore, the following sections will approach the different transports in the electrode and membrane, which include the diffusion of gases in the PEMFC. Liquid water transport, though crucial for fuel cell modeling, will not be

discussed in detail because the developed model assumes that only water vapor exists in the electrodes. Also, the transport of water and protons in the membrane will be discussed, but gas permeation will not, as it is most often neglected in modeling (NÓBREGA, 2023).

3.5.1 Flux balance

A common technique to analyze PEMFC is the usage of a flux balance because it ties all fluxes to the current density, enabling the description of molar fluxes in the fuel cell (O'HAYRE et al., 2016, p. 208). It is the base of the important Springer *et al*. (1991) model, which presented some modeling approaches that are still used (NÓBREGA, 2023).

To describe this balance, the PEMFC represented in Figure 11 will be used. It is considered that the anode is fed with humidified hydrogen and the cathode with humidified air (a mixture of O_2 and N_2).

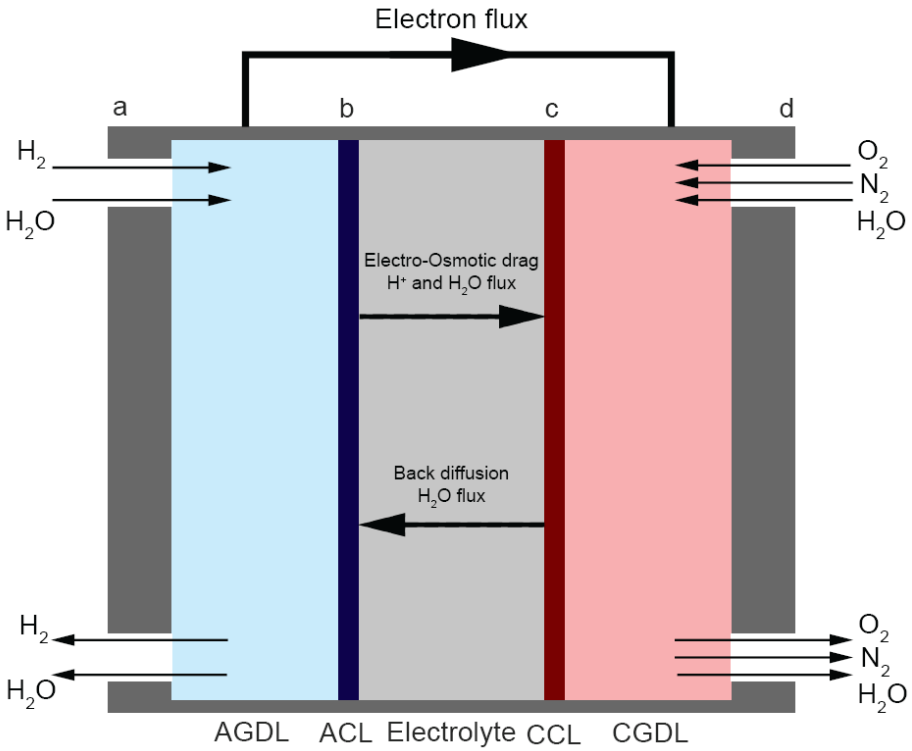

Figure 11 - Fluxes in a PEMFC.
Source: (CARNEIRO et al., 2024).

If the only reactions in this system are the HOR and ORR, the net flux – that is, inlet flux - outlet flux – of every species can be related to the reaction rate, as steady state is assumed. This rate, according to the discussion made in section 3.2, is directly related to the charge flux, as shown in Equation 47. In it, $S_{H_2O}^C$ is the water generated by the reaction in the cathode, which must be equal to the net flux of hydrogen under these conditions due to stoichiometry.

$$J_{e^-} = J_{H_2,in}^A - J_{H_2,out}^A = \frac{J_{H^+,in}^M - J_{H^+,out}^M}{2} = 2\left(J_{O_2,in}^C - J_{O_2,out}^C\right) = S_{H_2O}^C \tag{47}$$

Considering that J_i is the net molar flux of species i, it is possible to write the previous equation as Equation 48.

$$\frac{j}{2F} = J_{H_2}^A = \frac{J_{H^+}^M}{2} = 2J_{O_2}^C = S_{H_2O}^C \tag{48}$$

To describe the water generation term, an unknown α*[2] is defined as a ratio between water flux in the membrane and net hydrogen flux – Equation 49.

$$\alpha^* \equiv \frac{J_{H_2O}^M}{J_{H_2}^A} = \frac{J_{H_2O}^M}{\frac{j}{2F}} \tag{49}$$

Considering the definition of α*, it is possible to write a flux balance for water in a fuel cell and relate it to the current density, as shown in Equation 50.

$$\frac{j}{2F} = \frac{J_{H_2O}^A}{\alpha^*} = \frac{J_{H_2O}^M}{\alpha^*} = \frac{J_{H_2O}^C}{(1+\alpha^*)} \tag{50}$$

Finally, by combining the two balances, Equation 51 is reached, which represents the flux balance for a PEMFC fuel cell in the steady state.

$$\frac{j}{2F} = J_{H_2}^A = \frac{J_{H^+}^M}{2} = 2J_{O_2}^C = \frac{J_{H_2O}^A}{\alpha^*} = \frac{J_{H_2O}^M}{\alpha^*} = \frac{J_{H_2O}^C}{(1+\alpha^*)} \tag{51}$$

3.5.2 Gas transport

Diffusion of gases in the porous layers has a major role in the PEMFC's performance (NÓBREGA, 2023). This is explained by the fact that, among other parameters, the reaction depends on the concentration of reactants in the catalyst layer (O'HAYRE et al., 2016, p. 167). Thus, if the transport is inefficient, the reaction rate will be low and a considerable amount of power will be lost.

[2] The asterisk is used to differentiate this definition from the transfer coefficient, as proposed by O'Hayre *et al*. (2016).

A proposal used by several authors to describe this system is a steady-state Fickian diffusion (NÓBREGA, 2023). In this case, Fick's first law, represented by Equation 52 for 1D transport, is used to describe the molar flux of each species, where D^{eff} is the effective diffusivity of the gas in the system and c is its total concentration.

$$J_i = -cD^{eff}\frac{dx_i}{dz} \tag{52}$$

This expression can be simplified to Equation 53 if the gases are ideal. In it, x_i is the molar fraction of i.

$$J_i = -D^{eff}\left(\frac{P}{RT}\right)\frac{dx_i}{dz} \tag{53}$$

The previously developed flux balance can be used to describe the molar fluxes of all species in the system, thus, using Fick's law in association with them can provide concentration profiles for the gases (H_2 and O_2) in the system. Water can also be described using this method if it is only present as vapor, however, if two phases exist, the diffusive flux for liquid and gases must be considered separately. This direct approach was used by O'Hayre *et al.* (2016, p. 203-237) in their development of a simple model. The concentration profile is obtained by integrating the resulting expressions between the concentration value in the bulk (considered equal to the inlet value) and at an arbitrary position z.

A more general proposition, if steady-state Fickian diffusion is assumed, is the usage of the continuity equation for every species in the fuel cell, which was done by Vetter *et* Schumacher (2019) and Yuan *et al.* (2021). This formulation is described by Equation 54 for a generic species i.

$$\nabla \cdot J_i = S_i \tag{54}$$

Note that a source term (S) is needed for every species, as molar quantities change as a consequence of the reaction. Naturally, they are described as a function of the current density, as it is directly related to the reaction rate. By using this description along with Fick's law, it is possible to evaluate systems whose properties vary along the analyzed direction, such as non-isothermal systems. This will result in a system of coupled ODEs for 1D models, which will need to be solved.

Even though Fickian diffusion is considerably used in models and, according to the work of Lindstrom and Wetton (2017), provides good results for the diffusion in the cathode when air is used as an oxidant, it is a model for binary diffusion and may not represent well all systems. In low densities, the Stefan-Maxwell model can be used to describe the multi-component diffusion, which may be useful considering that more

than one species diffuses in each electrode. This model is presented in Equation 55, where C is the total concentration of the system ($PR^{-1}T^{-1}$ for ideal gases) (GLASGOW, 2010, p. 189-190) (BENÍTEZ, 2009, p. 14-15).

$$\frac{dx_i}{dz} = \sum_{\substack{j=1 \\ j \neq i}}^{n} \frac{x_i J_j - x_j J_i}{C \cdot D_{i,j}^{eff}} \tag{55}$$

Differently from the Fickian case, here, the molar fractions are written as a function of the fluxes, not the inverse. This description is also present in models, such as the seminal work by Springer *et al.* (1991), where the flux balance was used to write the relations between the concentrations and current density.

Regardless if Stefan-Maxwell or Fickian diffusion is used, describing the effective diffusion coefficient in the fuel cell condition is necessary. This was done differently by many authors. A commonly used description for the binary coefficients is the usage of a relation developed by Slattery and Bird (1958) based on the kinetic theory. It is shown in Equation 56.

$$\frac{pD_{AB}}{(p_{cA}p_{cB})^{1/3}(T_{cA}T_{cB})^{5/12}\left(\frac{1}{M_A}+\frac{1}{M_B}\right)^{1/2}} = a\left(\frac{T}{\sqrt{T_{cA}T_{cB}}}\right)^{b} \tag{56}$$

Here, D_{AB} is the binary diffusion coefficient ($cm^2 \cdot s^{-1}$), p is the pressure (atm), M is the molecular weight ($g\ mol^{-1}$), and the subscript c indicates the critical value of the property. For nonpolar gas pairs, except helium and hydrogen, $a = 2.745 \cdot 10^{-4}$ and $b = 1.823$, while for a pair of nonpolar gas and water $a = 3.640 \cdot 10^{-4}$ and $b = 2.334$ (BIRD; STEWART; LIGHTFOOT, 2002, p. 521). This equation was used in Springer *et al.* (1991), for example. Another relation used to calculate binary diffusion coefficients is the one proposed in the Chapman-Enskog kinetic theory. It describes the diffusion coefficient ($m^2 \cdot s^{-1}$) for an ideal gas by Equation 57, where σ_{AB} is the collision diameter (m), T is the temperature (K), P is the pressure (Pa), Ω_D is the dimensionless collisional integral, and MM is the molecular mass ($g \cdot mol^{-1}$) (BIRD; STEWART; LIGHTFOOT, 2002, p. 526).

$$D_{AB} = \frac{1.8583 \cdot 10^{-27} T^{3/2}}{\left(\frac{P}{101325}\right)\sigma_{AB}^2 \Omega_D}\left(\frac{1}{MM_A}+\frac{1}{MM_B}\right)^{\frac{1}{2}} \tag{57}$$

These binary diffusion coefficients may be used in the anode (H_2 and H_2O) and in the calculations involving the Stefan-Maxwell model, nevertheless, for Fickian descriptions of the Cathode, a diffusion coefficient for the species in the mixture should be used. In this case, usually, Equation 58 is used, where the relations with

temperature and pressure predicted by the Chapman-Enskog model are used along with a reference value for the diffusion coefficient. This was used in the works of Vetter *et* Schumacher (2019), Lazar *et al.* (2019), and Berasategi *et al,* (2024), for example.

$$D_{AB} = D_{AB,ref}\left(\frac{T}{T_{ref}}\right)^{1.5}\left(\frac{P_{ref}}{P}\right) \tag{58}$$

The reference values used in the work of Vetter *et* Schumacher (2019) are presented in Table 4, for a T_{ref} of 353.15 K and P_{ref} equal to 101325 Pa. Note that they define those values for air, instead of N_2 and O_2 separately in the cathode. This enables the usage of the simpler Fickian model, however, losses in flexibility, as the description is only valid if the proportion of N_2 and O_2 is equal to the one in air.

Table 4 - Reference values for diffusion coefficients.

System	Value (m^2/s)
H_2 in water vapor	$1.24 \cdot 10^{-4}$
O_2 in air	$0.28 \cdot 10^{-4}$
$H_2O(g)$ in H_2	$1.24 \cdot 10^{-4}$
$H_2O(g)$ in air	$0.36 \cdot 10^{-4}$

Source: VETTER; SCHUMACHER, 2019a.

Another type of diffusion that can be important in the catalyst layer and microporous layer is the Knudsen diffusion (NÓBREGA, 2023). In this type of diffusion, the molecules collide more frequently with the pore's walls than with other molecules (Cussler, 2009), thus it is especially relevant when larger molecules pass through small pores. The Knudsen diffusivity can be obtained by Equation 59, where d is the pore diameter and M_i is the molar mass of species i (WEBER et al., 2014).

$$D_{K,A} = \left(\frac{d}{3}\right)\left(\frac{8RT}{\pi M_i}\right)^{\frac{1}{2}} \tag{59}$$

The Knudsen diffusivity is a parallel resistance to the diffusivity of one species in the mixture, thus, the global diffusion coefficient can be calculated by Equation 60.

$$D_{A,global} = \left(\frac{1}{D_{AB}} + \frac{1}{D_{K,A}}\right)^{-1} \tag{60}$$

Finally, a correction should be made in the diffusion coefficient to consider the characteristics of the diffusion medium. This microstructure influence may be represented by a dimensionless M-factor, which is a function of the material's porosity (ε) and tortuosity (τ) (ANDERSSON et al., 2016). The porosity is defined as the pore

volume divided by the total volume (BIRD; STEWART; LIGHTFOOT, 2002, p. 149), while the tortuosity represents the additional diffusion length related to the tortuous nature of the pores (MILLS; COIMBRA, 2015, p. 811). This M-factor is represented in a generalized form by Equation 61, where n and m are empirical constants (ANDERSSON et al., 2016). Table 5 presents values used in some works for n and m.

$$M = \frac{\varepsilon^n}{\tau^m} \tag{61}$$

Table 5 - Values for n and m in the literature.

Reference	Medium	n	m
Bernardi et Verbrugge, 1992	Electrode	1.5	-
Andersson *et al*., 2016	Carbon paper	3.6	-
Vetter *et* Schumacher, 2019a	GDL and CL	1	2
Berasategi et al, 2023	Electrode	1	2

Source: the author.

Another possibility to calculate a correction is Equation 62, derived from the percolation theory (WEBER et al., 2014).

$$M = \left(\frac{\varepsilon - \varepsilon_p}{1 - \varepsilon_p}\right)^{\alpha} \tag{62}$$

Here, ε_p is the percolation threshold and α is an empirical constant. Table 6 shows values for both of those variables found in the literature.

Table 6 - Values for percolation threshold and α in different works.

Reference	Medium	ε_p	α
Tomadakis *et* Sotirchos, 1993	1D Fiber structure	0.33	0.707
	2D Fiber structure	0.11	0.785
Zamel *et* Li, 2013	Carbon paper	0.11	0.785
Chaudhary *et al*., 2014	Electrode	0.11	0.785

Source: the author.

Also, a correction is made to consider the liquid water saturation, that is, the fraction of space in the pore filled by liquid water (s). The correction factor is commonly made by Equation 63, where n is an empirical constant. Some values for this constant are presented in Table 7.

$$M_s = (1 - s)^n \tag{63}$$

Table 7 - Values for the constant in water saturation correction.

Reference	Medium	n
Zamel *et* Li, 2013	Carbon paper	2
Chaudhary et al., 2014	Electrode	1.5
Vetter *et* Schumacher, 2019	GDL and CL	3
Vetter et Schumacher, 2019b	GDL	3
	CL	1.5
Berasategi *et al*., 2024	Electrode	3

Source: the author.

As some water is immobile in the GDL pores, the effective value of s is smaller than the total liquid water saturation (ANDERSSON et al., 2016). To consider this effect, the effective saturation (s_{eff}), given by Equation 64, can be used, where s_{im} is the immobile water saturation (NÓBREGA, 2023) (ANDERSSON et al., 2016).

$$s_{eff} = \begin{cases} \dfrac{s - s_{im}}{1 - s_{im}}, & s_{im} < s \leq 1 \\ 0, & s = s_{im} \end{cases} \tag{64}$$

Considering these corrections, the effective diffusivity of the gas in a medium can be calculated from Equation 65. Note that M can be obtained by Equation 61 or 62, according to what is considered more accurate.

$$D_{AB}^{eff} = M \cdot M_s \cdot D_{AB} \tag{65}$$

3.5.2.1 Depletion effects

Even though advection in the gas channels is not discussed in this work, to accurately describe the diffusion in the fuel cell, the bulk concentration of each species must be known, as it is used when modeling the electrode's diffusion. If an infinite supply of fuel and air is assumed, this bulk value will be equal to the inlet value, as the amount consumed by the reaction is insignificant when compared to the fed quantity (O'HAYRE et al., 2016, p. 224). However, if this is not the case, the bulk concentration will be lower than the inlet, resulting in a less effective cell.

To consider these gas depletion effects, it is useful to define the stoichiometric number (λ). This value is the ratio between the inlet flux of a species and the amount of this species that is consumed in the reaction (O'HAYRE et al., 2016, p. 226). Therefore, for a PEMFC fuel cell, the stoichiometric numbers for hydrogen and oxygen are defined as Equation 66 and 67, respectively.

$$\lambda_{H_2} = \frac{J_{H_2,inlet}}{J^A_{H_2}} \tag{66}$$

$$\lambda_{O_2} = \frac{J_{O_2,inlet}}{J^C_{O_2}} \tag{67}$$

Using these definitions, it is possible to relate the inlet flux with the net flux of reactants in a fuel cell. Other important relations are obtained if a perfect mixture is assumed in the bulk, that is, the outlet value is equal to the bulk value. Considering this, Equations 68 can be written, where i is any of the present species and E is either anode (A) or cathode (C).

$$x_{i,bulk} = \frac{J^E_{i,outlet}}{\sum_{j=1}^{n} J^E_{i,outlet}} \tag{68}$$

Knowing that the outlet flux of a species is equal to the inlet flux minus the consumed or generated amount, it is possible to deduce expressions for bulk concentrations as a function of the stoichiometric numbers and net fluxes. If the flux balance presented in section 3.5.1 is used, Equations 69 to 72 can be obtained (SPRINGER; ZAWODZINSKI; GOTTESFELD, 1991). Here, the same notation used in section 3.5.1 is used, that is, “a” is the anode bulk, and “d” is the cathode bulk. Also, “dry” denotes the value of the molar fraction on a dry basis.

$$x^A_{H_2O,a} = \frac{\lambda_{H_2} x^A_{H_2O,in} - \alpha^*\left(1 - x^A_{H_2O,in}\right)}{x^A_{H_2O,in} - \alpha^*\left(1 - x^A_{H_2O,in}\right) + \lambda_{H_2} - 1} \tag{69}$$

$$x^A_{H_2,a} = 1 - x^A_{H_2O,a} \tag{70}$$

$$x^C_{H_2O,d} = \frac{\left(\lambda_{O_2} x^C_{H_2O,in}\right) + 2(1+\alpha^*)\left(1 - x^C_{H_2O,in}\right)x^C_{O_2,dry,in}}{\lambda_{O_2} + (2\alpha^* + 1)\left(1 - x^C_{H_2O,in}\right)x^C_{O_2,dry,in}} \tag{71}$$

$$x^C_{O_2,d} = \frac{\left(\lambda_{O_2} - 1\right)\left(1 - x^C_{H_2O,in}\right)x^C_{O_2,dry,in}}{\lambda_{O_2} + (2\alpha^* + 1)\left(1 - x^C_{H_2O,in}\right)x^C_{O_2,dry,in}} \tag{72}$$

By using these equations, it is possible to obtain the actual bulk values in the electrode, which should be used in the diffusion calculations.

3.5.3 Water transport in the membrane

Membrane transport properties are strongly dependent on water content (WEBER; NEWMAN, 2004a), therefore, modeling its value (λ) inside the membrane is important for an accurate description of the fuel cell. To do this, it is necessary to know both the λ value at the membrane boundaries when exposed to the system inlet and how this water will be transferred inside the membrane. This enables the description

of the water content through the membrane, which is necessary for evaluating its properties, such as the protonic conductivity discussed in section 3.4.1.

3.5.3.1 Sorption isotherms

The description of the water content at the boundaries is made by using the equilibrium value, represented by a sorption isotherm that relates λ to the water activity (a_{H_2O}) on the membrane (DICKINSON; SMITH, 2020). The isotherm varies if the membrane is in equilibrium with water vapor (vapor-equilibrated, VE) or with liquid water (liquid-equilibrated, LE), even if the water activity is the same. This phenomenon is the previously mentioned Schroeder's paradox (DICKINSON; SMITH, 2020).

In order to express the isotherm for VE conditions, the activity of water activity is approximated by the ratio between water's partial pressure and its saturation pressure, that is, the relative humidity (O'HAYRE et al., 2016, p. 138). This relation is presented in Equation 73.

$$a_{H_2O} = \frac{p_{H_2O}}{p_{sat,H_2O}(T)} = \frac{x_{H_2O}P}{p_{sat,H_2O}(T)} \tag{73}$$

To describe the saturation pressure relation with temperature, it is possible to use the Antoine equation, presented in Equation 74. The constants (A, B, and C) are dependent on the temperature interval evaluated. Table 8 presents values for these constants available in NIST's online database (LINSTROM; WILLIAM, 2003).

$$p_{sat,H_2O}(T) = e^{\left[A - \frac{B}{(T+C)}\right]} \tag{74}$$

Table 8 - NIST data for water's Antoine equation.

Temperature (K)	A	B	C
379 – 573	3.55959	643.748	-198.043
273 – 303	5.40221	1838.675	-31.737
304 – 333	5.20389	1733.926	-39.485
334 – 363	5.0768	1659.793	-45.854
344 – 373	5.08354	1663.125	-45.622
293 – 343	6.20963	2354.731	7.559

255.9 – 373	4.6543	1435.264	-64.848

Source: LINSTROM; WILLIAM, 2003.

In LE conditions, it is typical to use a pseudo-two-phase description where the activity range is extended above 1 while extending the isotherm to fit values for liquid water, which permits the description of Schroeder's paradox (DICKINSON; SMITH, 2020). More rigorous approaches can be obtained by using two-phase models that have a specific equation for both VE and LE conditions.

The sorption isotherm that is most common in the literature is the one proposed by Springer *et al*. (1991) based on empirical data for Nafion 117 at 30°C (DICKINSON; SMITH, 2020). This relation – Equation 75 – used the extension of the activity range that was described in the last paragraph.

$$\lambda_{eq} = \begin{cases} 0.043 + 17.81a_{H_2O} - 39.85a_{H_2O}^2 + 36.0a_{H_2O}^3, & 0 \leq a_{H_2O} < 1 \\ 14 + 1.4(a_{H_2O} - 1), & 1 \leq a_{H_2O} < 3 \end{cases} \quad (75)$$

Despite this relationship being constructed for 30°C, as most data suggest that the temperature dependence is weak up to 90°C, its usage in the higher real operating conditions of PEMFCs is common (DICKINSON; SMITH, 2020).

Hinatsu *et al*. (1994), when evaluating Nafion 117 and 125 membranes at 80°C, concluded that both can be reasonably described by Equation 76. Note that this fit is only valid for VE systems.

$$\lambda_{eq} = 0.300 + 10.8a_{H_2O} - 16.0a_{H_2O}^2 + 14.1a_{H_2O}^3, 0 \leq a_{H_2O} < 1 \quad (76)$$

Kulikovsky (2003) proposed an isotherm based on the data of Hinatsu *et al*. (1994), but using the extension of activities to describe LE values. Their result is presented in Equation 77.

$$\lambda_{eq} = 0.3 + 6a_{H_2O}\left[1 - \tanh\left(a_{H_2O} - 0.5\right)\right] + 3.9\sqrt{a_{H_2O}}\left[1 + tanh\left(\frac{a_{H_2O} - 0.89}{0.23}\right)\right] \quad (77)$$

These empirical relations are specific to a certain membrane, thus, Dickinson and Smith (2020) advise that they should be used with caution even for other materials in the Nafion family.

In the literature, there are also propositions of isotherms based on the fundamental properties of the membrane (DICKINSON; SMITH, 2020). One example is the Meyers-Newman model (2002), which was adapted to better fit experimental data with empirical corrections by Weber and Newman (2004). For VE Nafion, this model can be described by Equations 78, which have to be simultaneously solved, Equations 79, which describes the coefficients, and data from Table 9. In those

equations, $\lambda_{H_3O^+}$ is the ratio between moles of hydronium and moles of sulfonic sites, and is the other variable calculated while solving Equations 78.

$$a_{H_2O} = K_2\left(\lambda_{eq} - \lambda_{H_3O^+}\right)e^{\left(\phi_2\lambda_{H_3O^+}\right)}e^{(\phi_3\lambda_{eq})} \tag{78a}$$

$$\frac{\lambda_{H_3O^+}}{(1-\lambda_{H_3O^+})(\lambda_{eq}-\lambda_{H_3O^+})}e^{\left(\phi_1\lambda_{H_3O^+}\right)}e^{(\phi_2\lambda_{eq})} = K_1 \tag{78b}$$

$$\phi_1 = \frac{2}{EW}\left(E^*_{0,0} - 2E^*_{H_3O^+,H^+} - 2E^*_{0,H_3O^+}\right) \tag{79a}$$

$$\phi_2 = \frac{2}{EW}\left(E^*_{0,H_3O^+} - 2E^*_{0,0}\right) \tag{79b}$$

$$\phi_3 = \frac{2}{EW}E^*_{0,0} \tag{79c}$$

$$K_2 = 0.217e^{\left[\frac{1000J/mol}{R}\left(\frac{1}{303.15K}-\frac{1}{T}\right)\right]} \tag{79d}$$

Table 9 - Parameters for Nafion to the Meyers-Newman isotherm.

Coefficient	Value
K_1	100
$E^*_{0,0}$	-0.0417 kg mol^{-1}
E^*_{0,H_3O^+}	-0.052 kg mol^{-1}
$E^*_{H_3O^+,H^+}$	-3.7216 kg mol^{-1}

Source: (WEBER; NEWMAN, 2004a).

Another equation that must be used in this model is an empirical correction proposed by Weber and Newman (2004) to ensure accurate prediction at very low activity. This is presented in Equation 80.

$$\lambda_{eq,adjusted} = \lambda_{eq}\left(1 + e^{(0.3-\lambda_{eq})}\right) \tag{80}$$

To illustrate the discussed isotherms, Figure 12 presents them in a plot. Note that most curves present a similar profile, but Springer's result deviates the most from the others. This may indicate that using values measured at low temperatures is impactful in the result, even if the temperature dependence is weak. Several other relations for sorption isotherms are presented in the work of Vetter and Schumacher (2019b).

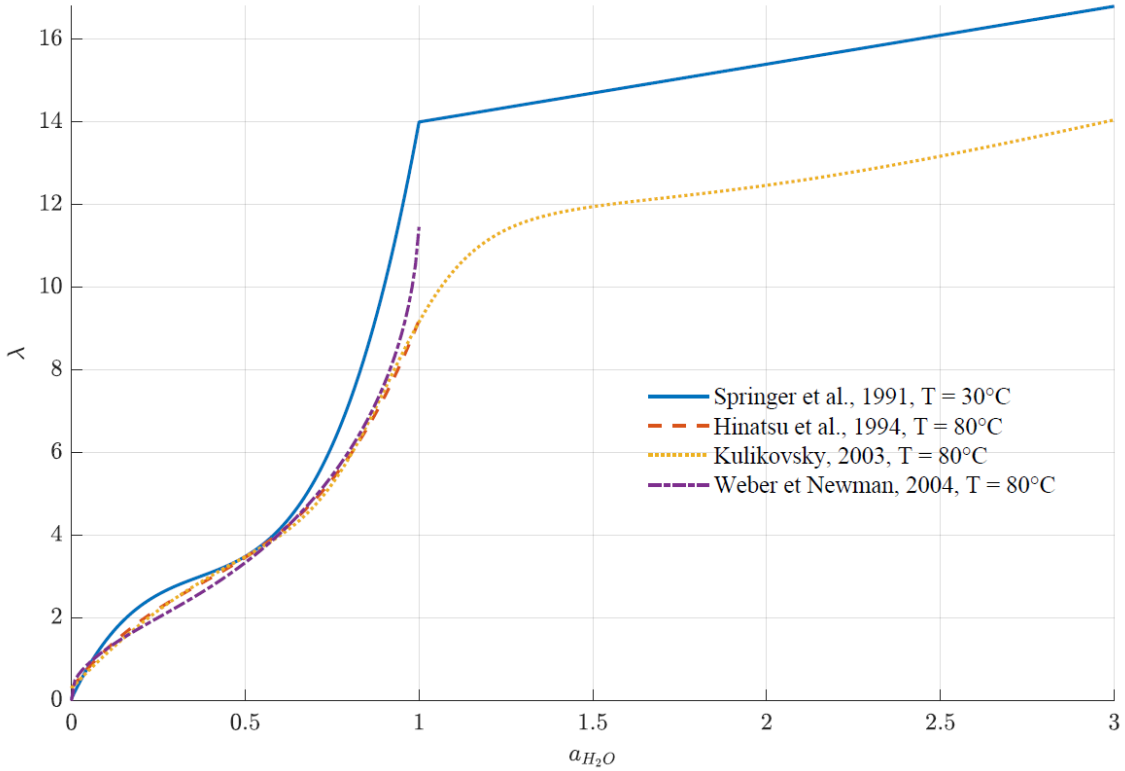

Figure 12 - Plot of the sorption isotherms.
Source: The author.

Another factor that affects the water content in a membrane is compression, as described by Weber and Newman (2004b). In their work, these authors showed that constraining causes the water content of the membrane to decrease and increases the back-flux of water. Nevertheless, even if most membranes operate constrained – that is, they cannot freely swell – this effect will not be considered in this work.

3.5.3.2 Water transport inside the membrane

Inside the membrane, there are four basic water transport mechanisms: back diffusion, electro-osmotic drag, hydraulic permeation, and thermo osmosis flux (UDDIN; SAHA; OSHIMA, 2014). Among these mechanisms, electro-osmotic drag and back diffusion are considered the most impactful (YUAN et al., 2021); thus, only they are addressed in this work.

Electro-osmotic drag is the water transport caused by proton movement, as they are transported in $(H_2O)_nH^+$ clusters (ABDEREZZAK, 2018, p. 107). This transport happens from the anode to the cathode, because they follow the proton flow (UDDIN;

SAHA; OSHIMA, 2014). The number of water molecules carried by a proton in the absence of a concentration gradient is defined as the electro-osmotic drag coefficient, ξ (WEBER; NEWMAN, 2004a).

The other important phenomenon is back diffusion, which is the diffusive movement of water molecules caused by a concentration gradient (UDDIN; SAHA; OSHIMA, 2014). In this case, the direction is from cathode to anode because the concentration in the cathode tends to be significantly higher due to the reaction and electro-osmotic drag (O'HAYRE et al., 2016, p. 141).

To conciliate both mechanisms, some models have been proposed in the literature. Among the most used is the one established by Springer *et al*. (1991) (DICKINSON; SMITH, 2020). In it, they use the concept of electro-osmotic drag coefficient to write the flux of water caused by electro-osmotic drag as presented in Equation 81.

$$J_{H_2O,drag} = \xi J_{H^+} \tag{81}$$

If the developed flux balance in section 3.5.1 is used, Equation 82 can be reached, which expresses the electro-osmotic drag in the function of its coefficient and current density.

$$J_{H_2O,drag} = \xi \frac{j}{F} \tag{82}$$

Then, to describe back diffusion, Fickian diffusion is assumed, resulting in Equation 83.

$$J_{H_2O,BD} = -D_{H_2O} \nabla c_{H_2O} \tag{83}$$

To relate this equation to λ and eliminate the necessity of tracking the membrane swelling in the model, Springer *et al.* (1991) defined the corrected diffusion coefficient D_λ and used a new coordinate, z, which is fixed to the dry membrane. Using these concepts and considering a 1D model in the z-direction, Equation 84 is obtained.

$$J_{H_2O,BD} = -D_\lambda \left(\frac{\rho_{m,dry}}{EW}\right) \frac{\mathrm{d}\lambda}{dz} \tag{84}$$

Adding both of the contributions, it is possible to obtain Springer's proposition for describing water flux in the membrane, Equation 85.

$$J^M_{H_2O} = \xi \frac{j}{F} - D_\lambda \left(\frac{\rho_{m,dry}}{EW}\right) \frac{\mathrm{d}\lambda}{dz} \tag{85}$$

Using the flux balance to describe the water flux, Equation 86 is reached, which describes the water content at each point across the membrane. Its usage, however, is not direct, as α^* is unknown. In their article, Springer *et al*. (1991) obtained its value

by using an iterative solution involving this equation, their description of ξ and D_λ, a sorption isotherm, and the concentrations after depletion effects.

$$\frac{\mathrm{d}\lambda}{dz} = (2\xi - \alpha^*)\frac{EW}{2F\rho_{m,dry}D_\lambda}j \tag{86}$$

To complete the system's description, it is necessary to describe both ξ and D_λ, as both are dependent on the water content λ (O'HAYRE et al., 2016, p. 140-141). Considering first the electro-osmotic drag coefficient, Springer *et al*. (1991) proposed the usage of a linear relation between λ and ξ, which goes from 0 (completely dry membrane) to 2.5 (the value they measured for a fully hydrated membrane at 30°C). This relation is presented in Equation 87.

$$\xi = 2.5\frac{\lambda}{22} \tag{87}$$

Even though the previous relation is still commonly used in models, later works indicate that VE membranes are better described by $\xi = 1$ (VETTER; SCHUMACHER, 2019b). Weber and Newman (2004a), for example, propose the usage of Equation 88 for VE membranes.

$$\xi = \min\{\lambda, 1\} \tag{88}$$

To account for both VE and LE conditions, Meier and Eigenberger (2004) used a polynomial fit, shown in Equation 89.

$$\xi = 1 + 0.028\lambda + 0.0026\lambda^2 \tag{89}$$

Another proposition to consider VE and LE conditions used in the literature is the usage of piecewise linear functions that have the form presented in Equation 90, where λ_{VE} is the value of λ for a VE membrane at water activity equal to 1 and ξ_l is the value at LE conditions (VETTER; SCHUMACHER, 2019b).

$$\xi = \begin{cases} \lambda, & 0 \le \lambda < 1 \\ 1, & 1 \le \lambda \le \lambda_{VE} \\ 1 + (\xi_l - 1)\dfrac{\lambda - \lambda_{VE}}{\lambda_{LE} - \lambda_{VE}}, & \lambda_{VE} < \lambda \le \lambda_{LE} \end{cases} \tag{90}$$

Regarding the temperature correction for ξ, Weber and Newman (2004a) assumed that it is independent of T for VE conditions, but in LE membranes, they fitted the Arrhenius dependence on temperature presented in Equation 91.

$$\xi_l = 2.55e^{\left[\frac{4000}{R}\left(\frac{1}{303.15} - \frac{1}{T}\right)\right]} \tag{91}$$

More relations for these coefficients can be found in Vetter and Schumacher's work (2019b), where they argue that a conclusive and reliable correlation between ξ, λ, and T still does not exist.

As for the description of D_λ, the original proposal by Springer *et al.* (1991) was the usage of Equation 92a. However, it is now considered obsolete, as it was reported incompletely (DICKINSON; SMITH, 2020). The fit of the values below 4 based on Springer's data was provided as a piecewise function proposed by Mazumder (2005) and is presented in Equation 92b.

$$D_\lambda(\lambda,T) = (2.563 - 0.33\lambda + 0.0264\lambda^2 - 0.000671\lambda^3)10^{-10}e^{\left[2416\left(\frac{1}{303}-\frac{1}{T}\right)\right]}, \qquad \lambda > 4 \tag{92a}$$

$$D_\lambda(\lambda,T) = \begin{cases} 1\cdot 10^{-10}e^{\left[2416\left(\frac{1}{303}-\frac{1}{T}\right)\right]}, & 2 \le \lambda \\ [1+2(\lambda-2)]10^{-10}e^{\left[2416\left(\frac{1}{303}-\frac{1}{T}\right)\right]}, & 2 < \lambda \le 3 \\ [3-1.38(\lambda-3)]10^{-10}e^{\left[2416\left(\frac{1}{303}-\frac{1}{T}\right)\right]}, & 3 < \lambda \le 4 \end{cases} \tag{92b}$$

Another parametrization was proposed by Motupally *et al.* (2000) and is shown in Equation 93. It is considered a refinement of Springer's previous proposition (DICKINSON; SMITH, 2020).

$$D_\lambda(\lambda,T) = \begin{cases} 3.1\cdot 10^{-7}\lambda\left(-1+e^{0.28\lambda}\right)e^{\left(\frac{-2436}{T}\right)}, & \lambda < 3 \\ 4.17\cdot 10^{-8}\left(1+161e^{-\lambda}\right)e^{\left(\frac{-2436}{T}\right)}, & 3 \le \lambda < 17 \end{cases} \tag{93}$$

Finally, Vetter *et* Schumacher (2019a) proposed a continuous polynomial fit that includes different types of Nafion, presented in Equation 94. It also includes the Bruggeman correction to enable the usage of the equation in the catalyst layer. Other work by those authors (VETTER; SCHUMACHER, 2019b) compiles other models for diffusivity present in the literature.

$$D_\lambda(\lambda,T) = {\epsilon_i}^{1.5}\frac{3.842\lambda^3 - 32.03\lambda^2 + 67.74\lambda}{\lambda^3 - 2.115\lambda^2 - 33.013\lambda + 101.37}10^{-10}e^{\left[\frac{20000}{R}\left(\frac{1}{353.15}-\frac{1}{T}\right)\right]} \tag{94}$$

3.5.4 Liquid water transport in the electrodes

Considering that PEMFCs operate at low temperatures, produce water as a product, and are fed with humidified gases, liquid water is expected to exist inside the electrodes. Describing this two-phase water flow is an area of active research (O'HAYRE et al., 2016, p. 212), and it is critical for the water management of fuel cells (NÓBREGA, 2023).

Due to the complexity of describing this transport, some authors make hypotheses in their model for avoiding it (NÓBREGA, 2023). For example, Liso *et al.* (2016) proposed that liquid water was present as finely dispersed droplets, such that

no distinction is made between liquid and gas. Nevertheless, this hypothesis is only reasonable, as highlighted by the authors, if the amount of excess water is small.

Regarding the description of the two-phase flow, the most used equation is Darcy's law (NÓBREGA, 2023). Using it, the liquid water flux can be written as Equation 95 (VETTER; SCHUMACHER, 2019a).

$$J_s = -\left(\frac{\rho_{H_2O} k^{eff}}{\mu_{H_2O} MM_{H_2O}}\right) \frac{\partial p_c}{\partial s} \nabla s \tag{95}$$

Here, ρ_{H_2O} is liquid water density, μ_{H_2O} the water viscosity, MM_{H_2O} its molar mass, k^{eff} is the effective permeability, s is the liquid water saturation and p_c is the capillary pressure. This final parameter is defined as the pressure difference between two immiscible fluids that are in equilibrium in a pore space (SPIEGEL, 2008, p. 201). In some works, the effective liquid water saturation described in section 3.5.2 (s_{eff}) is used instead of s (NÓBREGA, 2023).

As liquid water is not considered in the analysis developed in this work, further discussion about important topics – such as the description of capillary pressure as a function of s – is not presented. For this specific topic, the review by Si *et al.* (2015) is recommended.

3.5.5 Concentration overvoltage

After describing the mass transport in a fuel cell, it is possible to calculate the overvoltage associated with its limitations – the concentration overvoltage (η_{conc}). In models that calculate the concentration through the fuel cell, this overpotential is already accounted for by the usage of the concentration of each species in the catalyst layer, along with an adequate description of thermodynamic potential and activation overvoltage (NÓBREGA, 2023). Examples of models that use this direct approach are the ones proposed by Goshtasbi *et al*. (2020) and Vetter *et* Schumacher (2019a). However, when the effects of transport are not directly considered – which is the most common approach – a specific parametrization should be used to make this description (NÓBREGA, 2023).

This description is usually made by considering the difference caused by not using the CL concentration in the thermodynamic potential and activation overvoltage (whose concentration dependence is present in the exchange current density).

Considering both of those contributions, a common parametrization used for calculating the overvoltage is presented in Equation 96, where x is either the anode or cathode, present in O'Hayre *et al.* (2016, p. 178), Spiegel (2008, p. 113) and used in the model by Schröder *et al.* (2021). Here, the equation is presented slightly different from the ones proposed by those sources to account for the description given in this work for the transfer coefficient, which follows IUPAC's recommendation (GUIDELLI et al., 2014b).

$$\eta_{conc,x} = \left(\frac{RT}{F}\right)\left(\frac{1}{n_x} + \frac{1}{\alpha_x}\right)\ln\left(\frac{j_L}{j_L - j}\right) \tag{96}$$

The term j_L in this equation is the limiting current density, defined as the current that would drop the reactant concentration on the CL to zero (O'HAYRE et al., 2016, p. 175) This value can either be considered a constant in a model or calculated by setting the concentration on the CL to zero (NÓBREGA, 2023). Using this second methodology and considering a linear concentration profile along the electrode, Equation 97 is obtained for this description, where t^E is the diffusion layer thickness and $c_{R,bulk}$ is the concentration of the reactant in the system bulk (O'HAYRE et al., 2016, p. 174-175).

$$j_L = nFD^{eff}\frac{c_{R,bulk}}{t^E} \tag{97}$$

By this equation, it is possible to conclude that the transport-related losses can be decreased by reducing the thickness of the electrode, increasing the diffusion coefficients, and having a good flow channel design to ensure a high $c_{R,bulk}$ (O'HAYRE et al., 2016, p. 175). Doing this enables the cell to operate in higher current densities without being depleted. For example, using pure oxygen instead of air and increasing the pressure in the system can significantly increase the value of $c_{R,bulk}$, improving cell performance by means of reducing concentration losses.

The previously described approach, although common, has some problems. It usually underestimates considerably the concentration overvoltage of real fuel cells, so Equation 98 is often used, where c is an empirical parameter (O'HAYRE et al., 2016, p. 180).

$$\eta_{conc,x} = c\ln\left(\frac{j_L}{j_L - j}\right) \tag{98}$$

Kulikovsky (2019, p. 89) also criticizes this approach, as the Nernst equation – used when deducing this equation – only describes the concentration dependence in

equilibrium. Therefore, the correct value would need to be calculated from kinetic equations.

An alternative approach for describing concentration losses in fuel cells was proposed by Beale (2004), where a more rigorous description is made. In it, the mass transfer factor is obtained as a function of a generalized mass transfer driving force (B). Using this description, Beale obtained Equation 99a for reactants and 99b for products, where B and r are respectively described by Equations 100a and 100b.

$$\eta_{conc,react} = \left(\frac{RT}{\alpha nF}\right) \ln\left(\frac{1 + rB}{1 + B}\right) \tag{99a}$$

$$\eta_{conc,prod} = \left(\frac{RT}{\alpha nF}\right) \ln\left(\frac{1 + B}{1 + rB}\right) \tag{99b}$$

$$B = \frac{m_{bulk} - m_{wall}}{m_{wall} - m_t} \tag{100a}$$

$$r = \frac{m_t}{m_{bulk}} \tag{100b}$$

Here, m_{bulk} and m_{wall} are the mass fractions in the bulk and wall, respectively, and m_t is the value at the transferred-substance state. The other expression is only valid for very dilute mixtures and in chemical catalysis without net mass transfer at the boundary, while this approach is more general (BEALE, 2015).

3.6 PEMFC Heat Transport

Many phenomena in a fuel cell involve heat generation or consumption. Among those, the electrochemical reaction, joule effect, and water phase transition can be highlighted (ABDEREZZAK, 2018, p. 125). Their impact may be relevant because, as can be seen in the previous sections, most of the properties involved in a fuel cell depend on the system temperature. This is especially important for saturation pressure, as it can vary significantly even with small temperature variations (NÓBREGA, 2023).

Even though temperature is an important parameter for almost all fuel cell phenomena, Nóbrega (2023) reported in their review that most system-level studies consider an isothermal system. The temperature can either be an input parameter of the model or obtained by solving a global energy balance, such as the one in Equation 101 (NÓBREGA, 2023). Here, C_{stack} is the heat capacity of the stack – that is, the

amount of heat energy that, when supplied to the stack, will increase its temperature by one kelvin –, Q_{amb} is the heat transfer to the ambient, Q_{cool} is the heat transfer to the cooling system and W_{ele} is the electrical work produced by the system.

$$C_{stack}\frac{dT_{stack}}{dt} = \sum\left(\dot{n}\overline{H}\right)_{in} - \sum\left(\dot{n}\overline{H}\right)_{out} + \dot{Q}_{amb} + \dot{Q}_{cool} + \dot{W}_{ele} \quad (101)$$

This can significantly simplify the analysis because considering spatial temperature variation involves solving coupled equations due to the variety of phenomena that release or absorb heat. However, temperature differences of 5 ºC or more have been reported in experiments, so this hypothesis may result in inaccuracies (BHAIYA; PUTZ; SECANELL, 2014).

Also, a general form for calculating the total heat generation in a fuel cell is the usage of Equation 102 (ZHANG; KANDLIKAR, 2012). In it, E_{tn} is the thermoneutral voltage, which represents the theoretical voltage if the efficiency was 100%, that is, all reaction enthalpy would be converted to electrical work (O'HAYRE et al., 2016, p. 66). As previously discussed, even in a reversible PEMFC, this would be impossible, but it is a useful value for some theoretical calculations. Nevertheless, this general approach does not give information about temperature profiles and demands the knowledge of real voltage. Thus, it cannot be used to describe temperature in the fuel cell model.

$$\dot{Q}_{cell} = (E_{tn} - V_{cell}) \cdot i \cdot A_{cell} \quad (102)$$

Considering that the developed model is isothermal, more detailed descriptions of the energy balance in the fuel cell are not discussed. Nevertheless, models with this description exist in the literature, for example, the steady-state one by Vetter *et* Schumacher (2019a) or even the transient description of Yang *et al.* (2019).

3.7 Types of fuel cell models

Considering the diversity of models that exist in the literature, it is useful to classify them according to their characteristics. In their review on fuel cell modeling, Nóbrega (2023) classified models according to their dimensions (0D up to 3D), time dependence, number of phases in the system, and temperature profile. It is also possible to differentiate them based on the scale of the analysis – in other words, if the system is analyzed as a continuum or not – and if the modeling is empirical or phenomenological (HAMDOLLAHI; JUN, 2023) (NÓBREGA, 2023).

First, the dimension of a model is the number of different dimensions in which properties can vary. Among those, the simplest is a 0-D model, where each electrode is considered a single control volume with homogeneous properties, such as a continuously-stirred tank reactor (NÓBREGA, 2023). They are usually empirical and are interesting for initial analysis (HAMDOLLAHI; JUN, 2023). On the other hand, 1D models evaluate the system's properties according to a specific spatial discretization that can either be done in the through-plane direction or the flow channel direction (NÓBREGA, 2023). Models with more dimensions will permit the description of discretization points in more directions at the cost of computational performance. It is also possible to combine models of lower dimensions to describe them in an uncoupled way, such as 1D+1D or 2D+1D models (NÓBREGA, 2023). Regarding this possibility, Weber *et al*. (2014) argue that 1D+2D models may be the ideal framework for describing the system accurately with good computational time.

Considering the time dependence, models can be either transient – that is, consider dynamic effects – or steady-state. Nóbrega (2023) proposes that the first type is useful, among other applications, for control strategies, while the second is interesting for optimizing fuel cell performance.

They can also be classified according to the description of the properties. A model can, as discussed in section 3.5.4, consider that water is only present in one phase or may describe the equilibrium between liquid and gas. They may also be isothermal or use different descriptions for representing temperature gradients in each layer, as seen in section 3.6.

Finally, models may also be differentiated based on the scale of the modeling and how they describe phenomena. Most often, they are macroscopic and based on conservation equations, however, as many phenomena occur in pore scale in a fuel cell, they demand microscopic modeling for accurate description (NÓBREGA, 2023). Then, regarding how the phenomena are described, it is possible to make empirical descriptions based on data alone or phenomenological models, which aim at a precise description based on theoretical models (HAMDOLLAHI; JUN, 2023).

Zhang *et al*. (2020) affirm that there are two main approaches to PEMFC models. The first one calculates the cell voltage using the Nernst equation, Kirchhoff-Ohm relation, and activation overpotential, as exemplified by Equation 103. They consider the catalyst layers as an interface and usually neglect anode overpotential. An example of this model is the Springer *et al.* (1991) model. Nóbrega (2023) refers to

these models as “semi-empirical”, as they use semi-empirical parametrizations. These models have as upsides their simplicity, computational efficiency, and ease of fitting them to experimental data (NÓBREGA, 2023).

$$V = E_{thermo} - \eta_{act} - j \cdot ASR \tag{103}$$

The other type is characterized by the modeling of the electrodes as volumetric regions, resulting in coupled Poisson equations for the description of potentials. This approach describes the conservation of its properties by a conservation equation that has the general form presented in Equation 104 (WEBER et al., 2014). In it, ψ is the property being evaluated. Note that the first term considers its time-variation in the control volume, the second is the flux of the property across the control surfaces of the system and the third one is the source term to account for generation or consumption inside the control volume. In this case, proton and electron conservation equations are solved in the fuel cell instead of the usage of semi-empirical relations (NÓBREGA, 2023).

$$\frac{\partial \psi}{\partial t} + \nabla \cdot J_{\psi} = S_{\psi} \tag{104}$$

Further details about considerations and equations used by different models in the literature are presented in the following section.

3.7.1 Literature models

Regarding the equations used to model each overvoltage, Table 10 presents what was used in some works in literature. All the presented models are one-dimensional (through-plane) and steady-state, as this is the type of model developed in this work.

Table 10 - Equations used to evaluate overvoltages in the literature.

Reference	E_{thermo}	η_{act} (cathode)	η_{act} (anode)	η_{ohm}	η_{conc}
Springer *et al*., 1991	ΔS=const.	Tafel	-	H^+ in membrane	Directly in η_{act}
Bernardi *et* Verbrugge, 1992	ΔS=const.	Butler-Volmer	Butler-Volmer	H^+ and e^-	Directly in η_{act}
Falcão *et al.*, 2009	ΔS=const.	Tafel	Tafel	H^+ in membrane	Directly in η_{act}
Salva *et al*., 2016	ΔS(T)	Tafel	Tafel	H^+, e^- and $R_{contact}$	Nernst + BV
Han *et al*., 2019	ΔS=const.	Other	-	H^+ in membrane	Agglomerate model
Vetter *et* Schumacher, 2019a	ΔS=const.	Butler-Volmer	Butler-Volmer	H^+ and e^-	Directly in η_{act}
Schröder *et al.*, 2021	ΔS=const.	Tafel	-	H^+ in membrane and CL	Nernst + BV

Source: the author.

It is noticeable that most authors consider that the reaction entropy is a constant with temperature, with the only exception being the model by Salva e*t al.* (2016), which used the Gibbs energy as a function of temperature. Han *et al.* (2019) calculate the activation overpotential using effective protonic and electronic conductivity and a local current density, as shown in Equation 105.

$$\frac{d\eta_{act}}{dz} = \frac{j_{local}}{\sigma_{H^+}^{eff}} + \frac{j_{local} - j_{total}}{\sigma_{e^-}^{eff}} \tag{105}$$

Another pattern observed is that most models neglect contact resistances in the fuel cell, which can be important, as previously discussed. Finally, the manner used to calculate concentration overpotential varies in the analyzed works. Most of the reviewed works do not use a unique term for describing this overpotential, but consider the concentration dependence in the calculation of the activation overpotential. Schröder *et al.* (2021) use the correction presented in this text (Equation 96), which considers both the concentration effects in the Nernst equation and in Butler-Volmer/ Tafel (O'HAYRE et al., 2016, p. 176-178). However, they also consider the concentration dependence in the exchange current density. Salva *et al*. (2016) used a hybrid approach, considering only the term relative to thermodynamic potential correction, but using the concentration dependence when calculating activation

overpotential. Han *et al.* (2019) use the agglomerate model, which already computes local rates of reaction, thus, none of the previously discussed equations were used.

The equations used to model the main phenomena in those models are presented in Table 11.

Table 11 - Equations used to model the phenomena in fuel cell models.

Reference	Catalyst layer	Gas transport	Liquid water in electrode	Water in membrane	Heat transport
Springer *et al.*, 1991	Interface	Steffan-Maxwell	Single-phase	Diffusive model	Isothermal
Bernardi *et* Verbrugge, 1992	Volume	Steffan-Maxwell	Schlögl's equation	Hydraulic model	Isothermal
Falcão *et al.*, 2009	Volume	Fick	Single-phase	Diffusive model	Conduction
Salva *et al.*, 2016	Volume	Fick	Darcy's law	Diffusive model	Conduction + Convection
Han *et al.*, 2019	Volume	Fick	Single-phase	Diffusive model	Isothermal
Vetter *et* Schumacher, 2019a	Volume	Fick	Darcy's law	Diffusive model	Conduction
Schröder *et al.*, 2021	Interface	Fick	Darcy's law	Diffusive model	Isothermal

Source: the author.

Among those models, the one by Bernardi and Verbrugge (1992) is the most different, mainly due to its description based on a hydraulic model for water transport. This hydraulic transport depends on the existence of a continuous liquid water phase within the membrane, which is only reasonable under LE conditions (DICKINSON; SMITH, 2020). It is also noticeable that, while the inaugural models used Steffan-Maxwell equations for gas transport, Fick's law is, at least among the analyzed models, more common recently.

3.7.2 Stack modeling

This work, as many others in the literature, focuses on modeling a single fuel cell. However, stacks of individual cells in series are used for most applications. Thus, this topic briefly presents some of the particularities for modeling a stack, though they are not considered in this work.

Among the simplest assumptions that can be made for modeling a stack, one may consider that all cells in a stack are equal, thus only one cell must be simulated

or they can be lumped as a system. This permits, considering the number of cells in the stack, the evaluation of the power produced by the stack. Although this is done in the literature – for example, in the work of Pukrushpan *et al*. (2004) – it is not a realistic consideration for most cases (CELIK; PAKALAPATI, 2008, p. 126). In reality, there are asymmetries between the cells, such as different fuel and oxygen quantities available to each cell and uneven temperature distribution related to cooling difficulties (CELIK; PAKALAPATI, 2008, p. 129). This makes assumptions like uniform temperature with the environment, considered reasonable for single cells, possibly inapplicable to stack models (CHU; JIANG, 1999). Nevertheless, the consideration of identical cell conditions is still the most common one used for system-level studies (NÓBREGA, 2023).

In order to describe in detail these heterogeneities, CFD has been used in the literature with good results. Still, due to their higher computational time and cost, many researchers use simplified models for the stack (ARIF; CHEUNG; ANDREWS, 2020). For more details about those stack-level models, Arif's *et al*. (2020) review is a good starting point.

4 METHODOLOGY

To evaluate the different propositions for modeling a fuel cell as well as their impact on the result and computational time, a model was developed in this work. The model, differently from what is normally done in the literature, has multiple possible descriptions for each phenomenon, enabling easy comparisons of the assumptions. It was implemented in MATLAB 2023b and run for all the tests on the same computer, using a Ryzen 7 2700 (~3.2GHz) CPU with 16 GB of RAM. The specific details and the methodology used for the comparisons are explained in the following sections.

4.1 Structure of the Model

The developed model is an implementation mainly based on Springer *et al.* (1991) proposal. It uses the flux balance presented in section 3.5.1 to describe the relations between the current density and material fluxes present in the cell. This aims to be a simplified approach, where phenomena are described in an as uncoupled as possible manner to obtain a computationally efficient model.

In its elaboration, the system is assumed to be in steady-state, isothermal, and one-dimensional. Also, water is considered to only be present in vapor form – even if its partial pressure is greater than the saturation value – and all gases are assumed to be ideal. Both catalyst layers are assumed to be infinitesimally thin and the gas channels are considered an ideal mixture of bulk gases, thus, only three control volumes exist in this system: the AGDL (anode gas diffusion layer), the membrane, and the CGDL (cathode gas diffusion layer). All those regions are considered homogeneous and isotropic, with the effect of clamping pressure in its properties neglected. The Nafion membrane is assumed to be able to swell freely, that is, effects related to their compression are not considered. Also, the membrane is assumed to be permeable only to water and protons.

The required inputs in this model can be divided into entry conditions, electrochemical data, and characteristics of the control volumes (electrodes and membrane). The first category is related to the reactant inlets, composed of the molar fraction of the dry gases, relative humidity of each inlet, temperature, and

stoichiometric number of hydrogen and oxygen. The demanded electrochemical data are the transfer coefficients for each half-reaction, reference exchange current density, as well as catalyst loading and activation energies of the reactions. Finally, the characteristics of each layer concern porosity, tortuosity, thickness, and membrane-specific parameters, such as equivalent weight, density, and λ values for liquid and vapor equilibrated Nafion. It should be noted that the water properties are given by the recommended description by the International Association for the Properties of Water and Steam (WAGNER; PRUSS, 1993) (HUBER et al., 2009) (HUBER et al., 2012). The values of current density in which the model is evaluated are also inputs to the model, whereas, in each evaluation, the current density is assumed to be homogeneous in all control volumes where electron flow exists.

For the description of the bulk value for the gases' molar fractions, the model considers the depletion effects using the concept of stoichiometric number, an input for the model, with the flux balance. These results are given by the previously presented Equations 69-72, which enable a description of the bulk values for hydrogen, oxygen, and water vapor with the assumption of an ideal mixture. A deduction of those equations is presented in Appendix C.

A particularity of models based on the flux balance (Equation 51) is the fluxes' dependence on the unknown α^*. As this value dictates the fluxes – and consequently the concentration values at the TPB – its determination is necessary for most of the other calculations. In this model, this is done by an iterative method that uses Equation 86 and two boundary conditions given by the sorption isotherm. The program solves the equation using the anode λ value given by the sorption isotherm as a boundary condition and a guess for α^*, then compares the obtained value in the cathode by the integration with the predicted by the sorption isotherm. According to the results, it proposes a new guess for α^*. This can also be thought of as an unrestricted optimization problem which has as variable α^* and objective minimizing the square difference between λ_{cat} predicted by the integration and isotherm. Note that transport equations – either Fick (Equation 53) or Stefan-Maxwell (Equation 55) – are needed for describing the water activity in the TPB, which is dependent on α^*, thus, they are coupled in the iterative solution. In this work, the Stefan-Maxwell model is chosen because of the multicomponent nature of the system's diffusion. Note that, as the depletion effect equations also depend on α^*, they are coupled in the solution as well. Another important point is that advective transport is neglected, which is the reason

why all presented equations have only the diffusional contribution for transport. Also, Knudsen diffusion is neglected. Appendix D presents the deduction of the equations when the flux balance is applied in a transport model. Even if only the Stefan-Maxwell equation is used, the result of applying Fick's model is also presented there. Figure 13 exemplifies this iterative procedure.

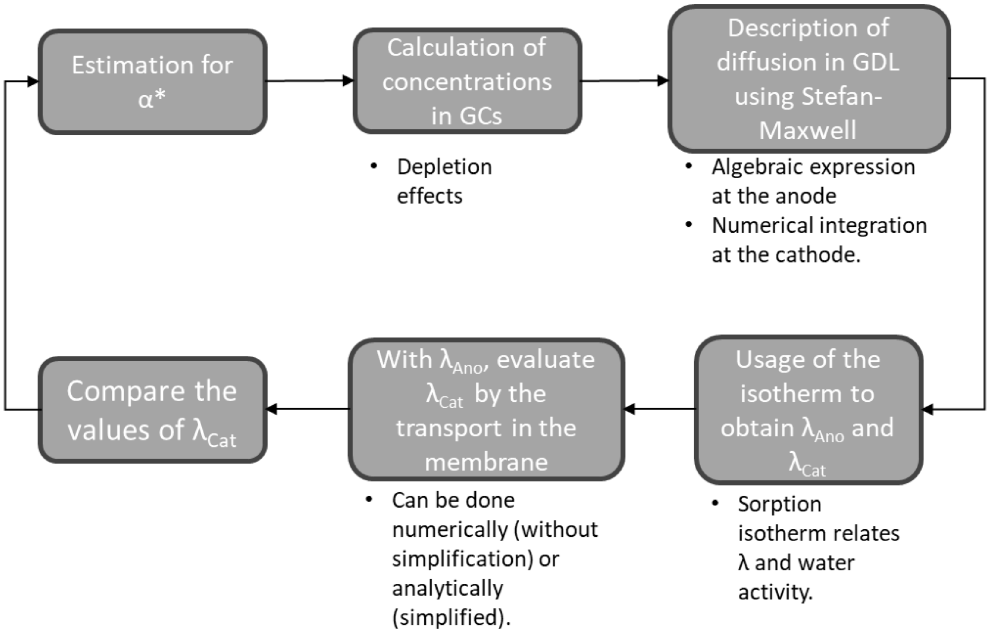

Figure 13 - Iterative procedure for finding α*.
Source: the author.

After the iterations, if the method converges, the actual value of α^* will be known, as well as the λ profile in the membrane. Thus, it is possible to calculate the membrane's protonic resistance (ASR_m) using a relation for its conductivity as a function of λ. In this model, the electronic and contact resistances are assumed to be negligible, and the correlation proposed by Springer *et al.* (1991) for conductivity is used. A slight adaptation was done in this expression to avoid numerical errors related to a conductivity of zero at low λ values: as shown in Equation 106, when the conductivity reaches a critical value – considered as a value 10% greater than the root of the expression –, it will linearly approach zero at $\lambda = 0$ instead of reaching zero in the root ($\lambda = 0.6344$). This results in the expected rapid growth of resistivity on a dry membrane, but without the numerical problems that would be caused by an infinite resistivity.

$$\sigma(\lambda, T) = \begin{cases} (0.5139\lambda - 0.326)e^{\left[1268\left(\frac{1}{303}-\frac{1}{T}\right)\right]}, & \lambda \geq 0.6978 \\ \left[0.0326 - 0.0326\left(\frac{0.6978-\lambda}{0.6978}\right)\right]e^{\left[1268\left(\frac{1}{303}-\frac{1}{T}\right)\right]}, & \lambda < 0.6978 \end{cases} \quad (106)$$

The proposed implementation calculates ASR_m by numerically integrating the resistivity – the inverse of the conductivity – along with the obtained description for $\lambda(z)$. With this value, the ohmic overvoltage at a given current density may be easily calculated using Equation 35.

Knowing α* also permits the description of the concentration values of each species at the TPB, which enables the calculation of the concentration overvoltage – evaluated in this model using Equation 107. Equation 96 is not used because, as the Stefan-Maxwell model is employed, its usage would be inconsistent considering that the limiting current density is calculated with Equation 97, based on Fick's law. However, even in this case, it is possible to use it as an approximation, but considering that the concentrations at TPB are already calculated, this is not expected to yield any advantages.

$$\eta_{conc.x} = \left(\frac{RT}{F}\right)\left\{\frac{1}{n_x}\ln\left[\left(\frac{x_i^{bulk}}{x_i^{TPB}}\right)^{\nu_i}\right] + \frac{1}{\alpha_{fwd,x}}\ln\left[\left(\frac{x_i^{bulk}}{x_i^{TPB}}\right)^{\gamma_i}\right]\right\} \quad (107)$$

The final overvoltage that should be calculated is the activation one. This can be done either using the Butler-Volmer or Tafel equation, as will be discussed in Section 4.2.

Finally, the thermodynamic voltage is calculated by the combination of Nernst Equation (Equation 9) with a temperature correction, either considering ΔS_{rxn} constant with temperature (Equation 7) or via integration (Equation 8). More details about both options are presented in Section 4.2.

With all those steps, it is possible to obtain the fuel cell voltage as a function of the current density in the PEMFC. Besides the voltage and current density, the model has as outputs the activation, ohmic, and concentration overvoltages calculated at each current density, and α* for those j values. Those results are presented graphically in the tested interval of current densities. Other graphs are also produced by the model, which are the values of the molar fraction of the gases in both electrodes and λ values along the membrane. As those are dependent on the current density, they are plotted in five different j values, equally spaced between (and including) initial and final current densities. Those concentration values are obtained by using the equations presented in Appendix D.

To illustrate the calculations described in the previous paragraphs, Figure 14 is presented. It is a simplification of the modules used in the program, as the actual model

is composed of many specialized functions, so explaining all of them would not be practical.

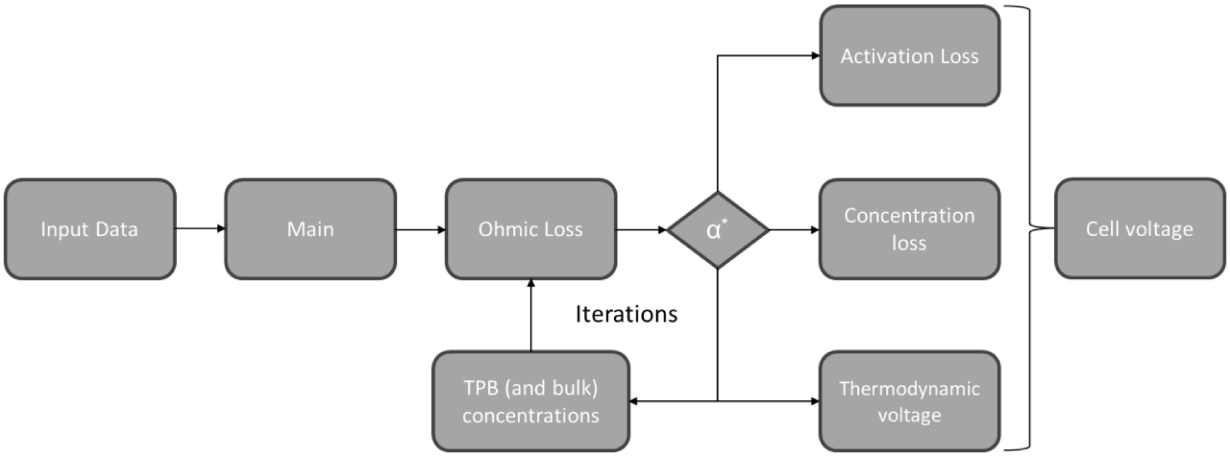

Figure 14 - Basic structure of the first model.
Source: the author.

4.1.1 Numerical considerations of the model

The developed model depends on the usage of numerical methods for multiple steps. For example, for solving the model at one specific current density, it is necessary to use an iterative solution to find α^*, whereas each step may potentially demand more than one numerical integration. Therefore, ensuring their convergence and efficiency is crucial.

First, as non-linear equations and ordinary differential equations are numerically solved, adequate methods and tolerances should be chosen. The non-linear equations are solved using MATLAB's "fsolve" function, which uses a trust-region approach with Powell dogleg procedure for computing the step (MATLAB, [s.d.]). The selected function and step tolerance used are 10^{-9}. Furthermore, the differential equations are solved using the 2-3rd order Runge-Kutta algorithm implemented in the "ode23" solver, with a relative tolerance of 10^{-6} and an absolute tolerance of 10^{-9} (SHAMPINE; REICHELT, 1997).

Special attention should be given to the iterative solution, as it is expected to be the most demanding part of the model. In the case where the complete description of D_λ is used – that is, without the simplification – the iterative method is solved using MATLAB's boundary value problem solver "bvp4c", an implementation of the three-stage Lobatto IIIa colocation formula (KIERZENKA; SHAMPINE, 2001). The number

of discretization points of the first mesh is 50, with an initial approximation of the solution given by a linear function between λ_{Ano} and λ_{Cat}. Moreover, the chosen relative tolerance and absolute tolerance are 10^{-6} and 10^{-9}, respectively. On the other hand, when the simplifying assumption is used, the solution is done by the "fsolve" function with the previously discussed tolerances. Both of those choices are based on preliminary tests, in which they had the best balance between stability and efficiency among all solving strategies.

Another crucial topic to the convergence of the methods is the initial guess used in the solvers. For the evaluation of activation overpotential when the Butler-Volmer equation is used, the value calculated by the Tafel equation at the same conditions is employed, as it should be a reasonable approximation. As for the one used to obtain α^*, the value of α^* calculated at the previous current density is utilized because, considering a reasonably small step in j, this should be close to the next value. For the initial current density, based on a hypothesis that the j value will be small (or even zero), the initial guess for α^* is zero, as the electro-osmotic drag is expected to be small when the reaction is not intense and, considering that the quantity of water produced will not be significant at those conditions, so will be the back-diffusion, resulting in a value near zero for water flux in the membrane.

Finally, the usage of regularization functions is proposed to avoid some numerical problems that could happen due to the discontinuity of the derivatives of the piecewise functions used both on the piecewise liner description of the electro-osmotic drag coefficient (ξ) and water diffusivity in the membrane (D_λ). These regularization functions are expressions that have the property presented in Equation 108 (SOUZA, 2007, p. 43). Here, "par" is a parameter that determines how step-like this function is.

$$\mathrm{H}(arg, par) \cong \begin{cases} 1, & arg < 0 \\ 0, & arg \geq 0 \end{cases} \tag{108}$$

Using them enables writing a continuous expression for piecewise functions, which solves the discontinuity in the derivatives. For example, Equation 109a can be written as 109b using these properties (SOUZA, 2007, p. 43).

$$\mathrm{f(t,x)} = \begin{cases} g_1(t,x), & \mathrm{f(t,x)} < f_{max} \\ g_2(t,x), & \mathrm{f(t,x)} \geq f_{max} \end{cases} \tag{109a}$$

$$\mathrm{f(t,x)} \cong \mathrm{H}(f - f_{max}, par) \cdot g_1(t,x) + [1 - \mathrm{H}(f - f_{max}, par)] \cdot g_2(t,x) \tag{109b}$$

In this work, the used regularization function – Equation 110 – is a version of the well-known logistic function. The k value on this function is defined as the inverse of the parameter (par = 1/k) to maintain the intuition that smaller parameter values imply

a more step-like function. The justification behind the proposition of this function is that some equations have exponential terms, which can increase significantly and result in a considerable term in the continuous equation when its value should be around zero if the regularization function is not small enough. Thus, the proposition of a function that exponentially approaches zero can possibly be more adequate for those specific cases.

$$\mathrm{H}(arg, k) = 1 - \frac{1}{1 + e^{-k \cdot arg}} \tag{110}$$

The behavior of the proposed function is presented in Figure 15. Note that it has the desired characteristic, therefore it should be capable of adequately removing the discontinuities.

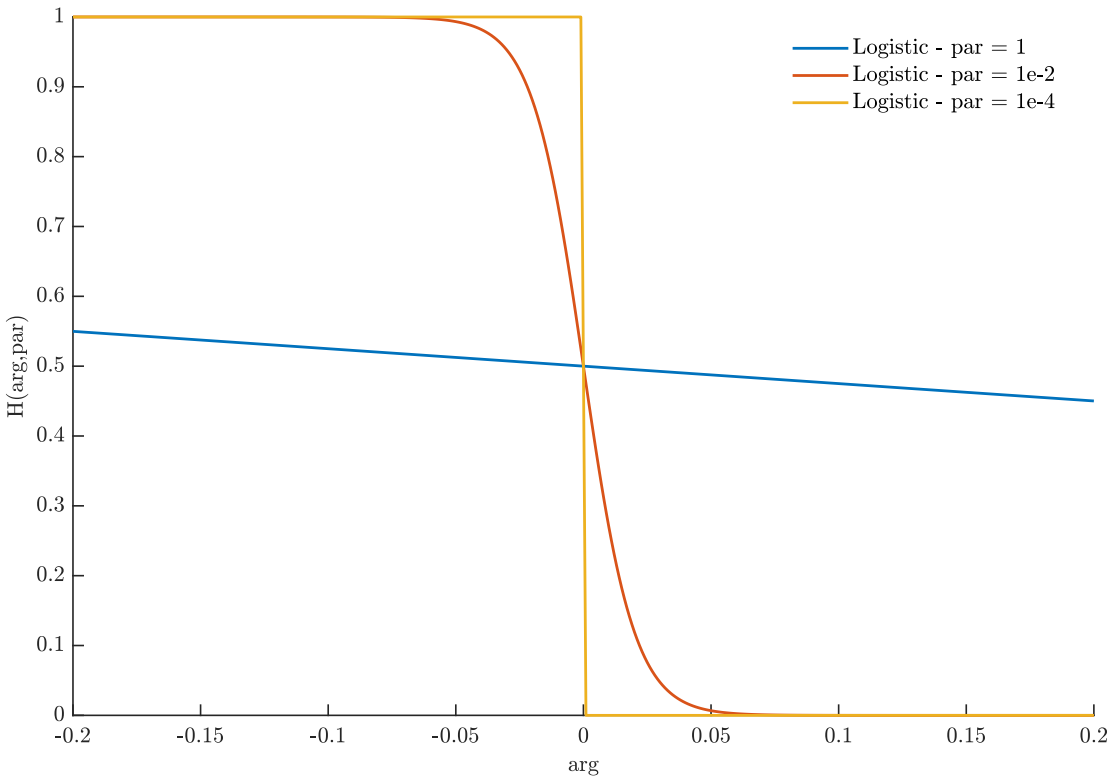

Figure 15 - Regularization function obtained using different parameters.
Source: the author.

For more details on the continuous expressions obtained by the usage of those regularization functions, the reader is referred to Appendix E.

4.2 Tested Variations

The selection of variations of the models was made aiming at evaluating descriptions that affect each overvoltage and are commonly used in the literature. An important point about these tests is that, though each variation targets mainly one overpotential, the coupling of properties makes it so that the others are probably affected as well. Therefore, a global analysis in some cases is justified.

Firstly, regarding the thermodynamic voltage, the proposed variation is in the description of the temperature correction. This can either be done considering a constant ΔS_{rxn} with temperature, as done in most articles, or integrating the temperature dependence. Note that, for this specific case, the simplifying assumption is commonly used in the literature, while the alternative description proposed is the non-simplified approach. For this work, the temperature dependence of ΔS_{rxn} is described using Shomate's Equation – Equation 111 –, with parameters obtained from Chase (1998). They are presented in Table 12.

$$S_i^0(t) = A_i \ln(t) + B_i t + C_i \frac{t^2}{2} + D_i \frac{t^3}{3} - \frac{E_i}{2t^2} + G_i;\ where\ t = \frac{T}{1000} \tag{111}$$

Table 12 - Parameters used in the Shomate Equation.

Constant	H_2O (l)	H_2O (g)	H_2 (g)	O_2 (g)
A	-203.6060	30.09200	33.066178	31.32234
B	1523.290	6.832514	-11.363417	-20.23531
C	-3196.413	6.793435	11.432816	57.86644
D	2474.455	-2.534480	-2.772874	-36.50624
E	3.855326	0.082139	-0.158558	-0.007374
F	-256.5478	-250.8810	-9.980797	-8.903471
G	-488.7163	223.3967	172.707974	246.7945
H	-285.8304	-241.8264	0.0	0.0

Source: Adapted from CHASE, 1998.

As this equation is easily integrated, the implemented expression is already the analytical integral, thus, the usage of the more complete description should not yield a considerably larger computational demand.

Furthermore, the chosen variation for activation overpotential is the usage of either the Butler-Volmer equation (Equations 24-25) or Tafel (Equation 29), both widely used in fuel cell modeling. When Butler-Volmer is chosen, it is necessary to solve a non-

linear equation, which is made numerically (using MATLAB's "fsolve" function) with the initial guess equal to the η_{act} value calculated by Tafel. Thus, the usage of that equation necessarily implies more operations. An important remark is that the exchange current density is calculated in this model considering that each concentration is equal to its inlet value in Equation 18, as the concentration overvoltage term will encompass the losses related to the actual concentrations at the TPB. Moreover, considering that the activation overvoltage should always be a positive value bearing in mind the description used in this work, if the value predicted by the Tafel equation is smaller than zero – which can happen if the current density is small – the program changes the value to zero.

As for the ohmic overpotential, variations in the description of D_λ and different sorption isotherms are tested. More parameters are evaluated here as this overpotential is the one with the largest quantity of different descriptions in the reviewed literature and was responsible for significant changes in the polarization curve in a previous work by the author (CARNEIRO et al., 2023).

The tested variation in D_λ is the usage of a constant value equal to the mean value for this diffusivity in the system, which is the subject of a published article by the author (CARNEIRO et al., 2024). This mean can either be obtained as the arithmetic mean of the diffusivities evaluated at the water content of the boundaries – Equation 112a – or by integrating the curve between λ_{Ano} and λ_{Cat} and dividing by the interval size, as proposed in Equation 112b. The second definition is more precise and should yield better results because it takes into account the curve's profile, an important factor given the irregular profile observed for this property. Therefore, it is the proposed methodology here.

$$D_{\lambda,mean} = \frac{D_\lambda(\lambda_{Ano}) + D_\lambda(\lambda_{Cat})}{2} \tag{112a}$$

$$D_{,mean} = \frac{1}{\lambda_{Cat} - \lambda_{Ano}} \int_{\lambda_{Ano}}^{\lambda_{Cat}} D_\lambda(\lambda) d\lambda \tag{112b}$$

Using this strategy along with Mazumder's (2005) expression for D_λ results in Equation 113, which is implemented in the model.

$$D_{\lambda,mean} = \begin{cases} K \cdot \begin{bmatrix} (2-\lambda_{Ano}) + 4.31 + \\ (2.563\lambda_{Cat} - 0.165\lambda_{Cat}^2 + 0.0088\lambda_{Cat}^3 \\ -0.00016275\lambda_{Cat}^4 - 8.132256) \end{bmatrix}, & 2 \le \lambda_{Ano} \\ K \cdot \begin{bmatrix} (3\lambda_{Ano} - \lambda_{Ano}^2) + 2.31 + \\ (2.563\lambda_{Cat} - 0.165\lambda_{Cat}^2 + 0.0088\lambda_{Cat}^3 \\ -0.00016275\lambda_{Cat}^4 - 8.132256) \end{bmatrix}, & 2 < \lambda_{Ano} \le 3 \\ K \cdot \begin{bmatrix} (0.69\lambda_{Ano}^2 - 7.14\lambda_{Ano} + 14.52) \\ +(2.563\lambda_{Cat} - 0.165\lambda_{Cat}^2 + 0.0088\lambda_{Cat}^3 \\ -0.00016275\lambda_{Cat}^4 - 8.132256) \end{bmatrix}, & 3 < \lambda_{Ano} \le 4 \\ K \cdot \begin{bmatrix} 2.563(\lambda_{Cat} - \lambda_{Ano}) - 0.165(\lambda_{Cat}^2 - \lambda_{Ano}^2) \\ +0.0088(\lambda_{Cat}^3 - \lambda_{Ano}^3) - 0.00016275(\lambda_{Cat}^4 - \lambda_{Ano}^4) \end{bmatrix}, & \lambda_{Ano} > 4 \end{cases} \quad (113)$$

$$K = \frac{10^{-10} e^{\left[2416\left(\frac{1}{303} - \frac{1}{T}\right)\right]}}{\lambda_{Cat} - \lambda_{Ano}}$$

By using this assumption of mean D_λ value, it is possible to integrate analytically Equation 86, which can possibly result in a significantly more efficient program, as each iteration of the full description demands solving an ODE numerically. The extent of this gain and the effect on the predicted results are evaluated by comparing the computational time for the model using both descriptions but with the same inputs. The expression obtained by this integration depends on the description of the electro-osmotic drag coefficient, as it is a function of λ. The equations obtained using the propositions made by Springer *et al.* (1991), Meier *et* Eigenberger (2004), and a piecewise linear function (VETTER; SCHUMACHER, 2019b) are presented, respectively, by Equations 114, 115, and 116. In all of those equations, it was assumed that λ_{Ano} is greater than 1 and that λ_{Cat} is always greater than λ_{Ano}.

$$\lambda(z) = \frac{11\alpha^*}{n_{drag}^{sat}} + \left(\lambda_{Ano} - \frac{11\alpha^*}{n_{drag}^{sat}}\right) \cdot \exp\left(\frac{jEW n_{drag}^{sat} z}{22 F \rho_{dry} D_{\lambda,mean}}\right) \quad (114)$$

$$\lambda(z) = \frac{-b}{2a} + \frac{\sqrt{4ac - b^2}}{2a} \tan\left[\tan^{-1}\left(\frac{2a\lambda_{Ano} + b}{\sqrt{4ac - b^2}}\right) + \left(\frac{\sqrt{4ac - b^2}}{2}\right) Kz\right] \quad (115)$$

$$a = 0.0026, \qquad b = 0.028, \qquad c = 1 - 0.5\alpha^*$$

$$\mathrm{K} = \frac{jEW}{F \rho_{dry} D_{\lambda,mean}}$$

$$\lambda(z) = \begin{cases} (1 - 0.5\alpha^*)\left(\frac{jEWz}{F\rho_{dry}D_{\lambda,mean}}\right) + \lambda_{Ano}, & 1 \le \lambda < \lambda_{VE} \\ \lambda_{VE} - \left(\frac{1 - 0.5\alpha^*}{k}\right) + \left(\frac{k\lambda_{VE} + 0.5\alpha^* - 1}{k}\right)\left[exp\left(\frac{j\ EW\ k\ z}{F\rho_{dry}D_{\lambda,mean}}\right)\right], & \lambda > \lambda_{VE} \end{cases} \quad (116)$$

$$where\ k = \left(\frac{\xi_{L,max} - 1}{\lambda_{LE} - \lambda_{VE}}\right)$$

In the previous descriptions, Equation 115 assumes that $b^2 - 4ac < 0$, and Equation 116 represents only the case where both λ_{Cat} and λ_{Ano} are in the same interval. As the piecewise description implies different expressions for each interval of

λ, it might be necessary to use different equations when integrating. For example, if $f(z)$ is the description valid until $\lambda = x$ and $g(z)$ is used for greater λ values, an expression such as Equation 117 should be used, where z_x is the z value that results in $\lambda = x$. More details about this integration and other nuances involved in obtaining the analytical expressions are discussed in Appendix F. This Appendix also has the equations for λ when two or more intervals coexist in the domain.

$$\lambda(z) = \int_0^{z_x} f(z)dz + \int_{z_x}^{t^M} g(z)dz \tag{117}$$

Finally, the sorption isotherm is also varied in this work to measure the impacts of different descriptions in the results. The selected isotherms are the ones proposed by Springer *et al.* (Equation 75) and Kulikovsky (Equation 77) because both permit the description of Schroeder's paradox in a monophasic model. Here, the simplification is not the use of a specific isotherm because membranes made of different materials are expected to have different absorption behaviors. This test aims to evaluate if considerable variation is observed when different sorption isotherms are used, to understand the validity of the common practice of using isotherms deduced for other types of membranes in models. It should be highlighted that, considering that neither isotherm demands a different solving procedure, the computational difference caused by these variations is mostly tied to the numerical convergence of the method, and not to the result of a simplification. Therefore, the greatest interest in this test is the impact on accuracy.

4.3 Evaluation of the model

After defining the model, the last necessity is to select the test conditions and evaluations that are made. Considering the large number of variables, it is impossible to thoroughly investigate them all, but choosing representative conditions of fuel cells should be an adequate approach to this limitation.

4.3.1 Test conditions

The test conditions of this work were chosen based on common literature values so that the results are representative and useful for future models. Most of the parameters have a single value in all tests, but some – due to their potentially significant impact on the results – have two, a high and a low value among what is present in the literature. This should permit the assumptions' evaluation under most of the relevant conditions.

Firstly, regarding the entry conditions, the pressure of both electrodes is established as 1.5 bar, an intermediate value between the span found in the literature (1 to 3 bar). Moreover, two temperatures are tested, 333.15 K and 353.15 K, as it can impact all the overvoltages. The same was done to relative humidity, with values of either 60% or 80%, whereas 80% is used when this parameter is not varied in the test of a specific simplification. Also, the stoichiometric numbers for hydrogen and oxygen are respectively 4 and 6, as used by Springer *et al*. (SPRINGER; ZAWODZINSKI; GOTTESFELD, 1991), because many models neglect depletion effects, therefore high values for ensuring only moderate effects were chosen.

Furthermore, the electrochemical parameters – namely reference exchange current densities, transfer coefficients, activation energy, and pressure dependency coefficient – are obtained from Neyerlin *et al.* (2006) (2007) experimental evaluations. In the specific case of the transfer coefficient, two values are proposed for each. Both the anode ones are possibilities analyzed in Neyerlin *et al*. (2007), while the value of 1 for the cathode is the proposition of this same author, and the value of 2 is the common value that arises from assuming a transfer coefficient of 0.5 and multiplying by the number of electrons involved in the cathodic half-reaction.

All these parameters are compiled in Table 13. It also presents the remaining ones, related to the electrode and membrane information. Among those, the one that should be highlighted is the membrane thickness, which varies significantly in the literature. Considering that in the reviewed works this value was in the interval of 25 to 175 μm, the chosen thicknesses are 50 and 125 μm, whereas the first one is typical for Nafion NRE-212 and the second for Nafion 115 (NISHIMURA et al., 2021).

Table 13 - Parameters used in the tests.

Entry conditions		
Parameter	**Value**	**Source**
$P_{Ano} = P_{Cat}$ (bar)	1.5	-
T (K)	333.15 and 353.15	-
RH (%)	60 and 80	-
λ_{H2}	4	Springer *et al.*, 1991
λ_{O2}	6	Springer et al., 1991
$x_{H2,in}$ (dry)	1	-
$x_{O2,in}$ (dry)	0.21	-
Electrochemical data		
Parameter	**Value**	**Source**
$\alpha_{fwd,Ano}$ and $\alpha_{bwd,Ano}$	0.5 or 1	Neyerlin *et al.*, 2007
$\alpha_{fwd,Cat}$ and $\alpha_{bwd,Cat}$	1 or 2	Neyerlin *et al*., 2006
$j_{0,Ano,ref}$ (A/cm^2 of Pt)	0.240	Neyerlin *et al.*, 2007
$j_{0,Cat,ref}$ (A/cm^2 of Pt)	2.47e-8	Neyerlin *et al*., 2006
$E_{c,Ano}$ (J/mol)	16000	Durst *et al.*, 2015
$E_{c,Cat}$ (J/mol)	67000	Neyerlin *et al*., 2006
γ_{Ano}	1	Assumed
γ_{Cat}	0.54	Neyerlin *et al*., 2006
$(a \cdot L_c)_{Ano}$ (cm_2 Pt/m_2)	3000000	Barbir, 2013
$(a \cdot L_c)_{Cat}$ (cm_2 Pt/m_2)	3000000	Barbir, 2013
Membrane and electrode data		
Parameter	**Value**	**Source**
EW (kg/m^3)	1.1	Schröder *et al.*, 2021
$\rho_{memb,dry}$ (kg/mol)	1980	Schröder *et al.*, 2021
ε_{GDL}	0.76	Vetter *et* Schumacher, 2019a
τ_{GDL}	1.6	Vetter et Schumacher, 2019a
t^A (µm)	250	-
t^C (µm)	250	-
t^M (µm)	50 and 125	Nishimura *et al*., 2021

Source: the author.

The effective diffusivity for all gases was evaluated with the Chapman-Enskog kinetic theory (Equation 57) along with an M-factor (Equation 61) using respectively 1 and 2 as the exponents for porosity and diffusivity, as done by Vetter *et* Schumacher (2019a) and Berasategi *et al.* (2024).

Lastly, considering that each simplification is affected only by specific parameters, Table 14 shows which of them are varied in the evaluations. Note that,

even with this pragmatic approach, the number of tests is still large, therefore a robust comparison methodology is needed to keep this work concise but conclusive.

Table 14 - Parameters varied in each test.

Assumption	Affects	Dependence	Varied parameters
ΔS_{rxn}	E_{Thermo}	T	T
Tafel	η_{act}	T, α_{Cat} and α_{Ano}	T, α_{Cat} and α_{Ano}
Sorption isotherm	α* (thus, all)	a_{H_2O}	T, RH, and t^M
Mean D_λ	α* (thus, all)	T and λ	T, RH, t^M and ξ

Source: the author.

4.3.2 Comparison methodology

In order to have a precise analysis of the impact of each modeling approach, the parameters considered for the comparison are standardized. This should permit a profound understanding of how each simplification affects the model. However, due to the used modeling strategy, as only simplifications that affect the calculated α^* value interfere in the transport – and consequently the concentrations –, the assumptions on the activation overvoltage and in the thermodynamic potential only affect the polarization curve. Therefore, the methodology used for them is different than for the other two. These specificities regarding each test are discussed in sections 4.3.2.1 and 4.3.2.2.

Even with those particularities, the comparison methodology for the polarization curve is similar in all the cases. Due to its practical importance, many analyses are done on it. The first one is its general profile, a qualitative analysis to verify if a specific region is more affected by the description. Furthermore, the current density in which the voltage is equal to zero is compared to verify the impact of the overpotentials in a more global manner. This value was obtained by analyzing steps of 0.01 $A \cdot cm^{-2}$ in current density until the potential was equal to zero. Also, the values of voltage and each overvoltage in specific current densities are evaluated, as they can provide more specific insights about the impacts caused by each variation. The selected current densities for these tests are based on harmonized test protocols for PEMFC made by the European Commission (TSOTRIDIS et al., 2015), and are 0.1 $A \cdot cm^{-2}$, 0.8 $A \cdot cm^{-2}$, and 1.8 $A \cdot cm^{-2}$ to evaluate regions representative for each overpotential. In specific cases where some of those current densities are not reached, different values are

used. Usually, those are selected as a value near the final current density for the specific test. Besides the profile evaluation, a numerical comparison of the curves is made using the standard error of the estimate (S_e), which represents how much the results with the simplification differ from the reference values. This is done using Equation 118, where y represents the voltage values without simplification, $\hat{y}$ are the voltages predicted by the simplified model, and n is the number of evaluated points (TRIOLA, 2006, p. 252).

$$S_e = \sqrt{\frac{\sum(y_i - \hat{y}_i)^2}{n-2}} \tag{118}$$

To permit the evaluation of the fit quality locally as well, the standard error of the estimate is also calculated separately for three parts of the polarization curve. The first interval is from the voltage calculated at j = 0 up to 0.75 V to represent the activation; the second goes from 0.75 V to 0.50 V to represent the ohmic overvoltage, and the last interval comprehends all remaining values, combining ohmic and concentration effects.

Moreover, the voltage, power, and current density at the system's optimal operation point – that is, maximum power – are calculated, as this point could be considered one of the most interesting for practical applications. Thus, understanding how much the simplifying assumptions shift the optimal is important.

Finally, the evaluation of the computational time for the model is also equal for all evaluations. The mean of ten model runs using current densities from zero to the first current density to yield 0 voltage is considered the time demanded, but twelve runs are made, whereas the highest and lowest time are discarded to remove possible outliers. The function selected for this evaluation is MATLAB's "tic toc" stopwatch timer, which uses high-accuracy timers (< 1μs) for obtaining the values (KNAPP-CORDES; MCKEEMAN, 2011). To ensure conclusive results for the model evaluations, this process is done with 100 and 500 points to see the effect of the simplification with a larger or smaller interval between solved current densities (Δj). It should be highlighted these tests only encompass the main function, as all other parts of the software – such as generating graphs – are equal among all tests, thus evaluating their time would dilute the effect of the variations.

4.3.2.1 Particularities for simplifications that do not affect α^*

The simplifications that do not affect α^*, namely the usage of a constant reaction entropy and Tafel equation, only affect the polarization curve. Therefore, the comparisons are only done with the voltage.

In the case of constant reaction entropy, the only parameter that affects the system is temperature because, even though the bulk value, affected by α^*, interferes with the cell's voltage, the simplification only affects the temperature correction – and not the concentration one – to the value. Thus, instead of comparing this value in the model, the chosen methodology is a direct comparison between the values predicted by Equation 7 and Equation 8 in a span of temperatures from 298.15 to 373.15 K. The entropy assumed for the constant case is -163.23 J mol^{-1} K^{-1}, the most common value in the literature. The final particularity is that the computational time of each description is evaluated separately and inside the model.

As for the comparison between Tafel and Butler Volmer equations, the polarization curve tests follow the general methodology. However, as the impact of the simplifying assumption is expected to be focused on the activation region, the polarization curve is only evaluated up to 0.1 $A \cdot cm^{-2}$, so that all the points are used in it. On the other hand, the computational time evaluation still used the whole span of current densities. Finally, a direct comparison of the Butler-Volmer, Tafel, and linear approximation of Butler-Volmer is made in the anode and cathode to highlight any particularities of either description.

4.3.2.2 Particularities for simplifications that affect α^*

The two other tests – mean D_λ and different sorption isotherms – are directly linked to the iterative method to evaluate α^*. Therefore, as they are expected to impact all system variables, all model results should be evaluated.

Besides the polarization curve and computational time evaluations – done exactly as previously presented – the properties along the through-plane direction are also analyzed. More specifically, the profiles of each property in specific current densities are investigated. These values are chosen as fractions of the analyzed

current density interval, with steps of 0.2 – that is, 0, 20%, 40% of the interval and so on until the last current density.

4.3.3 Summary of the tests

A detailed representation of each variation made is presented in Table 15 for clarity. As previously discussed, more than one condition is tested for each model. The idea is to compare the proposed variation with the results of test one, which is considered as the reference. Note that there are three conditions tied to this first test, related to the possible descriptions of the electro-osmotic drag coefficient. Nevertheless, the second and third variations (1.2 and 1.3) are only used for comparing with tests of mean D_λ, that is, tests 5.2 and 5.3, respectively.

Table 15 - Variations of the model tested.

Test number		$\Delta S_{rxn}(T)$	Reaction rate	Sorption isotherm	Water diffusivity in the membrane	Electro-osmotic drag coefficient
1	1.1	Variable	Butler-Volmer	Springer *et al.*, 1991	Variable	Springer *et al.*, 1991
	1.2	Variable	Butler-Volmer	Springer *et al.*, 1991	Variable	Meier *et* Eigenberger, 2004
	1.3	Variable	Butler-Volmer	Springer *et al.*, 1991	Variable	Piecewise linear
	2	Constant	Butler-Volmer	Springer *et al.*, 1991	Variable	Springer *et al.*, 1991
	3	Variable	Tafel	Springer *et al.*, 1991	Variable	Springer *et al.*, 1991
	4	Variable	Butler-Volmer	Kulikovsky, 2003	Variable	Springer *et al.*, 1991
5	5.1	Variable	Butler-Volmer	Springer *et al.*, 1991	Mean	Springer *et al.*, 1991
	5.2	Variable	Butler-Volmer	Springer *et al.*, 1991	Mean	Meier *et* Eigenberger, 2004
	5.3	Variable	Butler-Volmer	Springer *et al.*, 1991	Mean	Piecewise linear

Source: the author.

4.4 Statistical Analysis

Differently from all other tests, which always provide the same results under the same conditions, the measured computational time naturally oscillates between

measurements. Thus, even if the result presented is already the mean of ten tests, it is necessary to use an adequate statistical treatment to ensure that the observed differences are significant enough to draw a conclusion.

The chosen methodology is a hypothesis test for the mean value of two independent samples based on the assumption that the computational time of the program follows a normal distribution. For this analysis, the null hypothesis is that the mean value for the model without the simplifying assumption is equal to the one with them. Naturally, the alternative hypothesis is that the time for the first is larger than for the second. This comparison is made using a t-student distribution – the variance of the population is not known – with a significance of α = 0.05 and α = 0.01, but the first results are assumed as enough to draw conclusions. The critical values for the tests are evaluated with a t-student distribution using as degrees of freedom the nearest integer rounding down to the result of Equation 119 (MONTGOMERY; RUNGER, 2013, p. 387).Those are compared with the test statistic presented in Equation 120.

$$gl = \frac{\left(\frac{s_1^2}{n_1} + \frac{s_2^2}{n_2}\right)^2}{\frac{\left(\frac{s_1^2}{n_1}\right)^2}{n_1 - 1} + \frac{\left(\frac{s_2^2}{n_2}\right)^2}{n_2 - 1}} \tag{119}$$

$$t = \frac{(\bar{X}_1 - \bar{X}_2) - (\mu_1 - \mu_2)}{\sqrt{\frac{s_1^2}{n_1} + \frac{s_2^2}{n_2}}} \tag{120}$$

If the t value is larger than t_c, enough evidence exists to reject the null hypothesis under the selected significance, that is, to claim that the computational time for the simplified model is smaller than the non-simplified one.

5 RESULTS AND DISCUSSION

As seen in the methodology, special care was taken to ensure that the results are representative of as many conditions as possible. However, this implies a quantity of data that cannot be reasonably presented in this work. Therefore, though all tests were conducted, only relevant results are presented. As a general rule, polarization curve data for all tests are presented in tables, but graphs and other data, such as concentration profiles, are only shown in particular cases. The notable exception is the tests related to the assumption of mean diffusivity because the points presented in the table were found to be insufficient to represent the impact of the assumption.

5.1 Constant entropy of reaction

The comparison between the thermodynamic voltages predicted by the complete and simplified equations as a function of temperature is presented in Figure 16. It also shows the relative error between those values, given by the absolute value of their difference divided by the reference (variable entropy) value.

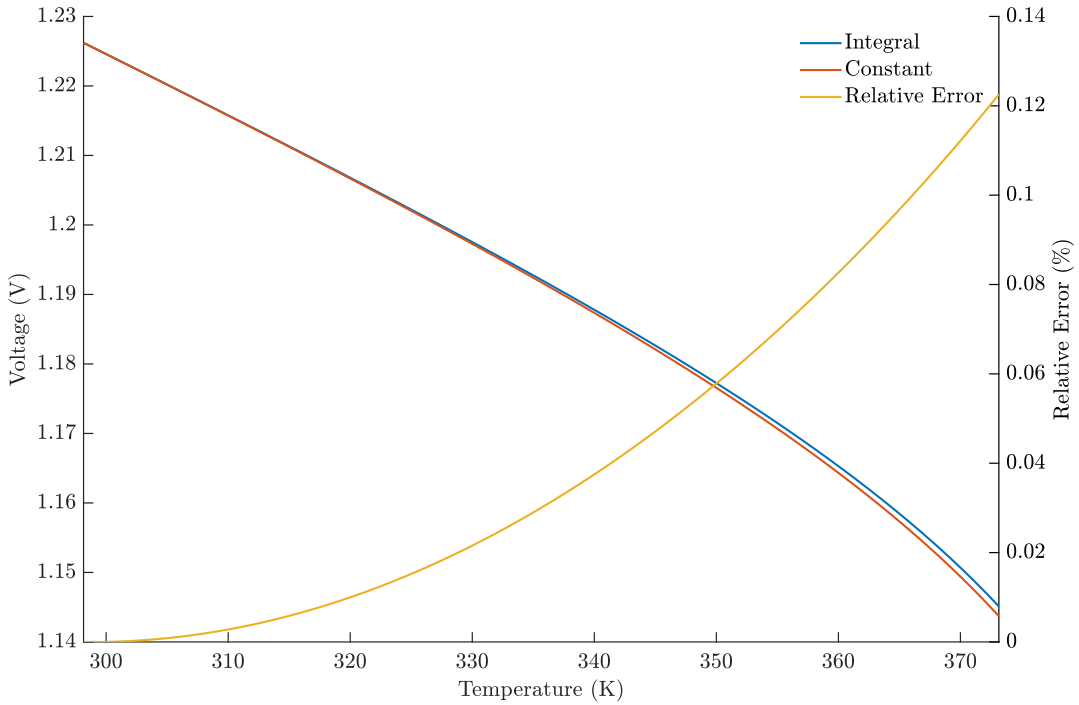

Figure 16 - Comparison between thermodynamic voltages predicted by the model. Source: the author.

Analyzing the graph, it is evident that the difference between both curves is small, with only 0.12% relative error at 373.15 K, a temperature above the operational value of PEMFCs. This indicates that the mathematical impact of the simplification is almost insignificant, which reinforces its usage in most modeling works.

Moreover, the computational time required to use both equations directly, along with the statistical analysis, are presented in Table 16. It is noticeable that a considerable improvement exists between both cases, indicating that even if the integration is done analytically, the simplified equation is still more efficiently evaluated. A high number of points was used in both cases to obtain a computational time higher than 0.1 seconds, which is recommended for the function used to evaluate the time.

Table 16 - Computational time test results for the direct analysis of the thermodynamical voltage simplification.

	100000 points		**500000 points**	
	Ref. (int)	**Constant**	**Ref. (int)**	**Constant**
Mean (s)	0.438541	0.309610	2.159197	1.556399
Std. Dev (s)	0.015355	0.003131	0.010461	0.012355
Improvement	29.40%		27.92%	
Significance	**t**	**t_c**	**t**	**t_c**
α = 0.05	26.017	1.833	117.745	1.740
α = 0.01	26.017	2.821	117.745	2.567
α = 0.05	Yes		Yes	
α = 0.01	Yes		Yes	

Source: the author.

Nevertheless, it should be noted that the time demanded per operation is considerably small. Thus, using Table 17 for the comparisons, which tests the simplification in the model instead of only the equations, can be more representative of their impact. The specific conditions of these tests were $T = 353.15\ K$, $t^M = 125\ \mu m$, and 80% relative humidity. It can be noticed that the improvement here is much smaller than in the direct comparison and has no statistical significance under either of the chosen α values.

Table 17 - Computational time test results for the model test of the thermodynamical voltage simplification.

	100 points		**500 points**	
	Ref. (int)	**Constant**	**Ref. (int)**	**Constant**
Mean (s)	2.976885	2.976645	9.794832	9.767382
Std. Dev (s)	0.024594	0.026992	0.084445	0.084810
Improvement	0.01%		0.28%	

Significance	t	t_c	t	t_c
α = 0.05	0.021	1.740	0.725	1.740
α = 0.01	0.021	2.567	0.725	2.567
α = 0.05	No		No	
α = 0.01	No		No	

Source: the author.

Therefore, it can be concluded that neglecting the temperature dependence of the reaction entropy has a small – or even insignificant for most applications – impact on the predicted value. Still, it did not yield any relevant computational advantage when used in the model. Considering this, even if an improvement is noticeable when only the equations are compared, the choice of using or not the assumption will not be relevant for most works.

5.2 Tafel Equation

Table 18 presents the nomenclature given to each test condition and the current density that first yielded zero voltage. Analyzing those values, it is noticeable that the usage of the simplification is not impacting this value enough with the used Δj of 0.01 A/cm^2 in any of the temperatures or transfer coefficients. Another interesting observation is that the change in the anodic transfer coefficient did not change the final current density – except in 3.2.3, where a slight change exists –, indicating that it has a small effect on the overvoltages.

Table 18 - Nomenclature for the activation tests.

Test	Subtest	T	$\alpha_{fwd,ano}$	$\alpha_{bwd,ano}$	$\alpha_{fwd,cat}$	$\alpha_{bwd,cat}$	j for V = 0 (BV)	j for V = 0 (Tafel)
1 (Low T)	3.1.1	333.15	0.5	0.5	1	1	1.41	1.41
	3.1.2	333.15	1	1	1	1	1.41	1.41
	3.1.3	333.15	0.5	0.5	2	2	1.61	1.61
	3.1.4	333.15	1	1	2	2	1.61	1.61
2 (High T)	3.2.1	353.15	0.5	0.5	1	1	2.30	2.31
	3.2.2	353.15	1	1	1	1	2.30	2.31
	3.2.3	353.15	0.5	0.5	2	2	2.75	2.76
	3.2.4	353.15	1	1	2	2	2.76	2.76

Source: the author.

This initial sign that the assumption is not significantly affecting the overvoltage is reinforced by comparing the activation overpotentials results – the only value directly affected by this simplification – presented in Table 19. Here, as all low-temperature

values do not reach 1.8 A/cm^2, the final value considered for them is 1.4 A/cm^2. Also, the test results with the high level of anodic transfer coefficient ($\alpha_{fwd,ano} = 1$) are omitted, as they presented no difference from the low level ($\alpha_{fwd,ano} = 0.5$) results. Still, they – and all other data tied to the polarization curve – are presented in Appendix G.

Table 19 - Activation overvoltage results for the comparison between Tafel and Butler-Volmer.

T = 333.15 K		**3.1.1**			**3.1.3**	
j (A/cm^2)	**η_{Act} (BV)**	**η_{Act} (Tafel)**	**Error (%)**	**η_{Act} (BV)**	**η_{Act} (Tafel)**	**Error (%)**
0.10	0.3353	0.3352	0.01%	0.1678	0.1678	0.03%
0.80	0.3958	0.3955	0.08%	0.1981	0.1977	0.16%
1.40	0.4121	0.4116	0.13%	0.2063	0.2058	0.26%
T = 353.15 K		**3.2.1**			**3.2.3**	
j (A/cm^2)	**η_{Act} (BV)**	**η_{Act} (Tafel)**	**Error (%)**	**η_{Act} (BV)**	**η_{Act} (Tafel)**	**Error (%)**
0.10	0.3174	0.3174	0.01%	0.1584	0.1583	0.02%
0.80	0.3809	0.3806	0.08%	0.1905	0.1903	0.15%
1.80	0.4060	0.4054	0.15%	0.2033	0.2027	0.30%

Source: the author.

The observed pattern is that the error increases with current density and with the larger cathode transfer coefficient, but even in those cases, the relative error is considerably small (less than 0.5%). This increase may seem odd, considering that Tafel is an approximation when the activation overvoltage – which increases with current density – is high, however, it is tied to the anodic behavior, where the Tafel equation may not have an adequate fit. This will be evident when the anodic fit with the linear Butler-Volmer approximation is presented at the end of this section. Furthermore, no difference is found between the different temperature level results.

Another key observation, seen in Table 20, is that the optimal point is almost the same for both equations in all tests. This reinforces the conclusion that Tafel is an adequate approximation for Butler-Volmer in PEMFC modeling.

Table 20 - Optimal points for the comparison between Tafel and Butler-Volmer.

Test	**Model**	**V (V)**	**j (A/cm^2)**	**W (W/cm^2)**
3.1.1	BV	0.5074	0.77	0.3928
	Tafel	0.5077	0.77	0.3931
3.1.2	BV	0.5076	0.77	0.3930
	Tafel	0.5077	0.77	0.3931
3.1.3	BV	0.6203	0.90	0.5604
	Tafel	0.6206	0.90	0.5607
3.1.4	BV	0.6204	0.90	0.5605

	Tafel	0.6206	0.90	0.5607
3.2.1	BV	0.4755	1.21	0.5764
	Tafel	0.4759	1.21	0.5769
3.2.2	BV	0.4757	1.21	0.5766
	Tafel	1.2122	1.21	0.5769
3.2.3	BV	0.5840	1.44	0.8432
	Tafel	0.5845	1.44	0.8439
3.2.4	BV	0.5844	1.44	0.8436
	Tafel	0.5846	1.44	0.8439

Source: the author.

As this result is homogeneous under all conditions, only the graphs of both extremes (subtests 3.1.1 and 3.2.4) are presented in Figure 17 – Figure 20 to illustrate the agreement.

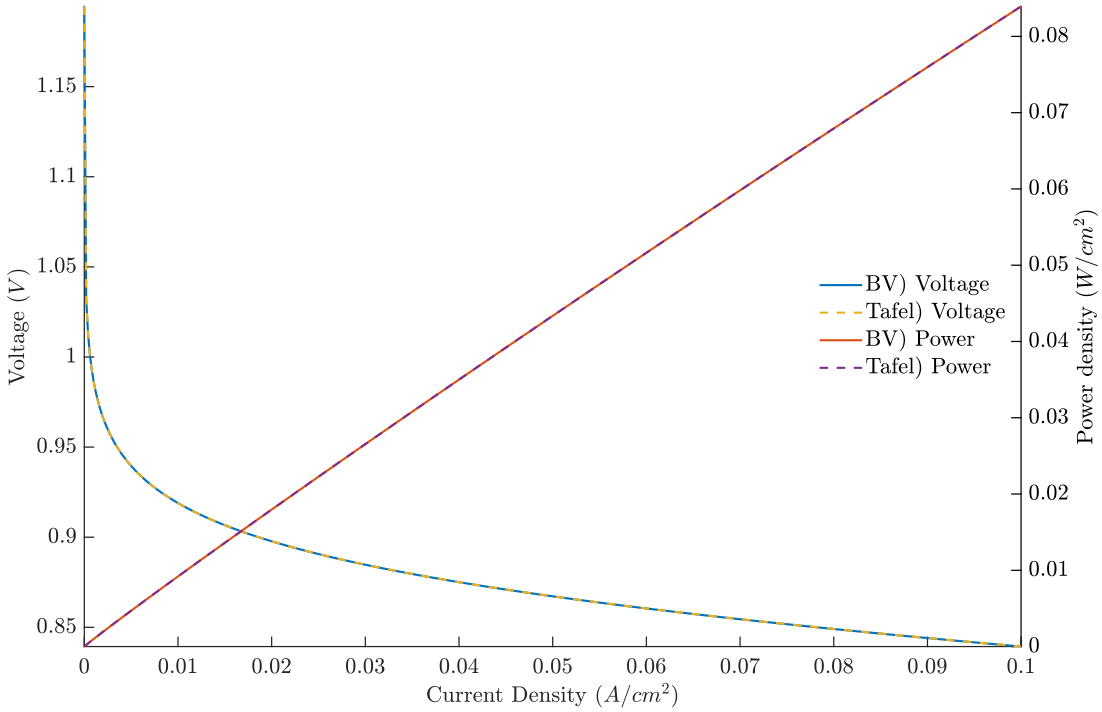

Figure 17 - Polarization curve for activation test 3.1.1.
Source: the author.

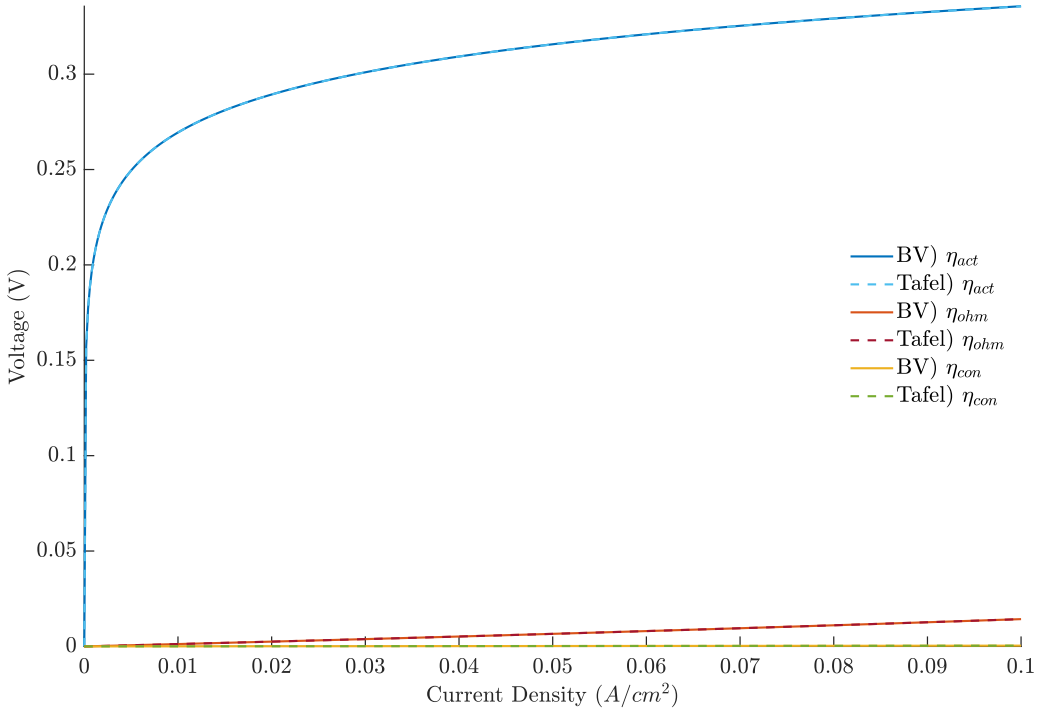

Figure 18 - Overvoltages of activation test 3.1.1.
Source: the author.

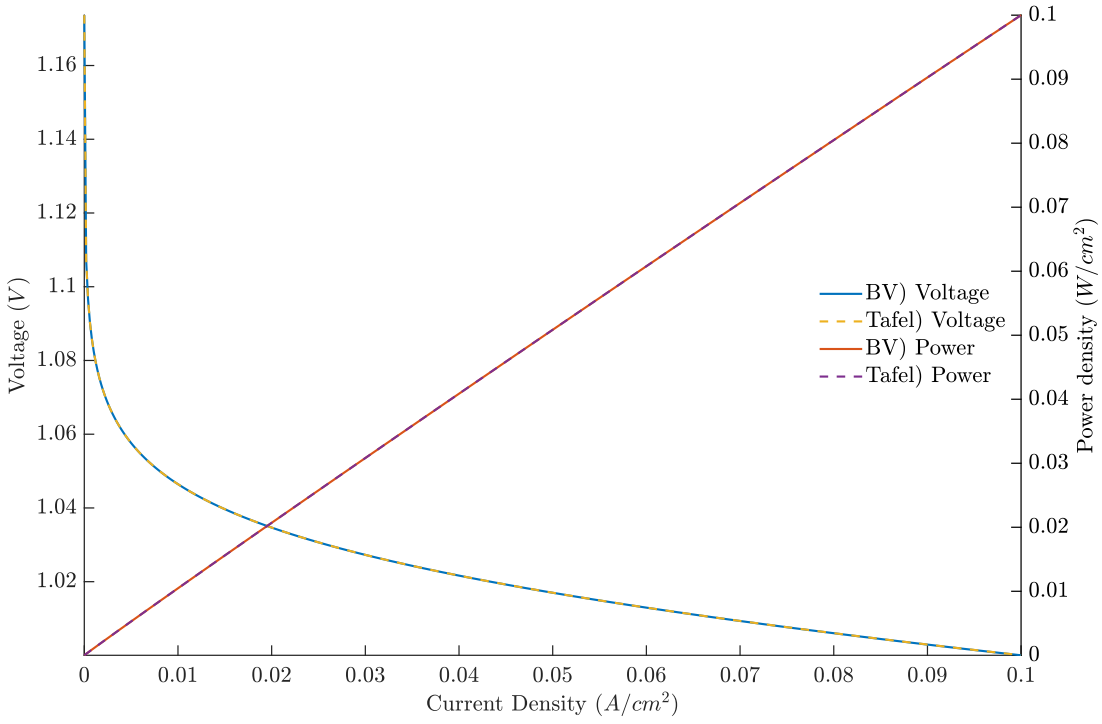

Figure 19 - Polarization curve for activation test 3.2.4.
Source: the author.

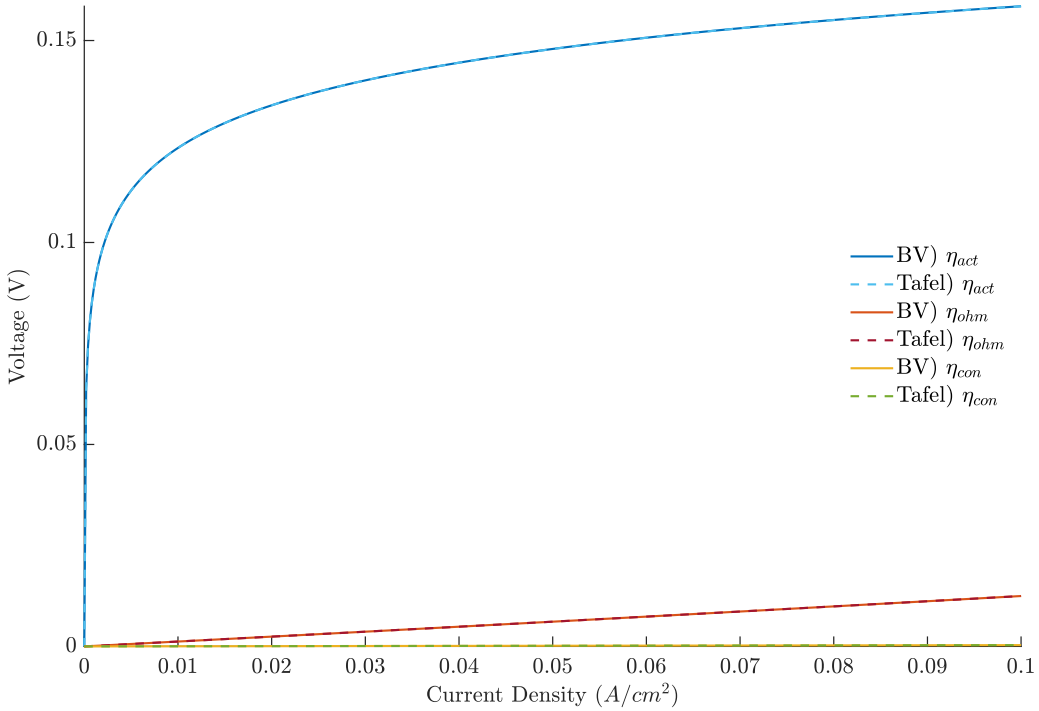

Figure 20 - Overvoltages of activation test 3.2.4.
Source: the author.

The quality of the description is also observed using the standard error of the estimate, shown in Table 21. In all the cases, the error is small, demonstrating that there is a good fit in the whole interval for all curves. Therefore, based on these results, under common PEMFC operational conditions, using the Tafel equation will not hinder in a significant manner the accuracy of the model.

Table 21 - Standard error for the comparison between Tafel and Butler-Volmer.

Experiment	Global S_e (V)	S_e 1 (V)	S_e 2 (V)	S_e 3 (V)
3.1.1	3.13E-04	7.88E-05	2.28E-04	4.26E-04
3.1.2	1.57E-04	3.94E-05	1.14E-04	2.13E-04
3.1.3	3.55E-04	1.63E-04	3.49E-04	5.13E-04
3.1.4	1.78E-04	8.16E-05	1.74E-04	2.56E-04
3.2.1	4.56E-04	8.97E-05	2.88E-04	6.01E-04
3.2.2	2.29E-04	4.49E-05	1.44E-04	3.01E-04
3.2.3	5.43E-04	2.10E-04	4.66E-04	7.57E-04
3.2.4	2.71E-04	1.05E-04	2.33E-04	3.78E-04

Source: the author.

Furthermore, regarding the computational time effect of the simplification, a similar result is also noticed in all tests: an improvement of between 2 and 4% in the computational time under both conditions (100 and 500 points). An interesting observation is that the improvement is slightly more relevant when 500 points are used,

which can be explained by the smaller number of iterations needed for the convergence of α^* in this case, as a smaller step in current density is used. This means that the iterative method constitutes a smaller part of the whole model, thus making improvements in the other areas more significant. Following what was previously done, only the results for subtests 3.1.1 and 3.2.4 are presented in Table 22 and Table 23.

Table 22 - Computational time test results for test 3.1.1.

	3.1.1) T = -1; α_A = -1 and α_C = -1			
	100 points		**500 points**	
	Ref. (BV)	**Tafel**	**Ref. (BV)**	**Tafel**
Mean (s)	3.810846	3.725712	11.295444	10.900236
Std. Dev (s)	0.034902	0.035131	0.029188	0.024070
Improvement	2.23%		3.50%	
Significance	**t**	**t_c**	**t**	**t_c**
α = 0.05	5.436	1.740	33.034	1.740
α = 0.01	5.436	2.567	33.034	2.567
α = 0.05	Yes		Yes	
α = 0.01	Yes		Yes	

Source: the author.

Table 23 - Computational time test results for test 3.2.4.

	3.2.4) T = 1; α_A = 1 and α_C = 1			
	100 points		**500 points**	
	Ref. (BV)	**Tafel**	**Ref. (BV)**	**Tafel**
Mean (s)	3.037049	2.957467	9.935707	9.522297
Std. Dev (s)	0.016201	0.009273	0.058435	0.027794
Improvement	2.62%		4.16%	
Significance	**t**	**t_c**	**t**	**t_c**
α = 0.05	13.481	1.761	20.203	1.782
α = 0.01	13.481	2.624	20.203	2.681
α = 0.05	Yes		Yes	
α = 0.01	Yes		Yes	

Source: the author.

Based on those results, it can be concluded that using the Tafel equation is beneficial for most modeling applications, as the impact on the result is insignificant. Nevertheless, it should be highlighted that even if the computational time difference exists and has statistical relevancy, the improvement is marginal. Thus, the main attractivity of this simplification is probably the additional ease of obtaining the transfer coefficients and not the time.

Finally, to further investigate the initial region of the curve, where the activation overvoltage changes rapidly, Figure 21 presents the cathodic overvoltage up to $2 \cdot 10^{-5}$

A·cm^{-2}. This is done at condition 3.2.1, but the discussions made are applicable for all others. In it, the difference with the Tafel equation is noticeable, where a better fit is obtained with the linear version of the Butler-Volmer equation (Equation 32). Nevertheless, as the current densities where this is true are restricted to such small values – with little interest for fuel cell applications –, this is not a significant downside for the usage of the Tafel Equation.

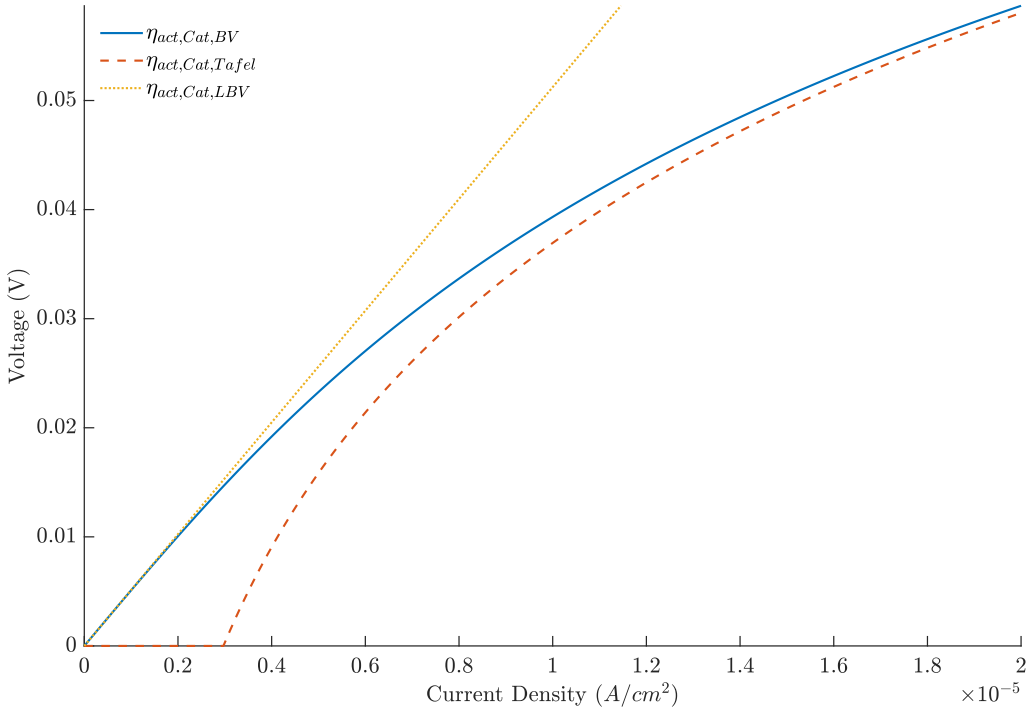

Figure 21 - Cathodic activation overvoltage comparison at small current densities for test 3.2.1. Source: the author.

On the other hand, when the anodic overvoltage is considered – Figure 22 – the results are different. The linear approximation holds for the whole domain, while the Tafel equation always predicts – due to the previously mentioned correction – the value zero. Note also that the domain is much larger here, going up to 0.1 A·cm^{-2}, further highlighting that this approximation is adequate under anodic conditions. However, considering that the anodic overvoltage predicted is four orders of magnitude smaller than the cathodic one, neglecting this term, as done in some works, is a viable alternative.

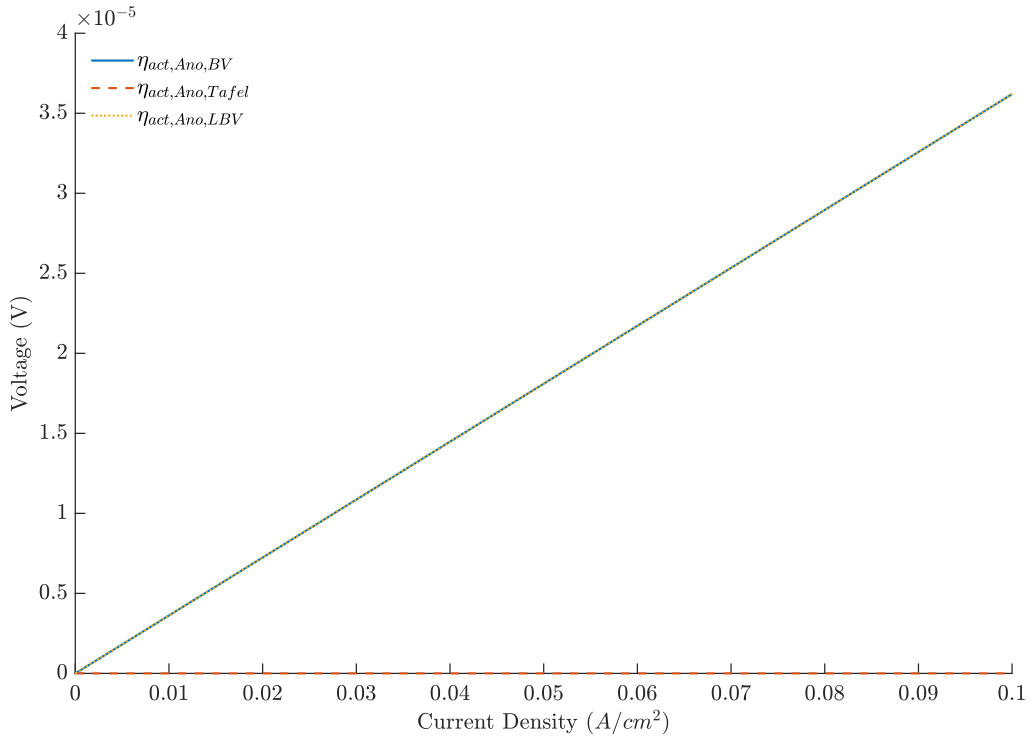

Figure 22 - Anodic activation overvoltage comparison for test 3.2.1.
Source: the author.

Observing this anodic and cathodic behavior separately further clarifies the previously presented explanation as to why the error on the activation overvoltage was increasing with current density. While the cathodic error rapidly reaches values close to zero, the anodic keeps increasing. Nevertheless, as the anodic overvoltage is much smaller than the cathodic one, even in high current densities, the error does not reach significant values.

Therefore, under all tested conditions, the usage of the Tafel equation for the cathodic activation overvoltage and the linear approximation of the Butler-Volmer equation for the anodic one is, in practical terms, as effective as using the complete Butler-Volmer equation.

5.3 Different Sorption Isotherms

Differently from the two previous tests, as the transport is affected by the sorption isotherm, all model results should be evaluated here. Table 24 explains all the tests made, as well as the final current density for each case.

Table 24 - Explanation of the sorption isotherm tests.

Test	Subtest	T	RH	t_M (μm)	j for V = 0 (Sp.)	j for V = 0 (Ku.)
1 (Low T)	1.1	333.15	60%	50	3.15	2.94
	1.2	333.15	60%	125	1.29	1.20
	1.3	333.15	80%	50	3.41	3.21
	1.4	333.15	80%	125	1.41	1.32
2 (High T)	2.1	353.15	60%	50	4.79	4.52
	2.2	353.15	60%	125	2.04	1.88
	2.3	353.15	80%	50	5.12	4.98
	2.4	353.15	80%	125	2.30	2.21

Source: the author.

Firstly, the overvoltage results are compared, starting with the ohmic overvoltage presented in Table 25. Note that for tests 4.1.2 and 4.1.4, where the maximum voltage does not reach 1.80 A/cm^2, the last point used for the comparison is 1.20 A/cm^2.

Table 25 - Ohmic overvoltage results for different sorption isotherms.

T = 333.15 K							
4.1.1				**4.1.2**			
j (A/cm^2)	**Springer**	**Kulikovsky**	**Error (%)**	**j (A/cm^2)**	**Springer**	**Kulikovsky**	**Error (%)**
0.10	0.0053	0.0079	48.40%	0.10	0.0149	0.0217	45.34%
0.80	0.0690	0.0862	24.88%	0.80	0.3255	0.3740	14.92%
1.80	0.2674	0.3089	15.50%	1.20	0.6735	0.7815	16.04%
4.1.3				**4.1.4**			
j (A/cm^2)	**Springer**	**Kulikovsky**	**Error (%)**	**j (A/cm^2)**	**Springer**	**Kulikovsky**	**Error (%)**
0.10	0.0053	0.0068	28.17%	0.10	0.0143	0.0182	27.58%
0.80	0.0649	0.0799	23.19%	0.80	0.3003	0.3414	13.70%
1.80	0.2471	0.2843	15.03%	1.20	0.5875	0.6604	12.40%
T = 353.15 K							
4.2.1				**4.2.2**			
j (A/cm^2)	**Springer**	**Kulikovsky**	**Error (%)**	**j (A/cm^2)**	**Springer**	**Kulikovsky**	**Error (%)**
0.10	0.0094	0.0114	21.62%	0.10	0.0249	0.0301	21.12%
0.80	0.0733	0.0911	24.41%	0.80	0.2276	0.2701	18.68%
1.80	0.1568	0.2068	31.87%	1.80	0.6317	0.7216	14.23%
4.2.3				**4.2.4**			
j (A/cm^2)	**Springer**	**Kulikovsky**	**Error (%)**	**j (A/cm^2)**	**Springer**	**Kulikovsky**	**Error (%)**
0.10	0.0048	0.0070	46.84%	0.10	0.0127	0.0186	47.07%
0.80	0.0443	0.0613	38.35%	0.80	0.1602	0.1979	23.52%
1.80	0.1370	0.1651	20.51%	1.80	0.5271	0.5719	8.50%

Source: the author.

The overvoltages are significantly different, indicating that changing the isotherm resulted in considerable variation in the membrane's resistivity. The variation is remarkably high at 0.10 A/cm^2 when the relative error is analyzed, but its absolute value is smaller at this point. In higher current densities, even if the relative error is smaller, it is still significant. It should also be noted that under all conditions, the overvoltage difference is high (more than 10% in almost every case), with emphasis on the low humidity test for low temperature and high humidity ones for high temperature, which presented especially large differences at 0.10 A/cm^2. This shows that the usage of different isotherms will have a noticeable impact regardless of the conditions.

Moreover, the concentration overvoltage results are presented in Table 26.

Table 26 - Concentration overvoltage results for different sorption isotherms.

T = 333.15 K							
4.1.1				**4.1.2**			
j (A/cm^2)	**Springer**	**Kulikovsky**	**Error (%)**	**j (A/cm^2)**	**Springer**	**Kulikovsky**	**Error (%)**
0.10	0.0004	0.0004	0.00%	0.10	0.0004	0.0004	0.01%
0.80	0.0033	0.0033	0.03%	0.80	0.0034	0.0034	0.08%
1.80	0.0083	0.0083	0.14%	1.20	0.0053	0.0053	0.27%
4.1.3				**4.1.4**			
j (A/cm^2)	**Springer**	**Kulikovsky**	**Error (%)**	**j (A/cm^2)**	**Springer**	**Kulikovsky**	**Error (%)**
0.10	0.0004	0.0004	0.04%	0.10	0.0004	0.0004	0.02%
0.80	0.0034	0.0034	0.09%	0.80	0.0036	0.0036	0.12%
1.80	0.0087	0.0087	0.34%	1.20	0.0056	0.0056	0.35%
T = 353.15 K							
4.2.1				**4.2.2**			
j (A/cm^2)	**Springer**	**Kulikovsky**	**Error (%)**	**j (A/cm^2)**	**Springer**	**Kulikovsky**	**Error (%)**
0.10	0.0004	0.0004	0.00%	0.10	0.0005	0.0005	0.01%
0.80	0.0038	0.0038	0.10%	0.80	0.0039	0.0039	1.28%
1.80	0.0094	0.0096	2.19%	1.80	0.0100	0.0100	0.10%
4.2.3				**4.2.4**			
j (A/cm^2)	**Springer**	**Kulikovsky**	**Error (%)**	**j (A/cm^2)**	**Springer**	**Kulikovsky**	**Error (%)**
0.10	0.0005	0.0005	0.01%	0.10	0.0005	0.0005	0.02%
0.80	0.0041	0.0041	0.06%	0.80	0.0043	0.0043	0.52%
1.80	0.0108	0.0108	0.19%	1.80	0.0112	0.0113	0.15%

Source: the author.

The error here is much smaller than what is observed for the ohmic overvoltage, indicating that the changes in the water concentration on the membrane are probably much more impactful for the voltage prediction than the changes in the reactant's molar fraction. Nevertheless, it is important to highlight that under all conditions, the

concentration overvoltage is always small compared to the others, which can be the reason for this behavior. Thus, considering that the concentration overvoltage has a logarithmic relation with concentration – thus its effect would be better evaluated if smaller concentrations are reached – a more conservative conclusion would be that the usage of the different isotherms does not considerably affect the concentration overvoltage when neither reactant is depleted.

In addition to the previous analysis, the standard error of the estimate for all tests is presented in Table 27. The results show that the error is significant in every case, and is smaller before the ohmic region. This reinforces all previous discussions.

Table 27 - Standard error for the comparison of sorption isotherms.

Experiment	Global S_e (V)	S_e 1 (V)	S_e 2 (V)	S_e 3 (V)
4.1.1	4.67E-02	8.42E-03	2.81E-02	6.94E-02
4.1.2	4.87E-02	1.26E-02	3.33E-02	7.25E-02
4.1.3	4.18E-02	6.28E-03	2.67E-02	5.92E-02
4.1.4	4.32E-02	8.73E-03	2.92E-02	6.21E-02
4.2.1	4.37E-02	7.05E-03	3.80E-02	5.32E-02
4.2.2	6.10E-02	8.70E-03	3.52E-02	8.24E-02
4.2.3	3.24E-02	9.96E-03	2.69E-02	4.01E-02
4.2.4	3.78E-02	1.50E-02	3.64E-02	4.45E-02

Source: the author.

To further demonstrate the discussed overvoltage behaviors, Figure 23 – Figure 26 show the polarization and overvoltage curves for tests 4.1.1 and 4.2.4, the two extremes. In those curves, it is noticeable that the ohmic overvoltage is the main cause for the large difference in the profiles.

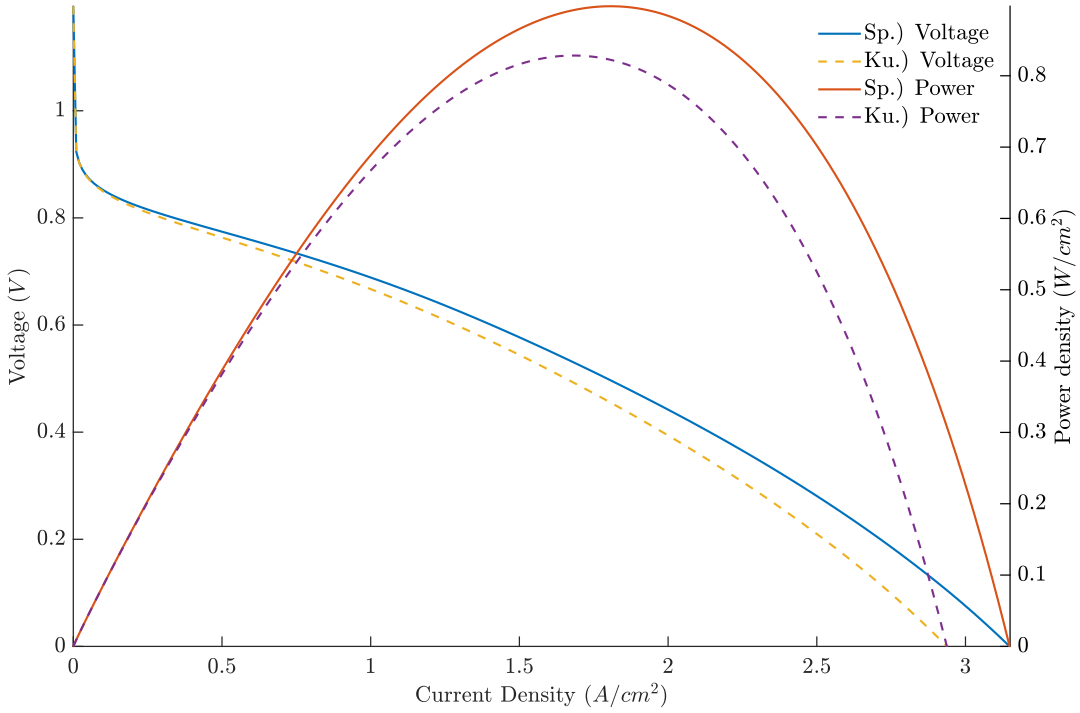

Figure 23 - Polarization result for test 4.1.1.
Source: the author.

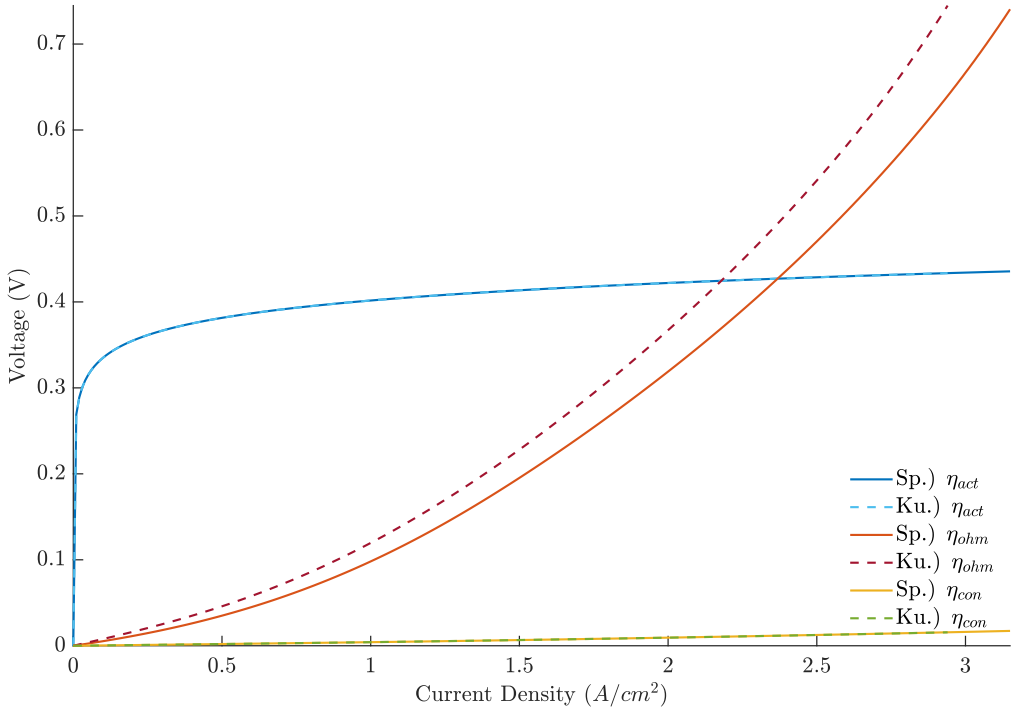

Figure 24 - Overvoltages for test 4.1.1.
Source: the author.

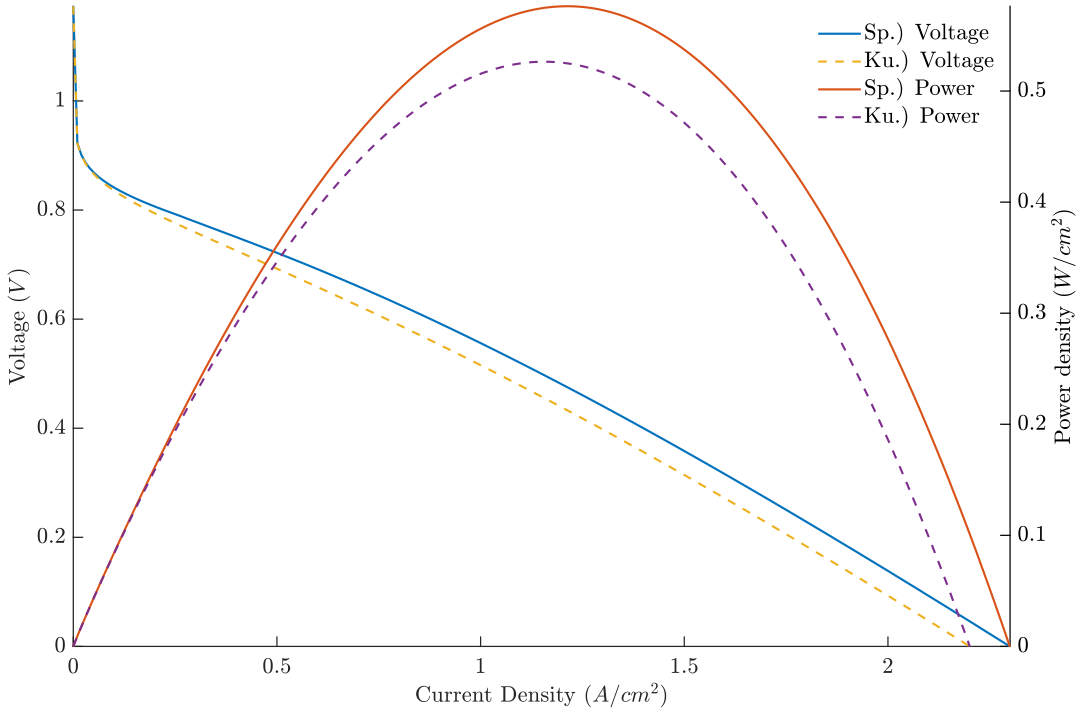

Figure 25 - Polarization result for test 4.2.4.
Source: the author.

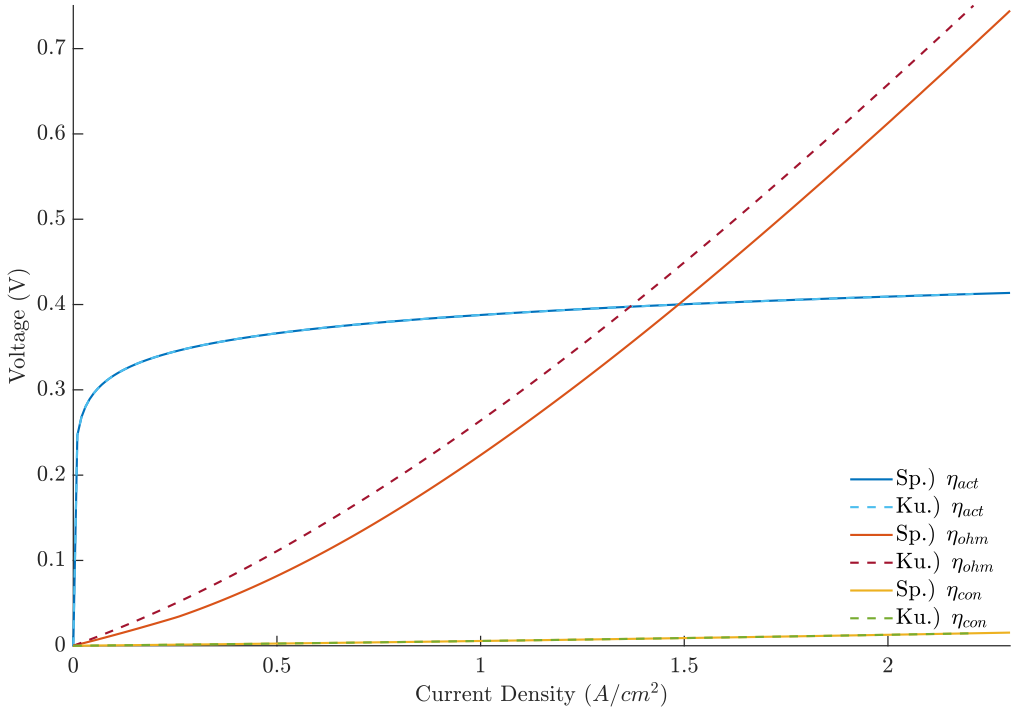

Figure 26 - Overvoltages for test 4.2.4.
Source: the author.

Other results tied to the polarization curve can be found in Appendix H, where it can be seen that the change of isotherm considerably impacted the predicted cell

voltage. Also, it is clear that the activation overvoltage is not significantly affected by this change, especially considering that bulk values – and not TPB ones – are used in the evaluation of the exchange current density in this overpotential.

Besides the polarization analysis, the concentration profiles of both cases are compared. Figure 27 presents them for test 4.1.1, and Figure 28 shows the ones for 4.2.4.

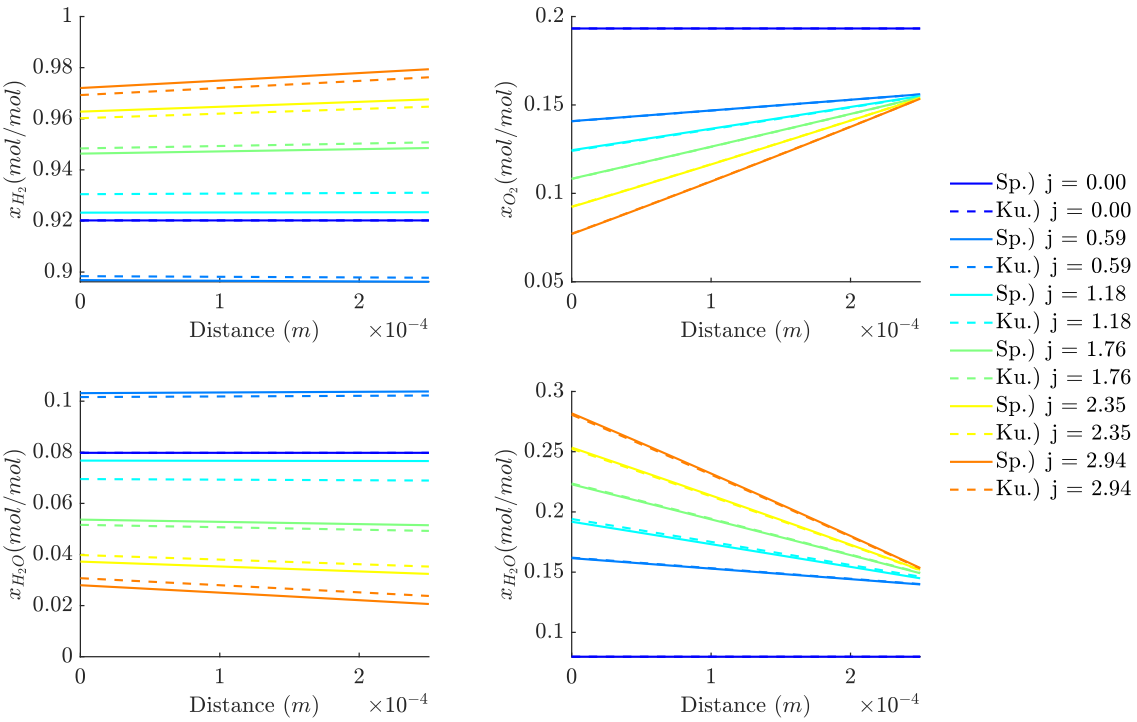

Figure 27 - Concentration profiles for test 4.1.1 .
Source: the author.

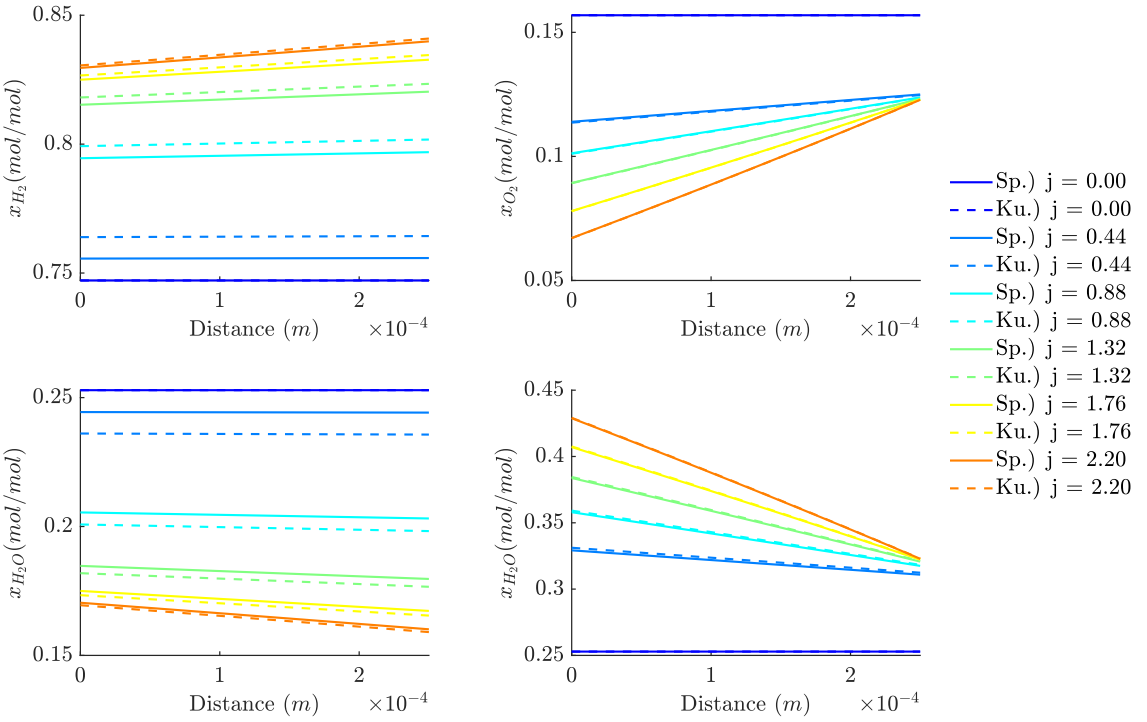

Figure 28 - Concentration profiles for test 4.2.4.
Source: the author.

As can be seen, the cathodic results are practically identical, indicating that the usage of different isotherms does not interfere significantly with the description of the diffusion in this electrode, even if it is indirectly coupled in the system due to water transport. Nevertheless, variations in the profiles are evident at the anode. Although they should not cause a noticeable impact on the concentration overvoltage because the hydrogen content is high, the variation in water content at the electrode/electrolyte interface may be responsible for some part of the ohmic overvoltage difference between the submodels. These behaviors are also observed in all other profiles, though they are not directly presented for the sake of brevity. This is aligned with the previous observation that the concentration overvoltage did not change significantly between both cases, but ohmic overvoltage is impacted. Thus, the cathodic concentration profiles, under the tested conditions, do not have a high sensitivity with the used sorption isotherm, but the impact on the anode may be among the causes for the observed effect on ohmic overvoltage.

Moreover, the λ profiles in the membrane under the same conditions are presented in Figure 29 and Figure 30.

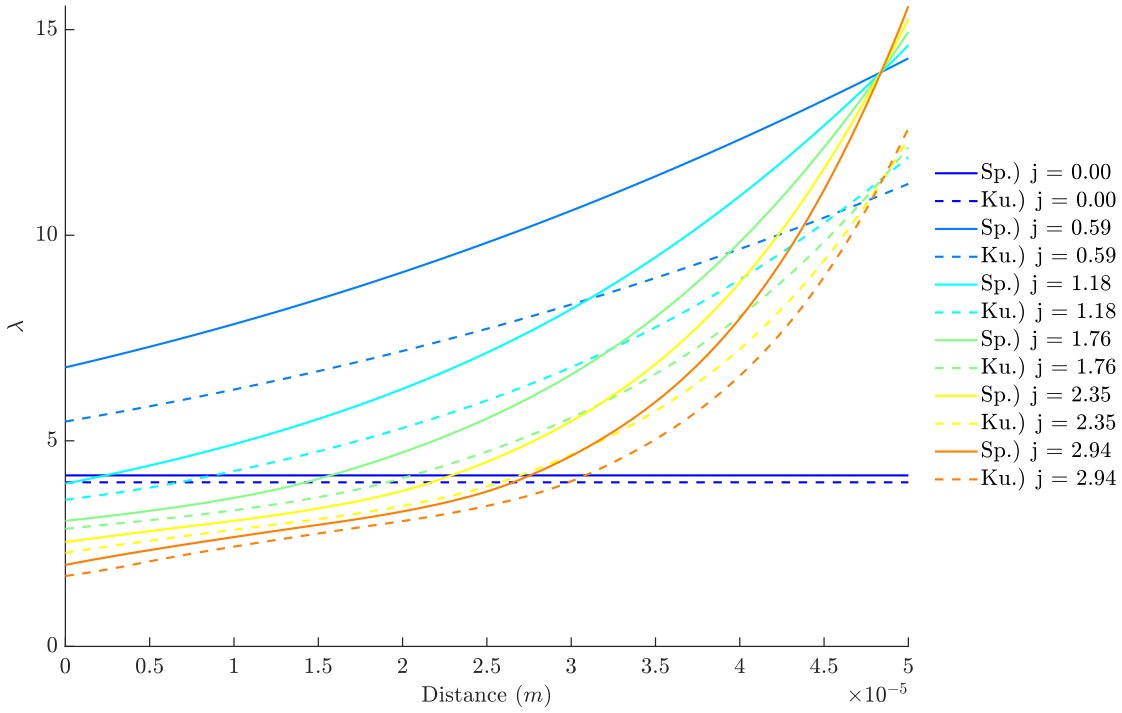

Figure 29 - λ profile for test 4.1.1.
Source: the author.

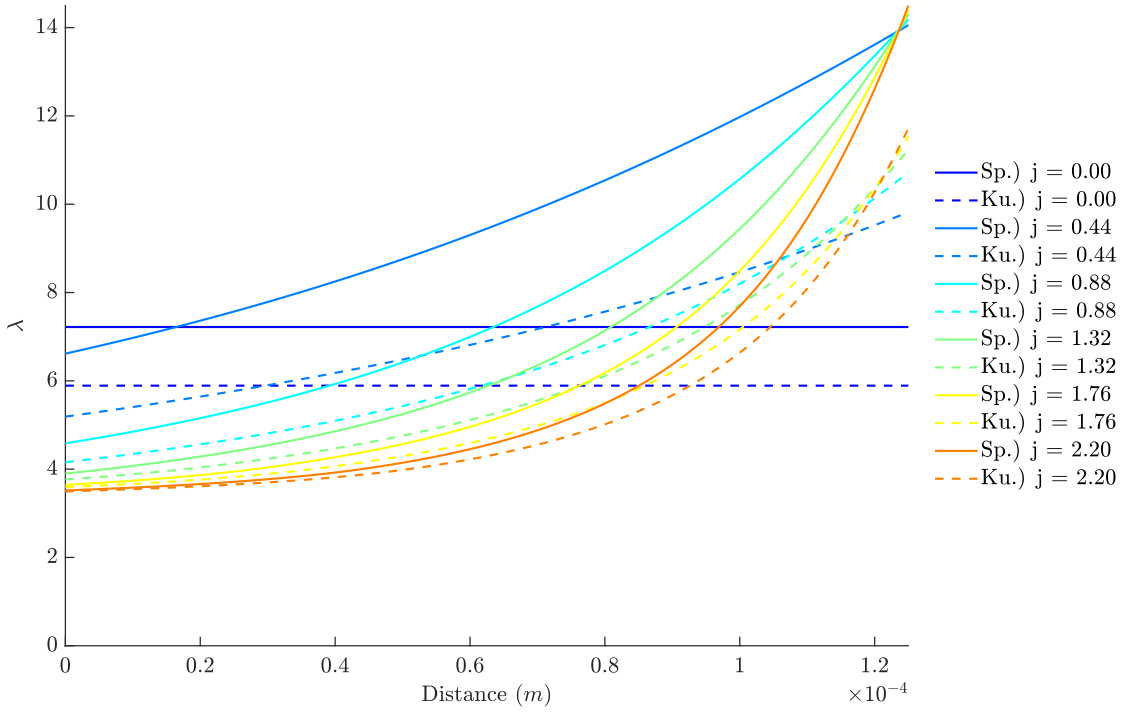

Figure 30 - λ profile for test 4.2.4.
Source: the author.

In those tests, as in all others, the profiles varied significantly between both conditions. The effect of changing the boundary conditions of the transport equation

used in the membrane is more noticeable at the cathode and for low current densities, but is still relevant for higher values in the anode. This also corroborates with the polarization results because this large difference in λ profiles causes a remarkable variation in the resistivity of the membrane, resulting in the ohmic overpotential difference. Hence, considering the significant effect on the ohmic overvoltage, the description of the water concentration inside the membrane shows itself as a crucial part of the model.

The computational time results are present in Appendix H as well. They are not extensively discussed because one isotherm is not a simplification of the other, thus there is not a direct interest in reducing computational time when one is chosen. Analyzing them, this is further highlighted because different isotherms present a lower computational time under different conditions, indicating that there is no intrinsic computational advantage of using a specific strategy.

Therefore, the selection of the sorption isotherm is expected to considerably affect the model. The changes produced in the λ values at the membrane's interface cause large changes in its water profile, which significantly affects the ohmic overvoltage. Also, because the water transport couples the control volumes, the anodic concentration profile is remarkably affected by the change of isotherm, but the cathodic one remains mostly unaltered. However, at least in conditions without hydrogen depletion, the observed differences do not affect the concentration overvoltage relevantly, though they are likely contributing to increasing the ohmic overvoltage difference. This highlights the importance of using an isotherm that specifically describes the relation for the used membrane, reinforcing Dickinson and Smith's (2020) advice that using a relation developed for other membranes, even of the same family, is not recommended. Furthermore, this shows that the lack of data for modern membranes is a significant hindrance to obtaining accurate fuel cell models.

5.4 Mean Water Diffusivity in the Electrolyte

Before discussing this section's results, it is worth pointing out that an article discussing this assumption was published by the author (CARNEIRO et al., 2024).

There, the analysis is done under slightly different cell conditions, but the same conclusions are reached, which further supports both works.

Table 28 presents the nomenclature and test conditions for all variations of the model used for this evaluation. They are divided into three major groups, classified using the electro-osmotic drag coefficient because different descriptions of this parameter imply different analytical equations when the simplification is used.

Table 28 - Test conditions for the mean water diffusivity evaluation.

Test	Subtest	T	RH	t_M (μm)	j for V = 0 (Var.)	j for V = 0 (Mean)
5.1 (Springer)	5.1.1	333.15	60%	50	3.15	2.99
	5.1.2	353.15	60%	50	4.79	4.86
	5.1.3	333.15	80%	50	3.41	3.28
	5.1.4	353.15	80%	50	5.12	5.13
	5.1.5	333.15	60%	125	1.29	1.22
	5.1.6	353.15	60%	125	2.04	2.07
	5.1.7	333.15	80%	125	1.41	1.36
	5.1.8	353.15	80%	125	2.30	2.31
5.2 (ME)	5.2.1	333.15	60%	50	1.25	1.21
	5.2.2	353.15	60%	50	2.36	2.29
	5.2.3	333.15	80%	50	1.34	1.30
	5.2.4	353.15	80%	50	3.04	2.93
	5.2.5	333.15	60%	125	0.50	0.48
	5.2.6	353.15	60%	125	0.96	0.93
	5.2.7	333.15	80%	125	0.54	0.52
	5.2.8	353.15	80%	125	1.27	1.22
5.3 (PL)	5.3.1	333.15	60%	50	1.71	1.71
	5.3.2	353.15	60%	50	3.51	3.50
	5.3.3	333.15	80%	50	1.86	1.85
	5.3.4	353.15	80%	50	4.73	4.72
	5.3.5	333.15	60%	125	0.68	0.68
	5.3.6	353.15	60%	125	1.44	1.44
	5.3.7	333.15	80%	125	0.74	0.74
	5.3.8	353.15	80%	125	2.08	2.08

Source: the author.

On preliminary analysis, it is clear that a major difference exists between the behavior of the different electro-osmotic drag coefficients. The final current density is larger when Springer's description is used than with the piecewise linear model, which itself has higher values than Meier *et* Eigenberger's description. Even if the objective of this work is not to compare the electro-osmotic drag descriptions directly, it is worth

noting that they appear to have a far greater impact on the model than any of the tested simplifications. Specific details of each condition are presented in their subsections.

5.4.1 Springer *et al.*, 1991

The behavior observed on the polarization curves varies significantly among the tests. However, this variation can be related to the test conditions, indicating that the validity of the simplification depends on them. Firstly, all tests at the low-temperature level presented considerable deviations after the activation region, with higher values near the optimal point and lower on the final part of the curve. This can be seen in Figure 31, presenting results for test 5.1.1.

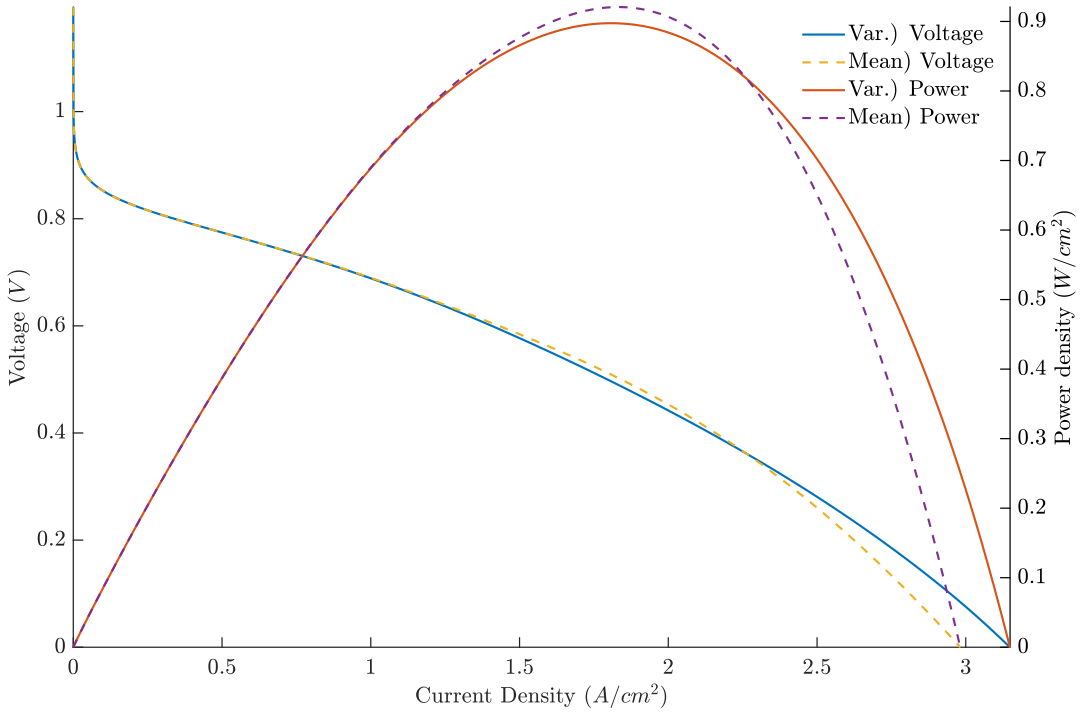

Figure 31 - Polarization results for test 5.1.1.
Source: the author.

On the other hand, tests with the high-temperature level but low humidity still had significant differences after the activation region, however, the general profile is maintained with the simplification. Also, in both of those tests, a noticeable slope change happens at a point in the ohmic region. This can be seen in Figure 32, relative to test 5.1.2. The cause for this change is likely the sudden change in the behavior of

the sorption isotherm that happens from a_{H_2O} lower and larger than one. This is a limitation of the single-phase cell assumption, as the transition in behavior is expected to be smother if the gradual formation of liquid water is modeled.

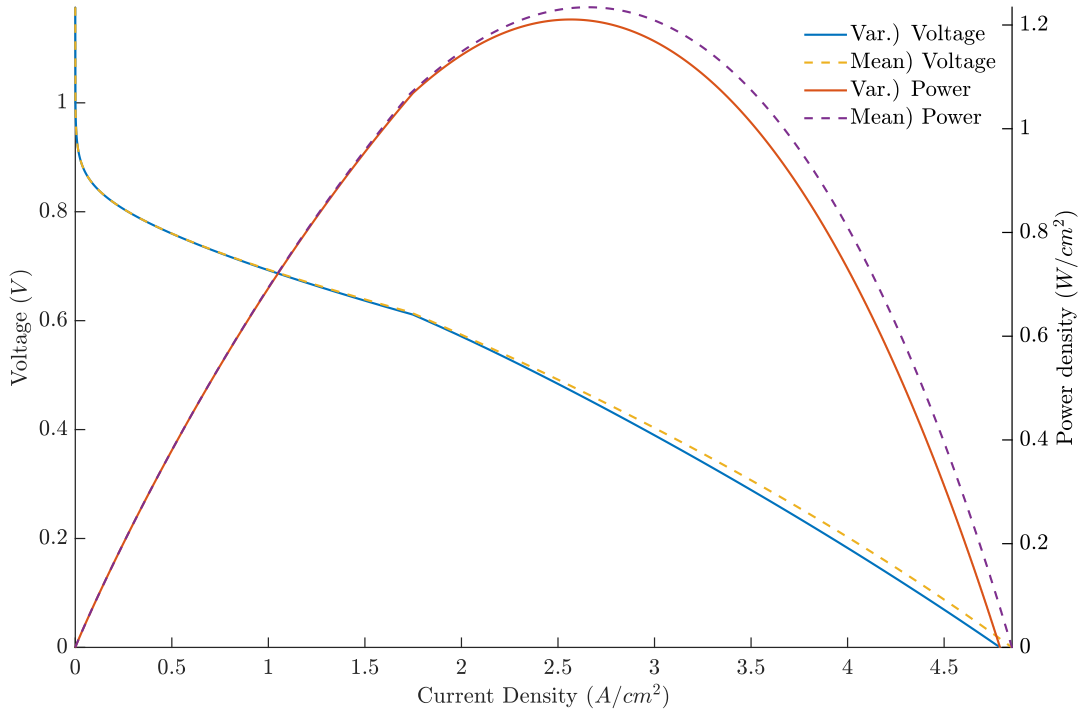

Figure 32 - Polarization results for test 5.1.2.
Source: the author.

The last observed behavior has a good fit throughout the polarization curve, as presented in Figure 33. This happened for both tests with high temperature and humidity levels. An important observation is that the membrane thickness did not interfere much with the quality of the simplification: when a bad fit was obtained with a thin membrane, it also happened with a thicker one.

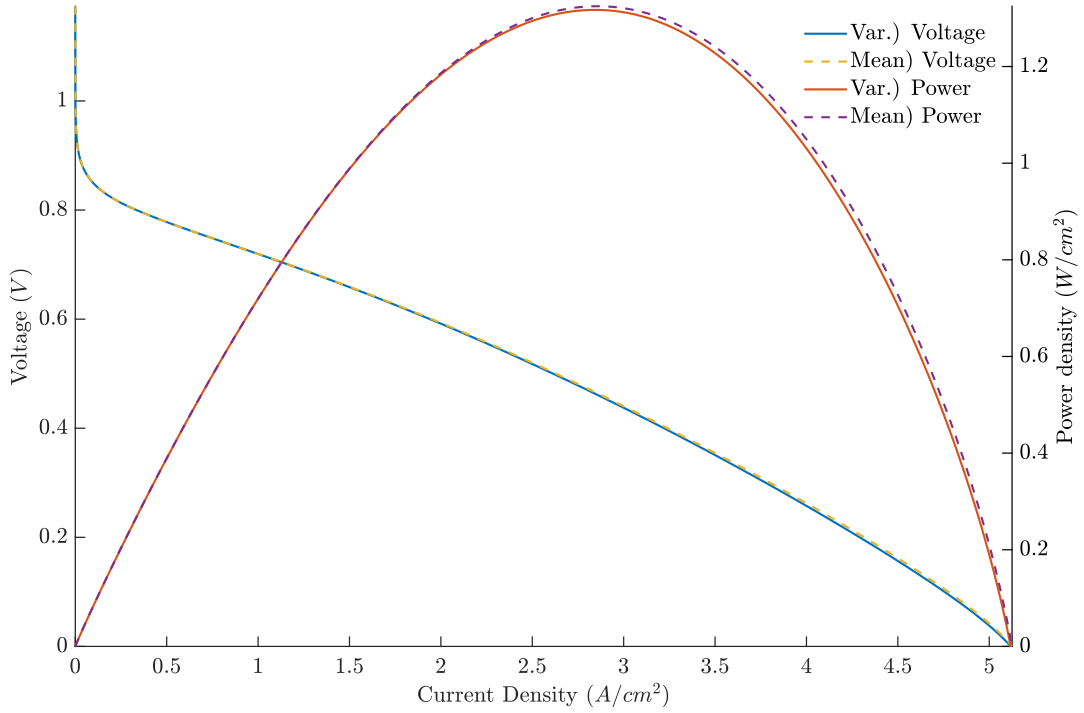

Figure 33 - Polarization results for test 5.1.4.
Source: the author.

The standard error of the estimate for all those tests – shown in Table 29 – corroborates with this previous analysis. Note that the error is small in the activation region, but increases in the others. However, this increase is smaller in tests 5.1.4 and 5.1.8, the ones with a higher humidity and temperature level.

Table 29 - Standard error for polarization curves of tests 5.1.

Experiment	Global S_e (V)	S_e 1 (V)	S_e 2 (V)	S_e 3 (V)
5.1.1	2.29E-02	5.57E-05	5.95E-03	3.60E-02
5.1.2	1.18E-02	1.05E-04	2.93E-03	1.66E-02
5.1.3	1.43E-02	2.86E-05	4.25E-03	2.14E-02
5.1.4	3.00E-03	1.19E-05	1.32E-03	4.14E-03
5.1.5	2.44E-02	1.92E-04	7.48E-03	3.90E-02
5.1.6	1.37E-02	2.04E-04	5.87E-03	1.84E-02
5.1.7	1.47E-02	1.29E-04	5.69E-03	2.22E-02
5.1.8	2.75E-03	3.58E-05	1.64E-03	3.67E-03

Source: the author.

Moreover, for all the tests, this deviation occurs at approximately the same current density for the α* curve. This is exemplified by Figure 34 and Figure 35, presenting the results for tests 5.1.1 and 5.1.2, respectively.

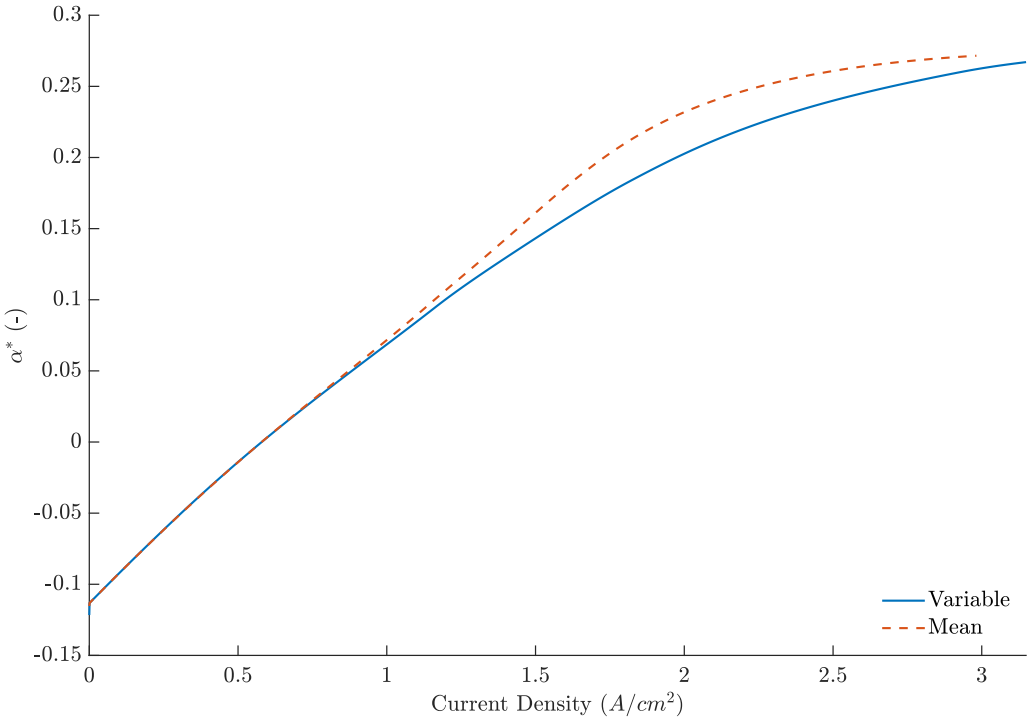

Figure 34 - α* values for test 5.1.1.
Source: the author.

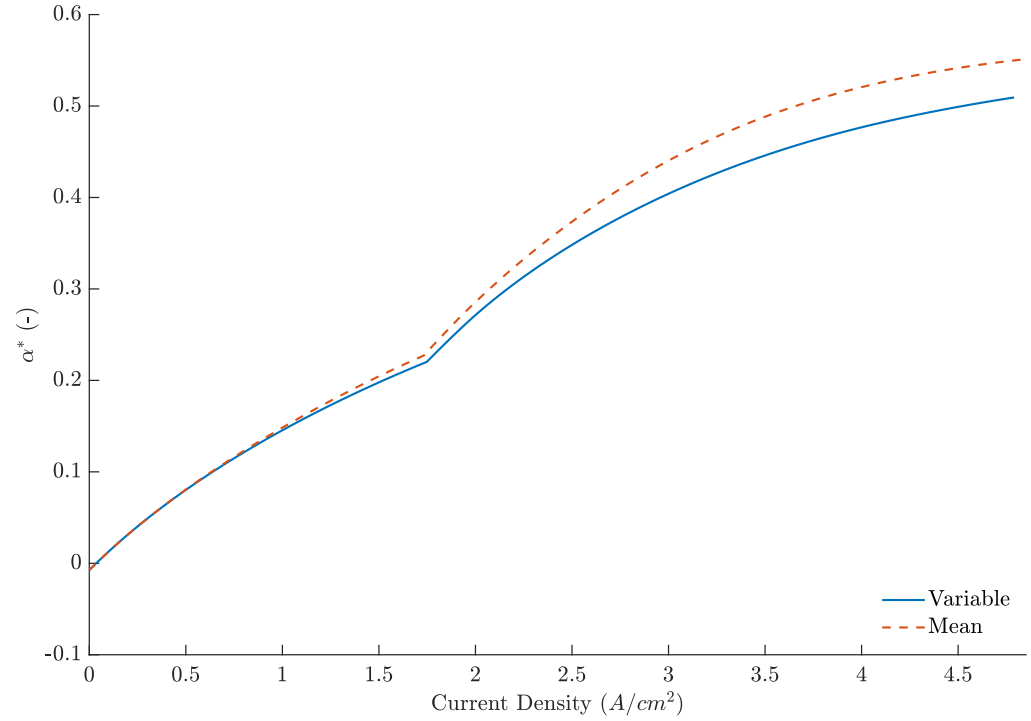

Figure 35 - α* values for test 5.1.2.
Source: the author.

Considering this correlation, it can be concluded that the simplifying assumption is causing a deviation in the transport behavior inside the membrane. This may lead to

effects on the concentration profiles because both transports are coupled due to their dependence on α^*. Appendix I explores this impact, where the influence of the water concentration profiles in the anode – linked to λ_{Ano} – is demonstrated to be significant for the ohmic overvoltage.

To further investigate these effects, it is useful to analyze the λ profiles because the sorption isotherm tests have highlighted its importance for the description of the ohmic overvoltage. These profiles are shown in Figure 36 to Figure 38, which present the results for the same tests of the polarization curves.

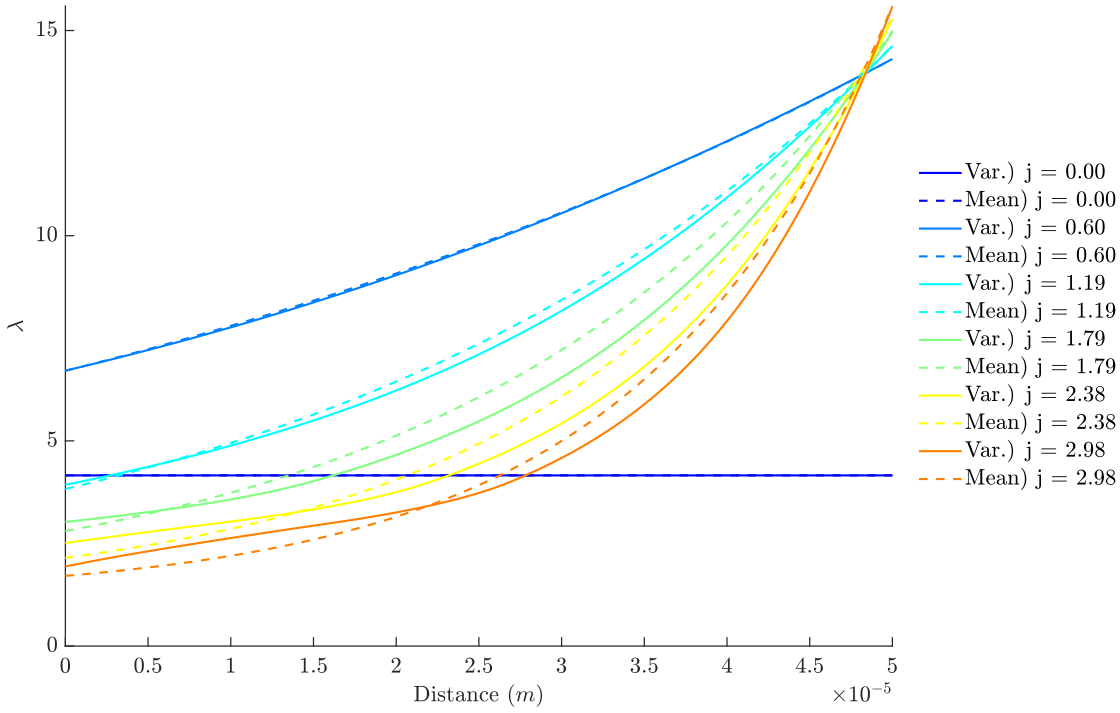

Figure 36 - λ profile for test 5.1.1
Source: the author.

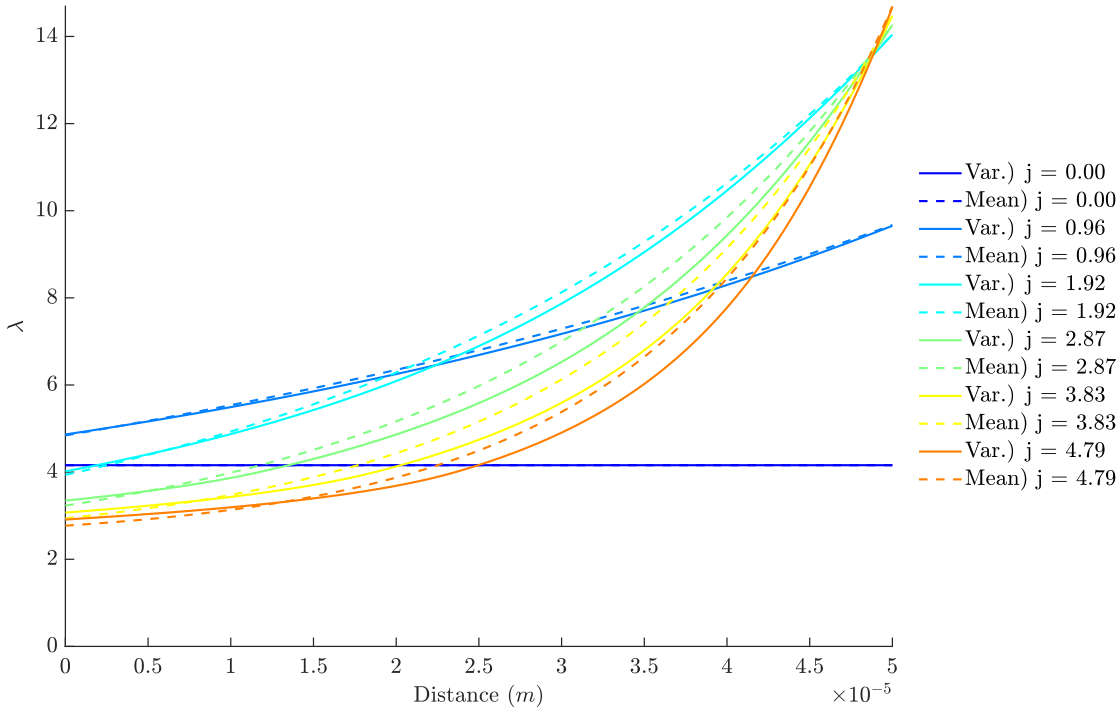

Figure 37 - λ profile for test 5.1.2.
Source: the author.

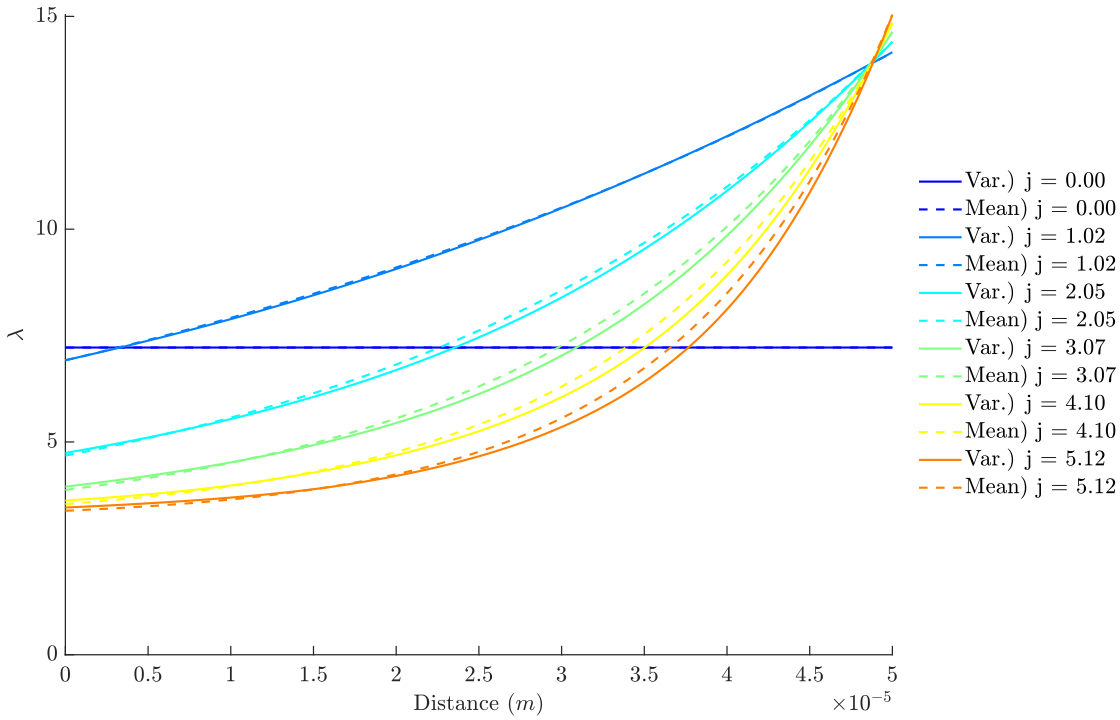

Figure 38 - λ profile for test 5.1.4.
Source: the author.

As can be seen, the results are coherent with the polarization ones. The difference between the profiles obtained with and without the simplifying assumption

in the low-temperature test is considerable, with an evident deviation seen near the anode and near the cathode. As for the results with high temperature and low humidity, the difference in profiles is still significant, but it is smaller near the anode. Finally, the ones with high temperature and humidity had the best agreement, though still not a great one, where the general profile of the curve is followed.

A pattern common to all the curves is that when higher current densities are reached, the λ values near the anode are underestimated, while they are overestimated in the rest of the membrane when the simplifying assumption is used. Another key observation is that the deviations are considerably larger in curves that reach λ values smaller than 4. Both of those remarks can be explained by the peak in diffusivity near $\lambda = 4$ in the used description for the diffusion coefficient, which makes the mean underestimate D_λ at values near the peak and overestimate them everywhere else. This explanation is also congruent with the observed results. Lowering the temperature decreases the saturation pressure, and, as the relative humidity and inlet pressure are fixed, this implies a lower water quantity in the cell. Also, reducing the relative humidity directly affects the amount of water present, lowering the λ values at the interfaces. This can result in values near the mentioned peak being reached. To highlight this effect, an additional simulation was made under the same conditions as test 5.1.4 – that is, $t^M = 50\ \mu m$ and $T = 353.15\ K$ – but with 100% relative humidity. The polarization curve, lambda profiles, and α* values of this test are presented in Figure 39, Figure 40, and Figure 41 respectively.

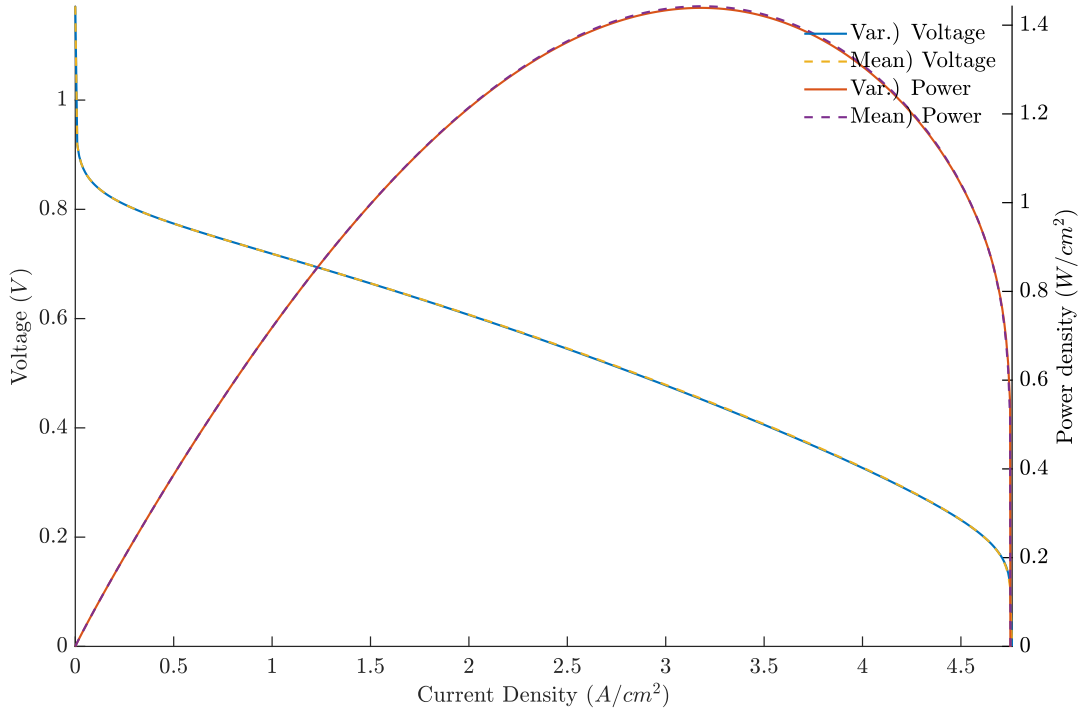

Figure 39 - Polarization curve for test 5.1.4 with 100% relative humidity.
Source: the author.

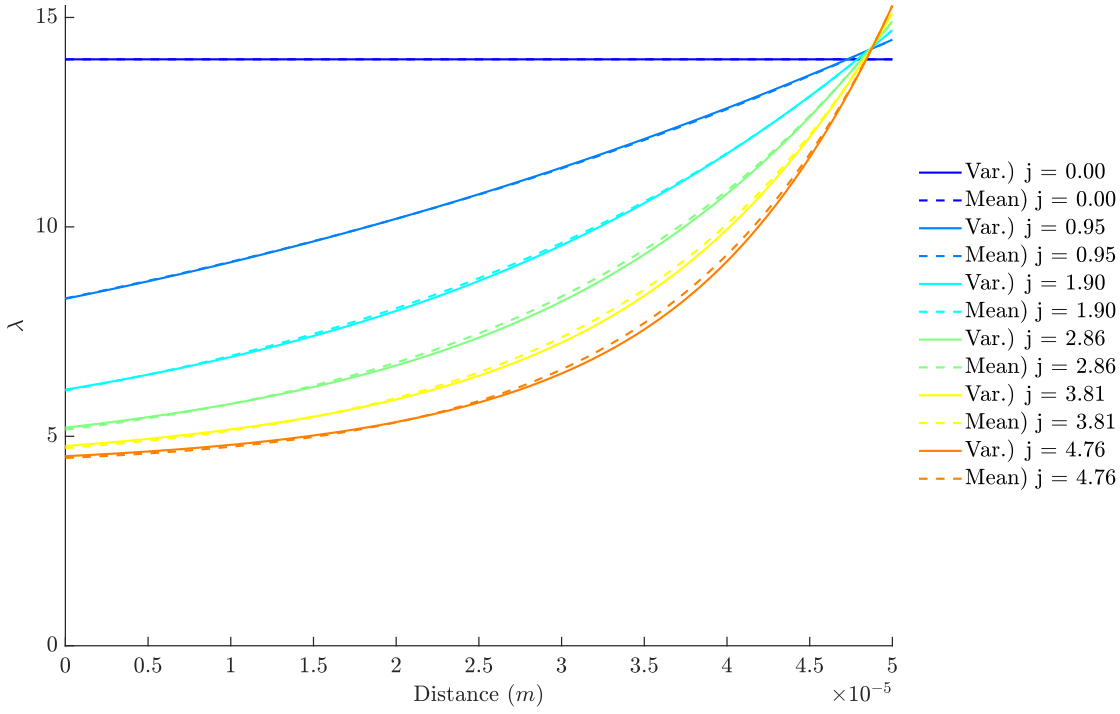

Figure 40 - λ profile for test 5.1.4 with 100% relative humidity.
Source: the author.

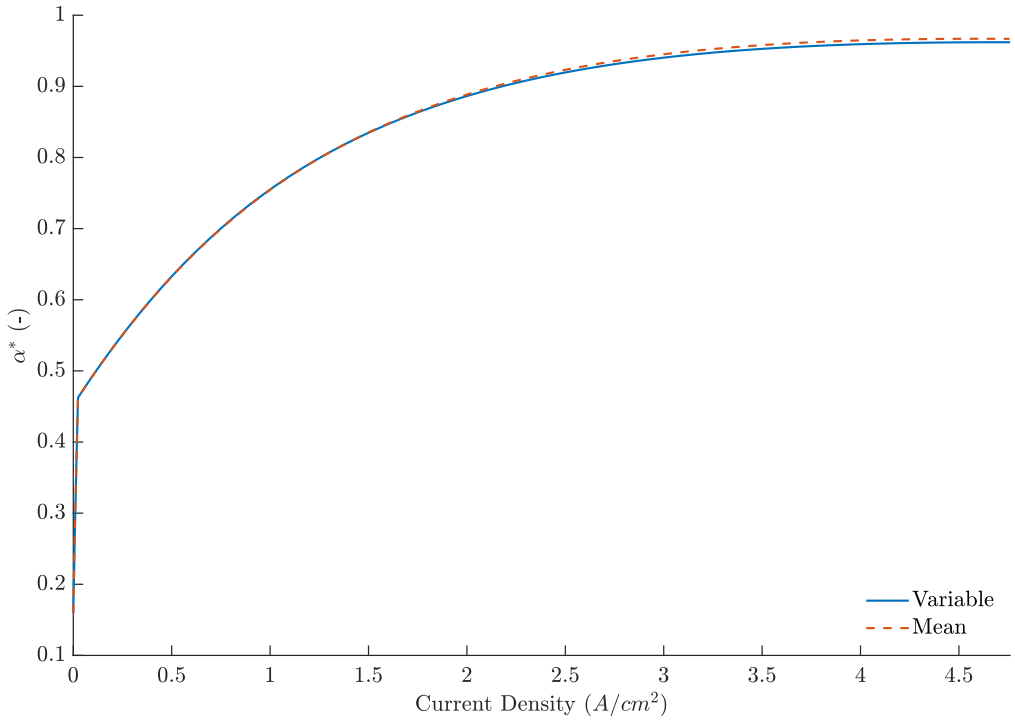

Figure 41 - α* values for test 5.1.4 with 100% relative humidity.
Source: the author.

Analyzing the graphs, it is clear that an excellent agreement is reached on both the polarization curve and the λ profile, indicating that the simplifying assumption is reasonable under this condition. It is also evident that the α* values have a much better agreement. Therefore, using a mean value for water diffusivity is an accurate approximation if the membrane is well-humidified, which happens when the temperature and relative humidity are higher.

Regarding the computational time, all tests presented a statistically significant computational gain when the simplification was used, which varied from 3.82% to 34.09%. Table 30 presents the mean and improvement for all tests, while the detailed data is presented in Appendix J. It should be highlighted that all improvements were statistically significant even with α = 0.01.

Table 30 - Computational time results for mean diffusivity comparison using Springer's description.

Test		Mean for 100 points (s)	Improvement for 100 points	Mean for 500 points (s)	Improvement for 500 points
5.1.1	Variable	3.576955	4.56%	10.901793	3.82%
	Mean	3.413682		10.485561	
5.1.2	Variable	3.098137	30.90%	9.781869	14.77%
	Mean	2.140917		8.337404	
5.1.3	Variable	3.400974	34.09%	10.608197	19.48%
	Mean	2.241603		8.541213	
5.1.4	Variable	2.785608	21.68%	9.649839	14.47%
	Mean	2.181565		8.253103	
5.1.5	Variable	3.890963	32.78%	11.697893	9.68%
	Mean	2.615437		10.565127	
5.1.6	Variable	3.118612	28.34%	9.658015	11.09%
	Mean	2.615437		8.586861	
5.1.7	Variable	3.591460	28.34%	13.359055	25.29%
	Mean	2.234660		9.980191	
5.1.8	Variable	2.860011	30.54%	9.649638	11.64%
	Mean	2.216024		8.526503	

Source: the author.

In general, the computational improvement for 100 points was about 30%, while for 500 points, it was between 10% and 20%. This difference is expected because, as the initial estimate for each iteration is the solution for the previous solved current density, a larger number of points – which decreases the interval between solved current densities – will improve the quality of the guess, thus decreasing the significance of the time demanded by this method for the overall solution. However, no clear pattern was found relating the improvement and the test conditions.

Thus, the usage of the analytical expression that arises from the simplifying assumption of mean diffusivity on the membrane provides a good approximation as long as the λ values are always greater than those at the diffusivity peak. Consequently, it should be reasonable under well-humidified conditions. When this is not true, significant deviations in the results may occur, especially on the λ profile and at high current densities. This simplification also proved to yield considerable computational benefits, which are more significant when fewer points are evaluated. So, if the cell is well humidified, this simplification will most likely provide a good improvement in computational time with a low impact on the results, which can be particularly valuable in conditions where the numerical method is troublesome.

5.4.2 Meier *et* Eigenberger, 2004

The polarization curves here follow the same pattern in all eight analyzed conditions. On the activation region, a good fit between the description with and without the simplifying assumption exists. After that, the voltage is overestimated by the simplified case up until a region near the optimal point, and then it falls sharply, underestimating the voltage of the complete case. This is exemplified in Figure 42 and Figure 43, which represent tests 5.2.1 and 5.2.8 – both extremes.

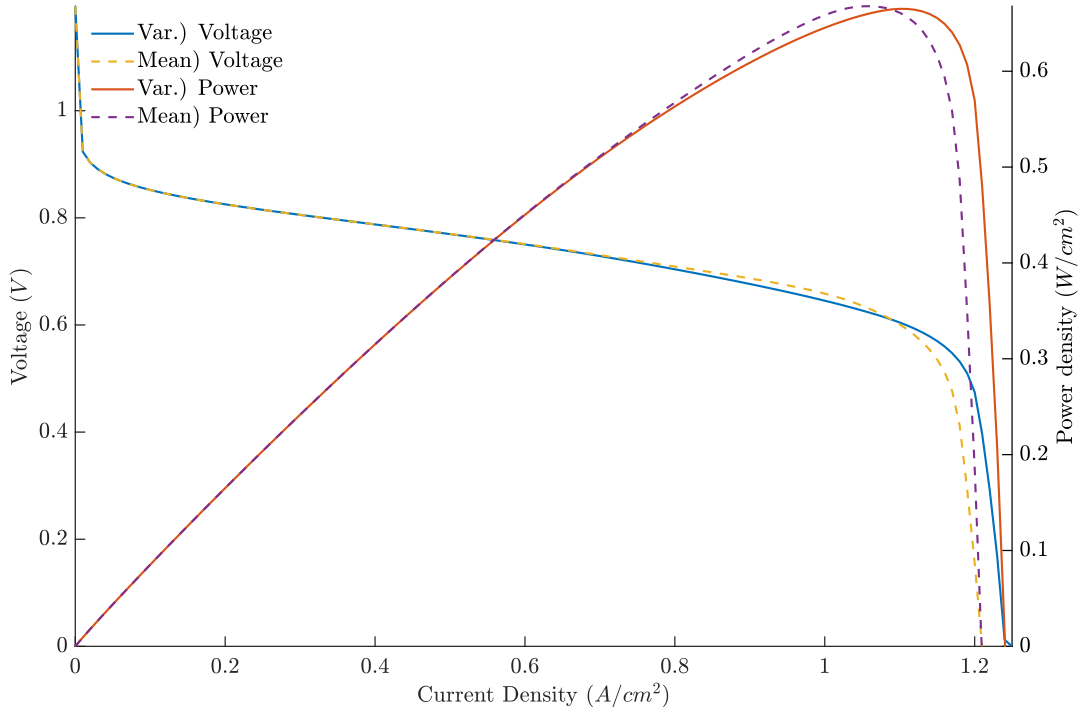

Figure 42 - Polarization results for test 5.2.1.
Source: the author.

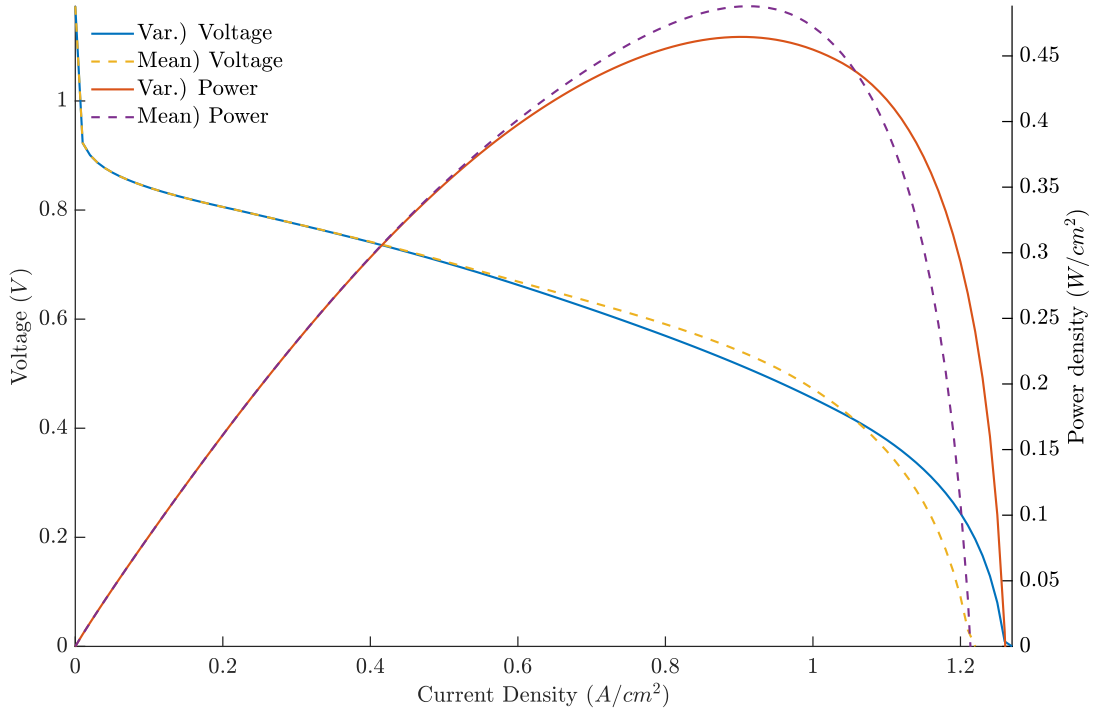

Figure 43 - Polarization results for test 5.2.8.
Source: the author.

The standard error, presented in Table 31, reinforces this discussion, showing that the error is small in the activation region but increases considerably in the other two. Even though the error is smaller on the ohmic region for tests 5.2.2, 5.2.4, 5.2.6, and 5.2.8 – all with $T = 353.15\ K$ – the difference is not considered big enough to be relevant.

Table 31 - Standard error for polarization curves of tests 5.2.

Experiment	Global S_e (V)	S_e 1 (V)	S_e 2 (V)	S_e 3 (V)
5.2.1	4.74E-02	2.23E-04	3.47E-02	3.85E-01
5.2.2	3.57E-02	3.26E-04	1.17E-02	9.34E-02
5.2.3	4.62E-02	1.43E-04	2.44E-02	3.43E-01
5.2.4	3.06E-02	2.51E-05	1.15E-02	5.77E-02
5.2.5	5.14E-02	6.87E-04	5.54E-02	4.57E-01
5.2.6	3.78E-02	8.39E-04	1.57E-02	1.14E-01
5.2.7	4.96E-02	5.03E-04	4.81E-02	4.55E-01
5.2.8	3.31E-02	1.73E-04	1.47E-02	6.51E-02

Source: the author.

It is worth noting that this sharp voltage drop on the final tail is not related to the concentration overvoltage but to the ohmic one. This is exemplified in Figure 44, the overvoltage results for case 5.2.8.

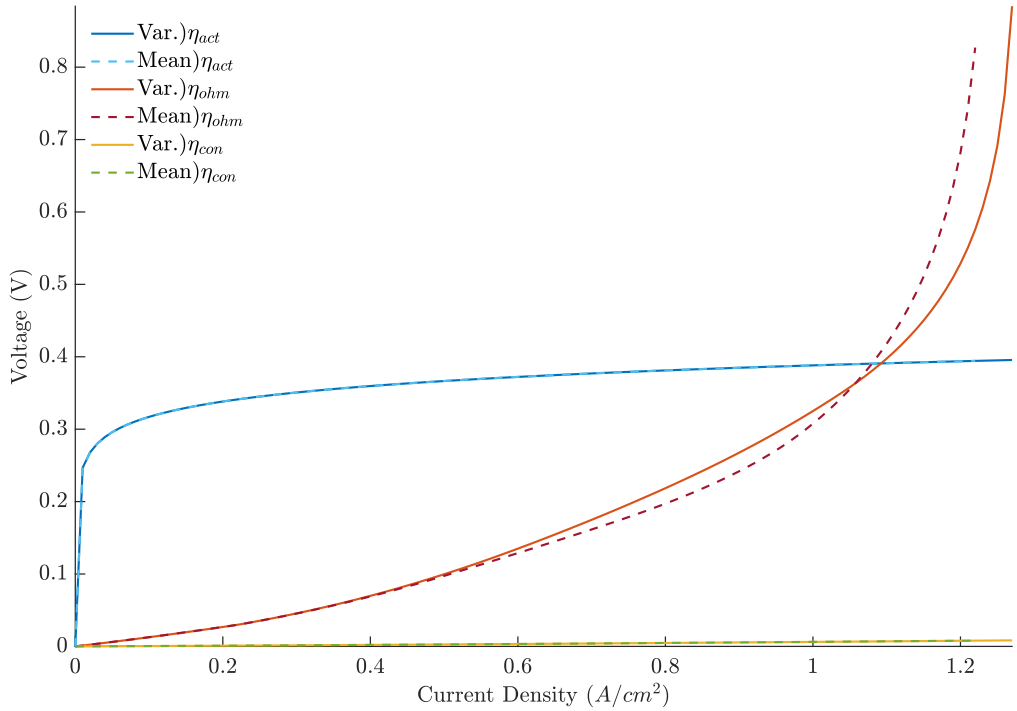

Figure 44 - Overvoltage results for test 5.2.8.
Source: the author.

Another important point is that, as in the previous case, the α* presents deviations after the activation regions. This is shown in Figure 45 and Figure 46, using tests 5.2.1 and 5.2.8.

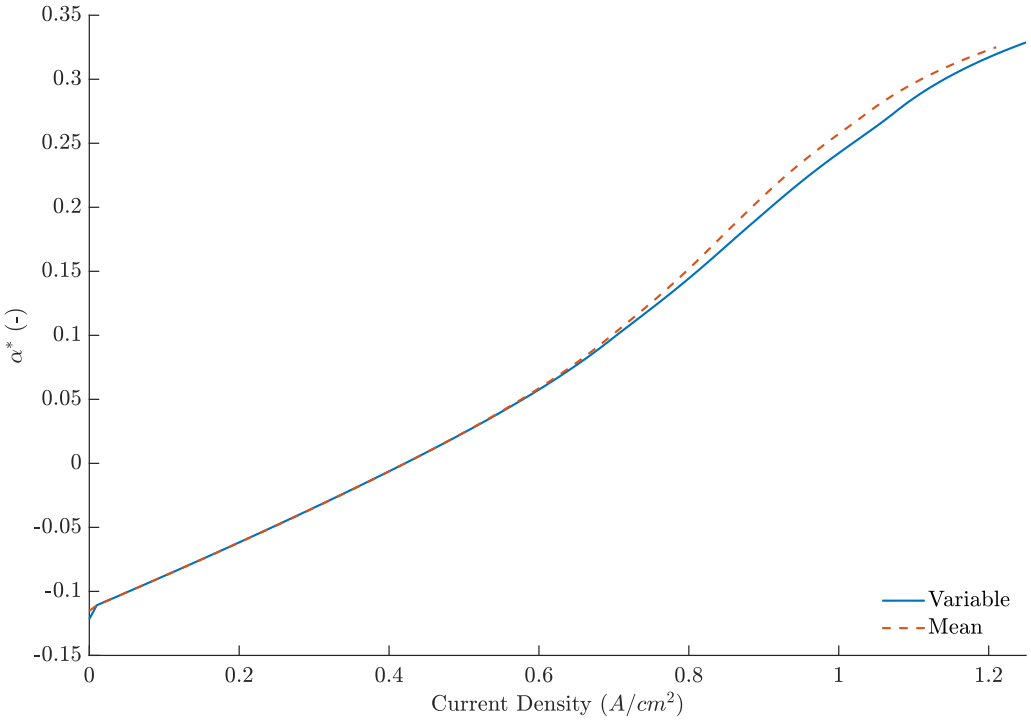

Figure 45 - α* values for test 5.2.1.
Source: the author.

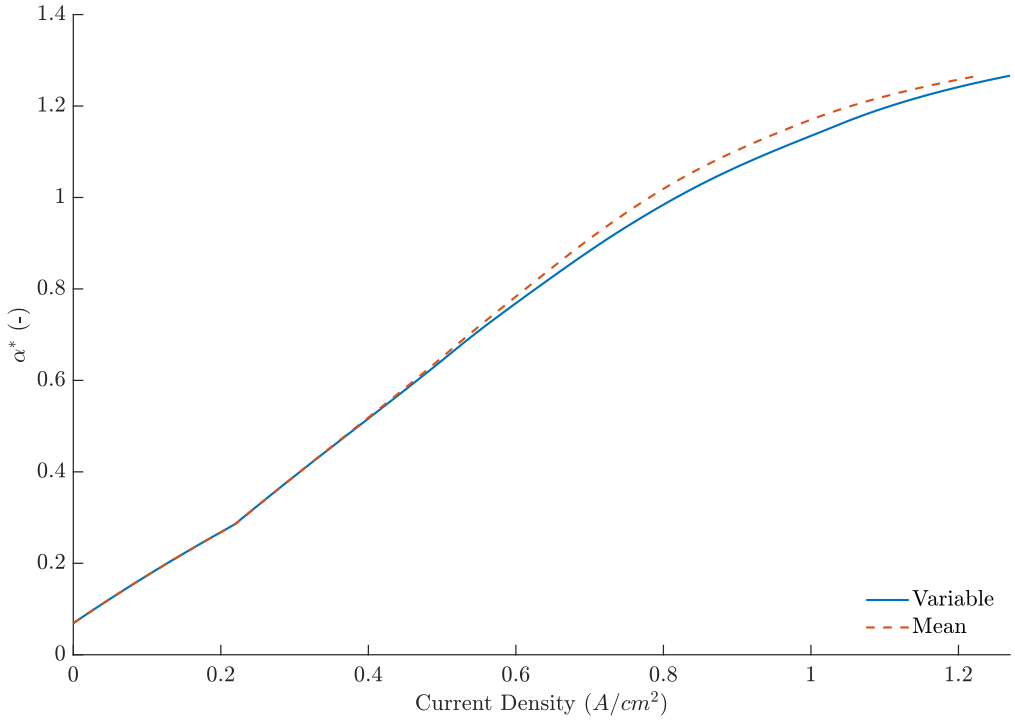

Figure 46 - α* values for test 5.2.8.
Source: the author.

This indicates that the assumption is affecting the water transport inside the membrane. Again, Appendix I presents the discussion concerning the concentration

profiles. To further understand the cause for these observations, the λ profiles are analyzed. Figure 47 and Figure 48 present them for tests 5.2.1 and 5.2.8.

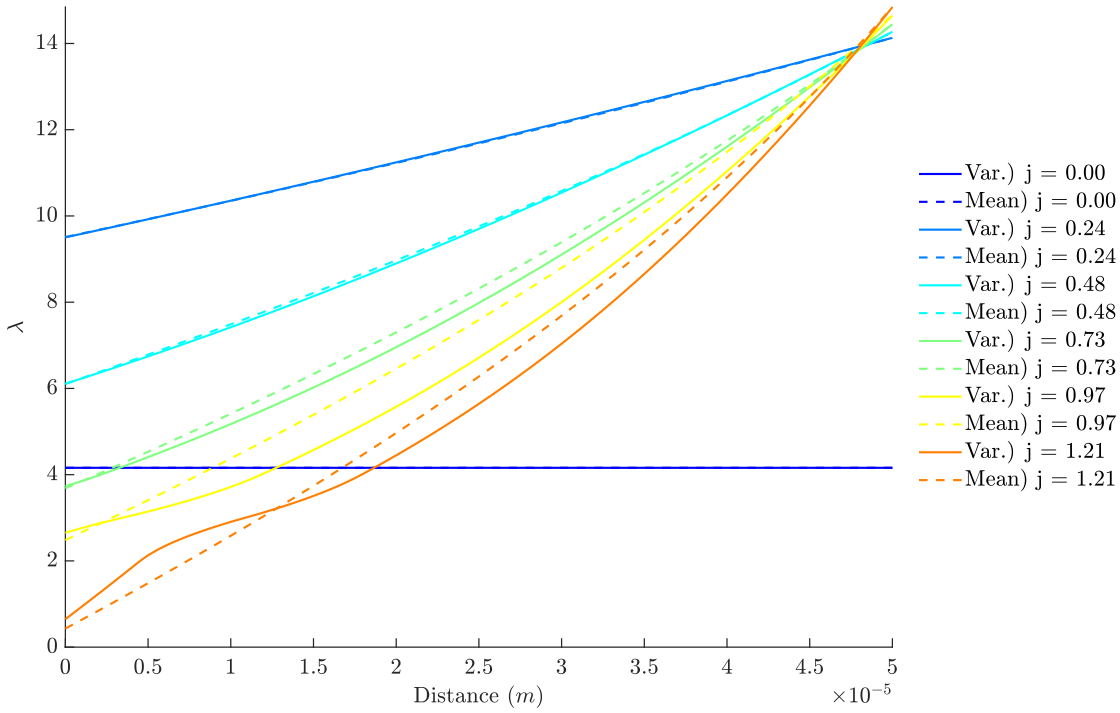

Figure 47 - λ profile for test 5.2.1.
Source: the author.

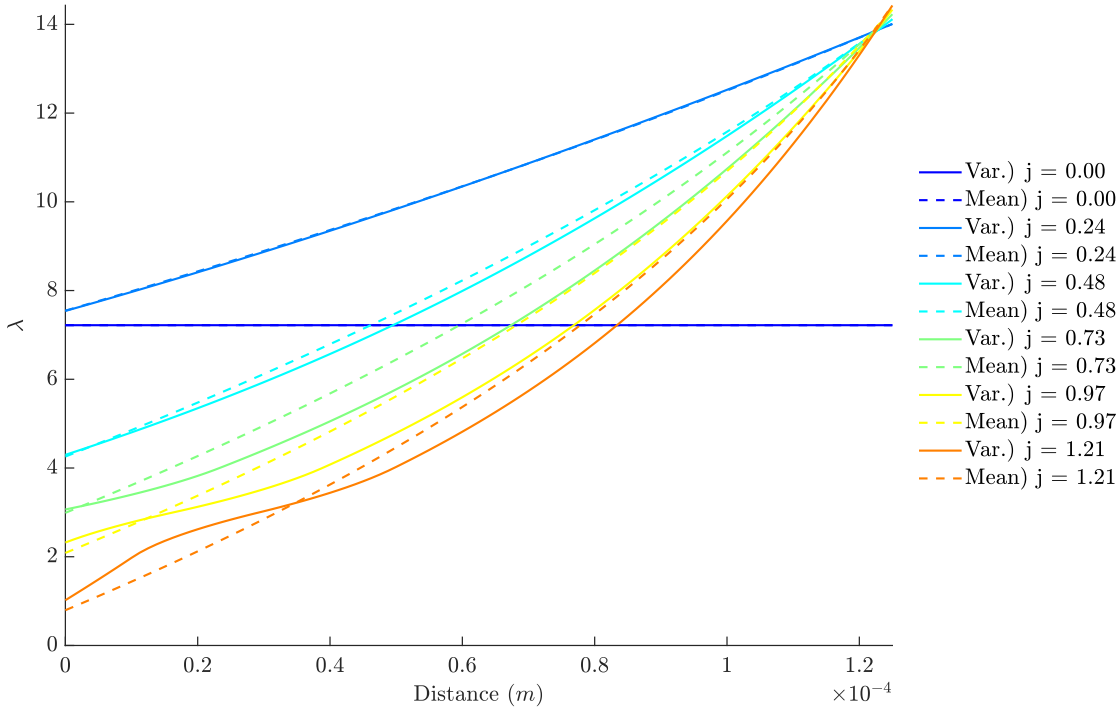

Figure 48 - λ profile for test 5.2.8.

Source: the author.

It is noticeable that under these – and all other – tested conditions, the water concentration rapidly reaches values near or below 4, which, as discussed in the previous section, causes considerable deviations due to the change in diffusivity. This explains the significant differences in the ohmic region and the drastic increase in the ohmic overvoltage because these low λ values rapidly decrease the membrane's protonic conductivity. Also, the profile is notably affected at high current densities, hindering the descriptive capability of the ohmic overvoltage. A possible explanation for why it first underestimates the losses and after overestimates it is that, considering that the curve underestimates λ near the anode and overestimates on the rest of the membrane, when λ is still high, the increase in conductivity on most of the domain will be more relevant than a small decrease on the beginning, however, as the λ values decrease, the impediment caused in this initial region will be severe, dominating the system.

To highlight the impact of humidification on the results, an additional case is proposed. It consists of the same conditions as test 5.2.8 but with a relative humidity of 150%. The polarization curve and the λ profiles are respectively presented in Figure 49 and Figure 50.

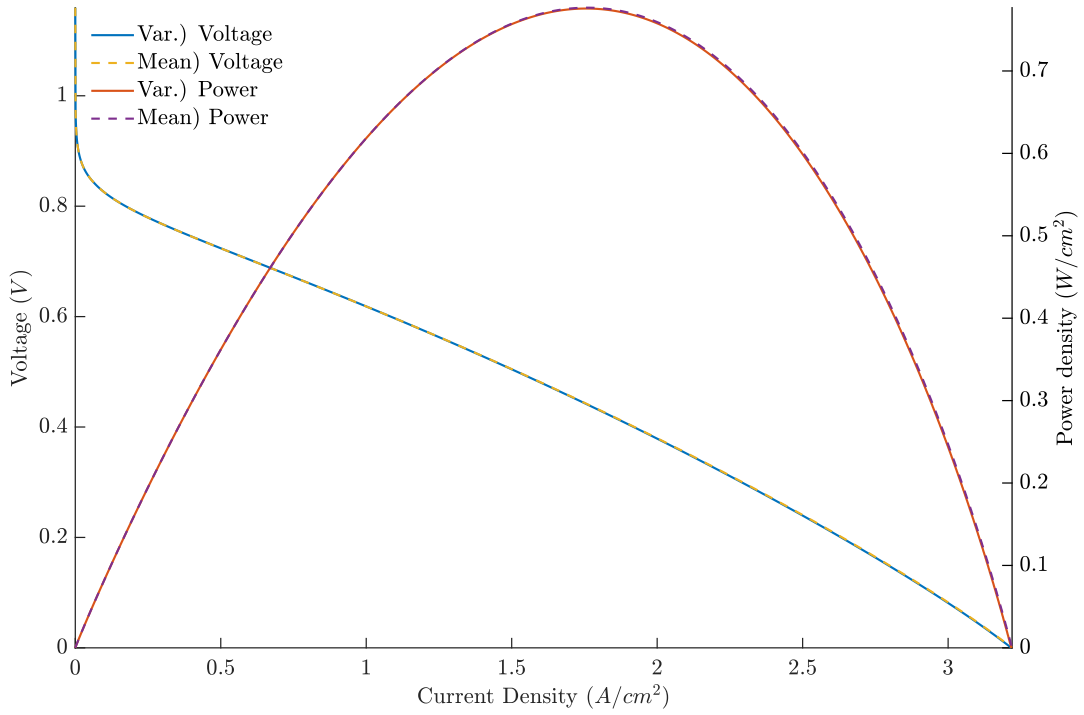

Figure 49 - Polarization curve for test 5.2.8 with RH = 150%.
Source: the author.

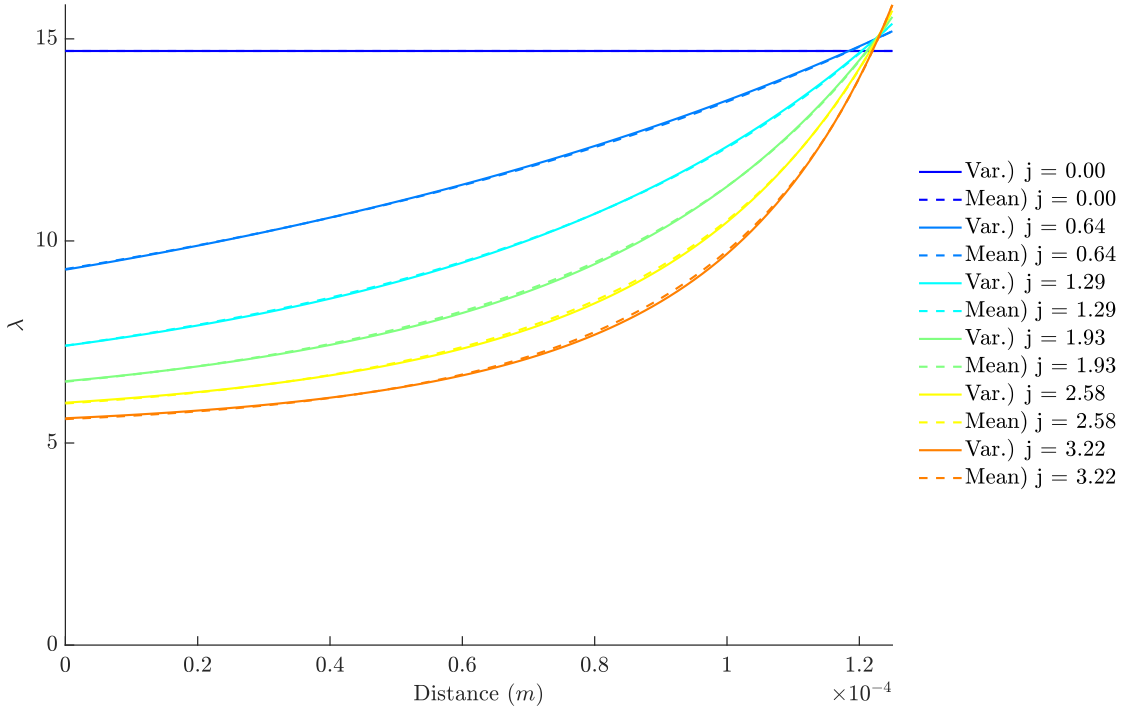

Figure 50 - λ profiles for test 5.2.8 with RH = 150%.
Source: the author.

Note that λ values are always greater than 4, resulting in a good adjustment on both curves. It should be highlighted that considering that the model neglects the existence of liquid water, it is possible that these results are not representative of reality. Nevertheless, they are adequate to reinforce the argument that the main parameter for a good agreement between the cases with and without the simplifying assumption is the water content.

Finally, the computational time analysis is presented in Table 32 – with the complete results in Appendix K.

Table 32 - Computational time results for mean diffusivity comparison using Meier and Eigenberger's description.

Test		Mean for 100 points (s)	Improvement for 100 points	Mean for 500 points (s)	Improvement for 500 points
5.2.1	Variable	3.881925	23.82%	11.710476	-1.33%
	Mean	2.957238		11.865836	
5.2.2	Variable	3.711456	22.46%	10.790080	-6.62%
	Mean	2.877975		11.504133	
5.2.3	Variable	3.790084	22.29%	11.681792	-1.33%
	Mean	2.945430		11.837423	
5.2.4	Variable	3.928169	27.29%	11.902396	3.47%
	Mean	2.856288		11.489367	
5.2.5	Variable	4.155021	19.50%	12.543249	-11.09%
	Mean	3.344883		13.934209	
5.2.6	Variable	4.068208	16.70%	11.565476	-22.95%
	Mean	3.344883		14.219683	
5.2.7	Variable	4.207036	16.70%	12.214009	-9.96%
	Mean	3.388770		13.430721	
5.2.8	Variable	4.350216	22.08%	12.545347	-5.58%
	Mean	3.254921		13.245127	

Source: the author.

An improvement of about 20% is present when 100 points are used, which indicates that the usage of the analytical equation is providing a considerable benefit for the resolution with larger intervals between current densities. However, a negative effect was observed for all tests, except 5.2.4, with 500 points. This shows that the complexity of the analytical equation, dependent on functions that are evaluated with a series (tan and $\tan^{-1}$, for example), becomes more relevant than the numerical method when Δj is small because the initial guess – given by the solution of the previous case – becomes better as Δj decreases. It is not clear why only case 5.2.4 had an increase in performance. A noteworthy feature of this case is that it has a slightly higher λ value at high current densities than many of the others, however, the difference is not significant from a case such as 5.2.8, which had a negative result. Thus, it is probably a specificity of the evaluated points in this test.

Considering all the results, it can be concluded that, as long as the system is well-humidified, this simplifying assumption provides a good approximation of the robust description. This is even more important here than if Springer's description of the electro-osmotic drag coefficient describes the system, as this ξ caused a rapid decrease of the λ values near the anode for all tested conditions. However, if the

system is not sufficiently humidified, the most affected region is the one near the point of maximum power, which can be problematic considering its importance. Regarding computational time, a significant increase exists when Δj is larger, but with smaller steps in current density, a hindrance in performance can be observed in most cases. Therefore, the usage of the developed analytical equation can be beneficial for well-humidified systems with large Δj, but not as significant as for Springer's case due to the complexity of the solution.

5.4.3 Piecewise linear

As for the final description of the electro-osmotic drag coefficient, the polarization results had similar behavior to the one with Meier *et* Eigenberger's description: a significant deviation in the ohmic region related to the ohmic overvoltage. However, different from the previous section, the last part of the curve is similar with and without the assumption, which explains why almost all tests had the same final current density between the complete and simplified descriptions. Figure 51 and Figure 52 show the polarization curves for both extremes (5.3.1 and 5.3.8), where all of those features are noticeable.

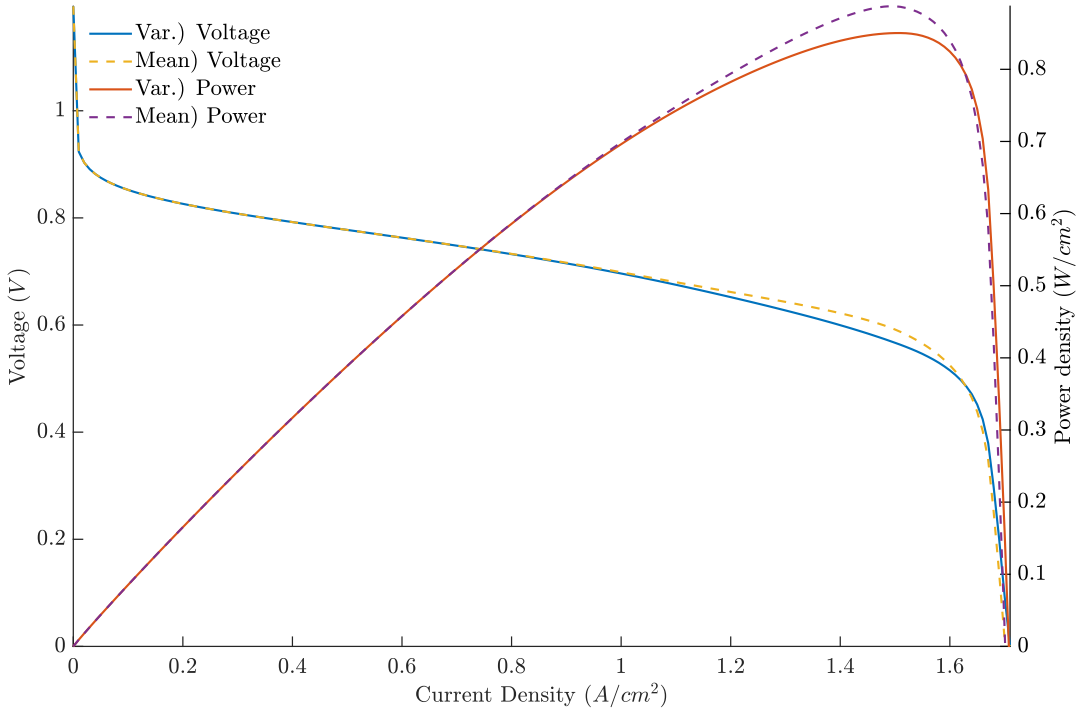

Figure 51 - Polarization curve for test 5.3.1.
Source: the author.

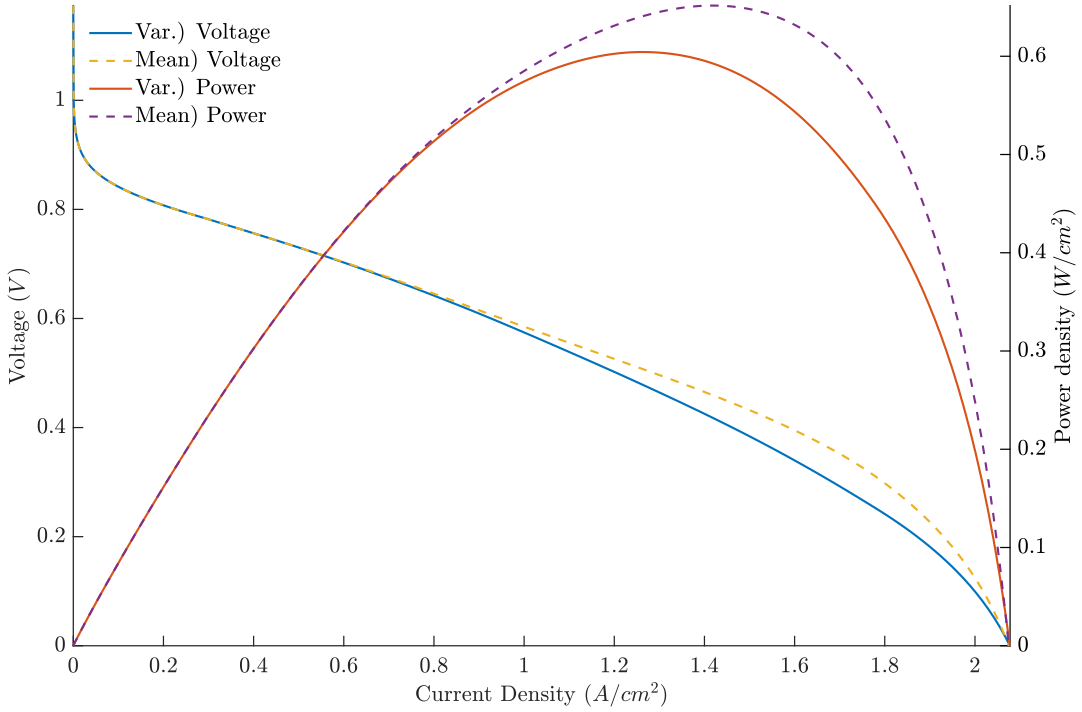

Figure 52 - Polarization curve for test 5.3.8.
Source: the author.

This behavior can also be observed in the values of the standard error of the estimate, presented in Table 33. Note that the error in the region between 0.5 V and

0.0 V is close to or smaller than for tests 5.2, but the error increases after the activation region is still present.

Table 33 - Standard error for polarization curves of tests 5.3.

Experiment	Global S_e (V)	S_e 1 (V)	S_e 2 (V)	S_e 3 (V)
5.3.1	1.30E-02	3.38E-05	1.30E-02	3.98E-02
5.3.2	1.93E-02	2.14E-04	1.13E-02	3.25E-02
5.3.3	1.47E-02	2.03E-05	1.35E-02	4.21E-02
5.3.4	2.61E-02	1.98E-05	5.99E-03	3.99E-02
5.3.5	1.19E-02	2.56E-04	1.46E-02	3.49E-02
5.3.6	2.21E-02	5.03E-04	2.01E-02	3.27E-02
5.3.7	1.31E-02	1.36E-04	1.51E-02	3.67E-02
5.3.8	2.98E-02	2.15E-05	9.78E-03	4.51E-02

Source: the author.

However, different from both previous cases, when the piecewise linear description is used, the α* is practically coincidental. Figure 53 and Figure 54 exemplify this using tests 5.3.1 and 5.3.8.

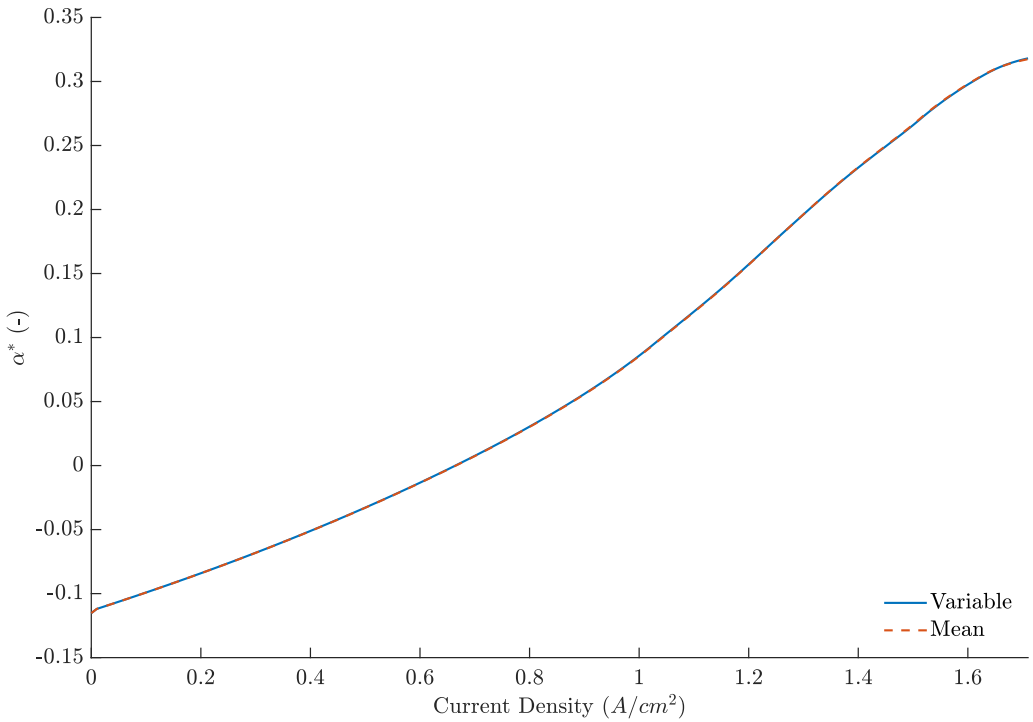

Figure 53 - α* values for test 5.3.1.
Source: the author.

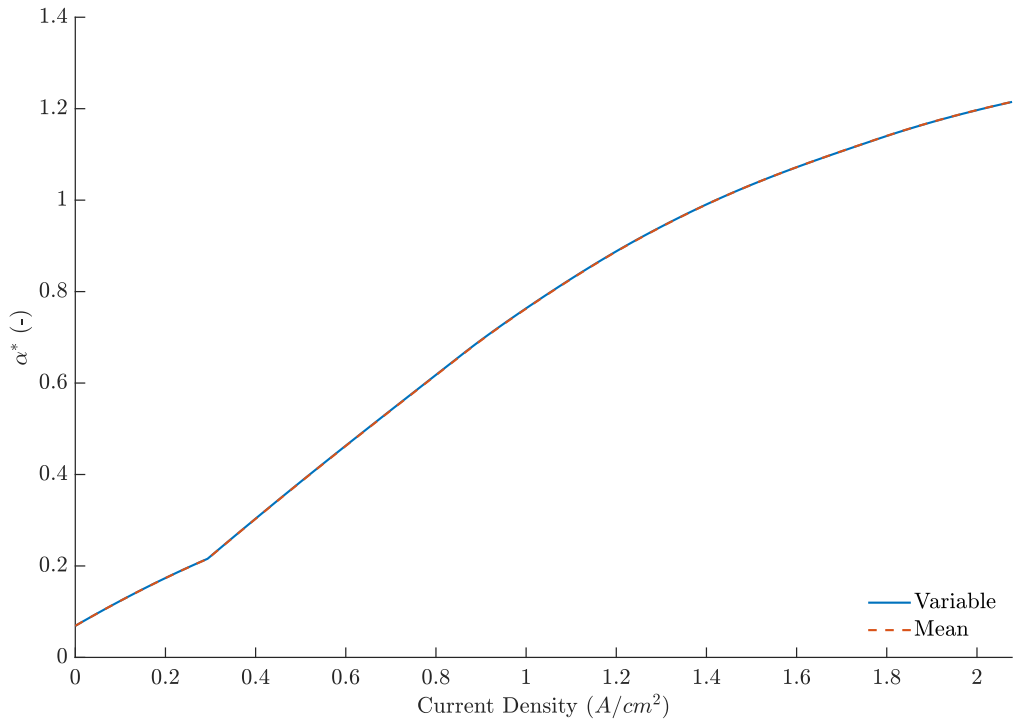

Figure 54 - α* values for test 5.3.8.
Source: the author.

This is an odd behavior because a difference in the polarization curves exists, indicating that the simplifying assumption must be affecting the system. However, this impact occurs in a manner that the fluxes that define α* are equally affected.

Also, Figure 55 is presented to highlight that the sharp decrease does not happen due to the concentration overvoltage, but to the ohmic one. This indicates that a similar reduction of the water concentration near the anode-membrane interface may be happening.

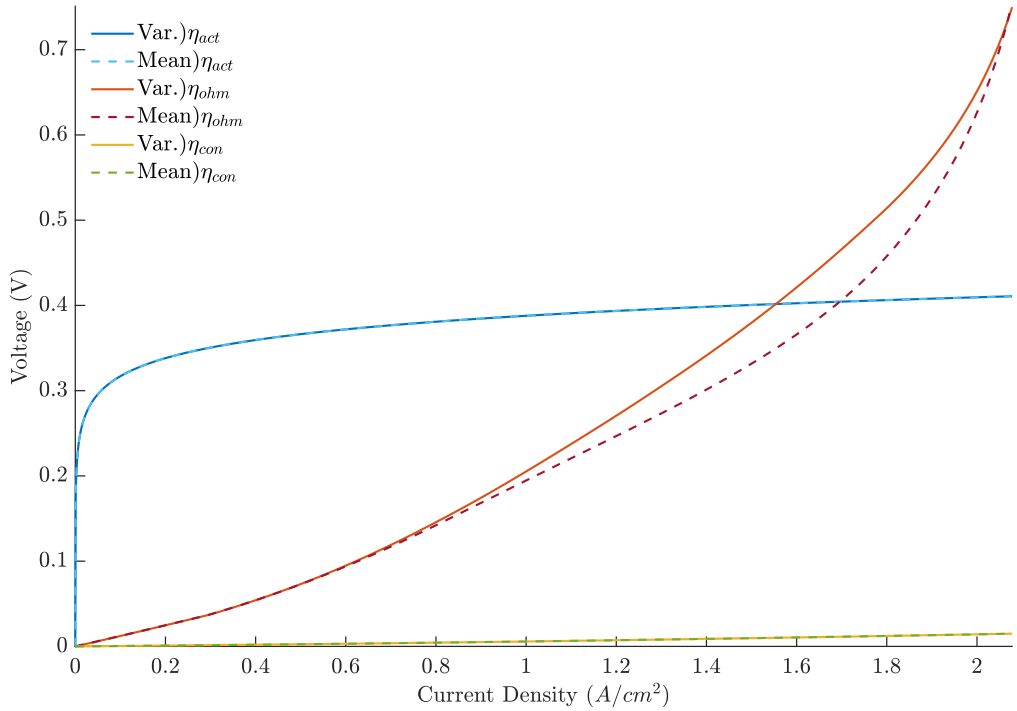

Figure 55 - Overvoltage results for test 5.3.8.
Source: the author.

To prove this hypothesis, Figure 56 and Figure 57, with the λ profiles for cases 5.3.1 and 5.3.8 are presented. It is highlighted that an analogous behavior occurs on the profiles that are not shown.

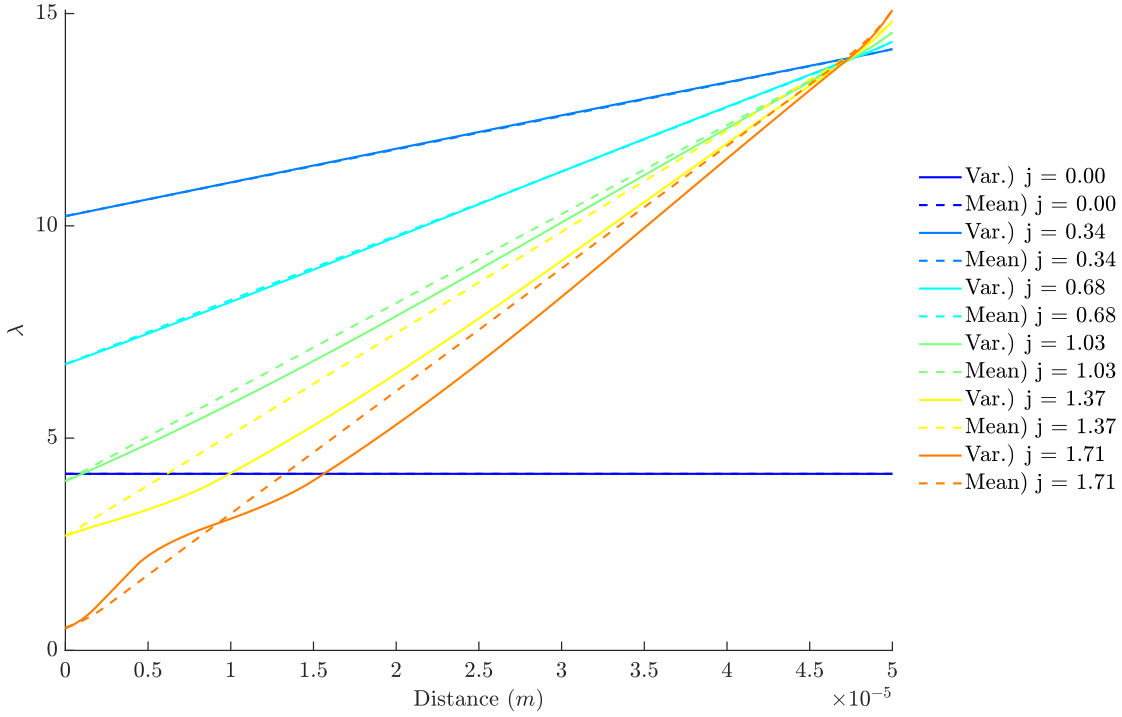

Figure 56 - λ profiles for test 5.3.1.
Source: the author.

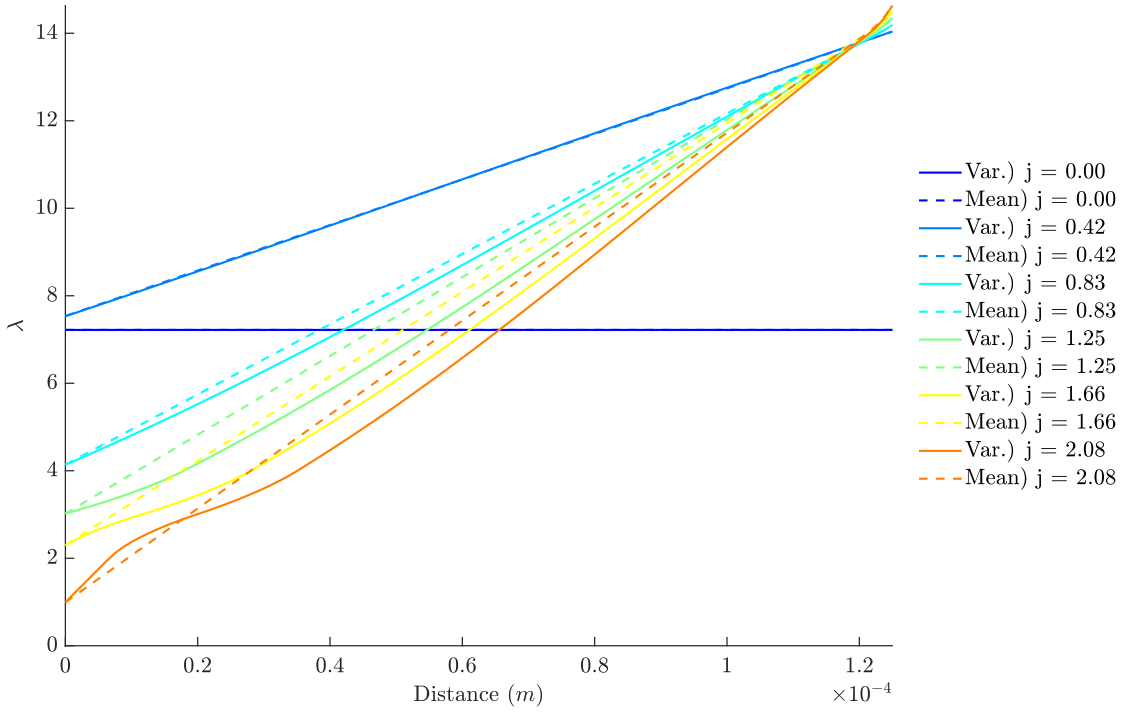

Figure 57 - λ profiles for test 5.3.8.
Source: the author.

Considerably low λ values near the anode are observed, which reinforces that the sharp increase in ohmic overvoltage occurs due to the low humidity levels. However,

an important difference here is that the value at the interface almost does not change with the simplifying assumption, even if the profile is considerably affected. A more in-depth explanation for why this happens is available in Appendix I, but, in summary, the reason is the almost coincidental α^* in both submodels, which likely happens due to the constant ξ for different values of λ in this description. As the profile is different, while λ_{Ano} is not low enough to result in a resistivity that will cause V = 0 the ohmic overvoltage is different between the robust and simplified descriptions. Nevertheless, as the λ value on the interface is almost equal, the resistivity on this initial region – which is the largest due to the low λ value – will be close in both cases, and because this resistivity is among the main contributors to the cell's overvoltage, the voltage will reach zero at similar current densities.

As was done in both previous cases, a test with a higher relative humidity is done to evaluate if the deviations are maintained at higher current densities. In this case, the same conditions for test 5.3.8 were used, but with a relative humidity of 130%. The polarization curve and λ profile for this case are shown in Figure 58 and Figure 59, respectively.

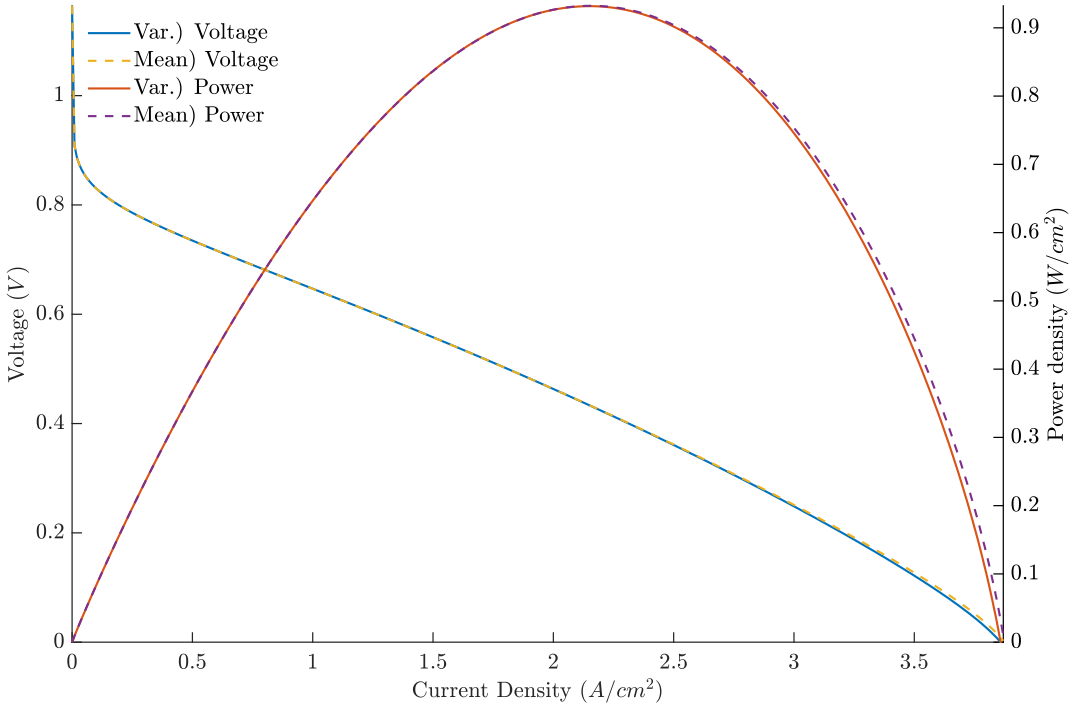

Figure 58 - Polarization curve for test 5.3.8 with RH = 130%.
Source: the author.

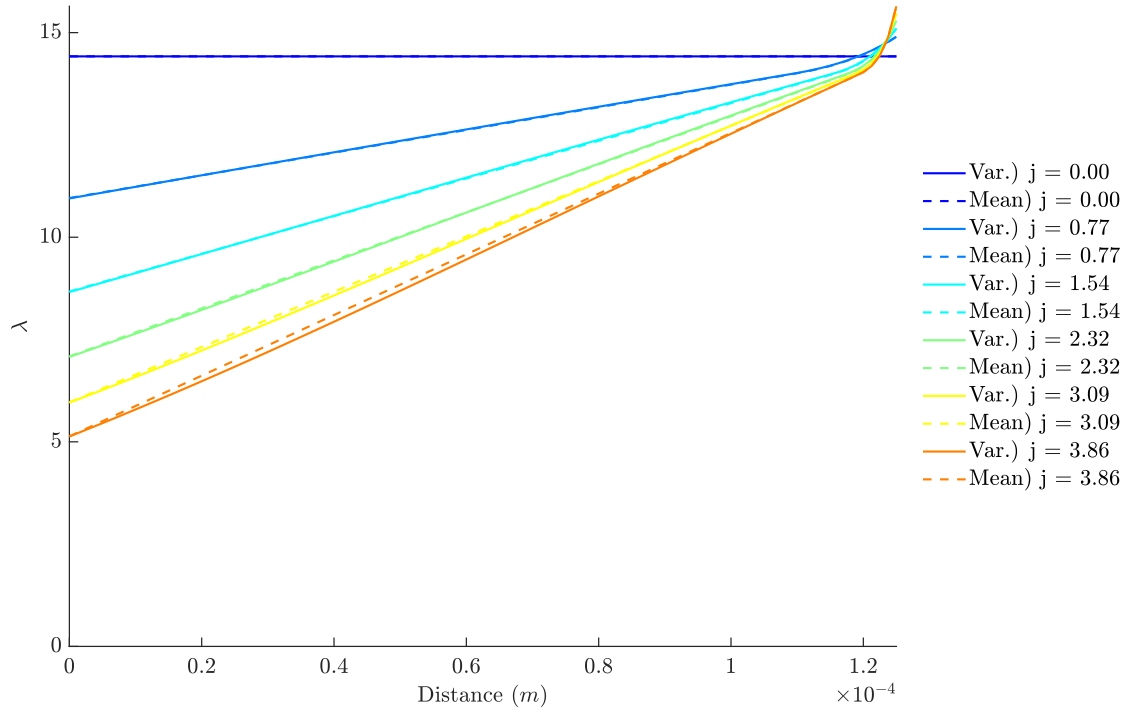

Figure 59 - λ profiles for test 5.3.8 with RH = 130%.
Source: the author.

Similarly to what was previously observed, the adjustment is good for this more humidified case, indicating that the cause for the variation on the profiles is also tied to the distortion caused by the mean when the peak is present.

As for the computational time, Table 34 presents the mean values and improvement for each case, with all details in Appendix L.

Table 34 - Computational time results for mean diffusivity comparison using the piecewise linear description.

Test		Mean for 100 points (s)	Improvement for 100 points	Mean for 500 points (s)	Improvement for 500 points
5.3.1	Variable	5.193663	43.46%	16.891775	31.88%
	Mean	2.936534		11.506852	
5.3.2	Variable	4.270269	33.86%	13.170973	13.69%
	Mean	2.824144		11.368390	
5.3.3	Variable	3.699689	24.91%	10.660134	-2.53%
	Mean	2.778145		10.929565	
5.3.4	Variable	3.925392	24.24%	11.064898	-6.15%
	Mean	2.973798		11.745111	
5.3.5	Variable	4.999421	37.96%	15.687852	19.10%
	Mean	3.101721		12.691066	
5.3.6	Variable	4.156957	22.35%	12.271850	-8.56%
	Mean	3.101721		13.322203	

5.3.7	Variable	4.038108	22.35%	11.602786	-8.61%
	Mean	3.227671		12.602338	
5.3.8	Variable	4.433927	23.08%	12.402737	-4.09%
	Mean	3.144507		12.910572	

Source: the author.

A noticeable improvement was observed when only 100 points were used, which varied from 22.35% to 43.46% - the most significant observed between the three electro-osmotic drag descriptions. Thus, when a relatively small interval between current densities is used, the analytical equation provides a significantly more efficient alternative.

Nevertheless, for 500 points, the result was not homogeneous: some cases presented significant improvements – up to 31.88% - and others were hindered by the expression. Considering that, even when an improvement was observed, it was smaller than for 100 points, the same conclusion for the other cases can be reached: with the smaller Δj, the initial guess becomes better, thus the impact of the analytical equation's additional complexity – with multiple cases to be analyzed according to the λ values at the interfaces – becomes more significant than the necessity of numerically integrating the equation.

An observed pattern was that the cases where the improvement was observed even with 500 points were those with the lower value for relative humidity (60%), with the exception of case 5.3.6. Also, the most significant improvements happened in cases 5.3.1 and 5.3.5, both with the low level of temperature and humidity. This seems to indicate that the assumption causes a greater improvement when the humidity in the system is low, but this does not explain, for example, why test 5.3.6 had a smaller improvement than 5.3.8, the same case but better humidified (RH = 80%). To test this general trend, the computational time was also evaluated for the extra case – equal to 5.3.8, but with a relative humidity of 130%. These results are presented in Table 35.

Table 35 - Computational time results for test 5.3.8 with RH = 130%.

	100 points		**500 points**	
	Variable (Ref.)	**Mean**	**Variable (Ref.)**	**Mean**
Mean (s)	3.002194	2.744036	7.878701	10.881071
Std. Dev (s)	0.033445	0.014863	0.049356	0.068787
Improvement	8.60%		-38.11%	
Significance	**t**	**t_c**	**t**	**t_c**
α = 0.05	22.306	1.782	-112.144	1.746
α = 0.01	22.306	2.681	-112.144	2.583
α = 0.05	Yes		No	
α = 0.01	Yes		No	

Source: the author.

Considering that this had the least significant improvement for 100 points and the largest decrease for 500, the previously stated observations seem to be true, that is, the improvement caused by the simplifying assumption is better for less humidified conditions. However, as this explanation does not explain some of the cases, it should be regarded as a general guideline, not a robust conclusion.

Therefore, the assumption of mean diffusivity using a piecewise linear description for the electro-osmotic drag coefficient should be carefully considered. While it presented a positive effect for all tests when larger intervals between current densities were used, when Δj was small, it caused hindrances in some cases. Also, the most considerable computational improvements – observed even for 500 points – occurred in the less humidified cases, but the simplifying assumption only presented accurate results compared to the robust description when the system was well humidified. As a good simplification should reduce the computational time while not compromising the accuracy, the consideration of a mean diffusivity for a system is only recommended in well-humidified systems with a large Δj.

6 CONCLUSIONS

In this dissertation, four different simplifying assumptions used in the literature were studied to evaluate their effect on the accuracy and computational time of a PEMFC model. Those assumptions varied from an almost ubiquitous one – the mean reaction entropy for evaluating the thermodynamic potential – to one where analytical solutions not previously available in the literature were proposed, the mean water diffusivity on the membrane. A one-dimensional, isothermal, and steady-state model based on Springer *et al.* (1991) was implemented, with the possibility of using or not each of those assumptions. As this model is among the most influential for PEMFC modeling, the conclusions are expected to be relevant for many other authors, providing important information for future models.

To ensure representative results, test conditions based on literature values were chosen, whereas critical parameters for each simplification were tested at high and low levels. The voltage, overvoltages, and α* in each evaluated current density were compared graphically and numerically in each case as a measurement of the accuracy of the model. Also, the concentration and λ profiles were compared to detect the variations caused by the assumption and to explain the observed behaviors on the voltage. Moreover, the computational time was analyzed to investigate the assumption's effect in the model's performance.

Firstly, the assumption of constant entropy was tested by comparing the predicted thermodynamic voltage using a mean reaction entropy with one that integrated the entropy dependence with temperature. It was found that, even if the constant entropy value used was the one for 298.15 K, as it is normally done in the literature, the relative error does not surpass 0.12% at PEMFCs operating temperatures. Considering that this difference is small, no significant accuracy loss is expected due to the usage of the simplification. As for the computational time, even if a gain was observed in a direct comparison of the two approaches, no statistically significant difference was found when they were applied to the model. Therefore, as the simplifying assumption does not remarkably affect either the accuracy or the efficiency, the consideration of a mean reaction entropy or the complete description of the entropy dependence with temperature are practically equivalent approaches for PEMFC modeling.

As for the usage of the Tafel equation as a simplification of the Butler-Volmer equation, under all test conditions, the activation overvoltage was practically the same

with both expressions. This indicates that the accuracy of the system is not hindered by the Tafel equation. The difference is only noticeable in current densities near zero, but the region is almost negligible. It was also observed that the anodic activation overvoltage is orders of magnitude smaller than the cathodic one, supporting the common practice of neglecting it. Another important observation is that, while the Tafel equation has good accuracy on the cathode, it does not have for the anode – the best simplification for this case, considering the low overvoltage, was the linear form of the Butler-Volmer equation. However, as the anodic activation overvoltage is so small, this did not have a significant effect on the model. Moreover, a slight, but statistically significant, improvement in the computational time was observed in all cases when the Tafel equation was used. This improvement was more significant when more points were used because, as the iterative process becomes faster when the interval between current densities is smaller, other improvements become more relevant. Thus, as the accuracy is maintained and a slight improvement in computational time is observed, employing the Tafel equation is recommended for describing the cathodic activation overvoltage as long as voltages close to zero current densities are not the focus – which is the case for most applications. Furthermore, the usage of this equation has the advantage of utilizing only one transfer coefficient, facilitating its experimental determination. Another recommendation is the usage of the linear Butler-Volmer equation for the anode if it is not neglected, as it presented a good fit throughout the activation region, but this is not expected to yield considerably more accurate results than simply neglecting it.

The comparison between two sorption isotherms showed the impact of using the parametrization developed for one membrane type for describing others. A considerable difference in the λ profile was caused by this variation, which resulted in major differences in the predicted ohmic overvoltage. Also, the anodic concentration profile was significantly affected, which, although not responsible for a relevant effect on the concentration overvoltage, is part of the reason for the difference in λ. Thus, the results indicate that special attention should be given to the choice of the correct sorption isotherm, with the common practice of using isotherms calculated for other materials – even of the same family – not recommended.

Finally, the robust analysis of the assumption of mean water diffusivity on the membrane, for which analytical expressions were deduced, provided general observations and specific ones for each electro-osmotic drag coefficient tested. For all

cases, the deviations between the model with variable and mean D_λ decreased considerably in well-humidified conditions. The explanation for this is the peak in diffusivity present around $\lambda = 4$, which makes the curve more irregular when these λ values are reached, reducing its capacity to be well represented by a mean value. However, the values of λ near the anode decreased much faster when Meier ***et*** Eigenberger or the piecewise linear descriptions for the electro-osmotic drag coefficient were used when compared to Springer's proposal. Thus, even more humidified conditions are needed if those coefficients are found to be representative of the system. As for the computational time, all tests presented a major improvement when the larger Δj (100 points) was used, but results varied for the smaller one. Springer's description still benefited from the assumption with 500 points, but the improvement was smaller. Meier and Eigenberger's one, on the other hand, had a decrease in performance in most cases, showing that the complexity of the analytical expression is greater than solving the ordinary differential equation numerically when the initial guess is better. Finally, the piecewise linear description – which had the highest improvement with 100 points – had a general tendency of small improvements in the conditions with low relative humidity and hindrances in performances in the other cases. Therefore, the usage of a mean diffusivity provided the best improvement on computational time between all tested simplifying assumptions when Δj is larger, but the improvement was not as significant – or even was harmful for performance – with smaller Δj. So, the benefits of using this simplification are only possible under well-humidified conditions (to ensure accuracy) and with larger intervals between current densities.

Even if the studied assumptions were among the most common in fuel cell modeling, many others are recommended to be analyzed in detail because, as shown by the results of this work, their impact may be significant. For example, the variation of the electro-osmotic drag coefficient caused major changes in the polarization curve for the same conditions, which is an important observation since the measurements for this value vary a lot between works. Also, the evaluation of assumptions on different models, such as one that considers the presence of liquid water, can be valuable data, thus, it is recommended as a continuation of this work. In conclusion, the adequate selection of assumptions for a model is a crucial step in its development, therefore, it is expected that a detailed analysis of its impact will considerably leverage the

construction of better PEMFC models and, consequently, improve this important technology for a sustainable future.

REFERENCES

ABDEREZZAK, B. **Introduction to transfer phenomena in PEM fuel cells**. First ed. [s.l.] Elsevier, 2018.

ALASWAD, A. et al. Technical and Commercial Challenges of Proton-Exchange Membrane (PEM) Fuel Cells. **Energies**, v. 14, n. 1, p. 144, 29 dez. 2020.

ANDERSSON, M. et al. A review of cell-scale multiphase flow modeling, including water management, in polymer electrolyte fuel cells. **Applied Energy**, v. 180, p. 757–778, out. 2016.

ARIF, M.; CHEUNG, S. C. P.; ANDREWS, J. Different Approaches Used for Modeling and Simulation of Polymer Electrolyte Membrane Fuel Cells: A Review. **Energy & Fuels**, v. 34, n. 10, p. 11897–11915, 15 out. 2020.

ASGHARI, S.; SHAHSAMANDI, M. H.; ASHRAF KHORASANI, M. R. Design and manufacturing of end plates of a 5kW PEM fuel cell. **International Journal of Hydrogen Energy**, v. 35, n. 17, p. 9291–9297, set. 2010.

BARBIR, F. **PEM Fuel Cells: Theory and Practice**. Second ed. [s.l.] Academic Press, 2013.

BAROUTAJI, A. et al. Materials in PEM Fuel Cells. Em: **Reference Module in Materials Science and Materials Engineering**. [s.l.] Elsevier, 2016.

BEALE, S. B. Calculation procedure for mass transfer in fuel cells. **Journal of Power Sources**, v. 128, n. 2, p. 185–192, abr. 2004.

BEALE, S. B. Mass transfer formulation for polymer electrolyte membrane fuel cell cathode. **International Journal of Hydrogen Energy**, v. 40, n. 35, p. 11641–11650, set. 2015.

BENÍTEZ, J. **Principles and Modern Applications of Mass Transfer Operations**. Second Edition ed. Hoboken, New Jersey: John Wiley & Sons, Inc, 2009.

BERASATEGI, J. et al. A hybrid 1D-CFD numerical framework for the thermofluidic assessment and design of PEM fuel cell and electrolysers. **International Journal of Hydrogen Energy**, v. 52, p. 1062–1075, jan. 2024.

BERNARDI, D. M.; VERBRUGGE, M. W. A Mathematical Model of the Solid-Polymer-Electrolyte Fuel Cell. **Journal of The Electrochemical Society**, v. 139, n. 9, p. 2477–2491, 1 set. 1992.

BHAIYA, M.; PUTZ, A.; SECANELL, M. Analysis of non-isothermal effects on polymer electrolyte fuel cell electrode assemblies. **Electrochimica Acta**, v. 147, p. 294–309, nov. 2014.

BIRD, R. B.; STEWART, W. E.; LIGHTFOOT, E. N. **Transport Phenomena**. Second Edition ed. [s.l.] John Wiley & Sons, Inc., 2002.

BOCKRIS, J. O. M. The hydrogen economy: Its history. **International Journal of Hydrogen Energy**, v. 38, n. 6, p. 2579–2588, fev. 2013.

BOCKRIS, J. O.; NAGY, Z. Symmetry factor and transfer coefficient. A source of confusion in electrode kinetics. **Journal of Chemical Education**, v. 50, n. 12, p. 839, 1 dez. 1973.

CARNEIRO, L. F. et al. **Análise do impacto de algumas simplificações em modelos de células a combustível PEMFC**. 24° Congresso Brasileiro de Engenharia Química. **Anais**...Salvador: 4 out. 2023. Disponível em: <https://proceedings.science/p/170782?lang=pt-br>

CARNEIRO, L. F. et al. Comparison Between Analytical and Numerical Solutions for Water Transport in the Membrane on a PEMFC Model. **Arabian Journal for Science and Engineering**, 15 set. 2024. Disponível em: <http://dx.doi.org/10.1007/s13369-024-09499-0>

CELIK, I. B.; PAKALAPATI, S. R. From a Single Cell to a Stack Modeling. Em: [s.l: s.n.]. p. 123–182.

CHASE, M. W. **NIST-JANAF Thermochemical Tables**. Fourth Edition ed. Washington, DC: American Chemical Society, 1998.

CHAUDHARY, S.; SACHAN, V. K.; BHATTACHARYA, P. K. Two dimensional modelling of water uptake in proton exchange membrane fuel cell. **International Journal of Hydrogen Energy**, v. 39, n. 31, p. 17802–17818, out. 2014.

CHU, D.; JIANG, R. Comparative studies of polymer electrolyte membrane fuel cell stack and single cell. **Journal of Power Sources**, v. 80, n. 1–2, p. 226–234, jul. 1999.

CHU, S.; MAJUMDAR, A. Opportunities and challenges for a sustainable energy future. **Nature**, v. 488, n. 7411, p. 294–303, 15 ago. 2012.

DICKINSON, E. J. F.; HINDS, G. The Butler-Volmer Equation for Polymer Electrolyte Membrane Fuel Cell (PEMFC) Electrode Kinetics: A Critical Discussion. **Journal of The Electrochemical Society**, v. 166, n. 4, p. F221–F231, 23 fev. 2019.

DICKINSON, E. J. F.; SMITH, G. Modelling the Proton-Conductive Membrane in Practical Polymer Electrolyte Membrane Fuel Cell (PEMFC) Simulation: A Review. **Membranes**, v. 10, n. 11, p. 310, 28 out. 2020.

DURST, J. et al. Hydrogen Oxidation and Evolution Reaction Kinetics on Carbon Supported Pt, Ir, Rh, and Pd Electrocatalysts in Acidic Media. **Journal of The Electrochemical Society**, v. 162, n. 1, p. F190–F203, 2015.

EG&G TECHNICAL SERVICES INC. **Fuel Cell Handbook**. Seventh ed. [s.l.] U.S. Department of Energy Office of Fossil Energy, 2004.

FALCÃO, D. S. et al. Water transport through a PEM fuel cell: A one-dimensional model with heat transfer effects. **Chemical Engineering Science**, v. 64, n. 9, p. 2216–2225, maio 2009.

FUTTER, G. A. et al. Physical modeling of polymer-electrolyte membrane fuel cells: Understanding water management and impedance spectra. **Journal of Power Sources**, v. 391, p. 148–161, jul. 2018.

GERTEISEN, D.; HEILMANN, T.; ZIEGLER, C. Modeling the phenomena of dehydration and flooding of a polymer electrolyte membrane fuel cell. **Journal of Power Sources**, v. 187, n. 1, p. 165–181, fev. 2009.

GLASGOW, L. A. **Transport phenomena: an introduction to advanced topics.** [s.l.] John Wiley & Sons, Inc., 2010.

GOSHTASBI, A. et al. A Mathematical Model toward Real-Time Monitoring of Automotive PEM Fuel Cells. **Journal of The Electrochemical Society**, v. 167, n. 2, p. 024518, 2 jan. 2020.

GUIDELLI, R. et al. Defining the transfer coefficient in electrochemistry: An assessment (IUPAC Technical Report). **Pure and Applied Chemistry**, v. 86, n. 2, p. 245–258, 1 fev. 2014a.

GUIDELLI, R. et al. Definition of the transfer coefficient in electrochemistry (IUPAC Recommendations 2014). **Pure and Applied Chemistry**, v. 86, n. 2, p. 259–262, 1 fev. 2014b.

HAMDOLLAHI, S.; JUN, L. A review on modeling of proton exchange membrane fuel cell. **Chemical Industry and Chemical Engineering Quarterly**, v. 29, n. 1, p. 61–74, 2023.

HAMOUR, M. et al. Electrical conductivity of PEMFC under loading. **Journal of Power Sources**, v. 289, p. 160–167, set. 2015.

HAN, J.; HWANG, J.; YU, S. A simulation of automotive fuel cell system for oxygen starvation trends by compressor surge under load follow-up. **Applied Thermal Engineering**, v. 154, p. 251–262, maio 2019.

HINATSU, J. T.; MIZUHATA, M.; TAKENAKA, H. Water Uptake of Perfluorosulfonic Acid Membranes from Liquid Water and Water Vapor. **Journal of The Electrochemical Society**, v. 141, n. 6, p. 1493–1498, 1 jun. 1994.

HUBER, M. L. et al. New International Formulation for the Viscosity of H2O. **Journal of Physical and Chemical Reference Data**, v. 38, n. 2, p. 101–125, 1 jun. 2009.

HUBER, M. L. et al. New International Formulation for the Thermal Conductivity of H2O. **Journal of Physical and Chemical Reference Data**, v. 41, n. 3, 1 set. 2012.

INCER-VALVERDE, J. et al. “Colors” of hydrogen: Definitions and carbon intensity. **Energy Conversion and Management**, v. 291, p. 117294, set. 2023.

IRANZO, A. et al. Experimental fuel cell performance analysis under different operating conditions and bipolar plate designs. **International Journal of Hydrogen Energy**, v. 35, n. 20, p. 11437–11447, out. 2010.

JIAO, K.; LI, X. Three-dimensional multiphase modeling of cold start processes in polymer electrolyte membrane fuel cells. **Electrochimica Acta**, v. 54, n. 27, p. 6876–6891, nov. 2009.

KIERZENKA, J.; SHAMPINE, L. F. A BVP solver based on residual control and the Maltab PSE. **ACM Transactions on Mathematical Software**, v. 27, n. 3, p. 299–316, set. 2001.

KNAPP-CORDES, M.; MCKEEMAN, B. **Improvements to tic and toc Functions for Measuring Absolute Elapsed Time Performance in MATLAB**. Disponível em: <https://www.mathworks.com/company/newsletters/articles/improvements-to-tic-and-toc-functions-for-measuring-absolute-elapsed-time-performance-in-matlab.html>. Acesso em: 21 dez. 2023.

KUHN, H.; WOKAUN, A.; SCHERER, G. G. Exploring single electrode reactions in polymer electrolyte fuel cells. **Electrochimica Acta**, v. 52, n. 6, p. 2322–2327, jan. 2007.

KULIKOVSKY, A. A. Quasi-3D Modeling of Water Transport in Polymer Electrolyte Fuel Cells. **Journal of The Electrochemical Society**, v. 150, n. 11, p. A1432, 2003.

KULIKOVSKY, A. A. **Analytical modelling of fuel cells**. Second Edition ed. [s.l.] Elsevier, 2019.

LAZAR, A. L.; KONRADT, S. C.; ROTTENGRUBER, H. Open-Source Dynamic Matlab/Simulink 1D Proton Exchange Membrane Fuel Cell Model. **Energies**, v. 12, n. 18, p. 3478, 9 set. 2019.

LEE, W. et al. The effects of compression and gas diffusion layers on the performance of a PEM fuel cell. **Journal of Power Sources**, v. 84, n. 1, p. 45–51, nov. 1999.

LINDSTROM, M.; WETTON, B. A comparison of Fick and Maxwell–Stefan diffusion formulations in PEMFC gas diffusion layers. **Heat and Mass Transfer**, v. 53, n. 1, p. 205–212, 8 jan. 2017.

LINSTROM, P. J.; WILLIAM, G. M. **NIST standard reference database number 69**.

LISO, V. et al. Modeling and experimental validation of water mass balance in a PEM fuel cell stack. **International Journal of Hydrogen Energy**, v. 41, n. 4, p. 3079–3092, jan. 2016.

MAIYALAGAN, T.; PASUPATHI, S. Components for PEM Fuel Cells: An Overview. **Materials Science Forum**, v. 657, p. 143–189, jul. 2010.

MAKHARIA, R.; MATHIAS, M. F.; BAKER, D. R. Measurement of Catalyst Layer Electrolyte Resistance in PEFCs Using Electrochemical Impedance Spectroscopy. **Journal of The Electrochemical Society**, v. 152, n. 5, p. A970, 2005.

MANN, R. F. et al. Development and application of a generalised steady-state electrochemical model for a PEM fuel cell. **Journal of Power Sources**, v. 86, n. 1–2, p. 173–180, mar. 2000.

MANSO, A. P. et al. Influence of geometric parameters of the flow fields on the performance of a PEM fuel cell. A review. **International Journal of Hydrogen Energy**, v. 37, n. 20, p. 15256–15287, out. 2012.

MATLAB. **Equation Solving Algorithms**. Disponível em: <https://www.mathworks.com/help/optim/ug/equation-solving-algorithms.html>. Acesso em: 13 set. 2023.

MAZUMDER, S. A Generalized Phenomenological Model and Database for the Transport of Water and Current in Polymer Electrolyte Membranes. **Journal of The Electrochemical Society**, v. 152, n. 8, p. A1633, 2005.

MEIER, F.; EIGENBERGER, G. Transport parameters for the modelling of water transport in ionomer membranes for PEM-fuel cells. **Electrochimica Acta**, v. 49, n. 11, p. 1731–1742, abr. 2004.

MEYERS, J. P.; NEWMAN, J. Simulation of the Direct Methanol Fuel Cell. **Journal of The Electrochemical Society**, v. 149, n. 6, p. A710, 2002.

MILLS, A. F.; COIMBRA, C. F. M. **Basic Heat and Mass Transfer**. Third Edition ed. San Diego: Temporal Publishing, LLC, 2015.

MONTGOMERY, D. C.; RUNGER, G. C. **Applied Statistics and Probability for Engineers**. Sixth Edition ed. [s.l.] Wiley, 2013.

MOTUPALLY, S.; BECKER, A. J.; WEIDNER, J. W. Diffusion of Water in Nafion 115 Membranes. **Journal of The Electrochemical Society**, v. 147, n. 9, p. 3171, 2000.

NEYERLIN, K. C. et al. Determination of Catalyst Unique Parameters for the Oxygen Reduction Reaction in a PEMFC. **Journal of The Electrochemical Society**, v. 153, n. 10, p. A1955, 2006.

NEYERLIN, K. C. et al. Study of the Exchange Current Density for the Hydrogen Oxidation and Evolution Reactions. **Journal of The Electrochemical Society**, v. 154, n. 7, p. B631, 2007.

NISHIMURA, A. et al. Numerical Simulation on Impacts of Thickness of Nafion Series Membranes and Relative Humidity on PEMFC Operated at 363 K and 373 K. **Energies**, v. 14, n. 24, p. 8256, 8 dez. 2021.

NITTA, I.; HIMANEN, O.; MIKKOLA, M. Contact resistance between gas diffusion layer and catalyst layer of PEM fuel cell. **Electrochemistry Communications**, v. 10, n. 1, p. 47–51, jan. 2008.

NÓBREGA, P. H. A. A review of physics-based low-temperature proton-exchange membrane fuel cell models for system-level water and thermal management studies. **Journal of Power Sources**, v. 558, p. 232585, fev. 2023.

O'HAYRE, R. et al. **Fuel Cell Fundamentals**. Third ed. Hoboken, New Jersey: John Wiley & Sons, Inc, 2016.

O'HAYRE, R.; BARNETT, D. M.; PRINZ, F. B. The Triple Phase Boundary. **Journal of The Electrochemical Society**, v. 152, n. 2, p. A439, 2005.

PAREKH, A. Recent developments of proton exchange membranes for PEMFC: A review. **Frontiers in Energy Research**, v. 10, 16 set. 2022.

PENNER, S. S. Steps toward the hydrogen economy. **Energy**, v. 31, n. 1, p. 33–43, jan. 2006.

PETRII, O. A. et al. Life of the Tafel equation: Current understanding and prospects for the second century. **Electrochimica Acta**, v. 52, n. 11, p. 3493–3504, mar. 2007.

PUKRUSHPAN, J. T.; PENG, H.; STEFANOPOULOU, A. G. Control-Oriented Modeling and Analysis for Automotive Fuel Cell Systems. **Journal of Dynamic Systems, Measurement, and Control**, v. 126, n. 1, p. 14–25, 1 mar. 2004.

RAZDAN, N. K.; LIN, T. C.; BHAN, A. Concepts Relevant for the Kinetic Analysis of Reversible Reaction Systems. **Chemical Reviews**, v. 123, n. 6, p. 2950–3006, 22 mar. 2023.

SALVA, J. A. et al. Validation of cell voltage and water content in a PEM (polymer electrolyte membrane) fuel cell model using neutron imaging for different operating conditions. **Energy**, v. 101, p. 100–112, abr. 2016.

SANTARELLI, M. G.; TORCHIO, M. F. Experimental analysis of the effects of the operating variables on the performance of a single PEMFC. **Energy Conversion and Management**, v. 48, n. 1, p. 40–51, jan. 2007.

SCHRÖDER, M. et al. Optimal operating conditions of PEM fuel cells in commercial aircraft. **International Journal of Hydrogen Energy**, v. 46, n. 66, p. 33218–33240, set. 2021.

SHABANI, B. **Solar-hydrogen combined heat and power systems for remote area power supply**. Doctor of Philosophy (PhD) Thesis—[s.l.] RMIT University, 2010.

SHAMPINE, L. F.; REICHELT, M. W. The MATLAB ODE Suite. **SIAM Journal on Scientific Computing**, v. 18, n. 1, p. 1–22, jan. 1997.

SI, C. et al. A Comprehensive Review on Measurement and Correlation Development of Capillary Pressure for Two-Phase Modeling of Proton Exchange Membrane Fuel Cells. **Journal of Chemistry**, v. 2015, p. 1–17, 2015.

SLATTERY, J. C.; BIRD, R. B. Calculation of the diffusion coefficient of dilute gases and of the self-diffusion coefficient of dense gases. **AIChE Journal**, v. 4, n. 2, p. 137–142, 17 jun. 1958.

SMITH, J. M. et al. **Introduction to Chemical Engineering Thermodynamics**. Eight ed. [s.l.] McGraw Hill, 2017.

SMITH, W. The role of fuel cells in energy storage. **Journal of Power Sources**, v. 86, n. 1–2, p. 74–83, mar. 2000.

SONG, C. et al. PEM fuel cell reaction kinetics in the temperature range of 23–120°C. **Electrochimica Acta**, v. 52, n. 7, p. 2552–2561, fev. 2007.

SOUZA, D. F. DE S. **Abordagem Algébrico-Diferencial Da Otimização Dinâmica De Processos**. Tese de Doutorado—Rio de Janeiro: Universidade Federal do Rio de Janeiro, 2007.

SPIEGEL, C. **PEM Fuel Cell Modeling and Simulation Using MATLAB®**. [s.l.] Academic Press, 2008.

SPRINGER, T. E.; ZAWODZINSKI, T. A.; GOTTESFELD, S. Polymer Electrolyte Fuel Cell Model. **Journal of The Electrochemical Society**, v. 138, n. 8, p. 2334–2342, 1 ago. 1991.

ŠTEKL, P.; KADLEC, P. **Influence of oxygen content at the PEM fuel cell cathode**. Joint conference Computational Problems of Electrical Engineering and Advanced Methods of the Theory of Electrical Engineering. **Anais**...Třebíč: 2015.

TANG, T. et al. A spatially resolved fuel cell stack model with gas–liquid slip phenomena for cold start simulations. **International Journal of Hydrogen Energy**, v. 42, n. 22, p. 15328–15346, jun. 2017.

TELLEZ-CRUZ, M. M. et al. Proton Exchange Membrane Fuel Cells (PEMFCs): Advances and Challenges. **Polymers**, v. 13, n. 18, p. 3064, 10 set. 2021.

TRIOLA, M. F. **Elementary Statistics**. 10th Edition ed. [s.l.] Pearson/Addison-Wesley, 2006.

TSOTRIDIS, G. et al. **EU harmonised test protocols for PEMFC MEA testing in single cell configuration for automotive applications**. Joint Research Centre: [s.n.].

UDDIN, K. M. S.; SAHA, L. K.; OSHIMA, N. Water Transport through the Membrane of PEM Fuel Cell. **American Journal of Computational and Applied Mathematics**, p. 225–238, 2014.

VETTER, R.; SCHUMACHER, J. O. Free open reference implementation of a two-phase PEM fuel cell model. **Computer Physics Communications**, v. 234, p. 223–234, jan. 2019a.

VETTER, R.; SCHUMACHER, J. O. Experimental parameter uncertainty in proton exchange membrane fuel cell modeling. Part I: Scatter in material parameterization. **Journal of Power Sources**, v. 438, p. 227018, out. 2019b.

WAGNER, W.; PRUSS, A. International Equations for the Saturation Properties of Ordinary Water Substance. Revised According to the International Temperature Scale of 1990. Addendum to J. Phys. Chem. Ref. Data **16** , 893 (1987). **Journal of Physical and Chemical Reference Data**, v. 22, n. 3, p. 783–787, 1 maio 1993.

WANG, C.-Y. Fundamental Models for Fuel Cell Engineering. **Chemical Reviews**, v. 104, n. 10, p. 4727–4766, 1 out. 2004.

WANG, Y. et al. A review of polymer electrolyte membrane fuel cells: Technology, applications, and needs on fundamental research. **Applied Energy**, v. 88, n. 4, p. 981–1007, abr. 2011.

WEBER, A. Z. et al. A Critical Review of Modeling Transport Phenomena in Polymer-Electrolyte Fuel Cells. **Journal of The Electrochemical Society**, v. 161, n. 12, p. F1254–F1299, 13 set. 2014.

WEBER, A. Z.; NEWMAN, J. Transport in Polymer-Electrolyte Membranes. **Journal of The Electrochemical Society**, v. 151, n. 2, p. A311, 2004a.

WEBER, A. Z.; NEWMAN, J. A theoretical study of membrane constraint in polymer-electrolyte fuel cells. **AIChE Journal**, v. 50, n. 12, p. 3215–3226, 11 dez. 2004b.

XU, L. et al. A reduced-dimension dynamic model of a proton-exchange membrane fuel cell. **International Journal of Energy Research**, v. 45, n. 12, p. 18002–18017, 10 out. 2021.

YANG, Z. et al. A comprehensive proton exchange membrane fuel cell system model integrating various auxiliary subsystems. **Applied Energy**, v. 256, p. 113959, dez. 2019.

YUAN, W.-W. et al. Analyzing and Modeling of Water Transport Phenomena in Open-Cathode Polymer Electrolyte Membrane Fuel Cell. **Applied Sciences**, v. 11, n. 13, p. 5964, 26 jun. 2021.

ZAMEL, N.; LI, X. Effective transport properties for polymer electrolyte membrane fuel cells – With a focus on the gas diffusion layer. **Progress in Energy and Combustion Science**, v. 39, n. 1, p. 111–146, fev. 2013.

ZHANG, G.; KANDLIKAR, S. G. A critical review of cooling techniques in proton exchange membrane fuel cell stacks. **International Journal of Hydrogen Energy**, v. 37, n. 3, p. 2412–2429, fev. 2012.

ZHANG, J. et al. PEM fuel cell relative humidity (RH) and its effect on performance at high temperatures. **Electrochimica Acta**, v. 53, n. 16, p. 5315–5321, jun. 2008.

ZHANG, S. et al. Polymer electrolyte fuel cell modeling - A comparison of two models with different levels of complexity. **International Journal of Hydrogen Energy**, v. 45, n. 38, p. 19761–19777, jul. 2020.

ZHOU, P.; WU, C. W.; MA, G. J. Contact resistance prediction and structure optimization of bipolar plates. **Journal of Power Sources**, v. 159, n. 2, p. 1115–1122, set. 2006.

ZHOU, Y. et al. Modeling of cold start processes and performance optimization for proton exchange membrane fuel cell stacks. **Journal of Power Sources**, v. 247, p. 738–748, fev. 2014.

APPENDIX A – RELATIONSHIP BETWEEN GIBBS ENERGY AND ELECTRICAL WORK

Equation A.1 presents the definition of Gibbs energy (Smith *et al.*, 2017 p. 211).

$$G \equiv U + PV - TS \tag{A.1}$$

Differentiating this equation, Equation A.2 is obtained.

$$dG = dU + VdP + PdV - TdS - SdT \tag{A.2}$$

In a closed system, the first law of thermodynamics may be written as presented in Equation A.3 (Smith *et al.*, 2017 p. 28).

$$dU = dQ + dW \tag{A.3}$$

In the considered system, the work can be separated into electrical work and mechanical, as proposed in Equation A.4 (O'Hayre *et al.*, 2016 p. 40). Note that the mechanical work has a negative sign, as the work is done by the system on the surroundings. Also, all the represented works here are assumed to be reversible.

$$dW = dW_{ele} + dW_{mech} = dW_{ele} - PdV \tag{A.4}$$

As the objective is to evaluate the maximum amount of work that a fuel cell could provide, the heat transfer process is considered reversible as well. Therefore, Equation A.5 can be used (Smith *et al.*, 2017 p. 174).

$$dQ_{rev} = TdS \tag{A.5}$$

Using the results of Equations A.4 and A.5 in A.3 and substituting it in A.2 results in Equation A.6.

$$dG = dW_{ele} - SdT + VdP \tag{A.6}$$

Thus, for a constant pressure and temperature system, ($dP = 0$ and $dT = 0$), Equation A.7 is reached.

$$dG = dW_{ele} \tag{A.7}$$

Finally, considering that the change in the Gibbs energy of the system is caused by a chemical reaction, Equation A.8 is obtained, which demonstrates that the maximum amount of electrical work (as a reversible process was assumed) is given by the variation of the Gibbs energy due to the reaction. Special attention should be given to the sign of work: in the convention used, the work done by the system is considered negative, and, as a spontaneous process, such as the chemical reactions that exist in a fuel cell, have negative values for ΔG, the equation is consistent with the definitions made.

$$\Delta G_{rnx} = W_{ele} \quad \text{(A.8)}$$

The restriction of constant pressure and temperature is reasonable for fuel cells, as they normally operate at those conditions and the equation only demands that this should be true during the reaction, and, therefore, is valid for any temperature and pressure (O'Hayre *et al.*, 2016 p. 40).

If the relation is desired to be written as a function of voltage instead of electrical work, one can combine Equations A.9 and A.10 in A.8, obtaining Equation A.11. In those equations, n is the number of moles of electrons transferred, Q is the charge which is moved and F is the Faraday constant.

$$W_{ele} = EQ \quad \text{(A.9)}$$

$$Q = nF \quad \text{(A.10)}$$

$$E = -\frac{\Delta G_{rnx}}{nF} \quad \text{(A.11)}$$

References:

SMITH, J. M. et al. **Introduction to Chemical Engineering Thermodynamics**. Eight ed. [s.l.] McGraw Hill, 2017.

APPENDIX B – DESCRIPTION OF THE VOLUME FRACTION OF WATER IN THE MEMBRANE

Considering constant additive molar volumes, the total volume of the membrane after swelling (V) is equal to the sum of dry membrane volume and water volume in the membrane. This assumption, as presented by Weber and Newman (2004b), is based on experimental data. Equation B.1 presents this relation.

$$V = \overline{V}_m + \lambda \overline{V}_{H2O} \tag{B.1}$$

The molar volume of a dry membrane ($\overline{V}_m$) can be calculated as the ratio between Nafion's equivalent weight (EW) and the membrane's dry density, as seen in Equation B.2. Equivalent weight is defined as the atomic weight of a species divided by its valence. Considering that the sulfonic group present in Nafion can only accept one proton (has a valence equal to one), it represents the average weight of the polymer chain capable of accepting one H^+ (O'Hayre *et al.*, 2016 p. 143). For Nafion, this value is typically between 1 and 1,1 $kg \cdot mol^{-1}$.

$$\overline{V}_m = \frac{EW}{\rho_{m,dry}} \tag{B.2}$$

Moreover, the molar volume of water at a given temperature can be obtained by the more available density value simply by using its molar mass of $MM_{H_2O} = 18.1528 \cdot 10^{-3}\ kg\ mol^{-1}$, as presented in Equation B.3.

$$\overline{V}_{H2O} = \frac{MM_{H2O}}{\rho_{H2O}} \tag{B.3}$$

The molar volume of water can be multiplied by λ – the ratio between moles of water and moles of sulfonic groups in the membrane – to obtain the volume of water per mol of sulfonic group. Dividing this value by the total volume given by Equation B.1 yields the volume fraction of water in the membrane, shown in Equation B.4.

$$\varphi = \frac{\lambda \overline{V}_{H2O}}{\overline{V}_m + \lambda \overline{V}_{H2O}} \tag{B.4}$$

To further explain this relation, a dimensional analysis of the numerator and denominator of Equation B.4 is presented, respectively, in Equation B.5 and B.6.

$$\lambda \overline{V}_{H2O} = \frac{moles\ of\ H_2O}{moles\ of\ SO_3^-H^+} \frac{m^3 of\ H_2O}{moles\ of\ H_2O} = \frac{m^3 of\ H_2O}{moles\ of\ SO_3^-H^+} \tag{B.5}$$

$$\overline{V}_m + \lambda \overline{V}_{H2O} = \frac{\frac{kg\ of\ dry\ Nafion}{moles\ of\ SO_3^- H^+}}{\frac{kg\ of\ dry\ Nafion}{m^3 of\ dry\ Nafion}} + \frac{m^3 of\ H_2O}{moles\ of\ SO_3^- H^+} \tag{B.6}$$

$$= \frac{m^3 of\ dry\ Nafion}{moles\ of\ SO_3^- H^+} + \frac{m^3 of\ H_2O}{moles\ of\ SO_3^- H^+}$$

Finally, considering both of the previous equations, it should be evident that φ is given by the volume of water divided by the total (membrane + water) volume, as expected.

References:

WEBER, A. Z.; NEWMAN, J. A theoretical study of membrane constraint in polymer-electrolyte fuel cells. **AIChE Journal**, v. 50, n. 12, p. 3215–3226, 11 dez. 2004b.

APPENDIX C – DEDUCTION OF THE EXPRESSIONS USED TO DESCRIBE THE DEPLETION EFFECTS

In this deduction, the flux balance (Equation 51) and the definition of stoichiometric number (Equations 66 and 67) are used. Also, the base hypothesis for this deduction is that a perfect mixture exists in the gas channel, which means that the bulk composition, present in the GC/GDL interface, is equal to the outlet one. The notation here follows the one presented in Figure 11, and Equation C.1 is used to simplify the notation.

$$I \equiv \frac{j}{2F} \tag{C.1}$$

Anode:

Based on the hypothesis of an ideal mixture and using the fact that the anode gas is a binary mixture of hydrogen and water, Equation C.2 can be written.

$$x^A_{H_2O,a} = \frac{J^A_{H_2,out}}{J^A_{H_2,out} + J^A_{H_2O,out}} \tag{C.2}$$

The outlet hydrogen flux is equal to the inlet flux minus what reacts. Using the concept of stoichiometric number to write the inlet flux as the product of this number and the flux used in the reaction, Equation C.3 is reached.

$$J^A_{H_2,out} = \lambda_{H_2} J^A_{H_2} - J^A_{H_2} = \left(\lambda_{H_2} - 1\right) \cdot I \tag{C.3}$$

The water inlet value in the anode is equal to the product of the total inlet flux in the anode and the molar fraction of water in the anode inlet. As the total inlet flux can be obtained as the ratio between hydrogen flux and hydrogen molar fraction, Equation C.4 is reached.

$$J^A_{H_2O,in} = \frac{J^A_{H_2,in}}{x_{H_2,in}} x^A_{H_2O,in} \tag{C.4}$$

As the mixture in binary, the molar fraction of hydrogen may be written as a function of the water one. Using this and the stoichiometric number, Equation C.5 is obtained.

$$J^A_{H_2O,in} = \lambda_{H_2} \left(\frac{x^A_{H_2O,in}}{1 - x^A_{H_2O,in}} \right) \cdot I \tag{C.5}$$

A similar procedure is used for describing the outlet water flux. In this case, the same relation with molar fractions and total flux is used, but now with outlet values, resulting in Equation C.6.

$$J^A_{H_2O,out} = \frac{J^A_{H_2,out}}{x_{H_2,out}} x_{H_2O,out} \tag{C.6}$$

By the ideal mixture, it is known that the outlet molar fractions are equal to the bulk values. Thus, using this and Equation C.2, Equation C.7 is obtained.

$$J^A_{H_2O,out} = (\lambda_{H_2} - 1)\left(\frac{x^A_{H_2O,a}}{1 - x^A_{H_2O,a}}\right) \cdot I \tag{C.7}$$

The net water flux in the anode is given by the inlet one minus the outlet flux of water, which, by the flux balance, is also equal to $I\alpha^*$. Therefore, Equation C.8 represents the net water flux.

$$J^A_{H_2O} = I\alpha^* = \lambda_{H_2}\left(\frac{x^A_{H_2O,in}}{1 - x^A_{H_2O,in}}\right) \cdot I - (\lambda_{H_2} - 1)\left(\frac{x^A_{H_2O,a}}{1 - x^A_{H_2O,a}}\right) \cdot I \tag{C.8}$$

Isolating the bulk water molar fraction in the previous expression, a description for the bulk molar fraction of water is reached (Equation C.9). Also, Equation C.10 can be easily obtained by remembering the binary nature of the mixture.

$$x^A_{H_2O,a} = \frac{\lambda_{H_2} x^A_{H_2O,in} - \alpha^*(1 - x^A_{H_2O,in})}{x^A_{H_2O,in} - \alpha^*(1 - x^A_{H_2O,in}) + \lambda_{H_2} - 1} \tag{C.9}$$

$$x^A_{H_2,a} = 1 - x^A_{H_2O,a} \tag{C.10}$$

Cathode:

The cathode is a ternary mixture of oxygen, nitrogen, and water. Considering this, the bulk concentration of oxygen can be described by Equation C.11.

$$x_{O_2,d} = \frac{J^C_{O_2,out}}{J^C_{O_2,out} + J^C_{N_2,out} + J^C_{H_2O,out}} \tag{C.11}$$

By an analogous procedure to what was done in the anode using the flux balance and definition of stoichiometric number, Equations C.12-C.15 are reached, where ω is defined by Equation C.16.

$$J^C_{O_2,in} = \lambda_{O_2}\frac{I}{2} \tag{C.12}$$

$$J^C_{O_2,out} = (\lambda_{O_2} - 1)\frac{I}{2} \tag{C.13}$$

$$J^C_{N_2,in} = \omega\lambda_{O_2}\frac{I}{2} \tag{C.14}$$

$$J^C_{N_2,out} = \omega\lambda_{O_2}\frac{I}{2} \tag{C.15}$$

$$\omega = \frac{x^C_{N_2,dry,in}}{x^C_{O_2,dry,in}} \tag{C.16}$$

The water inlet and outlet flows are described respectively by Equations C.17 and C.18. The first one is obtained in a similar manner to Equation C.5, but considering

that the mixture is ternary, instead of binary, when describing the total flux. The second one is a consequence of the flux balance.

$$J^C_{H_2O,in} = \lambda_{O_2}\left(\frac{x^C_{H_2O,in}}{1 - x^C_{H_2O,in}}\right)\cdot\frac{1}{x^C_{O_2,dry,in}}\cdot\frac{I}{2} \tag{C.17}$$

$$J^C_{H_2O,out} = J^C_{H_2O,in} + (1+\alpha^*)I \tag{C.18}$$

Using Equations C.13, C.15, and C.18, the total outlet flux in the cathode can be described with Equation C.19.

$$J^C_{total,out} = \left(\frac{\lambda_{O_2}}{2\left(1 - x^C_{H_2O,in}\right)x^C_{O_2,dry,in}} + \alpha^* + \frac{1}{2}\right)\cdot I \tag{C.19}$$

Finally, Equations C.20 and C.21 may be obtained using a combination of either C.13 or C.18 with C.19.

$$x^C_{O_2,d} = \frac{\left(\lambda_{O_2} - 1\right)\left(1 - x^C_{H_2O,in}\right)x^C_{O_2,dry,in}}{\lambda_{O_2} + (2\alpha^* + 1)\left(1 - x^C_{H_2O,in}\right)x^C_{O_2,dry,in}} \tag{C.20}$$

$$x^C_{H_2O,d} = \frac{\lambda_{O_2}x^C_{H_2O,in} + 2(1+\alpha^*)\left(1 - x^C_{H_2O,in}\right)x^C_{O_2,dry,in}}{\lambda_{O_2} + (2\alpha^* + 1)\left(1 - x^C_{H_2O,in}\right)x^C_{O_2,dry,in}} \tag{C.21}$$

Therefore, using the stoichiometric number, α^*, and the inlet values, it is possible to determine the bulk values of the electrodes.

APPENDIX D – DEDUCTION OF THE TRANSPORT EQUATIONS USING FICK AND STEFAN-MAXWELL MODELS

The flux balance in a fuel cell (Equation 51) can be used to associate the flux with current density, an input of the proposed fuel cell models. Thus, using it and a specific transport model it is possible to obtain a relation between concentration in an arbitrary z point of the electrode and system variables. This relation is deduced here for both Fickian diffusion and the Stefan-Maxwell model.

Fickian diffusion

Substituting the relation for water flow in the anode in Fick's law (Equation 53), the ordinary differential equation presented in Equation D.1 is reached.

$$\frac{dx_{H_2O}^A}{dz} = -\left(\frac{\alpha^* jRT}{2FP^A D_{Ano}^{Eff}}\right) \tag{D.1}$$

This is a separable ode, which can be integrated from 0 to the arbitrary point z, resulting in Equation D.2. Naturally, as the anode is composed of a binary mix, the hydrogen concentration can be obtained by Equation D.3.

$$x_{H_2O}^A(z) = x_{H_2O,a}^A - \left(\frac{\alpha^* jRT}{2FP^A D_{Ano}^{Eff}}\right) z \tag{D.2}$$

$$x_{H_2}^A(z) = 1 - x_{H_2O}^A(z) \tag{D.3}$$

A similar process can be done in the cathode. Substituting the flux expression on Fick's law for both oxygen and water, Equations D.4 and D.5 are reached. Note that the direction used here is z', which is positive when going from the cathode to the anode, the inverse of z.

$$\frac{dx_{O_2}^C}{dz'} = -\left(\frac{jRT}{4FP^C D_{Cat}^{Eff}}\right) \tag{D.4}$$

$$\frac{dx_{H_2O}^C}{dz'} = -\left(\frac{-(1+\alpha^*)jRT}{2FP^C D_{Cat}^{Eff}}\right) \tag{D.5}$$

Integrating both from 0 (GC/CGDL interface) until an arbitrary distance z', Equations D.6 and D.7 are reached.

$$x_{O_2}^C(z') = x_{O_2,d}^C - \left(\frac{jRT}{4FP^C D_{Cat}^{Eff}}\right) z' \tag{D.6}$$

$$x_{H_2O}^C(z') = x_{H_2O,d}^C + \left(\frac{(1+\alpha^*)jRT}{2FP^C D_{Cat}^{Eff}}\right) z' \tag{D.7}$$

Stefan-Maxwell model

The Stefan-Maxwell model is described by Equation D.8.

$$\frac{dx_i}{dz} = \left(\frac{RT}{P}\right)\sum_{j\neq i}\frac{x_i J_j - x_j J_i}{D_{i,j}^{eff}} \tag{D.8}$$

Using this equation to describe the water molar fraction in the anode, Equation D.9 is obtained.

$$\frac{dx_{H_2O}^A}{dz} = \left(\frac{RT}{P^A}\right)\left(\frac{x_{H_2O}^A J_{H_2} - x_{H_2O}^A J_{H_2O}}{D_{H_2O,H_2}^{eff}}\right) \tag{D.9}$$

Substituting the description of the flux balance, Equation D.10 is reached.

$$\frac{dx_{H_2O}^A}{dz} = \left(\frac{RT}{P^A}\right)\left(\frac{x_{H_2O}(I) - x_{H_2}(I\alpha^*)}{D_{H_2O,H_2}^{eff}}\right) \tag{D.10}$$

This previous equation can be integrated between 0 and an arbitrary position z, resulting in Equation D.11. Finally, as the mixture is binary, Equation D.12 can also be written.

$$x_{H_2O}^A(z) = \left(x_{H_2O,a}^A - \frac{\alpha^*}{1+\alpha^*}\right)e^{\left[\frac{RTI}{P^A D_{H_2O,H_2}^{eff}}(1+\alpha^*)z\right]} + \frac{\alpha^*}{1+\alpha^*} \tag{D.11}$$

$$x_{H_2}^A(z) = 1 - x_{H_2O}^A(z) \tag{D.12}$$

The same procedure can be applied to the cathode, resulting in Equation D.13 for water. Note that, as it was done when Fickian diffusion was assumed, here the z' axis is considered.

$$\frac{dx_{H_2O}^C}{dz'} = \left(\frac{RT}{P^C}\right)\left(\frac{x_{H_2O}^C J_{N_2}^C - x_{N_2} J_{H_2O}^C}{D_{H_2O,N_2}^{eff}} + \frac{x_{H_2O}^C J_{O_2}^C - x_{O_2}^C J_{H_2O}^C}{D_{H_2O,O_2}^{eff}}\right) \tag{D.13}$$

Substituting the fluxes, paying special attention to the fact that a negative sign should be added in the water flux to account for the fact that the z' axis is used, Equation D.14 is obtained.

$$\frac{dx_{H_2O}^C}{dz'} = \left(\frac{RTI}{P^C}\right)\left(\frac{(1+\alpha^*)\left(1 - x_{H_2O}^C - x_{O_2}^C\right)}{D_{H_2O,N_2}^{eff}} + \frac{0.5x_{H_2O}^C + x_{O_2}^C(1+\alpha^*)}{D_{H_2O,O_2}^{eff}}\right) \tag{D.14}$$

The oxygen molar fraction can be written similarly, also using the z' axis. This description yields Equation D.15.

$$\frac{dx_{O_2}^C}{dz'} = -\left(\frac{RTI}{P^C}\right)\left(\frac{0.5\left(1 - x_{H_2O}^C - x_{O_2}^C\right)}{D_{O_2,N_2}^{eff}} + \frac{(1+\alpha^*)x_{O_2}^C + 0.5x_{H_2O}^C}{D_{H_2O,O_2}^{eff}}\right) \tag{D.15}$$

Differently from the anode description, the integration here is not simple. Thus, a numerical solution of those differential equations is needed. For this, the boundary condition used is the value at z' = 0, which is equal to the bulk cathode molar fraction

for each gas, given either by the inlet value or by the equations deduced in Appendix C if depletion effects are considered.

APPENDIX E – CONTINUOUS EXPRESSIONS OBTAINED BY THE USAGE OF REGULARIZATION FUNCTIONS

In this topic, the continuous expressions obtained for piecewise models by the usage of a regularization function are presented. This function has the behavior described by Equation E.1.

$$\mathrm{H}(arg, par) \cong \begin{cases} 1, & arg < 0 \\ 0, & arg \geq 0 \end{cases} \tag{E.1}$$

All the expressions presented here were obtained following the procedures exemplified in Equation 109 and the function description.

Electro-osmotic drag coefficient:

Piecewise linear (Vetter *et* Schumacher, 2019b)

$$\begin{aligned} \xi(\lambda) = {} & \mathrm{H}(\lambda - 1, par) \cdot \lambda + [1 - \mathrm{H}(\lambda - 1, par)] \cdot \mathrm{H}(\lambda - \lambda_{VE}, par) \cdot 1 \\ & + [1 - \mathrm{H}(\lambda - \lambda_{VE}, par)] \cdot \left[1 + (\xi_l - 1)\frac{\lambda - \lambda_{VE}}{\lambda_{LE} - \lambda_{VE}}\right] \end{aligned} \tag{E.2}$$

Water diffusivity in Nafion:

Mazumder (2005)

$$\begin{aligned} D_\lambda(\lambda) = {} & \{\mathrm{H}(\lambda - 2, par) \cdot 1 + [1 - \mathrm{H}(\lambda - 2, par)] \cdot \mathrm{H}(\lambda - 3, par) \cdot [1 + 2(\lambda - 2)] \\ & + [1 - \mathrm{H}(\lambda - 3, par)] \cdot \mathrm{H}(\lambda - 4, par) \cdot [3 - 1.38(\lambda - 3)] \\ & + [1 - \mathrm{H}(\lambda - 4, par)](2.563 - 0.33\lambda + 0.0264\lambda^2 \\ & - 0.000671\lambda^3)\}10^{-10} e^{\left[2416\left(\frac{1}{303} - \frac{1}{T}\right)\right]} \end{aligned} \tag{E.3}$$

APPENDIX F – DETERMINATION OF INTEGRATION CONSTANTS AND INTERVALS ASSOCIATED WITH WATER CONTENT DESCRIPTION

The different electro-osmotic drag relations proposed in this text will yield varied expressions for the differential equation that describes water content (λ). Considering that, when the value of D_λ is assumed constant, the integration of the differential equation is done analytically and that some models use piecewise functions, the intervals of those integrations should be defined carefully.

The procedure to describe λ for each electro-osmotic coefficient is similar. A definite integral is made from λ_{Ano} to a generic λ, and from 0 to the corresponding z. However, if the expression was a piecewise function, its integration was divided into steps, as shown in Equation F.1. In this equation, z_c is the critical z value, which makes the first term equal exactly to its limit value of applicability.

$$\lambda(z) = \int_0^{z_C} f(z)dz + \int_{z_C}^{z} g(z)dz \tag{F.1}$$

This value of z_c is obtained by solving the resulting equation of substituting this limit λ value in the expression of the integral. Note that this is only necessary when z is greater than z_c.

The specific case of each model will be covered in the following topics, and those for Springer's and the Piecewise-Linear description are also present in an article published by the author (CARNEIRO et al., 2024). An important consideration made here is that the anode λ value is always assumed greater than the cathode one – resulting in a derivative that is positive for every z. This is reasonable, considering that there is water production in the cathode only.

Springer *et al.* (1991)

There is only one expression used in the whole integral, therefore, the solution is given by a single integration. Thus, the λ profile is determined by Equation F.2.

$$\lambda(z) = \frac{11\alpha^*}{n_{drag}^{sat}} + \left(\lambda_{Ano} - \frac{11\alpha^*}{n_{drag}^{sat}}\right) \cdot \exp\left(\frac{n_{drag}^{sat}}{22} \cdot \frac{jEWz}{F\rho_{dry}D_{\lambda,mean}}\right) \tag{F.2}$$

Meier *et* Eigenberger (2004)

This definition, such as Springer's model uses only one expression for the whole interval. However, the solution is not as straightforward. First, to summarize the notation, Equation F.3 presents some definitions.

$$\mathrm{K} = \frac{jEW}{F\rho_{dry}D_{\lambda,mean}} \tag{F.3}$$

$$a = 0.0026, \qquad b = 0.028, \qquad c = 1 - 0.5\alpha^*$$

The nature of this equation demands that different approaches to the integral are used according to the value of $\Delta = b^2 - 4ac$. The most common case is a negative value for Δ, which happens for α*< 1,84923. Therefore, the solution steps for this problem will be detailed, while only the final solution will be presented for the other cases (Δ = 0 and Δ > 0).

The integral that should be solved is presented in Equation F.4a. The strategy used for solving it is a trigonometric substitution after rewriting it as Equation F.4b.

$$\int_{\lambda_{Ano}}^{\lambda} \frac{1}{a\lambda^2 + b\lambda + c}\, d\lambda \tag{F.4a}$$

$$\int_{\lambda_{Ano}}^{\lambda} \frac{1}{\left(\lambda + \frac{b}{2a}\right)^2 + \left(\frac{\sqrt{4ac - b^2}}{2a}\right)^2}\, d\lambda \tag{F.4b}$$

The solution of this integral is given by Equation F.5.

$$\left(\frac{2}{\sqrt{4ac - b^2}}\right)\tan^{-1}\left(\frac{2a\lambda + b}{\sqrt{4ac - b^2}}\right)\Big|_{\lambda_{Ano}}^{\lambda} \tag{F.5}$$

Then this solution can be used along with the other integral (dependent on z), yielding Equation F.6. Finally, the expression can be manipulated to reach Equation F.7, which describes the profile.

$$\tan^{-1}\left(\frac{2a\lambda + b}{\sqrt{4ac - b^2}}\right) = \tan^{-1}\left(\frac{2a\lambda_{Ano} + b}{\sqrt{4ac - b^2}}\right) + \left(\frac{\sqrt{4ac - b^2}}{2}\right)Kz \tag{F.6}$$

$$\lambda(z) = \frac{-b}{2a} + \frac{\sqrt{4ac - b^2}}{2a}\tan\left[\tan^{-1}\left(\frac{2a\lambda_{Ano} + b}{\sqrt{4ac - b^2}}\right) + \left(\frac{\sqrt{4ac - b^2}}{2}\right)Kz\right] \tag{F.7}$$

Equation F.8 presents the final result for Δ > 0 and Equation F.9 for Δ = 0.

$$\lambda(z) = \frac{1}{2a - 2aAB}\left(-b + \sqrt{b^2 - 4ac} + AB\sqrt{b^2 - 4ac} + ABb\right) \tag{F.8}$$

$$A = \frac{2a\lambda_{Ano} + b - \sqrt{b^2 - 4ac}}{a\lambda_{Ano} + b + \sqrt{b^2 - 4ac}} \quad B = e^{\left(Kz\sqrt{b^2 - 4ac}\right)}$$

$$\lambda(z) = \frac{4a\lambda_{Ano} + 2abKz\lambda_{Ano} + b^2Kz}{4a - 4a^2\lambda_{Ano}Kz - 2abKz} \tag{F.9}$$

Piecewise Linear (Vetter et Schumacher, 2019b)

When the piecewise linear description for ξ is used, the problem should be divided into many cases. It can have up to three expressions coexisting in the domain, therefore, the approach shown in Equation F.1 must be used. Nevertheless, the integrals themselves, due to the linear nature of the expressions, are not complex. So, only the final results will be presented for each case.

For concise notation, the definition presented in Equation F.10 is used.

$$K = \left(\frac{jEW}{F\rho_{dry}D_{\lambda,mean}}\right) \tag{F.10}$$

Case 1: $\lambda_{Ano} < 1$ and $\lambda_{Cat} < 1$ (one interval)

Only one expression exists, which can be readily integrated to yield Equation F.11.

$$\lambda(z) = 0.5\alpha^* + (\lambda_{Ano} - 0.5\alpha^*) \cdot exp(Kz) \tag{F.11}$$

Case 2: $1 \leq \lambda_{Ano} < \lambda_{VE}$ and $1 \leq \lambda_{Cat} < \lambda_{VE}$ (one interval)

As in the previous case, only one interval exists. The solution is given by Equation F.12.

$$(z) = (1 - 0.5\alpha^*) \cdot \left(\frac{jEWz}{F\rho_{dry}D_{\lambda,mean}}\right) + \lambda_{Ano} \tag{F.12}$$

Case 3: $\lambda_{VE} \leq \lambda_{Ano} < \lambda_{LE}$ and $\lambda_{VE} \leq \lambda_{Cat} < \lambda_{LE}$ (one interval)

The solution – Equation F.13 – is analogous to the previous two cases.

$$\lambda(z) = \lambda_{VE} - \left(\frac{1 - 0.5\alpha^*}{C}\right) + \left(\frac{C\lambda_{VE} + 0.5\alpha^* - 1}{C}\right)[exp(CKz)] \tag{F.13}$$

$$C = \left(\frac{\xi_{L,max} - 1}{\lambda_{LE} - \lambda_{VE}}\right)$$

Case 4: $\lambda_{Ano} < 1$ and $1 \leq \lambda_{Cat} < \lambda_{VE}$ (Two intervals)

Here, two expressions exist. This demands the application of Equation F.1, which results in Equation F.14.

$$\lambda(z) = \begin{cases} 0.5\alpha^* + (\lambda_{Ano} - 0.5\alpha^*)exp(Kz), & z \leq z_c \\ 1 + (1 - 0.5\alpha^*)(Kz)(z - z_c), & x > z_c \end{cases} \tag{F.14}$$

$$z_c = \left(\frac{1}{K}\right)\ln\left(\frac{1-0.5\alpha^*}{\lambda_{Ano}-0.5\alpha^*}\right)$$

Case 5: $1 \le \lambda_{Ano} < \lambda_{VE}$ and $\lambda_{VE} \le \lambda_{Cat} < \lambda_{LE}$ (Two intervals)

Two expressions also are present here. The integral results in Equation F.15.

$$(z) = \begin{cases} (1-0.5\alpha^*)\cdot(Kz) + \lambda_{Ano}, & z \le z_c \\ \lambda_{VE} - \left(\frac{1-0.5\alpha^*}{C}\right) + \left(\frac{1-0.5\alpha^*}{C}\right)\left[exp\left(CK\ (z-z_c)\right)\right], & x > z_c \end{cases} \quad \text{(F.15)}$$

$$z_c = \left(\frac{\lambda_{VE}-\lambda_{Ano}}{1-0.5\alpha^*}\right)\cdot\left(\frac{1}{K}\right)$$

Case 6: $\lambda_{Ano} < 1$ and $\lambda_{VE} \le \lambda_{Cat} < \lambda_{LE}$ (Three intervals)

This is the most complex case, involving three expressions. Therefore, there is an extra integral when compared to Equation F.1, making it so that two critical z values exit. The final result of this careful integration is Equation F.16.

$$(z) = \begin{cases} 0.5\alpha^* + (\lambda_{Ano}-0.5\alpha^*)exp(Kz), & z \le z_{c1} \\ 1 + (1-0.5\alpha^*)(Kz)(z-z_{c1}), & z_{c1} < z \le z_{c2} \\ \lambda_{VE} - \left(\frac{1-0.5\alpha^*}{C}\right) + \left(\frac{1-0.5\alpha^*}{C}\right)\left[exp\left(CK\ (z-z_{c2})\right)\right], & z > z_{c2} \end{cases} \quad \text{(F.16)}$$

$$z_{c1} = \left(\frac{1}{K}\right)\ln\left(\frac{1-0.5\alpha^*}{\lambda_{Ano}-0.5\alpha^*}\right)$$

$$z_{c2} = z_{c1} + \left(\frac{\lambda_{VE}-1}{1-0.5\alpha^*}\right)\cdot\left(\frac{1}{K}\right)$$

APPENDIX G – RESULTS FOR THE SIMULATION COMPARING BUTLER-VOLMER AND TAFEL

		Type	V (V)	j (A/cm²)	W (W/cm²)	η_{Act}	η_{Ohm}	η_{Conc}
3.1.1	**Ref. (BV)**		0.8398	0.10	0.0840	0.3353	0.0141	0.0004
		Specific	0.4906	0.80	0.3925	0.3958	0.2996	0.0035
			0.0058	1.40	0.0081	0.4121	0.7650	0.0067
		Optimal	0.5074	0.77	0.3928	-	-	-
	Tafel		0.8399	0.10	0.0840	0.3352	0.0141	0.0004
		Specific	0.4909	0.80	0.3927	0.3955	0.2996	0.0035
			0.0063	1.40	0.0089	0.4116	0.7650	0.0067
		Optimal	0.5077	0.77	0.3931	-	-	-
3.1.2	**Ref.**		0.8399	0.10	0.0840	0.3353	0.0141	0.0004
		Specific	0.4908	0.80	0.3926	0.3956	0.2996	0.0035
			0.0061	1.40	0.0085	0.4119	0.7650	0.0067
		Optimal	0.5076	0.77	0.3930	-	-	-
	Sim.		0.8399	0.10	0.0840	0.3352	0.0141	0.0004
		Specific	0.4909	0.80	0.3927	0.3955	0.2996	0.0035
			0.0063	1.40	0.0089	0.4116	0.7650	0.0067
		Optimal	0.5077	0.77	0.3931	-	-	-
3.1.3	**Ref.**		1.0072	0.10	0.1007	0.1678	0.0143	0.0003
		Specific	0.6892	0.80	0.5514	0.1981	0.3000	0.0023
			0.2124	1.40	0.2973	0.2063	0.7665	0.0044
		Optimal	0.6203	0.90	0.5604	-	-	-
	Sim.		1.0073	0.10	0.1007	0.1678	0.0143	0.0003
		Specific	0.6895	0.80	0.5516	0.1977	0.3000	0.0023
			0.2129	1.40	0.2980	0.2058	0.7665	0.0044
		Optimal	0.6206	0.90	0.5607	-	-	-
3.1.4	**Ref.**		1.0073	0.10	0.1007	0.1678	0.0143	0.0003
		Specific	0.6894	0.80	0.5515	0.1979	0.3000	0.0023
			0.2126	1.40	0.2977	0.2061	0.7665	0.0044
		Optimal	0.6204	0.90	0.5605	-	-	-
	Sim.		1.0073	0.10	0.1007	0.1678	0.0143	0.0003
		Specific	0.6895	0.80	0.5516	0.1977	0.3000	0.0023
			0.2129	1.40	0.2980	0.2058	0.7665	0.0044
		Optimal	0.6206	0.90	0.5607	-	-	-
3.2.1	**Ref. (BV)**		0.8408	0.10	0.0841	0.3174	0.0127	0.0005
		Specific	0.6261	0.80	0.5009	0.3809	0.1614	0.0043
			0.2274	1.80	0.4092	0.4060	0.5285	0.0113
		Optimal	0.4755	1.21	0.5764	-	-	-
	Tafel		0.8408	0.10	0.0841	0.3174	0.0127	0.0005
		Specific	0.6264	0.80	0.5011	0.3806	0.1614	0.0043
			0.2280	1.80	0.4104	0.4054	0.5285	0.0113

		Optimal	0.4759	1.21	0.5769	-	-	-
3.2.2	**Ref.**	Specific	0.8408	0.10	0.0841	0.3174	0.0127	0.0005
			0.6262	0.80	0.5010	0.3808	0.1614	0.0043
			0.2277	1.80	0.4098	0.4057	0.5285	0.0113
		Optimal	0.4757	1.21	0.5766			
	Sim.	Specific	0.8408	0.10	0.0841	0.3174	0.0127	0.0005
			0.6264	0.80	0.5011	0.3806	0.1614	0.0043
			0.2280	1.80	0.4104	0.4054	0.5285	0.0113
		Optimal	0.4759	1.21	0.5769	-	-	-
3.2.3	**Ref.**	Specific	1.0002	0.10	0.1000	0.1584	0.0124	0.0003
			0.8188	0.80	0.6551	0.1905	0.1606	0.0028
			0.4340	1.80	0.7811	0.2033	0.5284	0.0074
		Optimal	0.5840	1.44	0.8432			
	Sim.	Specific	1.0003	0.10	0.1000	0.1583	0.0124	0.0003
			0.8191	0.80	0.6553	0.1903	0.1606	0.0028
			0.4346	1.80	0.7822	0.2027	0.5284	0.0074
		Optimal	0.5845	1.44	0.8439	-	-	-
3.2.4	**Ref.**	Specific	1.0002	0.10	0.1000	0.1584	0.0124	0.0003
			0.8180	0.80	0.6544	0.1905	0.1614	0.0029
			0.4362	1.80	0.7852	0.2030	0.5266	0.0074
		Optimal	0.5844	1.44	0.8436			
	Sim.	Specific	1.0002	0.10	0.1000	0.1584	0.0124	0.0003
			0.8182	0.80	0.6546	0.1903	0.1614	0.0029
			0.4365	1.80	0.7857	0.2027	0.5266	0.0074
		Optimal	0.5846	1.44	0.8439	-	-	-

APPENDIX H – RESULTS FOR THE SIMULATION COMPARING SORPTION ISOTHERMS

Polarization results:

		Type	V (V)	j (A/cm²)	W (W/cm²)	η_{Act}	η_{Ohm}	η_{Conc}
4.1.1	Springer	Specific	0.8521	0.10	0.0852	0.3351	0.0053	0.0004
			0.7252	0.80	0.5801	0.3952	0.0690	0.0033
			0.4978	1.80	0.8960	0.4190	0.2674	0.0083
		Optimal	0.4962	1.81	0.8975	-	-	-
	Kulikovsky	Specific	0.8495	0.10	0.0850	0.3351	0.0079	0.0004
			0.7080	0.80	0.5664	0.3952	0.0862	0.0033
			0.4563	1.80	0.8214	0.4190	0.3089	0.0083
		Optimal	0.4916	1.69	0.8284	-	-	-
4.1.2	Springer	Specific	0.8421	0.10	0.0842	0.3353	0.0149	0.0004
			0.4683	0.80	0.3746	0.3953	0.3255	0.0034
			0.1065	1.20	0.1278	0.4071	0.6735	0.0053
		Optimal	0.5128	0.74	0.3786	-	-	-
	Kulikovsky	Specific	0.8353	0.10	0.0835	0.3353	0.0217	0.0004
			0.4197	0.80	0.3358	0.3953	0.3740	0.0034
			0.0000	1.20	0.0000	0.4071	0.7815	0.0053
		Optimal	0.5053	0.69	0.3488	-	-	-
4.1.3	Springer	Specific	0.8475	0.10	0.0847	0.3364	0.0053	0.0004
			0.7257	0.80	0.5806	0.3956	0.0649	0.0034
			0.5143	1.80	0.9257	0.4195	0.2471	0.0087
		Optimal	0.4911	1.89	0.9288	-	-	-
	Kulikovsky	Specific	0.8461	0.10	0.0846	0.3364	0.0068	0.0004
			0.7107	0.80	0.5685	0.3956	0.0799	0.0034
			0.4771	1.80	0.8588	0.4195	0.2843	0.0087
		Optimal	0.4860	1.77	0.8597	-	-	-
4.1.4	Springer	Specific	0.8394	0.10	0.0839	0.3355	0.0143	0.0004
			0.4899	0.80	0.3919	0.3958	0.3003	0.0036
			0.1889	1.20	0.2266	0.4076	0.5875	0.0056
		Optimal	0.5073	0.77	0.3928	-	-	-
	Kulikovsky	Specific	0.8355	0.10	0.0836	0.3355	0.0182	0.0004
			0.4488	0.80	0.3590	0.3958	0.3414	0.0036
			0.1160	1.20	0.1392	0.4076	0.6604	0.0056
		Optimal	0.5028	0.72	0.3643	-	-	-
4.2.1	Springer	Specific	0.8478	0.10	0.0848	0.3154	0.0094	0.0004
			0.7170	0.80	0.5736	0.3794	0.0733	0.0038
			0.6033	1.80	1.0860	0.4043	0.1568	0.0094
		Optimal	0.4716	2.57	1.2106	-	-	-
	Kul	Specific	0.8458	0.10	0.0846	0.3154	0.0114	0.0004

			0.6992	0.80	0.5594	0.3794	0.0911	0.0038
			0.5534	1.80	0.9962	0.4044	0.2068	0.0096
		Optimal	0.4411	2.48	1.0924	-	-	-
4.2.2	**Springer**		0.8319	0.10	0.0832	0.3160	0.0249	0.0005
		Specific	0.5634	0.80	0.4508	0.3793	0.2276	0.0039
			0.1287	1.80	0.2316	0.4045	0.6317	0.0100
		Optimal	0.4293	1.17	0.5003	-	-	-
	Kulikovsky		0.8267	0.10	0.0827	0.3160	0.0301	0.0005
		Specific	0.5211	0.80	0.4168	0.3794	0.2701	0.0039
			0.0388	1.80	0.0698	0.4045	0.7216	0.0100
		Optimal	0.4396	0.99	0.4332	-	-	-
4.2.3	**Springer**		0.8491	0.10	0.0849	0.3168	0.0048	0.0005
		Specific	0.7429	0.80	0.5943	0.3805	0.0443	0.0041
			0.6189	1.80	1.1140	0.4059	0.1370	0.0108
		Optimal	0.4624	2.85	1.3172	-	-	-
	Kulikovsky		0.8469	0.10	0.0847	0.3168	0.0070	0.0005
		Specific	0.7260	0.80	0.5808	0.3806	0.0613	0.0041
			0.5908	1.80	1.0634	0.4059	0.1651	0.0108
		Optimal	0.4506	2.71	1.2208	-	-	-
4.2.4	**Springer**		0.8408	0.10	0.0841	0.3174	0.0127	0.0005
		Specific	0.6275	0.80	0.5020	0.3808	0.1602	0.0043
			0.2289	1.80	0.4120	0.4060	0.5271	0.0112
		Optimal	0.4754	1.21	0.5764	-	-	-
	Kulikovsky		0.8349	0.10	0.0835	0.3174	0.0186	0.0005
		Specific	0.5898	0.80	0.4718	0.3808	0.1979	0.0043
			0.1841	1.80	0.3313	0.4060	0.5719	0.0113
		Optimal	0.4557	1.16	0.5264	-	-	-

Computational time results:

	4.1.1) T = -1; RH = -1 and t_M = -1			
	100 points		**500 points**	
	Ref. (BV)	**Tafel**	**Ref. (BV)**	**Tafel**
Mean (s)	3.569455	3.591306	10.806125	10.852858
Std. Dev (s)	0.014441	0.084097	0.027781	0.080990
Improvement	-0.61%		-0.43%	
Significance	**t**	**t_c**	**t**	**t_c**
α = 0.05	-0.810	1.833	-1.726	1.796
α = 0.01	-0.810	2.821	-1.726	2.718
α = 0.05	No		No	
α = 0.01	No		No	
	4.1.2) T = -1; RH = -1 and t_M = 1			
	100 points		**500 points**	

	Ref. (BV)	Tafel	Ref. (BV)	Tafel
Mean (s)	3.883043	3.933062	11.519520	11.704123
Std. Dev (s)	0.011982	0.021810	0.056934	0.018501
Improvement	-1.29%		-1.60%	
Significance	**t**	**t_c**	**t**	**t_c**
α = 0.05	-6.356	1.771	-9.751	1.812
α = 0.01	-6.356	2.650	-9.751	2.764
α = 0.05	No		No	
α = 0.01	No		No	

4.1.3) T = -1; RH = 1 and t_M = -1

	100 points		500 points	
	Ref. (BV)	**Tafel**	**Ref. (BV)**	**Tafel**
Mean (s)	3.371521	3.309244	10.650247	10.259838
Std. Dev (s)	0.015543	0.006100	0.038296	0.043098
Improvement	1.85%		3.67%	
Significance	**t**	**t_c**	**t**	**t_c**
α = 0.05	11.795	1.796	21.414	1.740
α = 0.01	11.795	2.718	21.414	2.567
α = 0.05	Yes		Yes	
α = 0.01	Yes		Yes	

4.1.4) T = -1; RH = 1 and t_M = 1

	100 points		500 points	
	Ref. (BV)	**Tafel**	**Ref. (BV)**	**Tafel**
Mean (s)	3.672536	3.636320	13.317482	10.876145
Std. Dev (s)	0.018582	0.009124	0.062468	0.042765
Improvement	0.99%		18.33%	
Significance	**t**	**t_c**	**t**	**t_c**
α = 0.05	5.532	1.771	101.978	1.753
α = 0.01	5.532	2.650	101.978	2.602
α = 0.05	Yes		Yes	
α = 0.01	Yes		Yes	

4.2.1) T = 1; RH = -1 and t_M = -1

	100 points		500 points	
	Ref. (BV)	**Tafel**	**Ref. (BV)**	**Tafel**
Mean (s)	2.958439	2.955805	9.451413	8.983655
Std. Dev (s)	0.009929	0.011673	0.033515	0.051196
Improvement	0.09%		4.95%	
Significance	**t**	**t_c**	**t**	**t_c**
α = 0.05	0.544	1.740	24.173	1.753
α = 0.01	0.544	2.567	24.173	2.602
α = 0.05	No		Yes	
α = 0.01	No		Yes	

4.2.2) T = 1; RH = -1 and t_M = 1

	100 points		500 points	
	Ref. (BV)	**Tafel**	**Ref. (BV)**	**Tafel**

Mean (s)	2.994290	3.084140	9.379102	9.025993
Std. Dev (s)	0.013227	0.007492	0.034011	0.021615
Improvement	-3.00%		3.76%	
Significance	**t**	**t_c**	**t**	**t_c**
α = 0.05	-18.691	1.761	27.709	1.753
α = 0.01	-18.691	2.624	27.709	2.602
α = 0.05	No		Yes	
α = 0.01	No		Yes	
	4.2.3) T = 1; RH = 1 and t_M = -1			
	100 points		**500 points**	
	Ref. (BV)	**Tafel**	**Ref. (BV)**	**Tafel**
Mean (s)	2.795126	2.699450	9.559942	9.081459
Std. Dev (s)	0.007863	0.008867	0.033334	0.074291
Improvement	3.42%		5.01%	
Significance	**t**	**t_c**	**t**	**t_c**
α = 0.05	25.531	1.740	18.582	1.782
α = 0.01	25.531	2.567	18.582	2.681
α = 0.05	Yes		Yes	
α = 0.01	Yes		Yes	
	4.2.4) T = 1; RH = 1 and t_M = 1			
	100 points		**500 points**	
	Ref. (BV)	**Tafel**	**Ref. (BV)**	**Tafel**
Mean (s)	2.836284	2.815311	9.549006	9.146724
Std. Dev (s)	0.024545	0.007502	0.019364	0.047965
Improvement	0.74%		4.21%	
Significance	**t**	**t_c**	**t**	**t_c**
α = 0.05	2.584	1.812	24.594	1.796
α = 0.01	2.584	2.764	24.594	2.718
α = 0.05	Yes		Yes	
α = 0.01	No		Yes	

APPENDIX I – IMPACT OF THE MEAN DIFFUSIVITY ASSUMPTION ON THE CONCENTRATION PROFILES

As most phenomena in a fuel cell, the transport in the membrane and in the electrode are coupled. In the developed model, the dependence of the fluxes and bulk concentrations on α^* makes so that variations on the water transport inside the membrane affect the concentration profiles in the electrode. To better understand the extent of this impact, the concentration profiles for tests 5.1.1 (Springer), 5.2.1 (Meier *et* Eigenberger), and 5.3.1 (Piecewise liner) are presented respectively in Figures I.1, I.2, and I.3. Although only one case is considered here, the conclusions can be extended for the others.

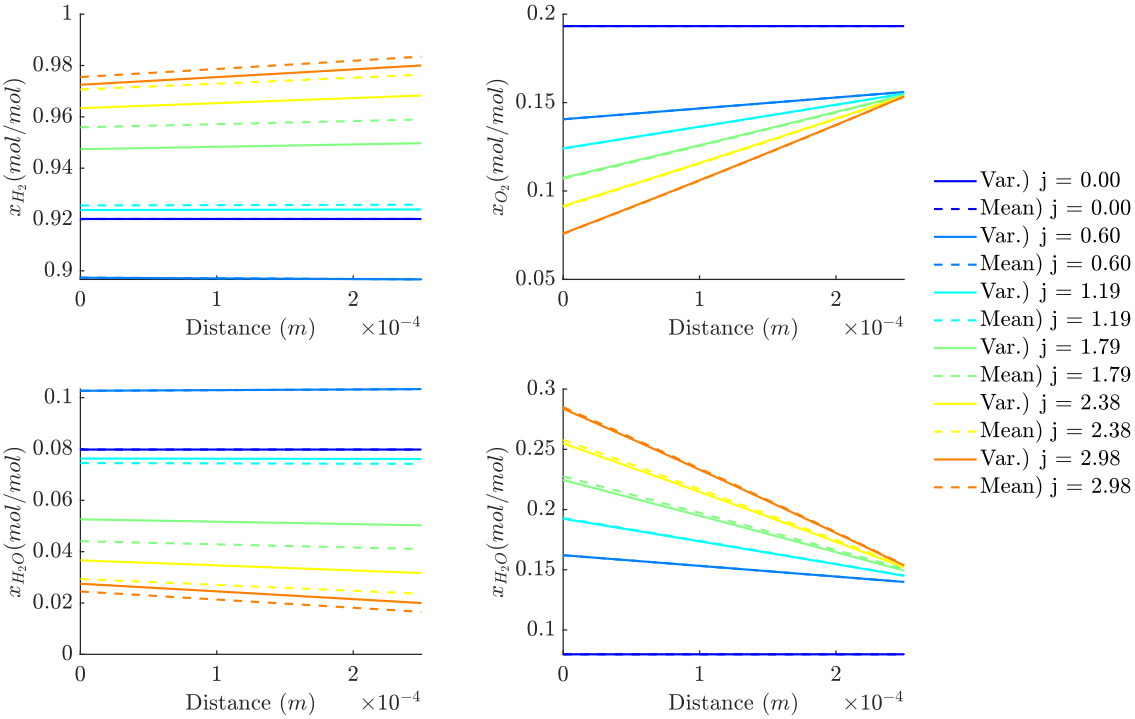

Figure I.1 – Concentration profiles for test 5.1.1.

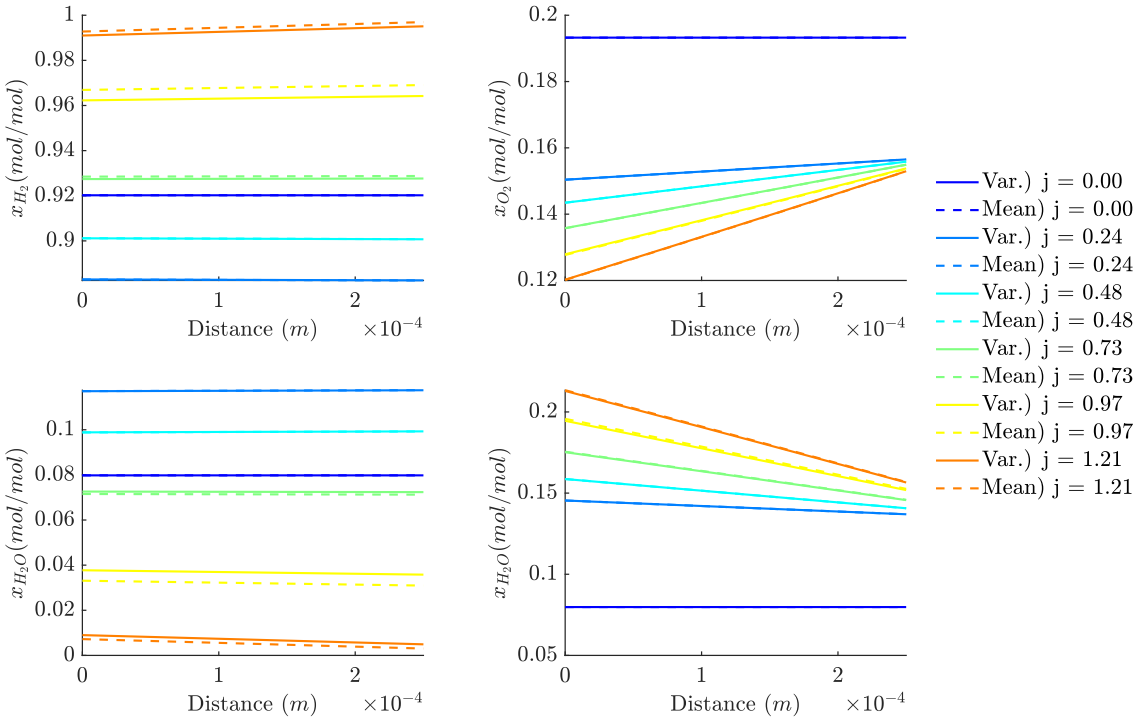

Figure I.2 – Concentration profiles for test 5.2.1.

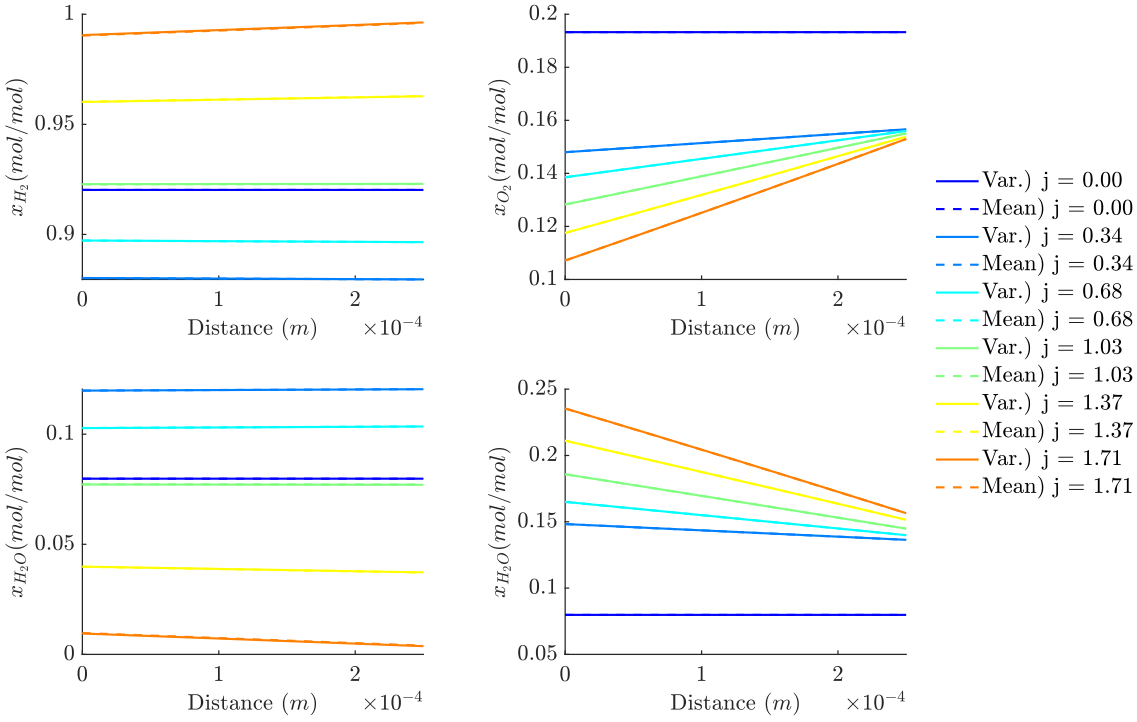

Figure I.3 – Concentration profiles for test 5.3.1.

All those curves have practically coincidental concentration profiles in the cathode. This indicates that the assumption likely does not affect the model's capability to predict overvoltages related to oxygen depletion.

However, conditions 5.1.1 and 5.2.1 have deviations in the anode. Although they are numerically small, they will affect λ at the interfaces. Considering the sharp drop of conductivity at low water contents, this effect may be a relevant part of the cause for the differences in ohmic overvoltages between submodels. Nevertheless, the profile inside the membrane – and not only the value at the interface – must be considered as well to understand this difference. For example, test 5.3.1 did not present a noticeable difference in concentration profiles and, consequently, in λ_{Ano}. However, the assumption impacted the λ profile inside the membrane, resulting in different ohmic overvoltages. The key characteristic of test 5.3.1 that enables this to happen is that α^* is practically the same between submodels, so the concentration profiles at the electrodes must be as well.

Therefore, although the cathodic profiles are mostly unaffected, the assumption is expected to affect the anodic ones under most conditions. Although the difference is small, it can be relevant for affecting the polarization curves due to the major dependence of conductivity and membrane humidification.

APPENDIX J – COMPUTATIONAL TIME RESULT FOR SPRINGER'S ELECTRO-OSMOTIC DRAG DESCRIPTION

	5.1.1) T = -1; RH = -1; t_M = -1			
	100 points		500 points	
	Variable (Ref.)	Mean	Variable (Ref.)	Mean
Mean (s)	3.576955	3.413682	10.901793	10.485561
Std. Dev (s)	0.101066	0.039719	0.042043	0.042511
Improvement	4.56%		3.82%	
Significance	t	t_c	t	t_c
α = 0.05	4.755	1.796	22.015	1.740
α = 0.01	4.755	2.718	22.015	2.567
α = 0.05	Yes		Yes	
α = 0.01	Yes		Yes	

	5.1.2) T = 1; RH = -1; t_M = -1			
	100 points		500 points	
	Variable (Ref.)	Mean	Variable (Ref.)	Mean
Mean (s)	3.098137	2.140917	9.781869	8.337404
Std. Dev (s)	0.052640	0.019318	0.067320	0.470743
Improvement	30.90%		14.77%	
Significance	t	t_c	t	t_c
α = 0.05	53.983	1.796	9.606	1.833
α = 0.01	53.983	2.718	9.606	2.821
α = 0.05	Yes		Yes	
α = 0.01	Yes		Yes	

	5.1.3) T = -1; RH = 1; t_M = -1			
	100 points		500 points	
	Variable (Ref.)	Mean	Variable (Ref.)	Mean
Mean (s)	3.400974	2.241603	10.608197	8.541213
Std. Dev (s)	0.013208	0.016947	0.016112	0.014908
Improvement	34.09%		19.48%	
Significance	t	t_c	t	t_c
α = 0.05	170.630	1.746	297.774	1.740
α = 0.01	170.630	2.583	297.774	2.567
α = 0.05	Yes		Yes	
α = 0.01	Yes		Yes	

	5.1.4) T = 1; RH = 1; t_M = -1	
	100 points	500 points

	Variable (Ref.)	Mean	Variable (Ref.)	Mean
Mean (s)	2.785608	2.181565	9.649839	8.253103
Std. Dev (s)	0.009662	0.039671	0.014415	0.014307
Improvement	21.68%		14.47%	
Significance	**t**	**t_c**	**t**	**t_c**
α = 0.05	46.782	1.812	217.477	1.740
α = 0.01	46.782	2.764	217.477	2.567
α = 0.05	Yes		Yes	
α = 0.01	Yes		Yes	

	5.1.5) T = -1; RH = -1; t_M = 1			
	100 points		**500 points**	
	Variable (Ref.)	**Mean**	**Variable (Ref.)**	**Mean**
Mean (s)	3.890963	2.615437	11.697893	10.565127
Std. Dev (s)	0.018115	0.015916	0.044872	0.050171
Improvement	32.78%		9.68%	
Significance	**t**	**t_c**	**t**	**t_c**
α = 0.05	167.270	1.740	53.218	1.740
α = 0.01	167.270	2.567	53.218	2.567
α = 0.05	Yes		Yes	
α = 0.01	Yes		Yes	

	5.1.6) T = 1; RH = -1; t_M = 1			
	100 points		**500 points**	
	Variable (Ref.)	**Mean**	**Variable (Ref.)**	**Mean**
Mean (s)	3.118612	2.234660	9.658015	8.586861
Std. Dev (s)	0.010475	0.006831	0.022406	0.008097
Improvement	28.34%		11.09%	
Significance	**t**	**t_c**	**t**	**t_c**
α = 0.05	223.529	1.753	142.179	1.796
α = 0.01	223.529	2.602	142.179	2.718
α = 0.05	Yes		Yes	
α = 0.01	Yes		Yes	

	5.1.7) T = -1; RH = 1; t_M = 1			
	100 points		**500 points**	
	Variable (Ref.)	**Mean**	**Variable (Ref.)**	**Mean**
Mean (s)	3.591460	2.494539	13.359055	9.980191
Std. Dev (s)	0.008467	0.008126	0.027909	0.038491
Improvement	30.54%		25.29%	
Significance	**t**	**t_c**	**t**	**t_c**
α = 0.05	295.589	1.740	224.733	1.746
α = 0.01	295.589	2.567	224.733	2.583

α = 0.05	Yes	Yes
α = 0.01	Yes	Yes

	5.1.8) T = 1; RH = 1; t_M = 1			
	100 points		500 points	
	Variable (Ref.)	**Mean**	**Variable (Ref.)**	**Mean**
Mean (s)	2.860011	2.216024	9.649638	8.526503
Std. Dev (s)	0.020350	0.006415	0.031179	0.030236
Improvement	22.52%		11.64%	
Significance	**t**	**t_c**	**t**	**t_c**
α = 0.05	95.440	1.812	81.776	1.740
α = 0.01	95.440	2.764	81.776	2.567
α = 0.05	Yes		Yes	
α = 0.01	Yes		Yes	

APPENDIX K – COMPUTATIONAL TIME RESULT FOR MEIER AND EIGENBERGER'S ELECTRO-OSMOTIC DRAG DESCRIPTION

	5.2.1) T = -1; RH = -1; t_M = -1			
	100 points		**500 points**	
	Variable (Ref.)	**Mean**	**Variable (Ref.)**	**Mean**
Mean (s)	3.881925	2.957238	11.710476	11.865836
Std. Dev (s)	0.075981	0.031384	0.031261	0.106127
Improvement	23.82%		-1.33%	
Significance	**t**	**t_c**	**t**	**t_c**
α = 0.05	35.570	1.796	-4.441	1.812
α = 0.01	35.570	2.718	-4.441	2.764
α = 0.05	Yes		No	
α = 0.01	Yes		No	

	5.2.2) T = 1; RH = -1; t_M = -1			
	100 points		**500 points**	
	Variable (Ref.)	**Mean**	**Variable (Ref.)**	**Mean**
Mean (s)	3.711456	2.877975	10.790080	11.504133
Std. Dev (s)	0.025740	0.032327	0.024706	0.037502
Improvement	22.46%		-6.62%	
Significance	**t**	**t_c**	**t**	**t_c**
α = 0.05	63.783	1.740	-50.280	1.753
α = 0.01	63.783	2.567	-50.280	2.602
α = 0.05	Yes		No	
α = 0.01	Yes		No	

	5.2.3) T = -1; RH = 1; t_M = -1			
	100 points		**500 points**	
	Variable (Ref.)	**Mean**	**Variable (Ref.)**	**Mean**
Mean (s)	3.790084	2.945430	11.681792	11.837423
Std. Dev (s)	0.023146	0.024024	0.024828	0.050116
Improvement	22.29%		-1.33%	
Significance	**t**	**t_c**	**t**	**t_c**
α = 0.05	80.066	1.740	-8.799	1.771
α = 0.01	80.066	2.567	-8.799	2.650
α = 0.05	Yes		No	
α = 0.01	Yes		No	

	5.2.4) T = 1; RH = 1; t_M = -1			
	100 points		**500 points**	
	Variable (Ref.)	**Mean**	**Variable (Ref.)**	**Mean**

Mean (s)	3.928169	2.856288	11.902396	11.489367
Std. Dev (s)	0.025130	0.008910	0.023569	0.037218
Improvement	27.29%		3.47%	
Significance	**t**	**t_c**	**t**	**t_c**
α = 0.05	127.129	1.796	29.649	1.753
α = 0.01	127.129	2.718	29.649	2.602
α = 0.05	Yes		Yes	
α = 0.01	Yes		Yes	

	5.2.5) T = -1; RH = -1; t_M = 1			
	100 points		**500 points**	
	Variable (Ref.)	**Mean**	**Variable (Ref.)**	**Mean**
Mean (s)	4.155021	3.344883	12.543249	13.934209
Std. Dev (s)	0.020655	0.010460	0.049076	0.114883
Improvement	19.50%		-11.09%	
Significance	**t**	**t_c**	**t**	**t_c**
α = 0.05	110.654	1.771	-35.210	1.782
α = 0.01	110.654	2.650	-35.210	2.681
α = 0.05	Yes		No	
α = 0.01	Yes		No	

	5.2.6) T = 1; RH = -1; t_M = 1			
	100 points		**500 points**	
	Variable (Ref.)	**Mean**	**Variable (Ref.)**	**Mean**
Mean (s)	4.068208	3.388770	11.565476	14.219683
Std. Dev (s)	0.023207	0.012122	0.026380	0.256116
Improvement	16.70%		-22.95%	
Significance	**t**	**t_c**	**t**	**t_c**
α = 0.05	82.061	1.771	-32.599	1.833
α = 0.01	82.061	2.650	-32.599	2.821
α = 0.05	Yes		No	
α = 0.01	Yes		No	

	5.2.7) T = -1; RH = 1; t_M = 1			
	100 points		**500 points**	
	Variable (Ref.)	**Mean**	**Variable (Ref.)**	**Mean**
Mean (s)	4.207036	3.278308	12.214009	13.430721
Std. Dev (s)	0.029153	0.013680	0.021406	0.058169
Improvement	22.08%		-9.96%	
Significance	**t**	**t_c**	**t**	**t_c**
α = 0.05	91.199	1.782	-62.075	1.796
α = 0.01	91.199	2.681	-62.075	2.718
α = 0.05	Yes		No	

α = 0.01	Yes	No

	5.2.8) T = 1; RH = 1; t_M = 1			
	100 points		500 points	
	Variable (Ref.)	**Mean**	**Variable (Ref.)**	**Mean**
Mean (s)	4.350216	3.254921	12.545347	13.245127
Std. Dev (s)	0.026281	0.021021	0.033872	0.043924
Improvement	25.18%		-5.58%	
Significance	**t**	**t_c**	**t**	**t_c**
α = 0.05	102.918	1.740	-39.895	1.746
α = 0.01	102.918	2.567	-39.895	2.583
α = 0.05	Yes		No	
α = 0.01	Yes		No	

APPENDIX L – COMPUTATIONAL TIME RESULT FOR PIECEWISE LINEAR ELECTRO-OSMOTIC DRAG DESCRIPTION

	5.3.1) T = -1; RH = -1; t_M = -1			
	100 points		500 points	
	Variable (Ref.)	Mean	Variable (Ref.)	Mean
Mean (s)	5.193663	2.936534	16.891775	11.506852
Std. Dev (s)	0.022939	0.017009	0.020631	0.044983
Improvement	43.46%		31.88%	
Significance	t	t_c	t	t_c
α = 0.05	249.939	1.746	344.092	1.782
α = 0.01	249.939	2.583	344.092	2.681
α = 0.05	Yes		Yes	
α = 0.01	Yes		Yes	

	5.3.2) T = 1; RH = -1; t_M = -1			
	100 points		500 points	
	Variable (Ref.)	Mean	Variable (Ref.)	Mean
Mean (s)	4.270269	2.824144	13.170973	11.368390
Std. Dev (s)	0.028461	0.029229	0.293700	0.249078
Improvement	33.86%		13.69%	
Significance	t	t_c	t	t_c
α = 0.05	112.095	1.740	14.802	1.740
α = 0.01	112.095	2.567	14.802	2.567
α = 0.05	Yes		Yes	
α = 0.01	Yes		Yes	

	5.3.3) T = -1; RH = 1; t_M = -1			
	100 points		500 points	
	Variable (Ref.)	Mean	Variable (Ref.)	Mean
Mean (s)	3.699689	2.778145	10.660134	10.929565
Std. Dev (s)	0.017178	0.016488	0.045178	0.025698
Improvement	24.91%		-2.53%	
Significance	t	t_c	t	t_c
α = 0.05	122.392	1.740	-16.393	1.761
α = 0.01	122.392	2.567	-16.393	2.624
α = 0.05	Yes		No	
α = 0.01	Yes		No	

5.3.4) T = 1; RH = 1; t_M = -1

	100 points		500 points	
	Variable (Ref.)	**Mean**	**Variable (Ref.)**	**Mean**
Mean (s)	3.925392	2.973798	11.064898	11.745111
Std. Dev (s)	0.011380	0.015993	0.077010	0.041812
Improvement	24.24%		-6.15%	
Significance	**t**	**t_c**	**t**	**t_c**
α = 0.05	153.308	1.746	-24.547	1.771
α = 0.01	153.308	2.583	-24.547	2.650
α = 0.05	Yes		No	
α = 0.01	Yes		No	

	5.3.5) T = -1; RH = -1; t_M = 1			
	100 points		**500 points**	
	Variable (Ref.)	**Mean**	**Variable (Ref.)**	**Mean**
Mean (s)	4.999421	3.101721	15.687852	12.691066
Std. Dev (s)	0.071423	0.008829	0.036750	0.049008
Improvement	37.96%		19.10%	
Significance	**t**	**t_c**	**t**	**t_c**
α = 0.05	83.386	1.833	154.705	1.746
α = 0.01	83.386	2.821	154.705	2.583
α = 0.05	Yes		Yes	
α = 0.01	Yes		Yes	

	5.3.6) T = 1; RH = -1; t_M = 1			
	100 points		**500 points**	
	Variable (Ref.)	**Mean**	**Variable (Ref.)**	**Mean**
Mean (s)	4.156957	3.227671	12.271850	13.322203
Std. Dev (s)	0.020529	0.028140	0.018553	0.020291
Improvement	22.35%		-8.56%	
Significance	**t**	**t_c**	**t**	**t_c**
α = 0.05	84.366	1.746	-120.806	1.740
α = 0.01	84.366	2.583	-120.806	2.567
α = 0.05	Yes		No	
α = 0.01	Yes		No	

	5.3.7) T = -1; RH = 1; t_M = 1			
	100 points		**500 points**	
	Variable (Ref.)	**Mean**	**Variable (Ref.)**	**Mean**
Mean (s)	4.038108	3.106030	11.602786	12.602338
Std. Dev (s)	0.012500	0.006657	0.024226	0.022185
Improvement	23.08%		-8.61%	
Significance	**t**	**t_c**	**t**	**t_c**
α = 0.05	208.128	1.771	-96.224	1.740

α = 0.01	208.128	2.650	-96.224	2.567
α = 0.05	Yes		No	
α = 0.01	Yes		No	

	5.3.8) T = 1; RH = 1; t_M = 1			
	100 points		**500 points**	
	Variable (Ref.)	**Mean**	**Variable (Ref.)**	**Mean**
Mean (s)	4.433927	3.144507	12.402737	12.910572
Std. Dev (s)	0.010918	0.008960	0.029506	0.161095
Improvement	29.08%		-4.09%	
Significance	**t**	**t_c**	**t**	**t_c**
α = 0.05	288.692	1.740	-9.806	1.833
α = 0.01	288.692	2.567	-9.806	2.821
α = 0.05	Yes		No	
α = 0.01	Yes		No	